The Oxidation of L-Tryptophan in Biology by Human Heme Dioxygenases

Thesis submitted for the degree of
Doctor of Philosophy
at the University of Leicester

by

Sara A. Rafice B.Sc. (Hons)

Department of Chemistry
Faculty of Science
University of Leicester

December 2009

STATEMENT

Unless otherwise acknowledged, the experimental work described in this thesis has been carried out by the author in the Henry Wellcome Laboratories for Structural Biology, at the University of Leicester between September 2006 and December 2009. The work has not been submitted, and is not presently being submitted for any other degree at this or any other university.

Signed: Date:

Department of Chemistry
University of Leicester
University Road
Leicester, LE1 7RH
UK

With appreciation…

To the Rafice Family;

Mum, Dad, Syed;

To the Shaw family;

James, Pat, Alan;

for their love and support.

ACKNOWLEDGEMENTS

The Raven Group

- I would like to thank my supervisor Prof. E. L. Raven for her guidance, support and help throughout the three years. Emma chose me for the TDO project, which has been very interesting leading edge work and I feel that my project has contributed to science and provided vital information for the study of some human diseases.
- Andrea Gumiero and Dr. Igor Efimov are my good friends whom I have shared hours of lab time with. I could not have made it through without them and it was also enjoyable to learn some Russia and Italian and spend many evenings eating wonderful foods (Picture left to right: Me, Igor and Andrea). Thank you to Dr. Clive Metcalfe and Phillip Raynor for your friendship and advice.

EPR Team

- A special thank you to Dr. Harriet Steward, Dr. Myles Cheeseman (UEA), Dr. Gerry Griffith and Mindy for advising, running and analysing my EPR work. Thank you to my friend Harriet for also giving me guidance on heme proteins!

Collaborations

- We collaborate with the crystallography lab, thank you to Dr. Peter Moody and Dr. Paul Elliot for your patience, we succeeded in growing IDO crystals!
- Thank you to Dr. Wei-Cheng Huang for all the discussions about cytochrome P450s and for your thoughts in general about heme containing enzymes.
- Thanks to our Edinburgh collaborators George Pantouris (my inhibition studies saviour), Dr. Sarah Thackray, Dr. Chris Mowat and Prof. Steve Chapman. I will miss our chats and best of luck in answering the huge number of dioxygenase questions.

Internal Services (University of Leicester)

- I spent a good deal of my PhD at The Protein Nucleic Acid Chemistry Laboratory (PNACL) with Dr. Sharad Mistry, Dr. Andrew Bottrill, Shairbanu Ibrahim and Joan Sutherland to work out whether I had the correct protein using MALDI and the correct DNA using sequencing, thanks for your help.
- Thank you to Dr. Xiaowen Yang and Andrew Prescott at the Protein and Expression Laboratory (PROTEX) for doing my mutagenesis, it saved me a lot of precious time.
- Thank you to the Biochemistry Departmental Services Office staff Barbara Birch, Jeff Morant, Dawn Goodey and Ayca Westgate for making my life easier especially when I was ordering supplies such as liquid helium and sending packages with dry ice.
- Thank you to the Chemistry Administration staff Phillip Acton, Saiful Choudhury, Ann Crane, Vicky Orson-Wright, Justin Shepard and Julie Spence for solving all my other problems!

Funding bodies

- Thank you finally to the EPSRC and the University of Leicester for funding.

ABSTRACT

THE OXIDATION OF L-TRYPTOPHAN BY HUMAN HEME DIOXYGENASES

SARA A. RAFICE

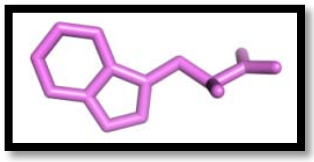

Tryptophan is an essential amino acid, which is catabolised via the kynurenine pathway leading to the formation of NAD. The initial and rate-limiting step of the kynurenine pathway is controlled by two hemoproteins called tryptophan 2,3-dioxygenase (TDO) and indoleamine 2,3-dioxygenase (IDO), which oxidise tryptophan to form *N*-formyl-kynurenine.

A bacterial expression system for hTDO was characterised in Chapter 2. Kinetic, spectroscopic and redox analyses determined that significant differences exist. It was found that hTDO does not form a stable ferrous-oxy complex and that the ferric form of the enzyme was catalytically active. In addition hTDO does not discriminate against substrate binding to the ferric derivative.

Site-directed mutagenesis of several active site residues and the role of each residue on substrate binding and in catalysis was examined in Chapter 3. The H76 residue was found to be involved in substrate binding. The phenylalanine variants of TDO showed that the hydrophobicity in the active site was essential for catalytic activity. Furthermore, the data showed that F72 is an important substrate binding residue. The highly conserved arginine residue was deemed to be an essential catalytic residue involved in substrate binding. The implications of these findings are discussed in terms of the current understanding of dioxygenase catalysis.

In Chapter 4, it was shown that 1-methyl-tryptophan was a substrate for wild type IDO and variants of TDO and IDO, which is contrary to previous findings in dioxygenase literature. No activity was observed for wild type hTDO. Previous crystallographic studies and modelling in combination with kinetic, spectroscopic and redox analyses indicated that the distal histidine in the TDO active site causes steric clashes with 1-methyl-L-tryptophan. This information indicated exclusion of the deprotonation of the indole N_1 mechanism, and an alternative reaction mechanism was presented.

A new expression system for IDO with a cleavable hexahistidyl tag was constructed in Chapter 5. The analyses indicated that the recombinant protein had the same characteristics as all other mammalian IDOs and that diffraction quality crystals can be grown from the system. Crystal structures of IDO are required to further the understanding of substrate binding and the catalytic mechanism.

TABLE OF CONTENTS

ABBREVIATIONS

Amino Acids are abbreviated according to the three-letter codes recommended by the I.U.P.A.C Joint Commission on Biochemical Nomenclature (1985).

ENZYMES

hTDO	Human tryptophan 2,3-dioxygenase
rhTDO	Recombinant human tryptophan 2,3-dioxygenase
xcTDO	*Xanthomonas campestris* tryptophan 2,3-dioxygenase
hIDO	Human indoleamine 2,3-dioxygenase
rhIDO	Recombinant human indoleamine 2,3-dioxygenase
Mb	Myoglobin
Hb	Hemoglobin
DNase	Deoxyribonuclease
BSA	Bovine serum albumin
TEV	Tobacco Etch Virus protease

CHEMICALS

L-Trp	L-Tryptophan
1-L-ME-TRP	1- L -Methyl-Tryptophan
Amp	Ampicillin
dNTPs	Deoxynucleotide triphosphates
DTT	Dithiothreitol
EDTA	Ethylenediaminetetraacetic acid
IPTG	Isopropyl-β-D-thiogalactopyanoside
Kan	Kanamycin
NBC	Nile blue chloride
PEG	Polyethylene Glycol
PIM	4 Phenolimidazole
PMSF	Phenylmethylsulphonyl fluoride
SDS	Sodium dodecyl sulphate
Tris	Trizma base (tri[hydroxymethyl]aminomethane)

TECHNIQUES

EPR	Electron paramagnetic resonance
FPLC	Fast protein liquid chromatography
PCR	Polyacrylamide gel electrophoresis
R_Z	Reinheitzahl
SDS-PAGE	Sodium dodecyl sulphate - polyacrylamide gel glectrophoresis
UV	Ultra violet

AMINO ACIDS

Ala	A	Alanine
Asn	N	Asparagine
Asp	D	Aspartic Acid
Arg	R	Arginine
Cys	C	Cysteine
Glu	E	Glutamic Acid
Gln	Q	Glutamine
Gly	G	Glycine
His	H	Histidine
Met	M	Methionine
Pro	P	Proline
Ser	S	Serine
Thr	T	Threonine
Tyr	Y	Tyrosine
Lys	K	Lysine
Leu	L	Leucine
Ile	I	Isoleucine
Phe	F	Phenylalanine
Trp	W	Tryptophan
Val	V	Valine

UNITS/SYMBOLS

A	Absorption
ε	Absorption coefficient
Å	Angström (1Å = 10^{-10} m)
bp	Base pairs
^{o}C	degrees Celcius
g	Grams
h	Hour
kb	Kilobases
kDa	Kilo Daltons
l	Litres
mV	milliVolts
min	Minutes
M	Molar
OD	Optical density
rpm	Revolutions per minute
s	Seconds
v/v	Volume to volume
λ	Wavelength
w/v	Weight per volume

OTHER

cDNA	Complementary deoxyribonucleic acid
CT band	Charge transfer band
DNA	Deoxyribonucleic acid
E. coli	*Escherichia coli*
I.U.P.A.C	International Union of Pure and Applied Chemistry
NAD	Nicotine adenine dinucleotide
PDB	Protein data bank
PNACL	Protein and Nucleic Acid Chemistry Laboratory

LIST OF FIGURES

CHAPTER 1

CHAPTER 2

CHAPTER 3

CHAPTER 6

CHAPTER 7

LIST OF TABLES

LIST OF SCHEMES

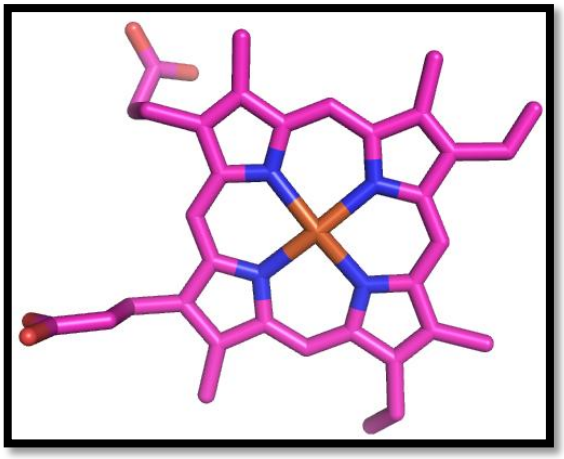

CHAPTER 1

INTRODUCTION

This chapter provides an introduction to the area of hemoproteins, in particular the dioxygenase enzymes tryptophan 2,3-dioxygenase (TDO) and indoleamine 2,3-dioxygenase (IDO).

1.1 The Chemical Properties of Dioxygen

Oxygen is the third most abundant element in the universe after hydrogen and helium and was discovered in the 1770s (*1, 2*). Most living organisms such as animals and fish utilise oxygen by respiration to survive, others produce oxygen, called photoautotrophs such as photosynthetic plants, algae and some bacteria. All main types of structural molecules in living organisms such as carbohydrates, fats and proteins contain atoms of oxygen. Respiration involves cleavage of dioxygen, (dioxygen is two atoms of oxygen joined by a double bond and constitutes 20.9 % of the volume of air (*3*)), which is an energetically favourable process.

Dioxygen has a triplet ground state configuration and is fairly unreactive at typical pressure and temperature. The electron configuration of dioxygen is a diradical with two unpaired electrons which are in the degenerate orbitals π_{2p}, which is favoured over singlet $^1O_2$ (Figure 1.1) (*4*).

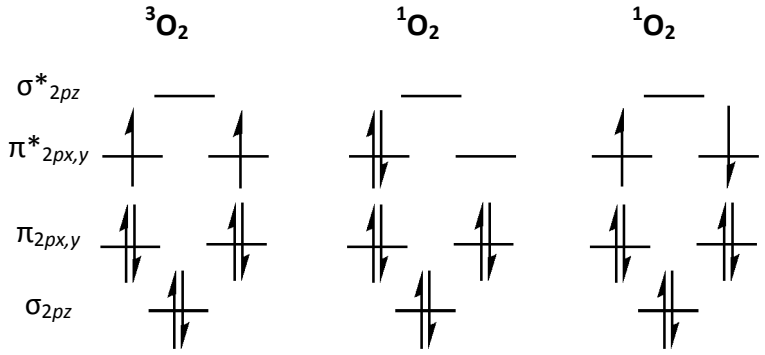

Figure 1.1 Molecular orbital diagram for triplet dioxygen $^3O_2$ and singlet oxygen $^1O_2$.

Although dioxygen has a triplet ground state, essentially all stable organic compounds are singlets, whereby all of their electrons are paired. Direct reactions of dioxygen with singlet organic reagents typically require high energy formation and therefore are rare apart from when triplet dioxygen reacts with organic radicals ($R^\bullet$), to form a stable radical intermediate (Equation 1.1).

Equation 1.1

$$R^{\bullet} + O_2 \rightarrow RO_2^{\bullet}$$

Another way to overcome the high kinetic barrier inherent to the reactions of triplet O_2 is to utilise a transition metal ion such as iron or copper as the cofactor in enzymes that carry out biological oxidations. Transition metals in the appropriate oxidation states are able to react readily with triplet O_2 to form dioxygen adducts that can participate in reaction pathways leading to either oxidation or the incorporation of oxygen atoms into organic substrates (*5*).

1.2 Oxygen Activation by Metal Ions

The use of transition metals for transport, activation and reduction of dioxygen is because most transition metals contain unpaired electrons, which allow reactions with triplet dioxygen. Secondly, transition metals have many shells of electrons, which allow for spin transitions apart from the first row of transition metals. Finally, transition metals often have several excited states with unpaired electrons close in energy to the ground state, which can be used to improve the likelihood of spin transition (*6*).

Transition metal ions, containing *3d* orbital unpaired electrons, can use three methods to activate dioxygen (*7*). Firstly, upon addition of dioxygen to a transition metal ion containing unpaired *3d* orbital electrons, the unpaired electrons in the dioxygen π^* orbitals are able to overlap with those on the metal ion (*8*). The reaction of such a transition metal-dioxygen with a singlet organic reagent is then allowed, provided that the overall number of unpaired electrons in the complex remains constant. Secondly the transition metals found in metallo-enzymes that activate dioxygen have two consecutive oxidation states (*e.g.* Fe^{II}/Fe^{III}, Cu^{I}/Cu^{II}), therefore the metal centre is able to carry out single electron transfer to the bound dioxygen. The triplet oxygen ground state can accept a single electron to form superoxide, which is one possible route for oxygen activation. Superoxide can then participate in a variety of 1- or 2-electron chemical reactions (*9, 10*). Finally, reaction of dioxygen via radical mechanisms is a possibility and has been proposed

for some non-heme dioxygenases, whereby a bound intermediate, which is a substrate radical can attack dioxygen to form a stable radical (*7, 11*)

1.3 Heme Prosthetic Group

Iron protoporphyrin IX, also known as heme, is a metal complex present in a variety of proteins in prokaryotes and eukaryotes. It is an iron-containing macrocycle that has a tetra-pyrrole structure connected by methene bridges (positions α, β, γ and δ) producing a square planar structure and contains eight side chains: four methyl (positions 1, 3, 5 and 8), two vinyl (positions 2 and 4) and two propionate (positions 6 and 7) (Figure 1.2A).

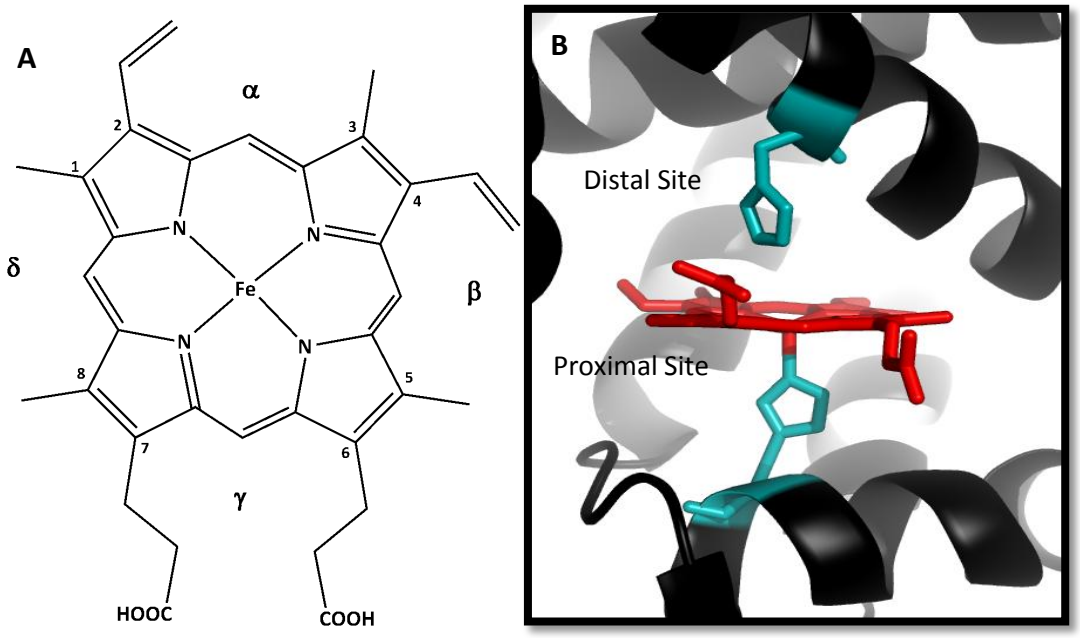

Figure 1.2 (**A**) Iron protoporphyrin IX contains eight side chains labelled 1 - 8 and four methene bridges labelled α, β, γ and δ. (**B**) The crystal structure of a subunit of human haemoglobin showing the distal and proximal sites above and below the heme plane respectively (red) , occupied by hisitidine residues (cyan).

Iron protoporphyrin IX has iron (3+) at the centre, which has up to six coordination sites, the fifth and sixth axial bonds are termed the proximal and distal coordination sites (Figure 1.2B). There is variation between the axial ligands in heme proteins,

however in the majority of cases the proximal ligand is a histidine. There is also variation in the oxidation state of iron, in some heme-containing proteins the iron can be either ferrous (Fe^{2+}) or ferric (Fe^{3+}) but in some cases such as peroxidase and cytochrome P450 enzymes the iron can also be ferryl (Fe^{4+}) (*12-16*).

1.4 Biological Function of Heme Proteins

Hemoproteins have a wide range of functions in eukaryotes, such as oxygen transport and storage, catalysis and active membrane transport/electron transfer. The biological function is determined by the sequence of amino acids forming the polypeptide chain and by the distal and proximal ligands to the heme, altering the ability for oxidation and reduction of the iron.

The primary dioxygen storage and transport proteins in humans are myoglobin and hemoglobin, which both have strongly bound proximal histidine residues coordinating to the iron (*17, 18*). Dioxygen is able to reversibly bind the protein weakly at the distal site. Peroxidases are hemoproteins for redox catalysis reactions, such as the monomeric protein cytochrome *c* peroxidase, which catalyses the production of hydrogen peroxide to water and has a proximal histidine coordinating to iron (*19*). Some of the heme containing cytochrome family, such as the cytochrome P450s are involved in the transfer of electrons due to their ability to rapidly convert between Fe^{3+} and Fe^{2+} oxidation states.

1.5 Oxygenases

Molecular oxygen serves two biological purposes for aerobic life. Firstly, it acts as the proton terminal acceptor for biological oxidation, whereby a single oxygen molecule is reduced to water, superoxide anion or hydrogen peroxide *e.g.*, by cytochrome oxidase, which catalyses the transfer of electrons from cytochrome *c* to molecular oxygen, in the respiratory chain. Secondly, it is a biosynthetic agent whereby oxygen is incorporated into dietary nutrients such as amino acids to produce biologically active compounds (*20*). The latter role is conducted by enzymes which are called oxygenases or oxidoreductase enzymes in plants, animals and microorganisms (*21, 22*). There are two types of oxygenase enzyme:

monooxygenases (Equation 1.2) and dioxygenases (Equation 1.3), which incorporate one or both atoms of dioxygen into the substrate respectively (*16*).

Equation 1.2 - Monooxygenases

$$XH + O_2^{\bullet} + 2e^- + 2H^+ \rightarrow X(O^{\bullet})H + H_2O^{\bullet}$$

Equation 1.3 - Dioxygenases

$$XH + O_2^{\bullet} \rightarrow X(O_2^{\bullet})H$$

Monooxygenases such as cytochrome P450 oxidases incorporate a single oxygen atom into the substrate and require two electrons to reduce the second oxygen atom of dioxygen to water (Equation 1.2) (*16*). The two electrons come from a reducing agent or from the substrate itself. Cytochrome P450s are found ubiquitously in mammalian tissues and organs as well as plants, bacteria, yeast and insects. Dioxygenases such as tryptophan 2,3-dioxygenase (TDO) and indoleamine 2,3-dioxygenase (IDO) are heme containing enzymes, which transfer two atoms of oxygen to the substrate for product formation (*21, 23*).

1.6 TDO and IDO Oxidation Reaction

Investigation of TDO and IDO is the topic of this thesis. TDO and IDO are heme-containing enzymes that catalyse the highly specific irreversible oxydative pyrole ring cleavage of L-tryptophan. The substrate L-tryptophan is an essential aromatic amino acid. The catabolism of L-tryptophan is the first rate limiting step in the kynurenine pathway forming the product *N*-formylkynurenine by incorporating dioxygen into the cleaved C_2-C_3 bond of L-tryptophan by the dioxygenases (Scheme 1.1). TDO and IDO are heme-containing dioxygenases that have been identified to catalyse the oxidation reaction of L-tryptophan and both dioxygenases use dioxygen for catalysis (*24*). In 1975, Hirata was able to demonstrate with the use of a heavy oxygen isotope ($^{18}O_2$) that molecular oxygen was directly incorporated into formyl-kynurenine (*25*).

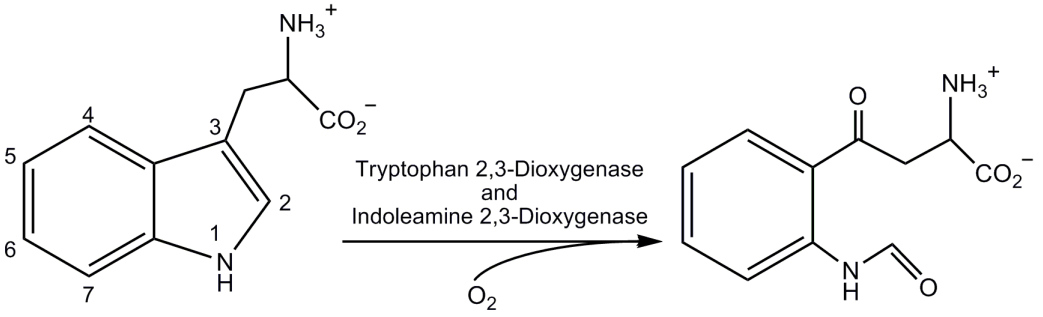

L-Tryptophan N-Formylkynurenine

Scheme 1.1 Oxidation of the substrate L-tryptophan to form the product *N*-formyl-kynurenine catalysed by TDO and IDO, IUPAC numbering indicated.

1.7 Discovery of TDO and IDO

TDO was initially discovered in rat liver in 1936, initially called tryptophan pyrrolase and later renamed to tryptophan 2,3-dioxygenase (Figure 1.3) (*26*). Then, TDO was first characterised in rat liver in 1955 and was later characterised in other organisms, which is discussed later. In 1951 TDO was shown to be a hemoprotein containing a prosthetic heme group protoporphyrin IX (*27*). IDO was later discovered in rabbit small intestine by Hayaishi and colleagues in 1963 shown to be similar to TDO by also catalysing the conversion of L-tryptophan to kynurenine (*28, 29*).

Studien über den intermediären Stoffwechsel des Tryptophans
XVIII—XXIV.

Von

Y. Kotake.

(Aus dem Biochem. Institut d. Medizin. Fakultät d. Kaiserl. Universität zu Ōsaka.)

(Der Schriftleitung zugegangen am 9. August 1936.)

XVIII. Über den Mechanismus der Kynurenin-bildung aus Tryptophan.

(I. Mitteilung.)

Von

Y. Kotake und T. Masayama.

(Unter Mitwirkung von Ch. Itagaki.)

Figure 1.3 The first page of the paper released in 1936 reporting the discovery of TDO (*24*).

1.8 Expression Systems for the Dioxygenases

TDO and IDO were obtained from the source species, which included mammals such as rats (*22, 30-32*), mice, oxen, goats, pigs, dogs and rabbits (*32*), rhesus monkeys (*Macaca mulatta*) and common marmosets (*Callithrix jacchus*) (*33*); insects such as *D. melanogaster* (*34*), bacteria *S. parvulus* (*35*) and *B. brevis* (*36*), yeast *S. cerevisae* (*37*) and humans (*32, 38*),

Table 1.1 Expression systems for a number of species of dioxygenase enzymes.

Enzyme	Species	Expression System	Reference
TDO	*H. sapiens*	*E. coli* pET28a hexa-histidyl tag	(*39*)
TDO	*H. sapiens*	*E.coli* pET14b hexa-histidyl tag	(*40*)
TDO	*H. sapiens*	*E.coli* pET15b hexa-histidyl tag	(*41*)
Bacterial TDO	*X. campestris*	*E.coli* pET21d hexa-histidyl tag	(*42*)
Bacterial TDO	*R. metallidurans*	*E.coli* pET28a hexa-histidyl tag	(*43*)
Mosquito TDO	*Ae. aegypti*	Baculovirus pBlueBac4.5 hexa-histidyl tag	(*44*)
Mosquito TDO	*A. gambiae*	*E.coli* pET16b hexa-histidyl tag	(*45*)
Zhikong Scallop TDO	*C. farreri*	*E.coli* pGEX 4T-3 GST-tag	(*46*)
Rat TDO	*R. Rattus*	*E. coli* pUC18 hexa-histidyl tag	(*47*)
Rat TDO	*R. norvegicus*	*E.coli* pTrc99A	(*48*)
Rat TDO	*R. Rattus*	*E. coli* pTrc99A	(*49*)
IDO	*H. sapiens*	*E. coli* pREP4 hexa-histidyl tag	(*50*)
IDO	*H. sapiens*	*E. coli* pQE9 hexa-histidyl tag	(*51*)
IDO	*H. sapiens*	*E.coli* pQE30	(*52*)
IDO	*H. sapiens*	*E.coli* pET-15b hexa-histidyl tag	(*53*)
IDO	*H. sapiens*	Yeast pARC25B	(*54*)
IDO	*H. sapiens*	*E.coli* pDEST17 hexa-histidyl tag	(*55*)
Bacterial IDO	*S. oneidensis*	*E.coli* pET21d hexa-histidyl tag	(*42*)
Mouse IDO	*M. musculus*	*E.coli* pDEST17 hexa-histidyl tag	(*55*)

Recently, expression systems emerged for studying the dioxygenases (Table 1.1). The first expression system was for human IDO in 1992 in *E. coli* with the vector pREP4 and the protein was purified using metal-ion affinity chromatography as a hexa-histidyl tag was added to the vector (*50*) (Table 1.1). Other expression systems rapidly followed, however the TDO expression systems only started to appear in

the last few years, even though TDO was discovered over 70 years ago (in comparison to IDO which was discovered only half a century ago). In consequence there is very little information in the literature regarding TDO in comparison to IDO.

1.9 Tryptophan Metabolism

Tryptophan is an essential amino acid, therefore it cannot be synthesised in humans and is obtained through diet. In most species, the kynurenine pathway represents the major route for L-tryptophan oxidative demolition (Scheme 1.2, right arm and 1.3) (*56, 57*). While the protein related pool of L-tryptophan is kept in constant balance between the processes of protein catabolism and protein synthesis, about 99 % of dietary intake of L-tryptophan is catabolised (Scheme 1.2) (*58*).

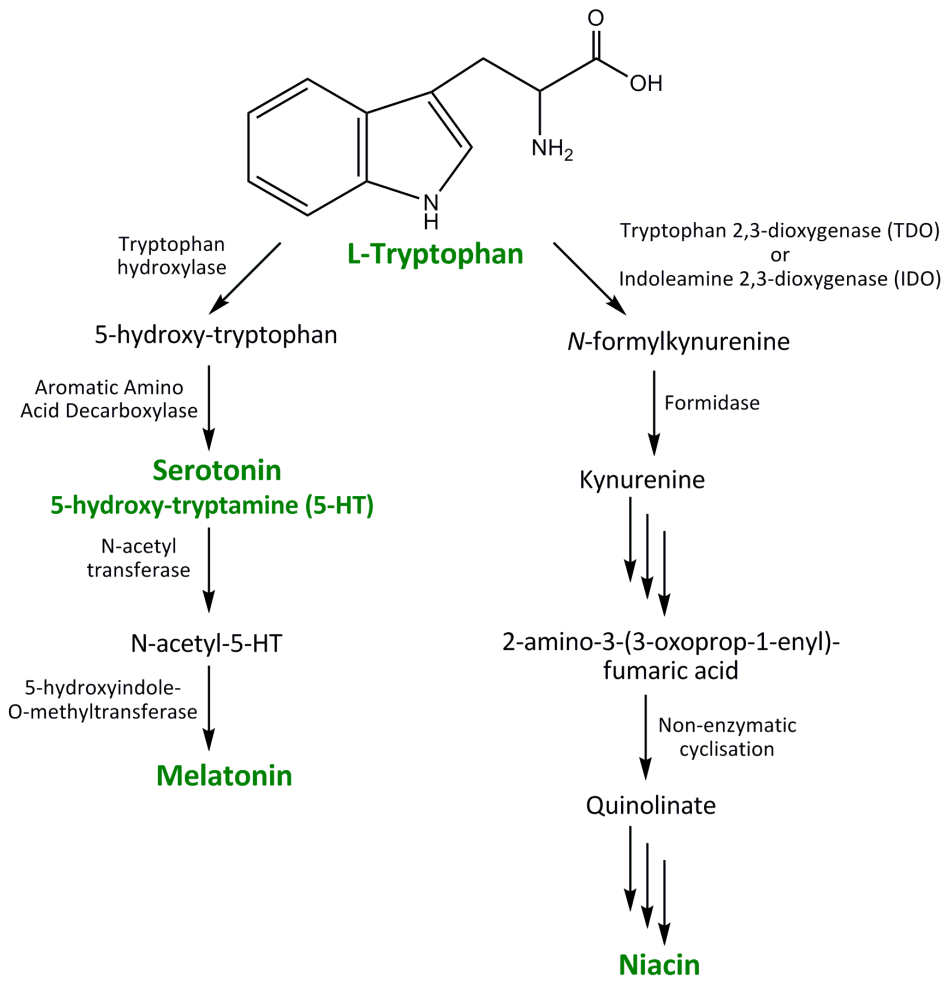

Scheme 1.2 Two metabolic routes of tryptophan metabolism, producing the important products serotonin, melatonin and niacin. Right arm is called the kynurenine pathway.

The metabolism of L-tryptophan, exceeding the protein synthesis requirements, proceeds through an enzymatic cascade, yielding a number of physiologically and pharmacologically relevant active compounds such as serotonin, melatonin and niacin, and other metabolites that play multiple roles in controlling basic aspects of the biology of most living organisms and can culminate in the *de novo* NAD biosynthesis (Scheme 1.3) (*59-61*).

Serotonin (5-hydroxy-tryptamine, 5-HT) is an aminergic neurotransmitter, which is primarily located in the gut for regulation of intestinal movements. A minority of serotonin is in the central nervous system controlling numerous functions including regulation of mood, sleep and some cognitive functions including memory and learning (Scheme 1.2) (*62*).

Serotonin has been found to also play an important role in personality traits such as depression, anxiety and bipolar disorder (*63*). Atypical levels of serotonin in criminals are considered to be the cause of anti-social behaviour [1]. The literature suggests that low levels of serotonin are involved with brain development and therefore disruption of serotonin production could lead to aggressiveness and impulsivity in adults and children (*64-66*).

Melatonin is a neurohormone found in animals and other living organisms including algae (Scheme 1.2) (*67*). Melatonin is involved in the regulation of the circadian rhythms of several biological functions, it is also a strong antioxidant and has an important role in protecting nuclear and mitochondrial DNA (*68-70*).

Niacin, also known as vitamin B_3, is a precursor to NAD in the kynurenine pathway, which plays an essential role in living cells. Niacin is involved in both DNA repair and the production of steroid hormones (Scheme 1.2) (*71*). Deficiency of niacin in the body causes a deficiency disease called pellagra (*72*).

[1] Personal communication between a criminologist and myself at the University of Leicester postgraduate research festival 2008.

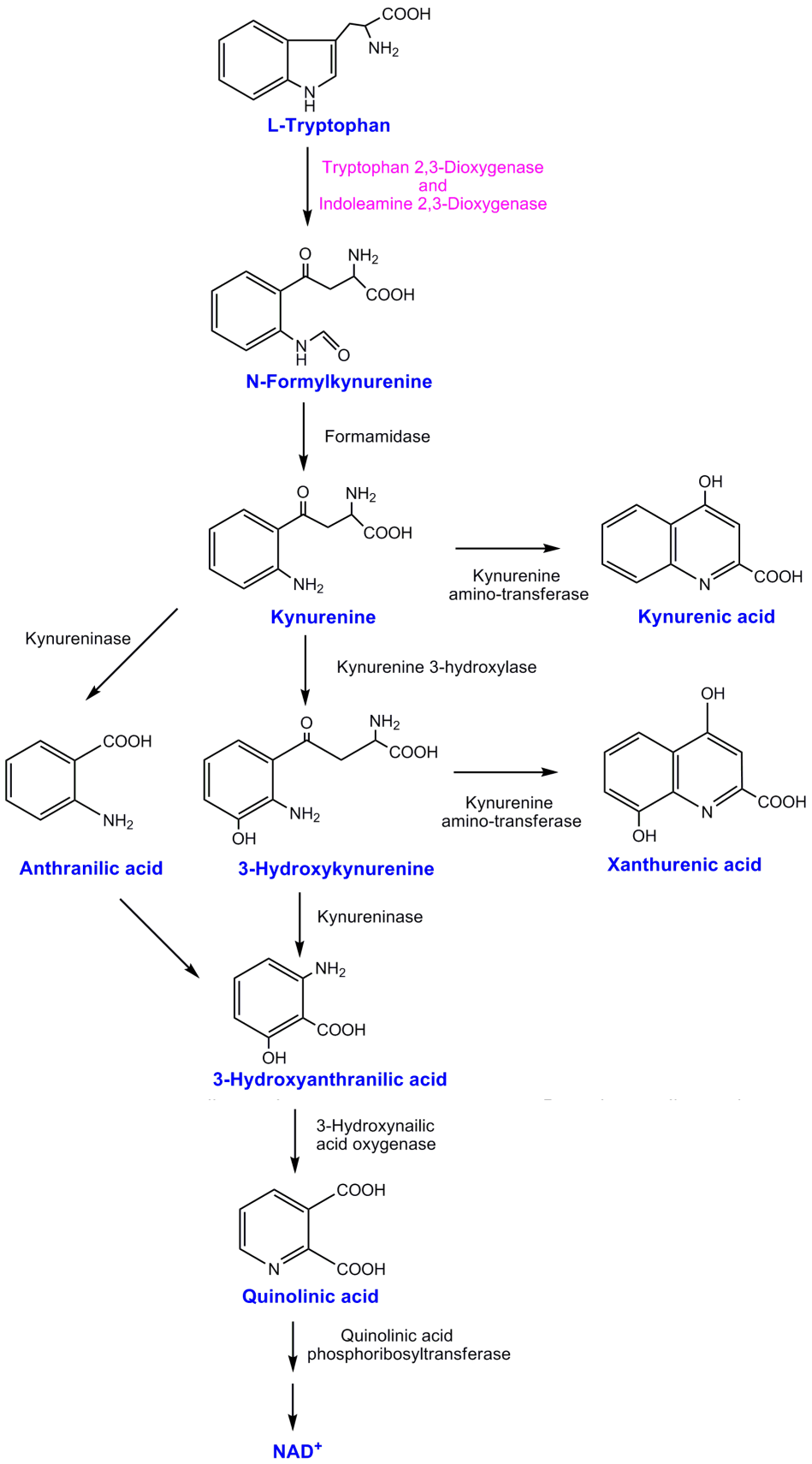

Scheme 1.3 The kynurenine pathway of tryptophan degradation in mammalian cells. The route involves the initial metabolism of tryptophan by TDO and IDO.

It is clear that the production of serotonin, melatonin and niacin is dependent on the level of tryptophan in the diet and that the enzymes, which catabolise tryptophan to these important products, are functioning properly. Furthermore, in most cases diseases and problems occur due to lack or low quantities of the compounds. The main focus of this thesis is on the enzymes TDO and IDO which are only involved in one arm of tryptophan metabolism (Scheme 1.2, right side and Scheme 1.3). The build up of pathway metabolites due to TDO and IDO induction or poor metabolism further along the pathway can lead to numerous conditions including pellagra, caused by lack of niacin production (*72, 73*).

The kynurenine pathway arm, which involves the enzymes TDO and IDO is important not only as a source of metabolites including niacin mentioned above, but also because of the effect of TDO and IDO production on the local tryptophan concentration. This arm of the kynurenine pathway is composed of two branches where the central metabolite L-kynurenine, discovered by Kotake was later demonstrated to be formed as the primary product from the TDO and IDO reaction with tryptophan followed by a second enzyme, formamidase, which hydrolysed the formyl group of formylkynurenine to yield kynurenine and formic acid (*27, 74, 75*). Kynurenine is then transformed, into the neurotoxic metabolite quinolinic acid (quinolate) or into the neuroprotective metabolite kynurenic acid (Scheme 1.2, right side and 1.3) (*74-76*).

High levels of quinolinic acid and kynurenine in cerebrospinal fluid (CSF) may be involved in various neurological disorders (e.g. cerebral malaria, ischemic brain injury, multiple sclerosis and AIDS related dementia (*77-80*)). Concentrations of these metabolites increase with the severity of neurological dysfunction or brain injury under a wide range of inflammatory conditions. For example, the kynurenine pathway metabolites 3-hydroxyanthranillic acid and 3-hydroxykynurenine are UV filters which can bind to the lens protein in the eye and have been implicated in cataract formation when present at high concentrations (*80*). In addition, some kynurenine pathway metabolites are immunomodulatory and can consequently contribute to immunosuppressive pathways and suppress proliferation (or even

cause apoptosis) of T cells (*81-83*). However, the mechanisms of action of such metabolites are unknown.

The local depletion of tryptophan by enzymatic action is mainly associated with an antimicrobial response by TDO or IDO, or immune regulation by IDO (*84*). Some pathogens are sensitive to tryptophan degradation, including viruses (herpes viruses), intra-cellular bacteria (Chlamydia and Rickettsia) and extra-cellular bacteria (Staphylococci) and this may be an effective mechanism for controlling their ability to proliferate.

1.10 Involvement of TDO and IDO in Pathophysiological and Physiological Processes

Early studies indicated that IDO had immunological effects in mammals as it was recognised for some time that elevated levels of various tryptophan metabolites were found in the urine of patients suffering from a variety of diseases, such as rheumatoid arthritis, tuberculosis, leukaemia, Hodgkins disease, bladder cancer, and prostrate disorders (*28, 32, 85*). However, TDO concentrations were not elevated in the liver in these patients and later the evidence followed that it was caused by IDO (*86, 87*). TDO simply appeared to only handle dietary catabolism of tryptophan, however both enzymes have been found to have immunological activity.

IDO has a wider range of biological functions than TDO in physiological and pathological conditions. IDO has an important role in disease, auto immunity and immune response such as T cell suppression, production of quinolinic acid as a neurotoxin, maternal tolerance to allogenic foetus and immune escape of cancers and is a target for drug discovery against cancer (*73, 88*).

IDO has been associated with antiviral and antiproliferative activities of the cytokine interferon (IFN). IFN is produced by immune defence cells namely T lymphocytes and natural killer cells, which induces protection of the body against nonviral pathogens, inhibition of cell growth, regulation of immune responses and induction of gene product synthesis (*89*). Numerous induced gene product are

involved in resistance to microbial infection such as *Chlamydia psittaci* (*90*). IFN also acts as an inducer of IDO expression as well as interferon, interleukin-1 and tumour necrosis factor.

The gene *BIN1* was recently discovered to control IDO expression in skin epithelial cells and also that cells lacking *BIN1* suffer from increased IDO expression, which form significantly large tumours (*91*). There are several cancers which have attenuated expression of *BIN1* including breast, prostate, lung and colon, so the link between the gene and IDO expression are being currently investigated (*92-95*).

In 2009 some knock-out mice studies, whereby the mice were deficient for TDO, demonstrated a link between systemic and brain tryptophan metabolism, neurogenesis and anxiety-related behaviour (*96*). Furthermore variations in the TDO gene have been associated with psychiatric diseases such as Tourette syndrome, depression and autism (*97, 98*).

TDO activity has also been related to the immune response and involved in tryptophan level regulation of early mouse concepti, rat hair growth, human schizophrenia and pigment synthesis of eye colour in insects and mosquitoes (*44, 99-103*).

1.11 Properties of TDO and IDO

TDO has four subunits forming a tetramer, ~190 kDa in eukaryotes and ~120 kDa in prokaryotes. Human TDO has been primarily localised to the liver and also expressed in the skin and brain (Table 1.2) (*73, 99*). One of the TDO subunits is approximately the same size as the monomeric mammalian IDO enzyme, at ~45 kDa which, is ubiquitously expressed throughout the body, apart from in the liver (Table 1.2). Both dioxygenases contain protoheme IX prosthetic group and the mammalian forms of the enzymes are ~400 amino acids in length.

Table 1.2 Comparison of Indoleamine 2,3-dioxygenase and tryptophan 2,3-dioxygenase

	TDO	**IDO**
Molecular Weight (kDa)	Mammalian ~190 Bacterial ~120	~45
Subunits	4	1
Prosthetic group	Protoheme IX (*27*)	Protoheme IX
Distribution	Liver	Ubiquitous (except liver)
Substrates	L-tryptophan, 5- and 6-fluoro-tryptophan	LD- tryptophan, 1-methyl-L-tryptophan, 5-hydroxyl-LD-tryptophan, tryptamine, serotonin
Crystal Structures PDBs	Ferric rhTDO (2NW7) (*42*) Ferrous rhTDO in complex with L-tryptophan (2NW8) (*42*) Ferrous rhTDO in complex with 6-fluoro-tryptophan (2NW9) (*42*) rhTDO variant H55A (3BK9) (*42*) rhTDO variant H55S (3E08)(*42*) Ferric rhTDO (2NOX) (*43*)	rhIDO in complex with 4-phenylimidazole (2D0T) (*53*) rhIDO in complex with cyanide (2D0U) (*53*)
Active form	Ferric and ferrous	Ferrous

1.12 Sequence Alignment of the Dioxygenases

The sequence similarities between TDO and IDO are extremely low, with approximately 10 % identity (Figure 1.4) (*42*). However, bacterial *X. campestris* TDO shares 34 % sequence identity with human TDO suggesting a closer conservation of residues between TDOs (Figure 1.4) (*42*). In contrast, prokaryotic IDOs (*S. oneidensis* IDO) have less sequence identity to the eukaryotic enzyme with ~14 % sequence identity. However, there is high sequence identity between eukaryotic IDOs at ≈61 % for human and mouse IDO (*43, 104, 105*).

```
Human TDO   1 ---MSGCPFLGNNFGYTFKK---LPVEGSEEDKSQ---TGVNRASKGGLIYGNYLHLEKVLNAQELQ 58
Xc TDO      1 ------MP-----VDKNLRD---LE-------------PGIHTDLEGRLTYGGYLRLDQLLSAQQPL 40
Human IDO   1 -------------MAHAMENSWTISKEYHIDEEVGFALPNPQENLPDF--YNDWMFIAKHLPDLIES 52

Human TDO  59 SETKGNKIHDEHLFI--ITHQAYELWFKQILWELDSVRE-IFQNGHVRDE--RNMLKVVSRMHRVSV 120
Xc TDO     41 SE---PAHHDEMLFI--IQHQTSELWLKLLAHELRAAIV-HLQRDEVWQC--RKVLA------RSKQ 93
Human IDO  53 GQLRERVEKLNMLSIDHLTDHKSQRLARLVLGCITMAYVWGKGHGDVRKVLPRNIAVPYCQLSKKLE 119

Human TDO 121 ILKLLV------QQFSILETMTALDFNDFREYLSPASGFQSLQFRLLENKIGVLQNMRVPYNRRHYR 181
Xc TDO     94 VLRQLT------EQWSVLETLTPSEYMGFRDVLGPSSGFQSLQYRYIEFLLG--------------- 139
Human IDO 120 LPPILVYADCVLANWKKKDPNKPLTYENMDVLFSFRDGDCSKGFFLVSLLVEIAAASAIKVIPTVFK 186

Human TDO 182 DNFKGEENELLLKSEQEKTLLELVEAWLERTPG-LEPHGFNFWGKLEKNITRGLEEEFIRIQAKEES 248
Xc TDO    140 ----NKNPQMLQVFAYDPAGQARLREVLE-APS-LYEEFLRYLARFGHAI---------------PQ 185
Human IDO 187 AMQMQERDTLLKALLEIASCLEKALQVFHQIHDHVNPKAF-------FSVLRIYLSGWKGNPQLSDG 246

Human TDO 249 EEKEEQVAEFQKQ------KEVLLSLFDEKRHEHLLSKGERRLSYRALQGALMIYFYREEPRFQVPF 309
Xc TDO    186 QYQARDWTAAHVA------DDTLRPVFER--------------------------IYENTDRYWREY 220
Human IDO 247 LVYEGFWEDPKEFAGGSAGQSSVFQCFDV------------LLGIQQTAGGGHAAQFLQDMRRYMPP 301

Human TDO 309 QLLTSLMDIDSLMTKWRYNHVCMVHRMLGSKAGTGGSSGY-HYLRSTVSDRYKVFVDLFNLSTYLIP 374
Xc TDO    221 SLCEDLVDVETQFQLWRFRHMRTVMRVIGFKRGTGGSSGV-GFLQQALALTF--FPELFDVRTSVGV 284
Human IDO 302 AHRNFLCSLESN---------PSVREFVLSKGDAGLREAYDACVKALVSLRS--YHLQIVTKYILIP 356

Human TDO 375 RHWIPK----------------MNPTIHKFLYTAEYCDSSYFSSDESD 406
Xc TDO    285 DNRPPQ----------------GSADAGKR------------------ 298
Human IDO 357 ASQQPKENKTSEDPSKLEAKGTGGTDLMNFLKTVRSTTEKSLLKEG-- 403
```

Figure 1.4 Sequence alignment of human and *Xanthamonas campetris* (Xc) TDO shown with the hIDO sequence. Highlighted in blue are active site residues shared between the dioxygenase family, residues F72, H76, F140, R144 and H240 for hTDO. Highlighted in red are the corresponding hIDO residues, F163, S167, F226, R231 and H364. The BLAST database was used for the sequence alignment.

1.13 TDO and IDO Crystal structures

In the past four years, three groups independently obtained X-ray crystal structures of TDO and IDO and advanced our understanding of the structure of the dioxygenase enzymes (Figure 1.5, 1.6 and Table 1.2) (*42, 53*). The crystal structure for TDO was determined in 2007 from *X. campestris* (PDB code 1YW0) (Figure 1.5, Table 1.2). Several crystal structures for TDO have been solved including the ferric and ferrous form with various substrates bound (L-tryptophan and 6-fluoro-tryptophan) and two histidine variants of TDO were solved (Figure 1.5A and B, Table 1.2) (*42, 43, 106*). The ferric TDO crystal structures of *R. metallidurans* and *X. campestris* share 47 % sequence identity and the regions of essentially identical residues are located near the active site.

The TDO structure is an α-helical homotetramer (α4) (Figure. 1.5A), where each monomer contains 13 α-helices (Figure 1.5B). Helices αB and αC create a hydrophobic interface connecting two of the monomers by salt-bridges, hydrophobic and hydrogen-bond interactions, the N-terminal of each monomer forms part of the substrate binding site in the adjacent monomer (Figure 1.5B). Each dimer contains two heme prosthetic groups and two distal cavities for substrate binding, thus the overall structure contains four active sites (*42*).

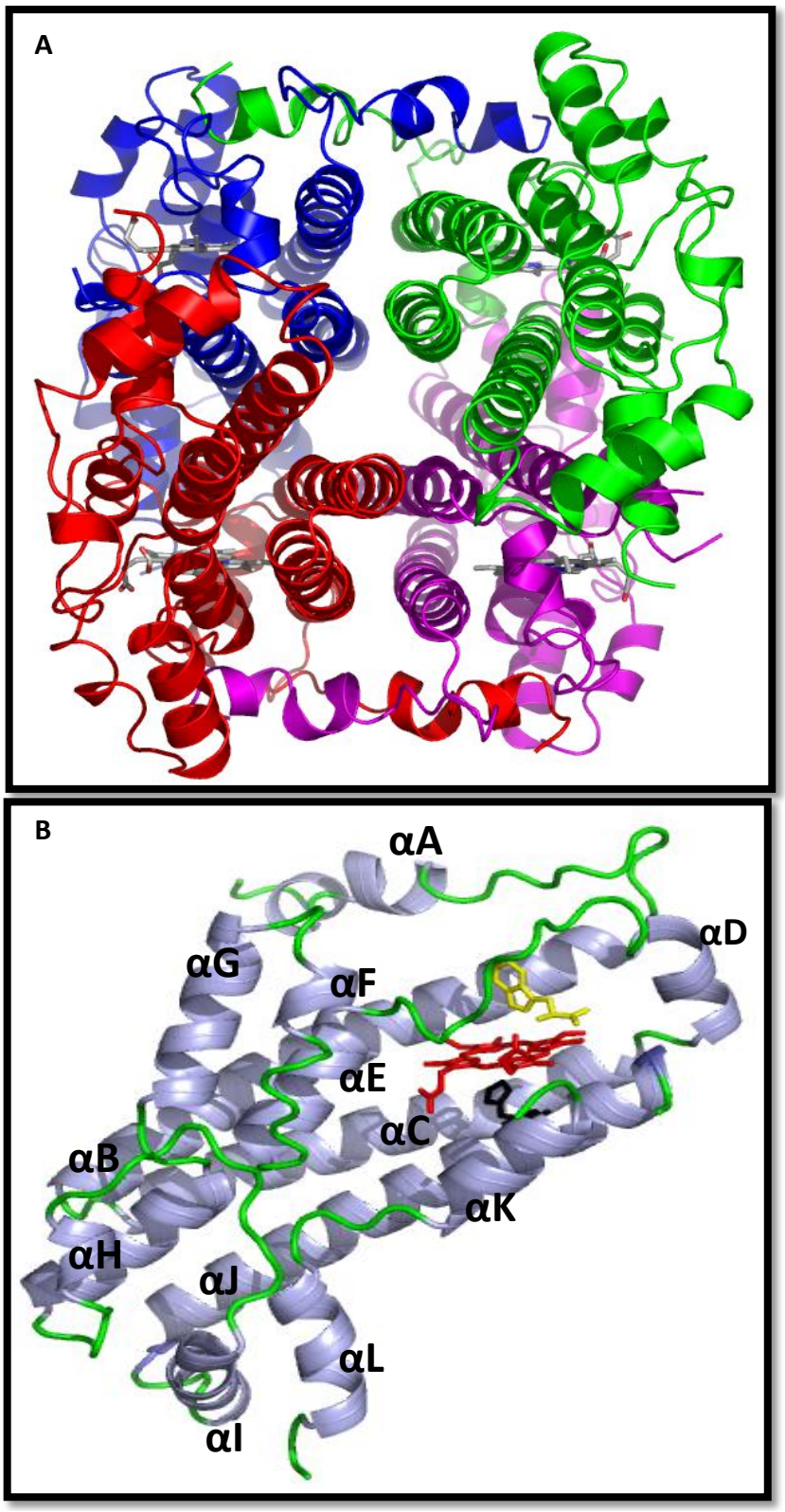

Figure 1.5 Crystal structures of *X. campestris* TDO. (**A)** The crystal structure of the tetramer *X. campestris* TDO. (**B)** The crystal structure of the *X. campestris* TDO monomer, the heme prosthetic group (red), substrate tryptophan (yellow) and the proximal histidine residue 240 (black).

In comparison to the numerous crystal structures for TDO, there are only two structures for IDO; ferric IDO in complex with either the inhibitor 4-phenylimidazdole or cyanide (Figure 1.6, Table 1.2) (*53, 107*). Interestingly the crystals took three months to grow and crystallised as a dimer, with a disulphide bridge between the cysteine 308 residues on each monomer (Figure 1.6). To date all literature suggests that IDO is only functional as a monomer and that the crystallisation of IDO as a dimer is most likely an artifact from the process (Table 1.2).

IDO is a monomer with a large domain (pink), which contains the catalytic pocket and a small domain (yellow) and in contrast to TDO, IDO contains both α-helices and β-strands (Figure 1.6). The large domain is composed solely of 15 α-helicies, whereby one helix provides the endogenous proximal ligand, histidine 346 (Figure 1.6B, H346 (black)). The small domain is composed of nine α-helices and two β-sheets and the domains are joined together by a loop of 17 residues (Figure 1.6 residues 250-267 (green)), which also contributes to part of the catalytic pocket cavity on the distal side (Figure 1.6).

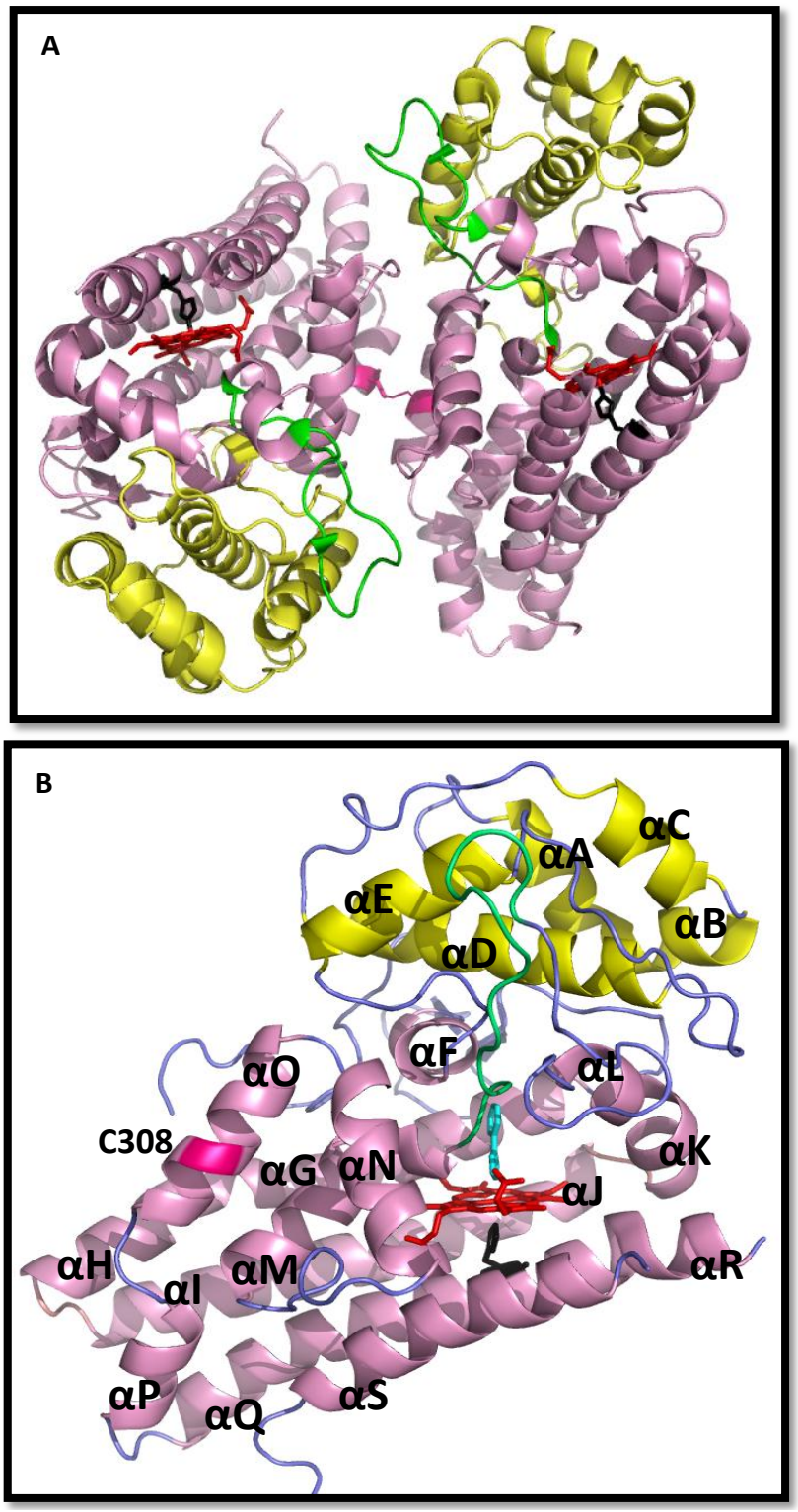

Figure 1.6 Crystal structure of hIDO showing the small domain (yellow) and the large domain (pink), connected by a loop (green). (**A)** The crystal structure of the dimer hIDO, joined by a disulphide bridge formed by the cysteine 308 residues of each monomer (magenta). (**B)** The crystal structure of the monomer hIDO showing the proximal histidine residue 346 (black), coordinating with the heme (red) and the ligand 4-phenylimidazole (cyan) bound at the distal site.

1.14 TDO and IDO Active Site

As mentioned earlier, despite the low sequence identity between the two dioxygenases, the active site is relatively conserved (Figure 1.7, Table 1.2) (*42, 53*). The overlaid crystal structures of the TDO and IDO active site show residues required for binding tryptophan, for TDO the residues are R117, Y113, F51, H55, H240 and for IDO the residues are R231, F226, F163, S167, H364 (Figure 1.4, TDO residues (blue) and IDO residues (red) and Figure 1.7). The crystal structures of the dioxygenases also revealed that the active sites have an abundance of hydrophobic residues, which include some of the residues involved in substrate binding (Figure 1.7).

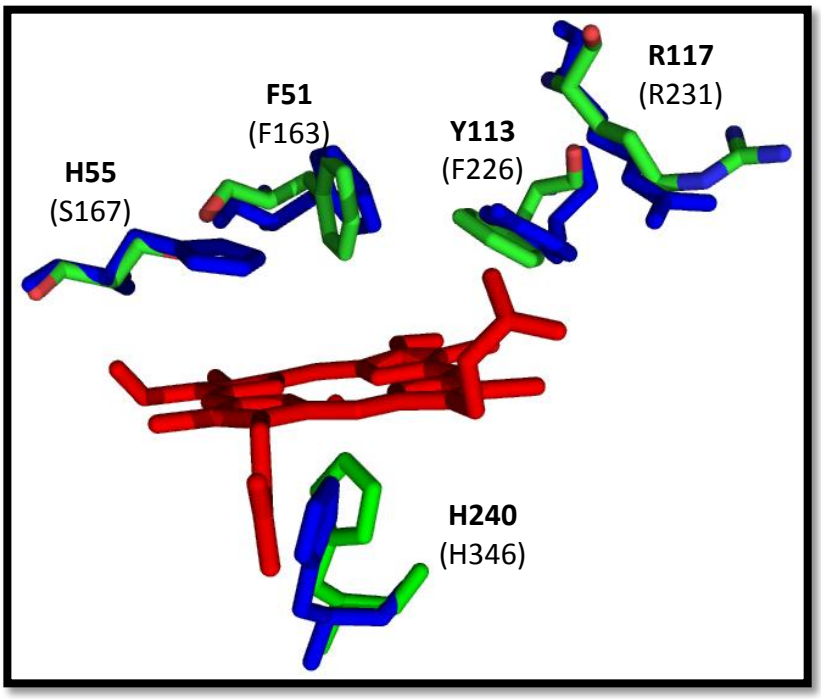

Figure 1.7 An overlay of the heme binding site of ferric *X. campestris* TDO (in blue) and ferric rhIDO (in green) (*42, 53*). The structures have been overlaid at the heme.

Some of the active site residues are highly conserved including the arginine, proximal histidine, and a phenylalanine (F51 for *X. campestris* TDO, F163 for IDO) (Figure 1.7). Another conserved type of amino acid is the aromatic hydrophobic amino acid residue 113 for *X. campestris* TDO and 226 for hIDO, however

approximately 50 % of the dioxygenases have tyrosine and the others have phenylalanine. The most important difference between the dioxygenase active sites is the presence of histidine in TDOs and serine in IDOs located on the distal site, close to the heme close (Figure 1.7). The histidine in TDOs is hydrogen bonded to the indole nitrogen of the substrate and could play a role in the reaction mechanism; the serine has been shown not to be involved in the reaction mechanism and further information regarding this residue can only be determined by an IDO structure with substrate bound (*106, 108*).

The structures have provided key information regarding the substrate protein interactions within the active site (Table 1.2). It was found that the dioxygenases change conformation in the presence of substrate, namely the arginine active site residue can interchange in the absence of substrate to forming electrostatic interactions with the carboxylate group of tryptophan. The arginine movement can be observed by comparing the ferric TDO structure in the absence of substrate (Figure 1.8A) and the ferrous TDO structure in the presence of substrate (Figure 1.8B).

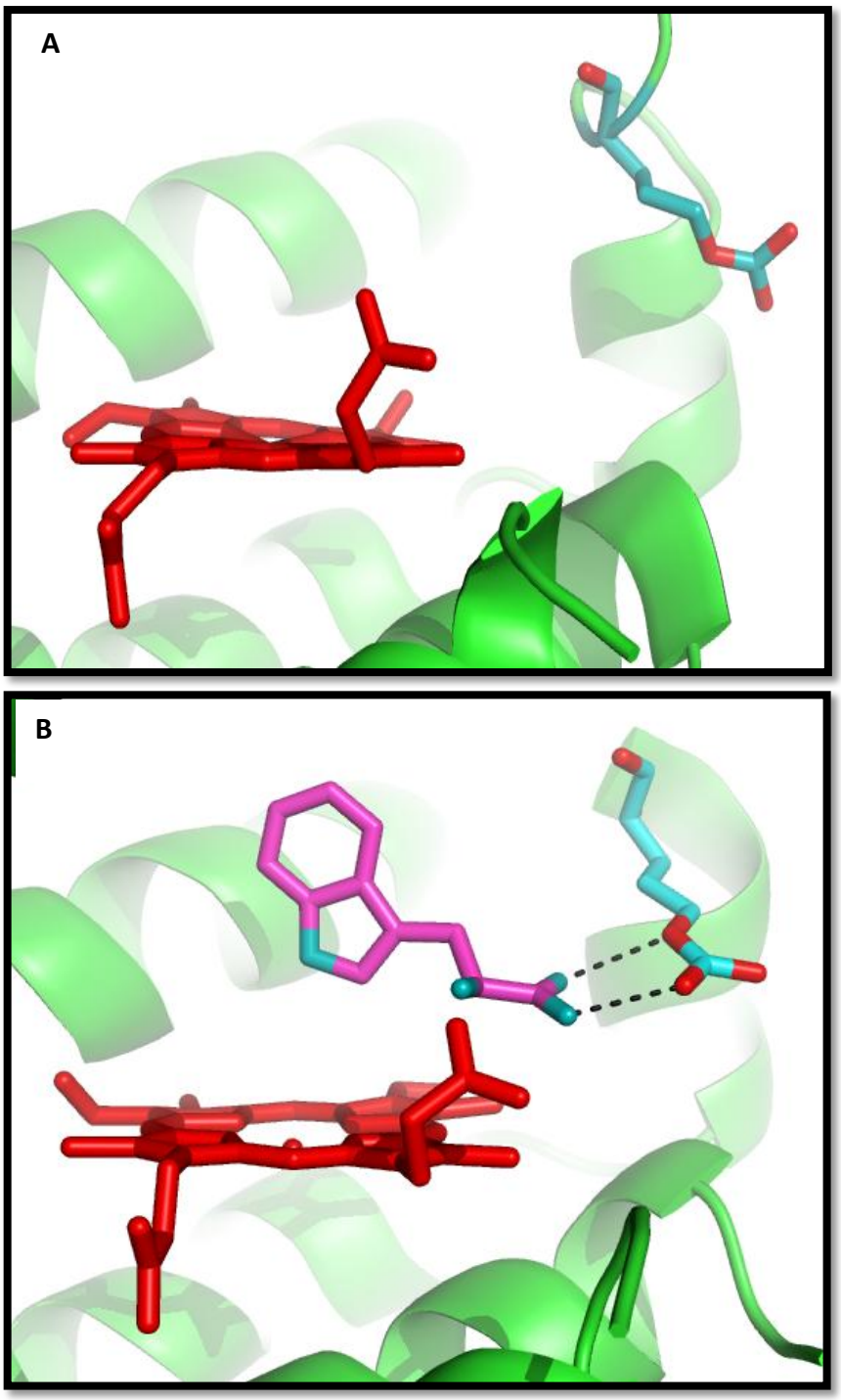

Figure 1.8 The crystal structures of ferric and ferrous *X. campestris* TDO with the active site residue R117 (blue) (A) ferric form in absence of substrate and (B) ferrous form interacting with L-tryptophan (pink) bound to the heme (red) (*42*).

1.15 Heme-Iron Coordination structures

Spectroscopic techniques, including electronic absorption, magnetic circular dichroism (MCD) and electro-paramagnetic resonance (EPR) spectroscopy, have been used to determine the distal environment in the ferric form of the dioxygenases in the absence and presence of substrate (*20*). The techniques revealed the presence of two species in ferric TDO and IDO, a high- and low- spin species and confirmed that the endogenous axial ligand coordinated to the heme prosthetic group was a histidine residue for both TDO and IDO (*39, 52, 109-114*). The high-spin species for IDO was suspected to arise from hisitidine/water ligation and the low-spin species was assigned as bis-nitrogenous ligation (Scheme 1.4) (*112, 113*). The high-spin species for TDO was likely to be coordinated by a water molecule, the same as for ferric myoglobin and the low-spin species was postulated to be hydroxide (*39, 100, 111, 114, 115*).

As discussed earlier both TDO and IDO crystal structures have been solved, which shed some light on the heme iron coordination environment. It is clear from the IDO structure that there is no distal histidine or any potential nitrogenous residues, which could ligate with the iron, therefore histidine ligation for IDO was ruled out and the sixth coordination ligand in IDO still remains unknown (Figure 1.7).

In the presence of substrate, three forms of ferric TDO and IDO were observed: a high- and a low-spin species and the formation of a new low-spin species. The new low-spin species was proposed to be hydroxide and also that the substrate L-tryptophan provides a hydrogen-bond acceptor to stabilise deprotonation of the bound water molecule (*52*). For TDO, this indicated that the ferric form of the enzyme causes increased deprotonation of the heme-bound water molecule and could be caused by the substrate deprotonating the bound water molecule, instead of the distal histidine. For IDO the hydroxide-bound species formation of the ferric form is unlikely as it lacks a hydrogen bond acceptor to facilitate deprotonation of the bound water molecule. However the spectra of the ferric substrate bound enzyme are pH dependent due to an ionisable interaction, which affects hydroxide formation in the active site, especially at an alkaline pH (pH > 7.5) (*114*). Therefore

tryptophan is suspected to act as a proton acceptor, thus deprotonating the water bound molecule and hence forming the hydroxide bound species as speculated for TDO.

1.16 Catalytic activity

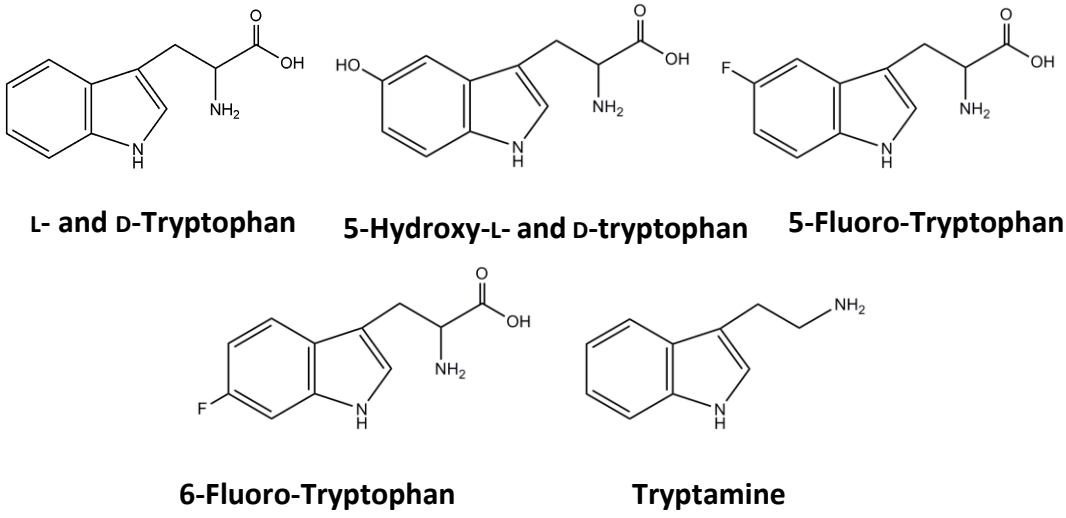

Figure 1.9 Structures of dioxygenase substrates, tryptophan and tryptophan analogues.

TDO utilises a highly specific range of substrates including L-tryptophan, 5- and 6-fluoro-tryptophan, in contrast to IDO that utilises a broader range of substrates including L- and D-tryptophan, 5-hydroxy L- and D-tryptophan, tryptamine and serotonin (Figure 1.9 and Table 1.2) (*29, 116, 117*). Rabbit IDO has an even broader range of substrates in comparison to human IDO, which includes 4-, 5- and 6-fluoro-tryptophan as well as the mammalian IDO substrates (*16*).

1.17 TDO and IDO Inhibition

In consequence of the several neurological and psychiatric pathologies caused by TDO and IDO, both enzymes have emerged as attractive drug targets (*76, 118*). The first natural inhibitors for TDO and IDO were discovered in 1984. These are β-carboline derivatives, which are found in plants and animals (*119*). One of the β-carboline derivatives called norharmen is a large ligand, which directly binds to the

heme iron of the dioxygenases as a nitrogen donor ligand and therefore is a potent inhibitor as it competes with oxygen (Figure 1.10A) (*107, 120*).

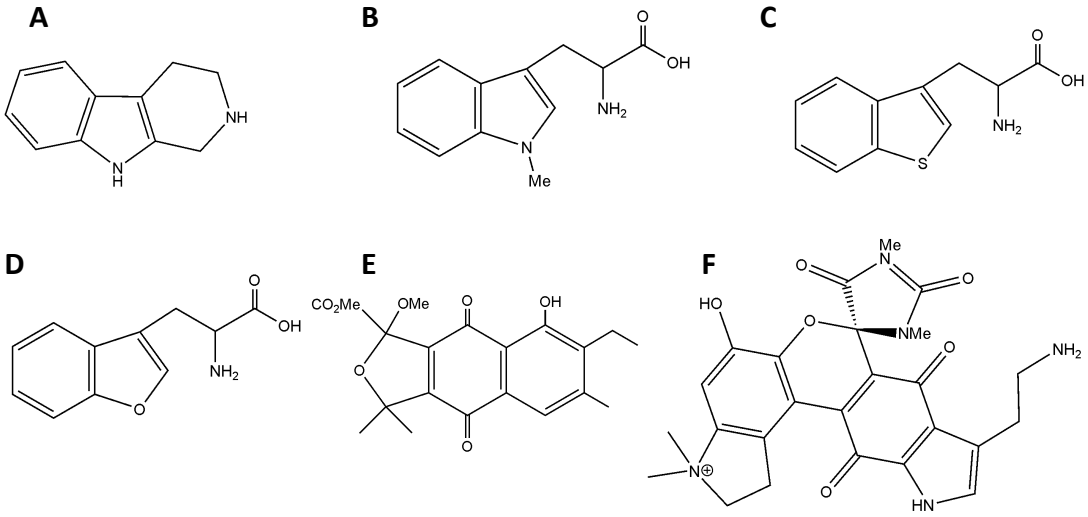

Figure 1.10 Structures of dioxygenase inhibitors. (A) norharman (β-carboline) (*120*), (B) 1-methyl-DL-tryptophan, (C) β-[3-benzo(b)thienyl]-DL-alanine, (D) β-[3-benzofuranyl]-DL-alanine, (E) annulin C and (F) exiguamine A.

Due to the discovery that IDO was immunologically active, resulting in numerous diseases, most investigations focused on IDO inhibitors. In the early nineties several tryptophan analogues, 1-methyl-DL-tryptophan, β-[3-benzo(b)thienyl]-DL-alanine and β-[3-benzofuranyl]-DL-alanine were discovered as competitive inhibitors for rabbit IDO (Figure 1.10 B-D) (*121*). All three analogues bound to the same site as the substrate L-tryptophan and the most potent was found to be 1-methyl-DL-tryptophan K_i ≈ 30 - 60 µM (*55, 121-123*). These results suggested that the free form of the indole nitrogen is important for binding and that replacement with more electron-inductive atoms such as sulfur and oxygen removes the ability of L-tryptophan to act as a substrate (Figure 1.10 B - D).

A wide range of the available IDO inhibitors are tryptophan analogues, which are not good drug candidates as they are only active at micromolar concentrations, therefore other natural inhibitors and synthetic alternatives were investigated. Annulin C (Ki 140 nM) and exiguamine A (210 nM), extracted from marine

organisms *Garveia annulata* and *Neopetrosia exigua* respectively, were found to be potent inhibitors of IDO with nanomolar concentrations required (Figure 1.10 E and F) (*124, 125*). Currently several groups worldwide are screening hundreds of inhibitors, synthetic and natural, to find more effective inhibitors and alternatives as further studies on human cells will be required to determine if they have potential as drug leads or cell biology tools.

1.18 Ternary Complex of TDO/IDO with O_2 and L-Tryptophan

The ternary complex was first identified in 1970, from IDO experiments (*30*). The resulting information with IDO showed that the active form of the enzyme was likely to be ferrous and that ferric enzyme was inactive (Scheme 1.4, Table 1.2) (*30*). It was suggested that the ferric form required either reducing compounds to become the active form or that cytochrome b_5 could act as an electron transfer protein and donate electrons to the ferric form of IDO *in vivo*. It is unknown whether TDO could be reduced by cytochrome b_5 (*116, 126*). Another suggestion was activation of the ferric form of the enzyme IDO by superoxide (*127*).

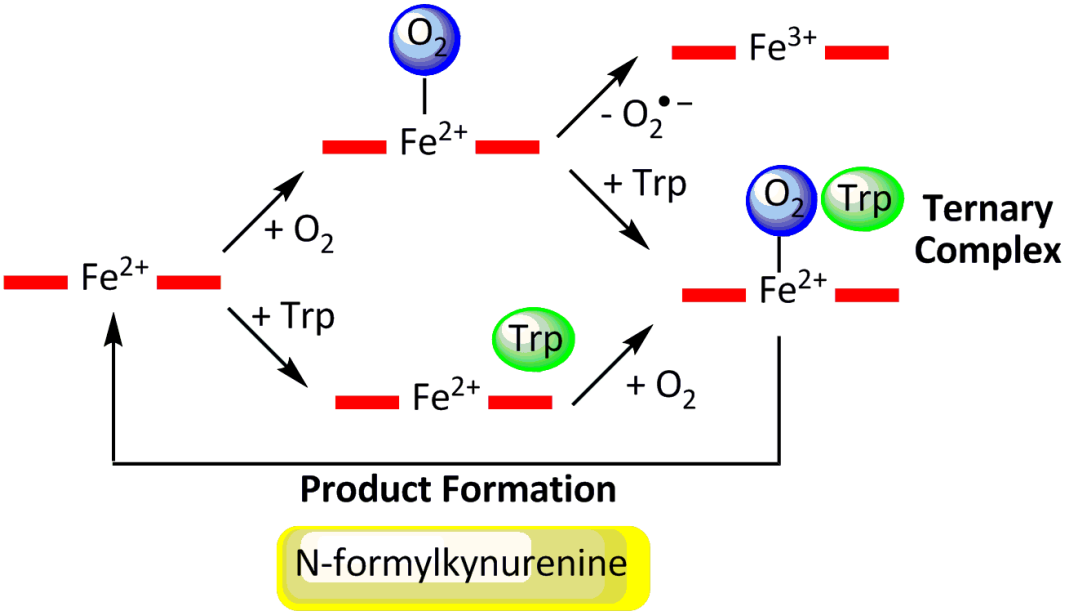

Scheme 1.4 Proposed catalytic reaction cycles for TDO and IDO. The heme (red) and the possible reaction intermediates are shown.

After reduction of the enzyme a mechanism for formation of the ternary complex was proposed based on IDO, which is also applicable for TDO, whereby the ferrous form of the enzyme binds either tryptophan or dioxygen, (the substrate binding order is currently unknown), to form the ternary complex (TDO/IDO^{2+}-tryptophan-O_2) (Scheme 1.4). After formation of the ternary complex it decomposes to yield the ferrous enzyme and product via reaction mechanisms discussed later (Scheme 1.4).

However, for TDO there are several complications. First it was recently determined that the active form differs between enzymes: IDO is only active in the ferrous form, however TDO is active as both oxidised and reduced forms (Table 2.1) (*16, 39, 41, 42, 128*). Reducing agents are required for the catalytic reaction but TDO turnsover substrate in the absence of reducing agents, which is atypical. Secondly the ferrous-oxy form of TDO cannot be detected therefore suggesting that tryptophan binds first and oxygen second, however two groups do observe ferrous-oxy formation with TDO and this complications are discussed in more detail in later chapters (Table 2.1) (*39-41, 128*).

1.19 Proposed Reaction Mechanisms

Unlike other heme-containing proteins such as the oxygenases, peroxidases, globins, and cytochrome P450s, the reaction mechanism of dioxygenases is poorly understood for several reasons. (*16, 129-132*). The crystal structures of the dioxygenases were solved only in the last four years, the catalytic intermediates have not been identified yet and finally the dioxygenase reaction mechanism is unique and is not similar to any other heme containing enzymes.

As mentioned earlier, the ternary complex is the starting complex for the reaction mechanism, with the substrate and dioxygen bound to the ferrous form of the enzyme. Excluding the fact that TDO is active without being reduced, which was a recent discovery, several mechanisms were proposed for the first step of the reaction either via an ionic or radical route (*16*). In 1993 a radical mechanism was

proposed based on rat liver TDO however, this mechanism was rejected as it was reported to be thermodynamically unfavourable (*16, 133*).

Later in the 1990s an ionic mechanism was proposed, which remained undisputed until the crystal structures were released, which is discussed in later chapters (Scheme 1.5) (*16, 134*). The mechanism involved deprotonation of the indole N_1 by an active site base, which could stimulate nucleophilic attack by the C_3 indole position, which is electron-rich, on the distal oxygen atom. This results in the formation of a 3-indolenylperoxy-Fe^{2+} intermediate, which was proposed to convert to the product *N*-formylkynurenine via two routes; the dioxetane (pink) or the Criegee (green) mechanisms (Scheme 1.5). The intermediate could undergo Criegee rearrangement, producing another intermediate, which would undergo further rearrangement to form the product or the intermediate could form a dioxetane intermediate, which would rearrange to form *N*-formylkynurenine.

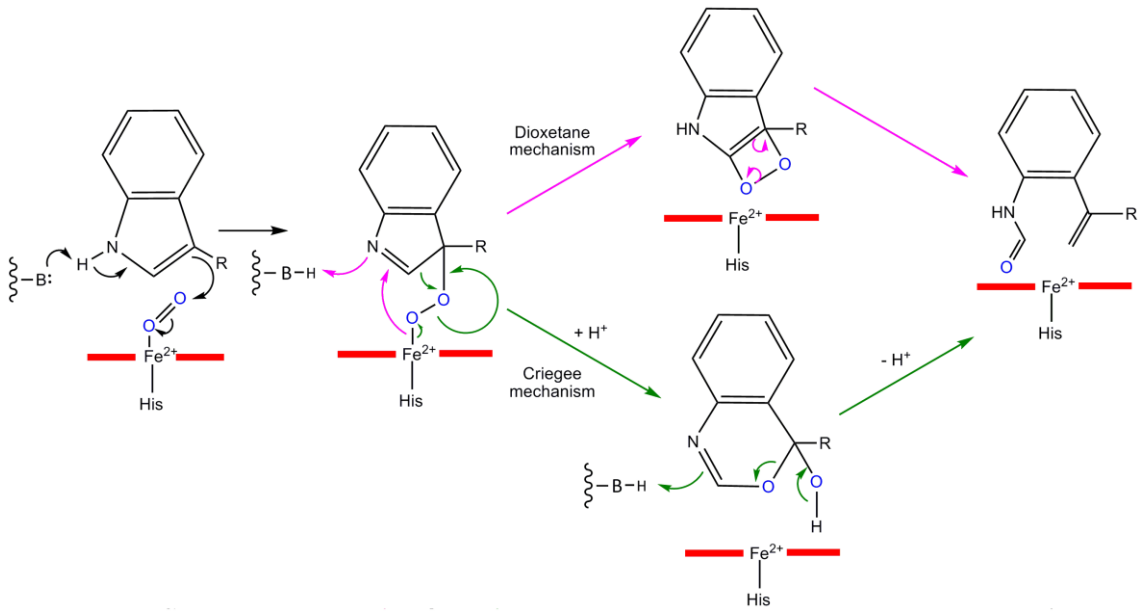

Scheme 1.5 Two proposed mechanisms for the formation of the substrate L-tryptophan to the product *N*-formylkynurenine catalysed by the enzymes TDO and IDO. Criegee rearrangement mechanism (green) Dioxetane mechanism (pink) (*16*).

The deprotonation of the indole N_1 of L-tryptophan by an active site base was suggested as an important part of the reaction mechanism for a number of reasons but mainly because various spectroscopies suggested that the distal residue for

ferric IDO was histidine under certain conditions and that the proximal ligand was nitrogenous, probably from a histidine imidazole ring (*29, 111, 112*). This suggested that the distal heme environment of ferrous IDO was similar to ferrous globins and a distal hisitidine was implied (Figure 1.11) (*135*). Sequence alignments for IDOs, which included mollusc IDO-like myoglobins, mammalian, mouse and a homologue in yeast revealed 37 % sequence identity with two conserved histidine residues H335 and H380 (*136*). It was assumed one of the residues, H380, corresponded to the proximal site and therefore the other, H335, was assigned as the distal histidine residue. Later reported alignments accompanied by experimental data showed other histidines in the sequence, which could be possible candidates for the proximal and distal sites in IDO including H346 and H303 respectively (*52*). The crystal structure solved this conundrum, no histidine was found in the distal site for IDO.

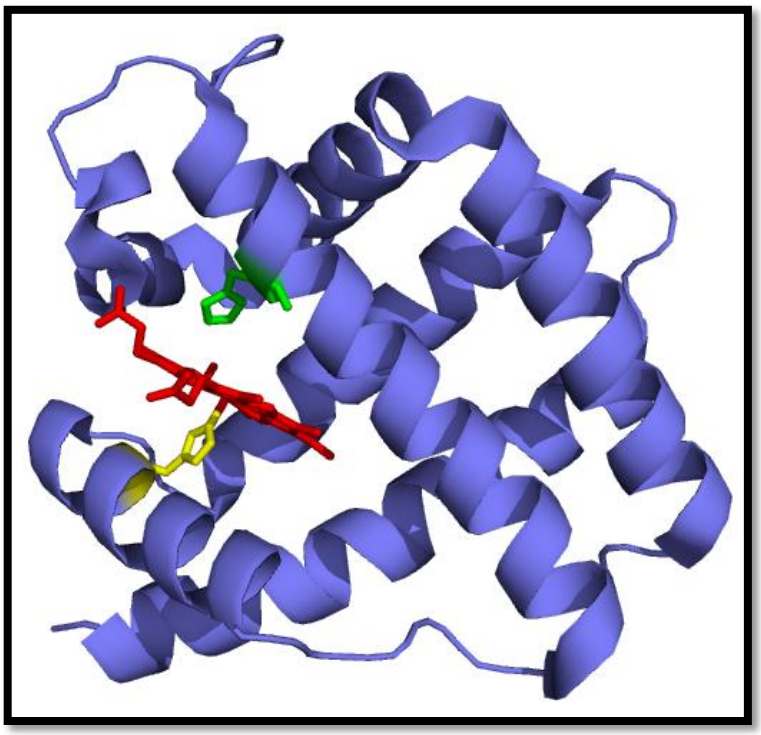

Figure 1.11 Crystal structure of horse heart myoglobin (purple) showing the active site of ferrous myoglobin, heme (red), distal histidine (green), proximal histidine (yellow) (*135*).

The final reason the mechanism was supported was from work in the early nineties, which found that 1-methyl-L-tryptophan was a competitive inhibitor of IDO, therefore methylation of the substrate tryptophan at the indole N_1 converts the compound into an inhibitor because deprotonation of 1-methyl-L-tryptophan is not possible (*121*). As it was firmly believed at the time that there was a distal histidine (suggested by EPR spectroscopy, MCD and sequence alignments), deprotonation of the indole N_1 seemed logical.

1.20 Unanswered questions

Investigation of the dioxygenases has been occurring for the past 70 years and yet there is still very little information regarding the enzymes due to the late development of expression systems. The unanswered questions can be summarised into two broad sections, the catalytic mechanism and the structure.

Currently several mechanisms have been proposed however, there is no hard evidence which supports a specific mechanism or intermediate. As mentioned above it is still unknown whether the substrates have a specfic binding order or whether it is random. This is in contrast to other heme containing enzymes such as the oxygenases and cytochrome P450s.

There are several crystal structures for bacterial TDO however there are only ferric crystal structures for IDO and no structures of mammalian TDO and to understand binding interactions and the role of the catalytic residues a ferrous structure is required with substrate bound in the pocket for IDO and a structure is required for mammalian TDO.

1.21 Aims

The major objectives of this thesis were:

1. Development of an expression and purification system for rhTDO.
2. Characterisation of the enzyme by spectroscopic, kinetic and redox techniques.
3. To investigate the roles of individual active site residues of rhTDO on substrate binding and in catalysis.
4. To elucidate the catalytic mechanism of the human heme dioxygenases.
5. To gain inhibition information for rhTDO.
6. To gain structural information for human IDO.

The results of the studies can be used to show the possible mechanism for the human heme dioxygenases and the information presented in this chapter can be used to inform our current understanding regarding the mechanism of heme dioxygenase catalysis.

1.22 References

1. Emsley, J. (2001) *Nature's building blocks : an A-Z guide to the elements*, Oxford University Press, Oxford.
2. Priestley, J. (1774) *Experiments and Observations on different kinds of Air*, 32 vol. London.
3. Hampel, C. A. (1968) *The encyclopaedia of the chemical elements*, Reinhold, New York ; London.
4. Kaim, W., and Schwederski, B. (1994) *Bioinorganic chemistry : inorganic elements in the chemistry of life : an introduction and guide*, Wiley, Chichester.
5. Valentine, J. S. (1995) *Active oxygen in biochemistry*, Blackie Academic & Professional, London.
6. Jensen, K. P., and Ryde, U. (2004) How O2 binds to heme: reasons for rapid binding and spin inversion, *J Biol Chem 279*, 14561-14569.
7. Bugg, T. D. H. (2003) Dioxygenase enzymes: catalytic mechanisms and model chemistry. , *Tetrahedron 59*, 7075-7101.
8. Jones, R. D., Summerville, D. A., and Basolo, F. (1979) Synthetic Oxygen Carriers Related to Biological Systems, *Chem. Rev. 79*, 139-179.
9. Winterhalter, K. H. (1976) *Chimia 30*, 9.
10. Lee-Ruff, E. (1977) The Organic Chemistry of Superoxide, *Chem. Soc. Rev. 6*, 195-214.
11. Que, L., Jr., and Ho, R. Y. (1996) Dioxygen Activation by Enzymes with Mononuclear Non-Heme Iron Active Sites, *Chem Rev 96*, 2607-2624.
12. English, A. M., and Tsaprailis, G. (1995) Catalytic and structure-function relationships in heme peroxidases, *Adv. Inorg. Chem. 43*, 79 - 125.
13. Wong, L. L. (1998) Cytochrome P450 monooxygenases, *Curr Opin Chem Biol 2*, 263-268.
14. Groves, J. T. (2005) *Cytochrome P450 : structure, mechanism, and biochemistry*, 3rd ed. ed., Kluwer Academic/Plenum Publishers, New York.
15. Makris, T. M., von Koenig, K., Schlichting, I., and Sligar, S. G. (2006) The status of high-valent metal oxo complexes in the P450 cytochromes, *J Inorg Biochem 100*, 507-518.
16. Sono, M., Roach, M. P., Coulter, E. D., and Dawson, J. H. (1996) Heme-Containing Oxygenases, *Chem Rev 96*, 2841-2888.
17. Antonini, M., and Brunori, E. (1971) *Haemoglobin and Myoglobin and their reactions with ligands*, North Holland Publishers, Amsterdam.
18. Takano, T. (1977) Structure of myoglobin refined at 2-0 A resolution. II. Structure of deoxymyoglobin from sperm whale, *J Mol Biol 110*, 569-584.
19. Finzel, B. C., Poulos, T. L., and Kraut, J. (1984) Crystal structure of yeast cytochrome c peroxidase refined at 1.7-A resolution, *J Biol Chem 259*, 13027-13036.
20. Hayaishi, O., and Yoshida, R. (1990) Indoleamine 2,3-dioxygenase: Properties and functions of a superoxide utilising enzyme, *Prog. Inorg. Chem. 38*, 75-94.

21. Mason, H. S., Fowelks, W. K., and Peterson, E. (1955) Oxygen transfer and electron transport by the phenolase complex, *J. Am. Chem. Soc 77*, 2914-2915.
22. Knox, W. E., and Auerbach, V. H. (1955) The hormonal control of tryptophan peroxidase in the rat, *J Biol Chem 214*, 307-313.
23. Hayaishi, O., Hirata, F., Ohnishi, T., Henry, J. P., Rosenthal, I., and Katoh, A. (1977) Indoleamine 2,3-dioxygenase: incorporation of 18O2-- and 18O2 into the reaction products, *J Biol Chem 252*, 3548-3550.
24. Stone, T. W. (1993) Neuropharmacology of quinolinic and kynurenic acids, *Pharmacol Rev 45*, 309-379.
25. Hirata, F., and Hayaishi, O. (1975) Studies on indoleamine 2,3-dioxygenase. I. Superoxide anion as substrate, *J Biol Chem 250*, 5960-5966.
26. Kotake, Y., and Masayama, I. (1936) The Intermediary metabolism of tryptophan. XVIII. The mechanism of formation of kynurenine from tryptophan, Z, *Physiol. Chem. 243*, 237-244.
27. Knox, W. E., and Mehler, A. H. (1951) The adaptive increase of the tryptophan peroxidase-oxidase system of liver, *Science 113*, 237-238.
28. Higuchi, K., and Hayaishi, O. (1967) Enzymic formation of D-kynurenine from D-tryptophan, *Arch Biochem Biophys 120*, 397-403.
29. Shimizu, T., Nomiyama, S., Hirata, F., and Hayaishi, O. (1978) Indoleamine 2,3-dioxygenase. Purification and some properties, *J Biol Chem 253*, 4700-4706.
30. Ishimura, Y., Nozaki, M., and Hayaishi, O. (1970) The oxygenated form of L-tryptophan 2,3-dioxygenase as reaction intermediate, *J Biol Chem 245*, 3593-3602.
31. Schutz, G., and Feigelson, P. (1972) Purification and properties of rat liver tryptophan oxygenase, *J Biol Chem 247*, 5327-5332.
32. Watanabe, Y., Fujiwara, M., Yoshida, R., and Hayaishi, O. (1980) Stereospecificity of hepatic L-tryptophan 2,3-dioxygenase, *Biochem J 189*, 393-405.
33. Drenzek, J. G., Breburda, E. E., Burleigh, D. W., Bondarenko, G. I., Grendell, R. L., and Golos, T. G. (2008) Expression of indoleamine 2,3-dioxygenase in the rhesus monkey and common marmoset, *J Reprod Immunol 78*, 125-133.
34. Searles, L. L., Ruth, R. S., Pret, A. M., Fridell, R. A., and Ali, A. J. (1990) Structure and transcription of the Drosophila melanogaster vermilion gene and several mutant alleles, *Mol Cell Biol 10*, 1423-1431.
35. Hitchcock, M. J., and Katz, E. (1988) Purification and characterization of tryptophan dioxygenase from Streptomyces parvulus, *Archives of Biochemistry and Biophysics 261*, 148-160.
36. Matsumura, M., Osada, K., and Aiba, S. (1984) L-tryptophan 2,3-dioxygenase of a moderate thermophile, Bacillus brevis. Purification, properties and a substrate-mediated stabilization of the quaternary structure, *Biochim Biophys Acta 786*, 9-17.
37. Iwamoto, Y., Lee, I. S., Tsubaki, M., and Kido, R. (1995) Tryptophan 2,3-dioxygenase in Saccharomyces cerevisiae, *Can J Microbiol 41*, 19-26.
38. Comings, D. E., Muhleman, D., Dietz, G., Sherman, M., and Forest, G. L. (1995) Sequence of human tryptophan 2,3-dioxygenase (TDO2): presence of

a glucocorticoid response-like element composed of a GTT repeat and an intronic CCCCT repeat, *Genomics 29*, 390-396.

39. Basran, J., Rafice, S. A., Chauhan, N., Efimov, I., Cheesman, M. R., Ghamsari, L., and Raven, E. L. (2008) A kinetic, spectroscopic, and redox study of human tryptophan 2,3-dioxygenase, *Biochemistry 47*, 4752-4760.
40. Batabyal, D., and Yeh, S. R. (2007) Human tryptophan dioxygenase: a comparison to indoleamine 2,3-dioxygenase, *J Am Chem Soc 129*, 15690-15701.
41. Fukumura, E., Sugimoto, H., Misumi, Y., Ogura, T., and Shiro, Y. (2009) Cooperative binding of L-trp to human tryptophan 2,3-dioxygenase: resonance Raman spectroscopic analysis, *J Biochem 145*, 505-515.
42. Forouhar, F., Anderson, J. L., Mowat, C. G., Vorobiev, S. M., Hussain, A., Abashidze, M., Bruckmann, C., Thackray, S. J., Seetharaman, J., Tucker, T., Xiao, R., Ma, L. C., Zhao, L., Acton, T. B., Montelione, G. T., Chapman, S. K., and Tong, L. (2007) Molecular insights into substrate recognition and catalysis by tryptophan 2,3-dioxygenase, *PNAS 104*, 473-478.
43. Zhang, Y., Kang, S. A., Mukherjee, T., Bale, S., Crane, B. R., Begley, T. P., and Ealick, S. E. (2007) Crystal structure and mechanism of tryptophan 2,3-dioxygenase, a heme enzyme involved in tryptophan catabolism and in quinolinate biosynthesis, *Biochemistry 46*, 145-155.
44. Li, J. S., Han, Q., Fang, J., Rizzi, M., James, A. A., and Li, J. (2007) Biochemical mechanisms leading to tryptophan 2,3-dioxygenase activation, *Archives of Insect Biochemistry and Physiology 64*, 74-87.
45. Paglino, A., Lombardo, F., Arca, B., Rizzi, M., and Rossi, F. (2008) Purification and biochemical characterization of a recombinant Anopheles gambiae tryptophan 2,3-dioxygenase expressed in Escherichia coli, *Insect Biochem Mol Biol 38*, 871-876.
46. Hu, X., Bao, Z., Hu, J., Shao, M., Zhang, L., Bi, K., Zhan, A., and Huang, X. (2006) Cloning and chracterisation of tryptophan 2,3-dioxygenase gene of Zhikong scallop Chlamys farreri (Jones and Preston 1904), *Aquaculture Research 37*, 1187-1194.
47. Manandhar, S. P., Shimada, H., Nagano, S., Egawa, T., and Ishimura, Y. (2002) Subunit structure of recombinant rat liver L-tryptophan 2,3-dioxygenase, *International Congress Series 1233*, 161-169.
48. Dick, R., Murray, B. P., Reid, M. J., and Correia, M. A. (2001) Structure--function relationships of rat hepatic tryptophan 2,3-dioxygenase: identification of the putative heme-ligating histidine residues, *Archives of Biochemistry and Biophysics 392*, 71-78.
49. Ren, S., Liu, H., Licad, E., and Correia, M. A. (1996) Expression of rat liver tryptophan 2,3-dioxygenase in Escherichia coli: structural and functional characterization of the purified enzyme, *Arch Biochem Biophys 333*, 96-102.
50. Maeda, H., Tone, S., Kadoya, A., Iwamonoto, Y., Y., M., and Kido, R. (1992) *Expression of human indoleamine 2,3-dioxygenase in E. coli*, Fujita Health University Press, Toyoake.
51. Littlejohn, T. K., Takikawa, O., Skylas, D., Jamie, J. F., Walker, M. J., and Truscott, R. J. (2000) Expression and purification of recombinant human indoleamine 2, 3-dioxygenase, *Protein Expr Purif 19*, 22-29.

52. Papadopoulou, N. D., Mewies, M., McLean, K. J., Seward, H. E., Svistunenko, D. A., Munro, A. W., and Raven, E. L. (2005) Redox and spectroscopic properties of human indoleamine 2,3-dioxygenase and a His303Ala variant: implications for catalysis, *Biochemistry 44*, 14318-14328.
53. Sugimoto, H., Oda, S., Otsuki, T., Hino, T., Yoshida, T., and Shiro, Y. (2006) Crystal structure of human indoleamine 2,3-dioxygenase: catalytic mechanism of O2 incorporation by a heme-containing dioxygenase, *PNAS 103*, 2611-2616.
54. Vottero, E., Mitchell, D. A., Page, M. J., MacGillivray, R. T., Sadowski, I. J., Roberge, M., and Mauk, A. G. (2006) Cytochrome b(5) is a major reductant in vivo of human indoleamine 2,3-dioxygenase expressed in yeast, *FEBS Lett 580*, 2265-2268.
55. Austin, C. J., Astelbauer, F., Kosim-Satyaputra, P., Ball, H. J., Willows, R. D., Jamie, J. F., and Hunt, N. H. (2009) Mouse and human indoleamine 2,3-dioxygenase display some distinct biochemical and structural properties, *Amino Acids 36*, 99-106.
56. Allegri, G., Ragazzi, E., Bertazzo, A., Costa, C. V., and Rocchi, R. (2003) Tryptophan metabolism along the kynurenine pathway in rats, *Adv Exp Med Biol 527*, 481-496.
57. Fujiwara, M., Shibata, M., Watanabe, Y., Nukiwa, T., Hirata, F., Mizuno, N., and Hayaishi, O. (1978) Indoleamine 2,3-dioxygenase. Formation of L-kynurenine from L-tryptophan in cultured rabbit fineal gland, *J Biol Chem 253*, 6081-6085.
58. Peters, J. C. (1991) Tryptophan nutrition and metabolism: an overview, *Adv Exp Med Biol 294*, 345-358.
59. Moroni, F. (1999) Tryptophan metabolism and brain function: focus on kynurenine and other indole metabolites, *Eur J Pharmacol 375*, 87-100.
60. Pogson, C. I., Knowles, R. G., and Salter, M. (1989) The control of aromatic amino acid catabolism and its relationship to neurotransmitter amine synthesis, *Crit Rev Neurobiol 5*, 29-64.
61. Ruddick, J. P., Evans, A. K., Nutt, D. J., Lightman, S. L., Rook, G. A., and Lowry, C. A. (2006) Tryptophan metabolism in the central nervous system: medical implications, *Expert Rev Mol Med 8*, 1-27.
62. Berger, M., Gray, J. A., and Roth, B. L. (2009) The expanded biology of serotonin, *Annu Rev Med 60*, 355-366.
63. Larsen, R. J., and Buss, D. M. (2002) *Personality psychology : domains of knowledge about human nature*, International ed. ed., McGraw-Hill, Boston ; London.
64. Morley, K., and Hall, W. (2003) Is there a genetic susceptibility to engage in criminal acts?, *Trends and Issues in Criminology 263*, 1-6.
65. Lowenstein, L. F. (2003) The genetic aspects of criminality., *Journal of Human Behavior in the Social Environment 8*, 63-78.
66. Elliot, F. A. (2000) *A neurological perspective of violent behavior.*, Civic Research Institute, Kingston, NJ.
67. Caniato, R., Filippini, R., Piovan, A., Puricelli, L., Borsarini, A., and Cappelletti, E. M. (2003) Melatonin in plants, *Adv Exp Med Biol 527*, 593-597.

68. Hardeland, R. (2005) Antioxidative protection by melatonin: multiplicity of mechanisms from radical detoxification to radical avoidance, *Endocrine 27*, 119-130.
69. Altun, A., and Ugur-Altun, B. (2007) Melatonin: therapeutic and clinical utilization, *Int J Clin Pract 61*, 835-845.
70. Reiter, R. J., Acuna-Castroviejo, D., Tan, D. X., and Burkhardt, S. (2001) Free radical-mediated molecular damage. Mechanisms for the protective actions of melatonin in the central nervous system, *Ann N Y Acad Sci 939*, 200-215.
71. Lehninger, A. L., Lehninger, A. L. P. o. b., Nelson, D. L., and Cox, M. M. (2000) *Lehninger principles of biochemistry*, 3rd ed. / David L. Nelson, Michael M. Cox. ed., Worth Publishers, New York.
72. Pitche, P. T. (2005) [Pellagra], *Sante 15*, 205-208.
73. Takikawa, O. (2005) Biochemical and medical aspects of the indoleamine 2,3-dioxygenase-initiated L-tryptophan metabolism, *Biochem Biophys Res Commun 338*, 12-19.
74. Kotake, Y., and Ito, N. (1937) Studien über den intermediären stoff wechsel des tryptophans: XXVI. Biochemisches über das d-Kynurenin, *Biochem J 26*, 161-165.
75. Kotake, Y., and Ito, N. (1937) Studien über den intermediären stoff-wechsel des tryptophans: XXV. Isolierung des d-Kynurenins, *Biochem J 25*, 71-78.
76. Stone, T. W., and Darlington, L. G. (2002) Endogenous kynurenines as targets for drug discovery and development, *Nat Rev Drug Discov 1*, 609-620.
77. Ohashi, H., Saito, K., Fujii, H., Wada, H., Furuta, N., Takemura, M., Maeda, S., and Seishima, M. (2004) Changes in quinolinic acid production and its related enzymes following D-galactosamine and lipopolysaccharide-induced hepatic injury, *Arch Biochem Biophys 428*, 154-159.
78. Saito, K., Fujigaki, S., Heyes, M. P., Shibata, K., Takemura, M., Fujii, H., Wada, H., Noma, A., and Seishima, M. (2000) Mechanism of increases in L-kynurenine and quinolinic acid in renal insufficiency, *Am J Physiol Renal Physiol 279*, F565-572.
79. Tankiewicz, A., Pawlak, D., and Buczko, W. (2001) [Enzymes of the kynurenine pathway], *Postepy Hig Med Dosw 55*, 715-731.
80. Aquilina, J. A., Carver, J. A., and Truscott, R. J. (1997) Oxidation products of 3-hydroxykynurenine bind to lens proteins: relevance for nuclear cataract, *Exp Eye Res 64*, 727-735.
81. Grohmann, U., Fallarino, F., and Puccetti, P. (2003) Tolerance, DCs and tryptophan: much ado about IDO, *Trends Immunol 24*, 242-248.
82. Munn, D. H., and Mellor, A. L. (2007) Indoleamine 2,3-dioxygenase and tumor-induced tolerance, *J Clin Invest 117*, 1147-1154.
83. Mellor, A. L., Munn, D., Chandler, P., Keskin, D., Johnson, T., Marshall, B., Jhaver, K., and Baban, B. (2003) Tryptophan catabolism and T cell responses, *Adv Exp Med Biol 527*, 27-35.
84. MacKenzie, C. R., Heseler, K., Muller, A., and Daubener, W. (2007) Role of indoleamine 2,3-dioxygenase in antimicrobial defence and immuno-regulation: tryptophan depletion versus production of toxic kynurenines, *Curr Drug Metab 8*, 237-244.

85. Yamamoto, S., and Hayaishi, O. (1967) Tryptophan pyrrolase of rabbit intestine. D- and L-tryptophan-cleaving enzyme or enzymes, *J Biol Chem 242*, 5260-5266.
86. Hayaishi, O., Takikawa, O., Yoshida, R., and Yasui, H. (1984) *Indoleamine-dioxygenase - A possible biological function*, W. de Gruyter, Berlin ; New York.
87. Hirata, H., Kosmakos, F. C., and Brodie, A. F. (1974) Active transport of proline in membrane preparations from Mycobacterium phlei, *J Biol Chem 249*, 6965-6970.
88. Munn, D. H., Zhou, M., Attwood, J. T., Bondarev, I., Conway, S. J., Marshall, B., Brown, C., and Mellor, A. L. (1998) Prevention of allogeneic fetal rejection by tryptophan catabolism, *Science 281*, 1191-1193.
89. Gupta, S. L., Carlin, J. M., Pyati, P., Dai, W., Pfefferkorn, E. R., and Murphy, M. J., Jr. (1994) Antiparasitic and antiproliferative effects of indoleamine 2,3-dioxygenase enzyme expression in human fibroblasts, *Infect Immun 62*, 2277-2284.
90. Byrne, G. I., Lehmann, L. K., and Landry, G. J. (1986) Induction of tryptophan catabolism is the mechanism for gamma-interferon-mediated inhibition of intracellular Chlamydia psittaci replication in T24 cells, *Infect Immun 53*, 347-351.
91. Muller, A. J., DuHadaway, J. B., Donover, P. S., Sutanto-Ward, E., and Prendergast, G. C. (2005) Inhibition of indoleamine 2,3-dioxygenase, an immunoregulatory target of the cancer suppression gene Bin1, potentiates cancer chemotherapy, *Nat Med 11*, 312-319.
92. Ge, K., Duhadaway, J., Sakamuro, D., Wechsler-Reya, R., Reynolds, C., and Prendergast, G. C. (2000) Losses of the tumor suppressor BIN1 in breast carcinoma are frequent and reflect deficits in programmed cell death capacity, *Int J Cancer 85*, 376-383.
93. Ge, K., Minhas, F., Duhadaway, J., Mao, N. C., Wilson, D., Buccafusca, R., Sakamuro, D., Nelson, P., Malkowicz, S. B., Tomaszewski, J., and Prendergast, G. C. (2000) Loss of heterozygosity and tumor suppressor activity of Bin1 in prostate carcinoma, *Int J Cancer 86*, 155-161.
94. Chang, M. Y., Boulden, J., Katz, J. B., Wang, L., Meyer, T. J., Soler, A. P., Muller, A. J., and Prendergast, G. C. (2007) Bin1 ablation increases susceptibility to cancer during aging, particularly lung cancer, *Cancer Res 67*, 7605-7612.
95. Chang, M. Y., Boulden, J., Sutanto-Ward, E., Duhadaway, J. B., Soler, A. P., Muller, A. J., and Prendergast, G. C. (2007) Bin1 ablation in mammary gland delays tissue remodeling and drives cancer progression, *Cancer Res 67*, 100-107.
96. Kanai, M., Funakoshi, H., Takahashi, H., Hayakawa, T., Mizuno, S., Matsumoto, K., and Nakamura, T. (2009) Tryptophan 2,3-dioxygenase is a key modulator of physiological neurogenesis and anxiety-related behavior in mice, *Mol Brain 2*, 8.
97. Comings, D. E. (2001) Clinical and molecular genetics of ADHD and Tourette syndrome. Two related polygenic disorders, *Ann N Y Acad Sci 931*, 50-83.

98. Nabi, R., Serajee, F. J., Chugani, D. C., Zhong, H., and Huq, A. H. (2004) Association of tryptophan 2,3 dioxygenase gene polymorphism with autism, *Am J Med Genet B Neuropsychiatr Genet 125B*, 63-68.
99. Ishiguro, I., Naito, J., Saito, K., and Nagamura, Y. (1993) Skin L-tryptophan-2,3-dioxygenase and rat hair growth, *FEBS Lett 329*, 178-182.
100. Suzuki, T., Watanabe, Y. H., Nagasawa, M., Matsuoka, A., and Shikama, K. (2000) Dual nature of the distal histidine residue in the autoxidation reaction of myoglobin and hemoglobin comparison of the H64 mutants, *Eur J Biochem 267*, 6166-6174.
101. Miller, C. L., Llenos, I. C., Dulay, J. R., Barillo, M. M., Yolken, R. H., and Weis, S. (2004) Expression of the kynurenine pathway enzyme tryptophan 2,3-dioxygenase is increased in the frontal cortex of individuals with schizophrenia, *Neurobiol Dis 15*, 618-629.
102. Phillips, J. P., and Forrest, H. S. (1980) *Ommochromes and pteridines*, Academic Press, London, UK.
103. Tatsumi, K., Higuchi, T., Fujiwara, H., Nakayama, T., Egawa, H., Itoh, K., Fujii, S., and Fujita, J. (2000) Induction of tryptophan 2,3-dioxygenase in the mouse endometrium during implantation, *Biochem Biophys Res Commun 274*, 166-170.
104. Tone, S., Takikawa, O., Habara-Ohkubo, A., Kadoya, A., Yoshida, R., and Kido, R. (1990) Primary structure of human indoleamine 2,3-dioxygenase deduced from the nucleotide sequence of its cDNA, *Nucleic Acids Res 18*, 367.
105. Habara-Ohkubo, A., Takikawa, O., and Yoshida, R. (1991) Cloning and expression of a cDNA encoding mouse indoleamine 2,3-dioxygenase, *Gene 105*, 221-227.
106. Thackray, S. J., Bruckmann, C., Anderson, J. L., Campbell, L. P., Xiao, R., Zhao, L., Mowat, C. G., Forouhar, F., Tong, L., and Chapman, S. K. (2008) Histidine 55 of tryptophan 2,3-dioxygenase is not an active site base but regulates catalysis by controlling substrate binding, *Biochemistry 47*, 10677-10684.
107. Sono, M. (1989) Enzyme kinetic and spectroscopic studies of inhibitor and effector interactions with indoleamine 2,3-dioxygenase. 2. Evidence for the existence of another binding site in the enzyme for indole derivative effectors, *Biochemistry 28*, 5400-5407.
108. Chauhan, N., Basran, J., Efimov, I., Svistunenko, D. A., Seward, H. E., Moody, P. C., and Raven, E. L. (2008) The role of serine 167 in human indoleamine 2,3-dioxygenase: a comparison with tryptophan 2,3-dioxygenase, *Biochemistry 47*, 4761-4769.
109. Bogumil, R., Maurus, R., Hildebrand, D. P., Brayer, G. D., and Mauk, A. G. (1995) Origin of the pH-dependent spectroscopic properties of pentacoordinate metmyoglobin variants, *Biochemistry 34*, 10483-10490.
110. Henry, Y., Ishimura, Y., and Peisach, J. (1976) Binding of nitric oxide to reduced L-tryptophan-2,3-dioxygenase as studied by electron paramagnetic resonance, *J Biol Chem 251*, 1578-1581.
111. Uchida, K., Shimizu, T., Makino, R., Sakaguchi, K., Iizuka, T., Ishimura, Y., Nozawa, T., and Hatano, M. (1983) Magnetic and natural circular dichroism of L-tryptophan 2,3-dioxygenases and indoleamine 2,3-dioxygenase. II.

Spectra of their ferric cyanide and ferrous carbon monoxide complexes and an oxygenated form, *J Biol Chem 258*, 2526-2533.

112. Sono, M., and Dawson, J. H. (1984) Extensive studies of the heme coordination structure of indoleamine 2,3-dioxygenase and of tryptophan binding with magnetic and natural circular dichroism and electron paramagnetic resonance spectroscopy, *Biochim Biophys Acta 789*, 170-187.
113. Terentis, A. C., Thomas, S. R., Takikawa, O., Littlejohn, T. K., Truscott, R. J., Armstrong, R. S., Yeh, S. R., and Stocker, R. (2002) The heme environment of recombinant human indoleamine 2,3-dioxygenase. Structural properties and substrate-ligand interactions, *J Biol Chem 277*, 15788-15794.
114. Makino, R., Sakaguchi, K., Iizuka, T., and Ishimura, Y. (1980) Acid-alkaline transition and thermal spin equilibrium of the heme in ferric L-tryptophan 2,3-dioxygenases, *J Biol Chem 255*, 11883-11891.
115. Patel, N., Jones, D. K., and Raven, E. L. (2000) Investigation of the haem-nicotinate interaction in leghaemoglobin. Role of hydrogen bonding, *Eur J Biochem 267*, 2581-2587.
116. Takikawa, O., Kuroiwa, T., Yamazaki, F., and Kido, R. (1988) Mechanism of interferon-gamma action. Characterization of indoleamine 2,3-dioxygenase in cultured human cells induced by interferon-gamma and evaluation of the enzyme-mediated tryptophan degradation in its anticellular activity, *J Biol Chem 263*, 2041-2048.
117. Hirata, F., and Hayaishi, O. (1972) New degradative routes of 5-hydroxytryptophan and serotonin by intestinal tryptophan 2,3-dioxygenase, *Biochem Biophys Res Commun 47*, 1112-1119.
118. Schwarcz, R., and Pellicciari, R. (2002) Manipulation of brain kynurenines: glial targets, neuronal effects, and clinical opportunities, *J Pharmacol Exp Ther 303*, 1-10.
119. Eguchi, N., Watanabe, Y., Kawanishi, K., Hashimoto, Y., and Hayaishi, O. (1984) Inhibition of indoleamine 2,3-dioxygenase and tryptophan 2,3-dioxygenase by beta-carboline and indole derivatives, *Arch Biochem Biophys 232*, 602-609.
120. Sono, M. (1990) Spectroscopic and equilibrium studies of ligand and organic substrate binding to indolamine 2,3-dioxygenase, *Biochemistry 29*, 1451-1460.
121. Cady, S. G., and Sono, M. (1991) 1-Methyl-DL-tryptophan, beta-(3-benzofuranyl)-DL-alanine (the oxygen analog of tryptophan), and beta-[3-benzo(b)thienyl]-DL-alanine (the sulfur analog of tryptophan) are competitive inhibitors for indoleamine 2,3-dioxygenase, *Arch Biochem Biophys 291*, 326-333.
122. Lu, C., Lin, Y., and Yeh, S. R. (2009) Inhibitory substrate binding site of human indoleamine 2,3-dioxygenase, *J Am Chem Soc 131*, 12866-12867.
123. Hou, D. Y., Muller, A. J., Sharma, M. D., DuHadaway, J., Banerjee, T., Johnson, M., Mellor, A. L., Prendergast, G. C., and Munn, D. H. (2007) Inhibition of indoleamine 2,3-dioxygenase in dendritic cells by stereoisomers of 1-methyl-tryptophan correlates with antitumor responses, *Cancer Res 67*, 792-801.

124. Pereira, A., Vottero, E., Roberge, M., Mauk, A. G., and Andersen, R. J. (2006) Indoleamine 2,3-dioxygenase inhibitors from the Northeastern Pacific Marine Hydroid Garveia annulata, *J Nat Prod 69*, 1496-1499.
125. Brastianos, H. C., Vottero, E., Patrick, B. O., Van Soest, R., Matainaho, T., Mauk, A. G., and Andersen, R. J. (2006) Exiguamine A, an indoleamine-2,3-dioxygenase (IDO) inhibitor isolated from the marine sponge Neopetrosia exigua, *J Am Chem Soc 128*, 16046-16047.
126. Maghzal, G. J., Thomas, S. R., Hunt, N. H., and Stocker, R. (2008) Cytochrome b5, not superoxide anion radical, is a major reductant of indoleamine 2,3-dioxygenase in human cells, *J Biol Chem 283*, 12014-12025.
127. Taniguchi, T., Hirata, F., and Hayaishi, O. (1977) Intracellular utilization of superoxide anion by indoleamine 2,3-dioxygenase of rabbit enterocytes, *J Biol Chem 252*, 2774-2776.
128. Batabyal, D., and Yeh, S. R. (2009) Substrate-Protein Interaction in Human Tryptophan Dioxygenase: The Critical Role of H76, *J Am Chem Soc*.
129. Denisov, I. G., Makris, T. M., Sligar, S. G., and Schlichting, I. (2005) Structure and chemistry of cytochrome P450, *Chem Rev 105*, 2253-2277.
130. Poulos, T. L. (2005) Structural biology of heme monooxygenases, *Biochem Biophys Res Commun 338*, 337-345.
131. Raven, E. L., Lad, L., Sharp, K. H., Mewies, M., and Moody, P. C. (2004) Defining substrate specificity and catalytic mechanism in ascorbate peroxidase, *Biochem Soc Symp*, 27-38.
132. Raven, E. L., and Mauk, A. G. (2001) Chemical reactivity of the active site of myoglobin, *Adv. Inorg. Chem. 51*, 1-49.
133. Leeds, J. M., Brown, P. J., McGeehan, G. M., Brown, F. K., and Wiseman, J. S. (1993) Isotope effects and alternative substrate reactivities for tryptophan 2,3-dioxygenase, *J Biol Chem 268*, 17781-17786.
134. Hamilton, G. A. (1969) Mechanisms of two- and four-electron oxidations catalyzed by some metalloenzymes, *Adv Enzymol Relat Areas Mol Biol 32*, 55-96.
135. Hersleth, H. P., Uchida, T., Rohr, A. K., Teschner, T., Schunemann, V., Kitagawa, T., Trautwein, A. X., Gorbitz, C. H., and Andersson, K. K. (2007) Crystallographic and spectroscopic studies of peroxide-derived myoglobin compound II and occurrence of protonated FeIV O, *J Biol Chem 282*, 23372-23386.
136. Suzuki, T., Kawamichi, H., and Imai, K. (1998) A myoglobin evolved from indoleamine 2,3-dioxygenase, a tryptophan-degrading enzyme, *Comp Biochem Physiol B Biochem Mol Biol 121*, 117-128.

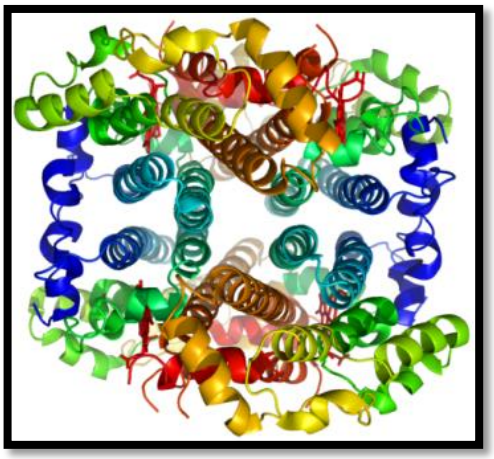

CHAPTER 2

CHARACTERISATION OF HUMAN TRYPTOPHAN 2,3-DIOXYGENASE

Tryptophan 2,3-Dioxygenase (TDO) is a heme-containing enzyme involved in the first rate limiting step in the L-kynurenine pathway, which is the major catabolic route of L-tryptophan metabolism in biology. L-Tryptophan is an essential amino acid and the L-kynurenine pathway processes over 90 % of L-tryptophan utilised by the body (*1*). Tetrameric TDO and its monomeric sister enzyme IDO catalyse the oxidation of L-tryptophan to *N*-formylkynurenine, (Scheme 2.1) by addition of dioxygen, which breaks the C_2-C_3 bond of the indole ring.

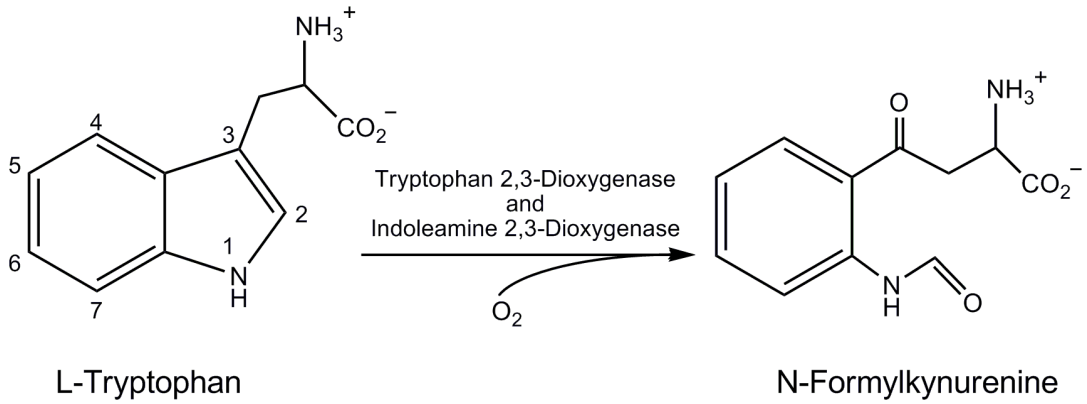

Scheme 2.1. Reaction catalysed by TDO and IDO, with IUPAC numbering indicated.

TDO is a heme containing dioxygenase enzyme that was first discovered in mammalian liver in 1936 and 27 years later the sister enzyme IDO was discovered (*2, 3*). The first characterisation of the enzyme TDO was in 1956 from rat liver (*4*) and more recently has been characterised in both prokaryotes and eukaryotes such as bacteria, insects, yeast and mammals; rats and mice (*5-13*). Due to advances in protein engineering the first year of my PhD was focused on the first characterisation of the full length human enzyme. This novel research was published in Biochemistry, 2008, 47: 4752 – 4760, titled "A Kinetic, Spectroscopic and Redox Study of Human Tryptophan 2,3-Dioxygenase" (*14*). Recently two truncated forms of human TDO have also been characterised (*15, 16*).

In this chapter an expression system for recombinant human TDO is described and the enzyme is analysed spectroscopically, kinetically and by electrochemically. The two dioxygenases have some differences such as low sequence identity between the enzymes, however the active sites of the enzymes share many conserved residues, which was determined by comparisons made between the bacterial TDO and the human IDO crystal structures (*5, 6, 17*). Further comparisons are drawn between the two dioxygenases and more broadly across the heme containing enzyme family regarding substrate binding and the catalytic reaction intermediates in this chapter.

2.1 Cloning of hTDO

The gene encoding hTDO is located on chromosome 4, which has in total 1367 genes. The gene was isolated by PCR amplification from a human liver cDNA library IMAGE clone ID 4071714[1]. The primers were designed with reference to the nucleic acid sequence of the gene (Figure 2.1) and the expression vector pET28a (Novagen) (Figure 2.2).

```
ATGAGTGGGT   GCCCATTTTT   AGGAAACAAC   TTTGGATATA   CTTTTAAAAA   ACTCCCCGTA
GAAGGCAGCG   AAGAAGACAA   ATCACAAACT   GGTGTGAATA   GAGCCAGCAA   AGGAGGTCTT
ATCTATGGGA   ACTACCTGCA   TTTGGAAAAA   GTTTTGAATG   CACAAGAACT   GCAAAGTGAA
ACAAAAGGAA   ATAAAATCCA   TGATGAACAT   CTTTTTATCA   TAACTCATCA   AGCTTATGAA
CTCTGGTTTA   AGCAAATCCT   CTGGGAGTTG   GATTCTGTTC   GAGAGATCTT   TCAGAATGGC
CATGTCAGAG   ATGAAAGGAA   CATGCTTAAG   GTTGTTTCTC   GGATGCACCG   AGTGTCAGTG
ATCCTGAAAC   TGCTGGTGCA   GCAGTTTTCC   ATTCTGGAGA   CGATGACAGC   CTTGGACTTC
AATGACTTCA   GAGAGTACTT   ATCTCCAGCA   TCAGGCTTCC   AGAGTTTGCA   ATTCCGACTA
TTAGAAAACA   AGATAGGTGT   TCTTCAGAAC   ATGAGAGTCC   CTTATAACAG   AAGACATTAT
CGTGATAACT   TCAAAGGAGA   AGAAAATGAA   CTGCTACTTA   AATCTGAGCA   GGAAAAGACA
CTTCTGGAAT   TAGTGGAGGC   ATGGCTGGAA   AGAACTCCAG   GTTTAGAGCC   ACATGGATTT
AACTTCTGGG   GAAAGCTTGA   AAAAAATATC   ACCAGAGGCC   TGGAAGAGGA   ATTCATAAGG
ATTCAGGCTA   AAGAAGAGTC   TGAAGAAAAA   GAGGAACAGG   TGGCTGAATT   TCAGAAGCAA
AAAGAGGTGC   TACTGTCCTT   ATTTGATGAG   AAACGTCATG   AACATCTCCT   TAGTAAAGGT
GAAAGACGGC   TGTCATACAG   AGCACTTCAG   GGAGCATTGA   TGATATATTT   TTACAGGGAA
GAGCCTAGGT   TCCAGGTGCC   TTTTCAGTTG   CTGACTTCTC   TTATGGACAT   AGATTCACTG
ATGACCAAAT   GGAGATATAA   CCATGTGTGC   ATGGTGCACA   GAATGCTGGG   CAGCAAAGCT
GGCACCGGTG   GTTCCTCAGG   CTATCACTAC   CTGCGATCAA   CTGTGAGTGA   TAGGTACAAG
GTATTTGTAG   ATTTATTTAA   TCTTTCAACA   TACCTGATTC   CCCGACACTG   GATACCGAAG
ATGAACCCAA   CCATTCACAA   ATTTCTATAT   ACAGCAGAAT   ACTGTGATAG   CTCCTACTTC
AGCAGTGATG   AATCAGATTA
```

Figure 2.1 The full nucleic acid sequence of the gene for hTDO, 1221 bases.

The primers were designed with an *Nco*I site on the forward primer and a *Xho*I site on the reverse primer, for directional cloning of TDO into the vector pET28a, which has a C-terminal hexahistidyl tag, producing the plasmid pEThTDO8 (Chapter 7, Table 7.1). rhTDO was first cloned into the pQE30 vector with a N-terminal hexahistidyl tag, which had low expression. Therefore the C-terminal hexahistidyl tag expression system was the preferred choice over the typical N-terminal tag due

[1] By Dr. Basran

to higher expression efficacy observed. The pET28a vector carries resistance to kanamycin (Figure 2.2). DNA sequencing confirmed that no spurious mutations occurred during PCR (Appendix II, Figure A2.1, Chapter 7, Section 7.2.2 and Appendix II, Figure A2.1).

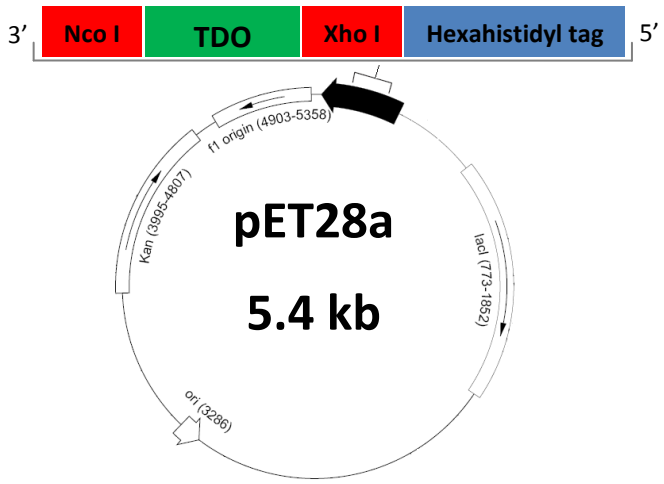

Figure 2.2 The expression vector pET28a (Novagen), (with the gene sequence TDO inserted in the multiple cloning site between the restriction sites *Nco*I and *Xho*I), with a C-terminal hexahistidyl tag and kanamycin resistance.

2.2 Expression and Purification of rhTDO

The pEThTDO8 plasmid was transformed into the *E. coli* strains DH5α and Rosetta (DE3) pLysS. DH5α was used because it has a particular chromosomal genotype which transforms with high efficiency and has a couple of mutations which prevent degradation of the plasmid DNA, namely *endA1* and *hsdR17*. Rosetta (DE3) pLysS is an expression competent cell line which has a T7 promoter, therefore expression is controlled by inducing the cells with IPTG. The pLysS encodes T7 phage lysozyme, which inhibits T7 polymerase and therefore reduces and eliminates expression for the T7 promoter in transformed cells until they are induced with IPTG. Expression cells lines without pLysS were trialed, however they had very low expression. The Rosetta strain also contains tRNA genes to supplement six rare codons to improve

expression. The transformed cells were grown to express full length rhTDO with a C-terminal hexahistidyl tag.

The enzyme was purified using a two step process, the first step was by metal-ion affinity chromatography, elution with an imidazole gradient and the second step was using an FPLC on a 200 pg 16/60 Sephadex gel filtration column (Chapter 7, section 7.4). The monomer is observed on the SDS-PAGE gel as the denaturing conditions of the gel separates the ≈190 kDa tetrameric enzyme into four similar sized subunits ~45 kDa, which is discussed in detail in chapter 6 (Figure 2.3 and Chapter 7, section 7.4.7).

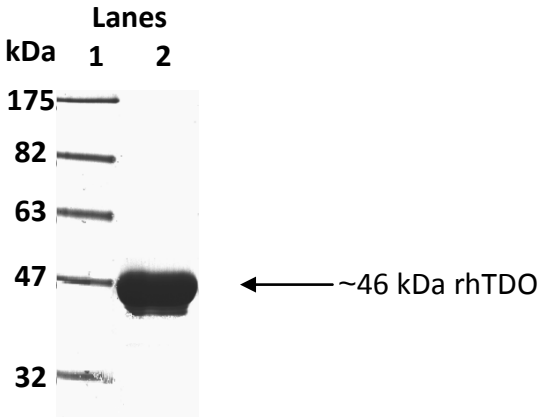

Figure 2.3 SDS-PAGE gel (12 %) showing a pure band of rhTDO after a two step purification process. Lane 1 marker, lane 2 eluted by an imidazole gradient 20 mM-500 mM on a Ni-NTA column, followed by a gel filtration.

The expression system gave ~15 mg/L yield of purified protein, which was reasonable compared to another hTDO expression system which gave 12 mg/L yield (*18*). Peptide mass fingerprinting was carried out on a sample of the enzyme, 45 % of the protein was identified which gave a clear indication that the protein band from the SDS-PAGE gel was rhTDO (Appendix III, Figure A3.1, Chapter 7, section 7.4.8). The concentration of the protein was calculated using absorption coefficients determined by the pyridine haemochromagen method (Appendix IV Table A4.1, Chapter 7, Section 7.5.3).

2.3 Electronic Absorption Spectroscopy

The absorption maxima for various ferric and ferrous derivatives of rhTDO are given in Table 2.1. Maxima for a few derivatives have been published for other human constructs, rat liver enzyme and bacterial *Bacillus brevis* and *Pseudomonas fluorescens* enzymes (*7, 12, 13, 15, 16*) and these are compared with rhTDO in Table 2.1. The spectrum of the ferric form of rhTDO has maxima at 409, 531, and 630 nm (Table 2.1 and Figure 2.4A), consistent with there being a mixture of high- and low-spin heme species. Reduction of ferric rhTDO results in a red shift in the Soret band (from 409 to 429 nm) and the formation of a sharp peak in the visible region (556 nm), which is consistent with the formation of a high-spin species seen by all TDOs (Figure 2.4A).

As observed for other human TDOs (*14, 15*), the binding of L-tryptophan to ferric rhTDO leads to a red shift of the Soret band (to 410 nm), increases in the low-spin signatures at 535 and 568 nm and decreases in absorbance at 630 nm (Figure 2.4B), all of which are consistent with the formation of a low-spin heme species.

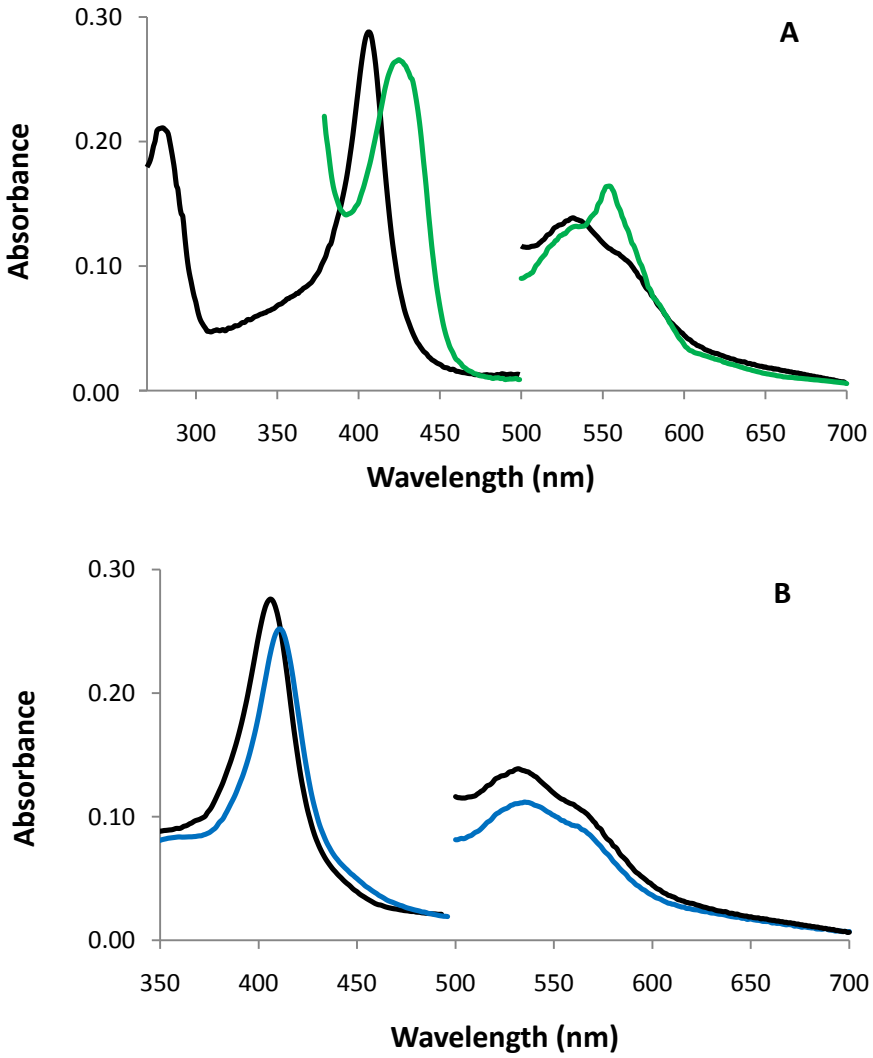

Figure 2.4 Electronic absorption spectrum of rhTDO. A) Ferric rhTDO (black) and ferrous rhTDO (green). B) Ferric rhTDO in the absence (black) and presence of 3 mM L-tryptophan (blue). Absorbance values in the visible region have been multiplied by a factor of 5. Reaction conditions: 50 mM Tris-HCl, pH 8.0, 25.0 ^{o}C.

2.4 EPR Spectroscopy

EPR spectroscopy was carried out by Dr. Myles Cheeseman (UEA) and was used as a means of providing further information on the heme coordination geometry in rhTDO. rhTDO was analysed by low-temperature X-band EPR and the spectrum shown in Figure 2.5 is dominated by an axial spectrum (g_{xy} = 5.71, g_z = 2.01) typical of high-spin ferric heme (Figure 2.5A). The presence of a minority low-spin form is evident (*g* values = 2.89, 2.30, 1.62) (Figure 2.5A). There is a high proportion of high-spin heme for ferric rhTDO compared to other dioxygenases such as rhIDO (*19*).

On addition of substrate (Figure 2.5B), there is a substantial decrease in the level of the high-spin species coupled with the emergence of a new low-spin form with *g*-values of 2.63, 2.20, 1.84 which have been assigned as arising from hydroxide-bound heme, which is in agreement with the UV–visible data presented above and was also seen for rhIDO (*19*).

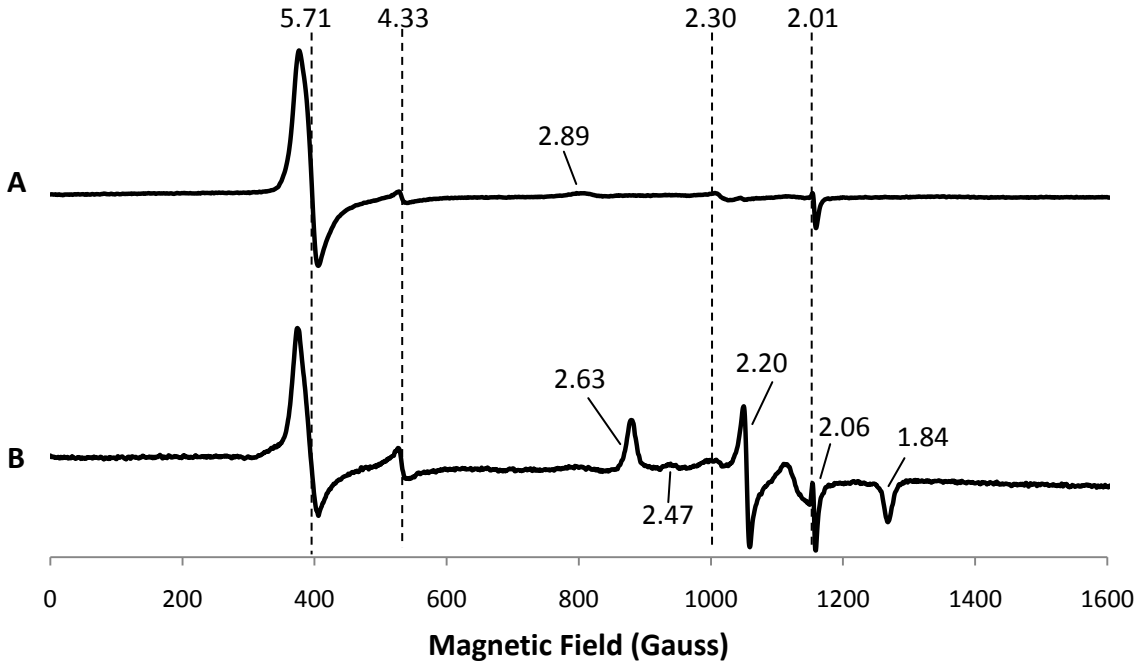

Figure 2.5 X-band EPR spectra of rhTDO in the absence (**A**) and presence (**B**) of 3 mM L-tryptophan. Spectra are adjusted to account for differences in receiver gain. Conditions: 10 K, 2.01 mW microwave power, frequency 9.67 GHz, modulation amplitude 1 mT.

Table 2.1: Absorption Maxima for various ferric and ferrous derivatives of rhTDO. Conditions: 50 mM Tris-HCl Buffer, pH 8.0, 25.0 °C

Derivative	rhTDO	rhTDO (*14*)	rhTDO (*15*)	rhTDO (*16*)	Rat liver (*7*)	*P. fluorescens* (*12*)	*B. brevis* (*13*)
Ferric	409, 531, 630^{sh}	408, 533, 621	406, 633	405, 504, 585, 632	406, 498, 632	405, 500, 635	407, 500, 630
Ferric + L-Trp	410, 535, 568^{sh}	410, 536, 565^{sh}	407	408, 574, 540	407, 498, 632	-	-
Ferrous	429, 534, 556	428, 533, 560	432, 556	-	430, 557	432, 553, 588	432, 555, 585
Ferrous + L -Trp	422, 556	426, 533, 560	433, 555	-	421, 557*d*	-	-
Ferrous-oxy	412	413	412	-	-	-	-
Ternary complex	-	-	417, 543, 576	-	-	418, 545, 580	-
Ferrous-CO	420, 539,565	421, 540, 564	420, 568, 538	-	420, 538, 569	-	-
Ferrous-CO + L -Trp	420, 539,565	421, 540, 564	421, 537, 567	-	420, 538, 569	-	-
Ferrous-cyanide	431, 535, 566	430, 534, 564	-	-	-	-	-
Ferric-azide	407, 535, 563^{sh}	415, 540	-	-	-	-	-
Ferric-cyanide	419, 540, 565^{sh}	419, 538, 566^{sh}	-	-	-	-	-
Ferric-fluoride	406, 528, 626	406, 527, 633	-	-	-	-	-

sh = shoulder

2.5 Binding of Non-Catalytic Ligands

The analysis of exogenous ligands bound at the heme iron provides further information about the distal coordination environment. The representative spectra for the ferric anionic ligand-bound derivatives of rhTDO are presented in Figure 2.6 and the absorption maxima for rhTDO is presented in Table 2.1. The absorption maxima for the cyanide derivative of rhTDO are consistent with the formation of a six-coordinate, low-spin species with a red-shift of the Soret band and disappearance of the CT_1 band in the visible region. A predominantly low-spin species containing small amounts of high-spin character was observed upon azide binding to rhTDO and its variants, whilst binding of fluoride results in a high-spin, six-coordinate species.

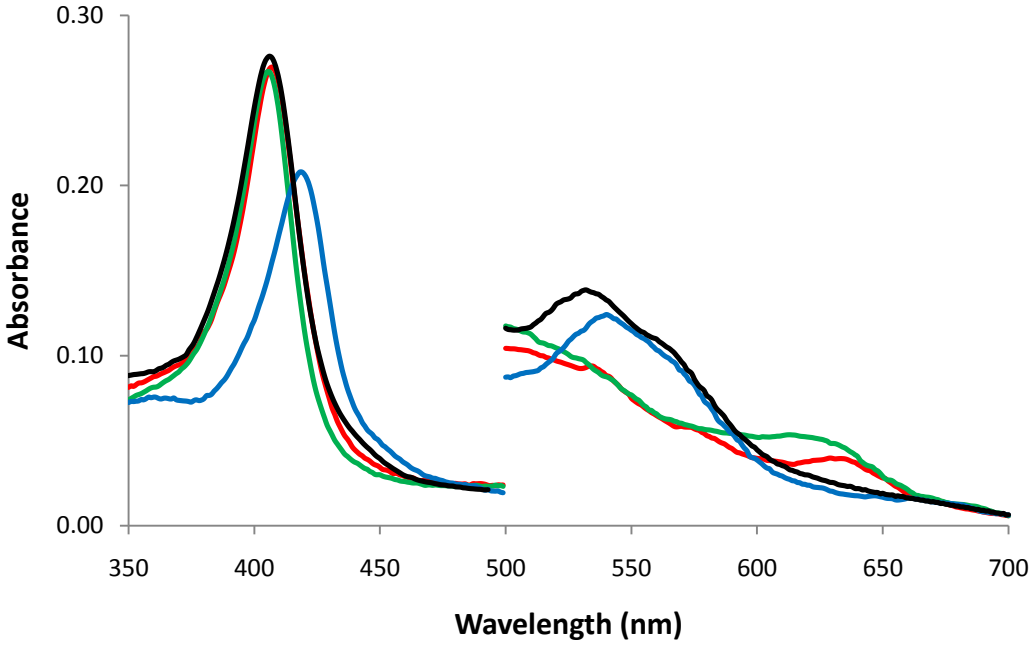

Figure 2.6 Absorption spectra of ferric anionic ligand-bound derivatives of rhTDO: ferric (black), ferric-cyanide (blue), ferric-azide (red) and ferric-fluoride (green). Absorbance values in the visible region have been multiplied by a factor of 5. Reaction conditions: 50 mM Tris-HCl, pH 8.0, 25.0 ˚C.

2.6 Binding of Cyanide and L-Tryptophan to Ferric rhTDO

The binding constant (K_D) for the rhTDO-cyanide complex was calculated to be 31 ± 1 μM (Figure 2.7 and inset), which is in agreement with the spectroscopic data presented in Table 2.1.

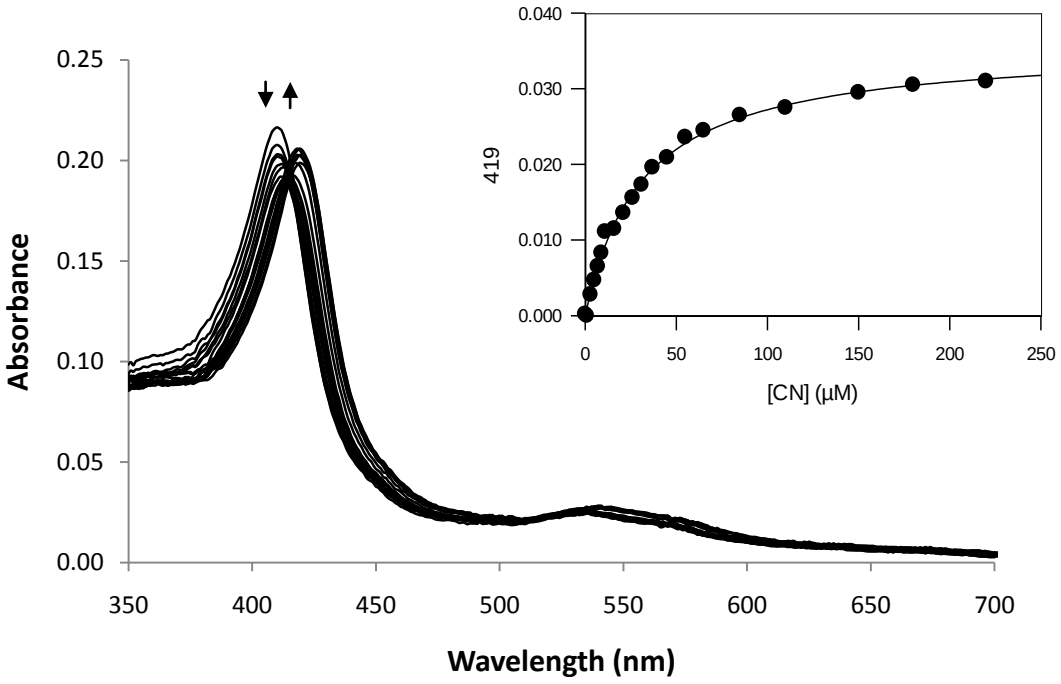

Figure 2.7 Reaction of ferric rhTDO (2 μM) with cyanide. Representative data set for the determination of K_D for binding of cyanide to rhTDO. The arrows indicate the direction of changes in absorbance upon successive additions of cyanide. Inset: Fit of data at 419 nm to Equation 7.4, Chapter 7. Conditions: 50 mM Tris-HCl, pH 8.0, 25.0 ^{o}C.

rhTDO exhibited characteristic spectroscopic changes upon binding of L-tryptophan at pH 8.0 (Table 2.1): the Soret band shifts to 410 nm, which is consistent with the loss of high-spin heme and the formation of a low-spin, hydroxide-bound species on binding of L-tryptophan. Absorbance changes observed upon binding of L-tryptophan to ferric rhTDO (under anaerobic conditions) gave a dissociation constant, K_D, of 162 ± 19 μM (Figure 2.8, inset), which is ~20 fold tighter than for *X.*

campestris TDO (K_D, of 3.8 ± 0.1 mM (*20*)) and similar to ferric rhIDO (K_D = 285 ± 6 μM (*21*)).

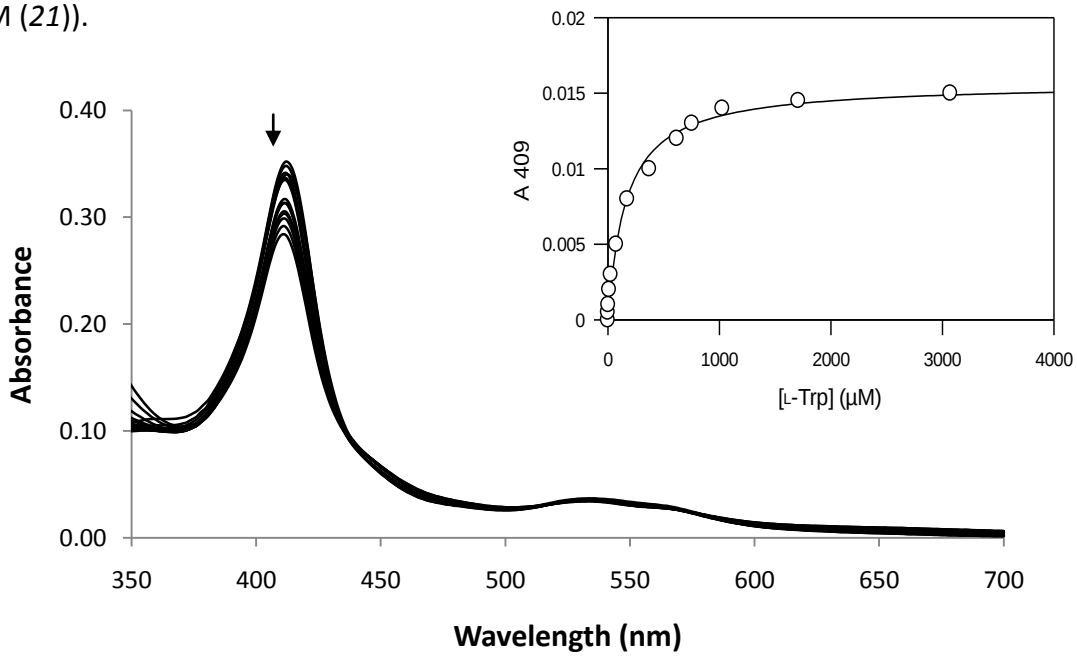

Figure 2.8 Reaction of ferric rhTDO (2 μM) with L-tryptophan. Representative data set for the determination of K_D for binding of L-tryptophan to rhTDO. The arrow indicates the direction of change in absorbance upon successive additions of L-tryptophan. Inset: Absorbance change at 409 nm upon successive additions of L-tryptophan and fit of the data (Chapter 7, Equation 7.4). Reaction conditions: 50 mM Tris-HCl, pH 8.0, 25.0 °C.

2.7 Steady-state Oxidation of L-Tryptophan and Other Tryptophan Analogues

A plot of the initial rate of dioxygenase activity (v/[E], s^{-1}), where v is the initial rate and [E] is the enzyme concentration in the reaction mixture versus L-tryptophan concentration (μM) shows a hyperbolic response. The data were fitted to the Michaelis-Menten equation (Chapter 7, Equation 7.5) and a representative plot for rhTDO is presented in Figure 2.9.

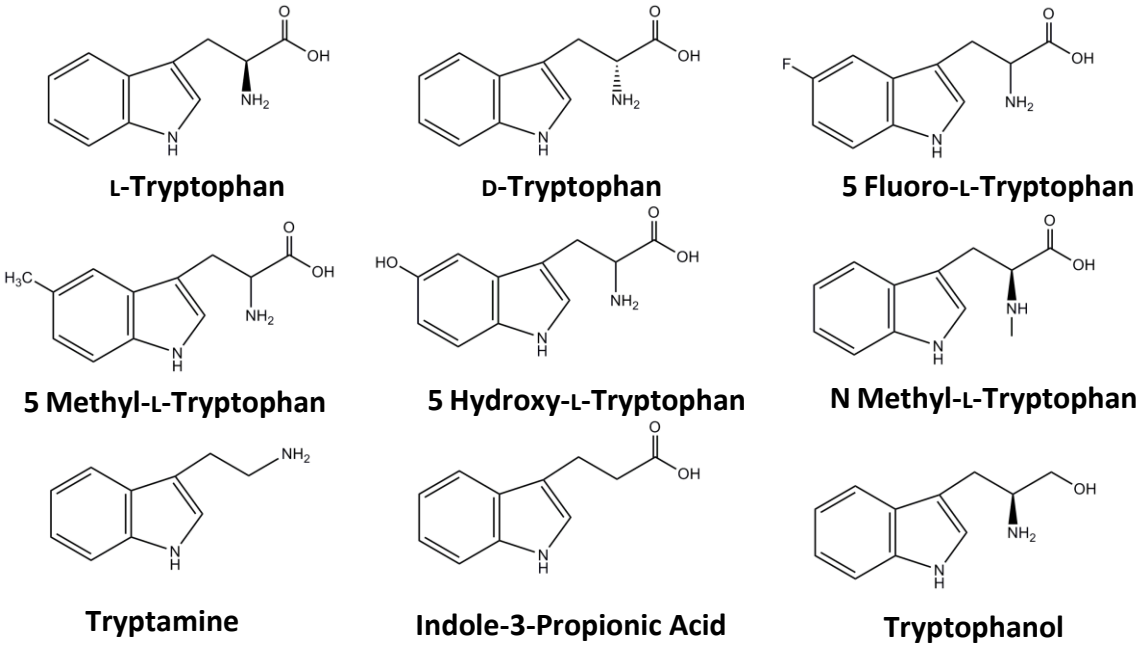

Scheme 2.2 Structures of tryptophan derivatives used in steady-state experiments.

Steady-state kinetic parameters for two constructs of rhTDO, *X. campestris* TDO and rhIDO with L-tryptophan and a number of substrate analogues (Scheme 2.2) are shown in Table 2.2. For rhTDO with L-tryptophan, k_{cat} 1.4 ± 0.1 s^{-1} and K_m 169 ± 18 μM (Figure 2.9). Similar values for k_{cat} and K_m were reported for a truncated form of rhTDO (Table 2.2) (*15*). The steady-state turnover rate (k_{cat}) for both rhTDO and rhIDO are the same (1.4 s^{-1}), although substrate binding for L-tryptophan is at least 15-fold weaker for rhTDO (K_m ≈ 170 μM) compared with ≈10 μM for rhIDO. Whereas rhTDO has a similar K_m for substrate binding compared to *X. campestris* TDO, however it has a ~14 fold faster turnover.

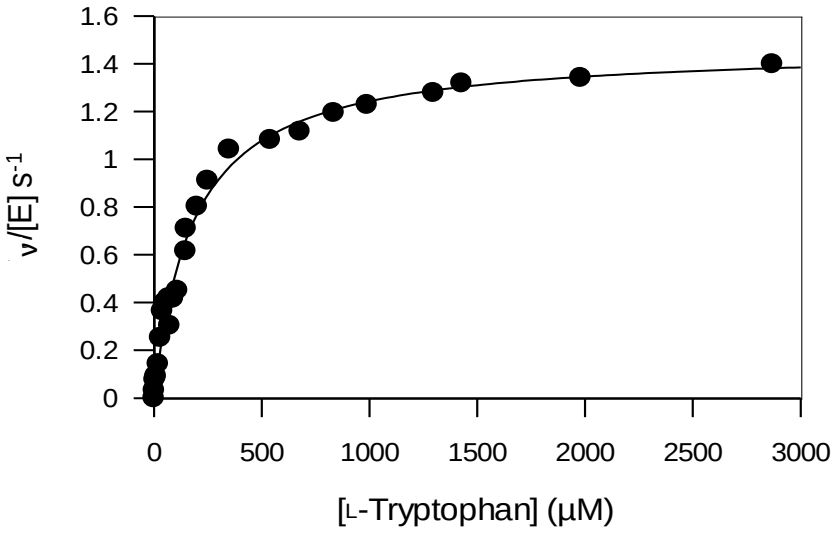

Figure 2.9 Steady-state oxidation of L-tryptophan by rhTDO. Solid line shows a fit of the data to the Michaelis-Menten Equation (Chapter 7, Equation 7.5)

For rhTDO there is evidence for oxidation of D-tryptophan, but the activity is very low, activity was also observed by another human and rat TDO (Table 2.2) (*8, 15, 22*). rhIDO is capable of turning over D-tryptophan k_{cat} 3.93 s^{-1} but the K_m is 100–fold higher than for L-tryptophan suggesting weaker binding for D-tryptophan (*14*). Given the relative binding affinities of the two enzymes for L-tryptophan, rhIDO binds substrate more strongly than rhTDO (rhIDO > rhTDO) and of the two substrates for the two enzymes, L-tryptophan binds stronger than D-tryptophan (L-tryptophan > D-tryptophan), this poor activity is likely to be a result of very weak binding of D-tryptophan to rhTDO, which was also observed by the truncated rhTDO (*15*).

Table 2.2 Steady-state kinetic data for oxidation of L-tryptophan and other substrate analogues by rhTDO. All data were fitted using the Michaelis-Menten equation (Chapter 7, Equation 7.5) where, each value is an average of at least three independent measurements. Reaction conditions: 50 mM Tris-HCl, pH 8.0, 25.0 ^{o}C

	rhTDO[a]		rhTDO[b] (*15*)		XcTDO[c] (*5*)		rhIDO[a] (*14*)	
Substrate	k_{cat} (s^{-1})	K_m (μM)	k_{cat} (s^{-1})	K_m (μM)	k_{cat} (s^{-1})	K_m (μM)	k_{cat} (s^{-1})	K_m (μM)
L-tryptophan	1.4 ± 0.1	169 ± 18	2.1[d]	190[d]	19.5 ± 1.2	114 ± 1	1.4 ± 0.1	7.0 ± 1.0
D-tryptophan[2]	e	e	0.2[d]	180[d]	0	16500 ± 3300	4.0 ± 0.1	1570 ± 100
5-fluoro-tryptophan[2]	0.2 ± 0.1	360 ± 28	-	-	2.40 ± 0.10	100 ± 48	1.00 ± 0.01	6 ± 1.0
5-methyl-tryptophan[2]	f	f	-	-	3.59 ± 0.05	357 ± 12	4.0 ± 0.2	98 ± 14
5-hydroxy-tryptophan[2]	No activity		-	-	-	-	0.10 ± 0.01	17.0 ± 1.0
N-methyl-tryptophan[2]	No activity		-	-	-	-	No activity	
Tryptamine	No activity		-	-	-	-	No activity	
Indole-3-propionic acid	No activity		-	-	No Activity		No activity	
Tryptophanol	No activity		-	-	-	-	No activity	

Steady state kinetics were calculated at a different pH for each enzyme [a] pH 8.0, [b] pH 7.0 and [c] pH 7.5. [d] Errors for k_{cat} and K_m are not published for rhTDO (*15*). [e] Catalytic turnover of D-tryptophan was only measured at one concentration (50 mM) as very little activity was detectable at lower concentrations. At a concentration of 50 mM D-tryptophan, the measured rate of catalytic turnover for rhTDO was 0.073 s^{-1}. [f] In these assays the initial velocity was linearly dependent on 5-methyl-tryptophan concentration across the experimental range; the value of k_{cat}/K_m determined from the slope of this plot was 0.0001 μM^{-1} s^{-1}.

[2] Measured by Dr. Basran

The heme dioxygenases can support insertion of dioxygen into a number of ring-substituted tryptophan analogues. For rhTDO, the only L-tryptophan analogues which were oxidised were 5-fluoro-L-tryptophan and 5-methyl-L-tryptophan (although the latter very slowly, Table 2.2); all other derivatives analysed gave no observable catalytic activity which was similar to rat TDO (*22*).

2.8 Oxidation of L-Tryptophan by Ferric TDO

The steady-state assays above use ferrous rhTDO as the catalytically reactive form of the enzyme. However, activity with the ferric form of rhTDO is also observed by rhTDO and several other TDOs (*15, 16, 23-26*). Activity in the ferric form was not observed for rat, bacterial *X. campestris* TDO and Pseudomonas, insect *Ae. Aegypti* TDO (*20, 27*). Incubation of ferric rhTDO with 3 mM L-tryptophan at atmospheric concentrations of oxygen results in an increase in absorption at 300–350 nm indicative of product formation (Figure 2.10).

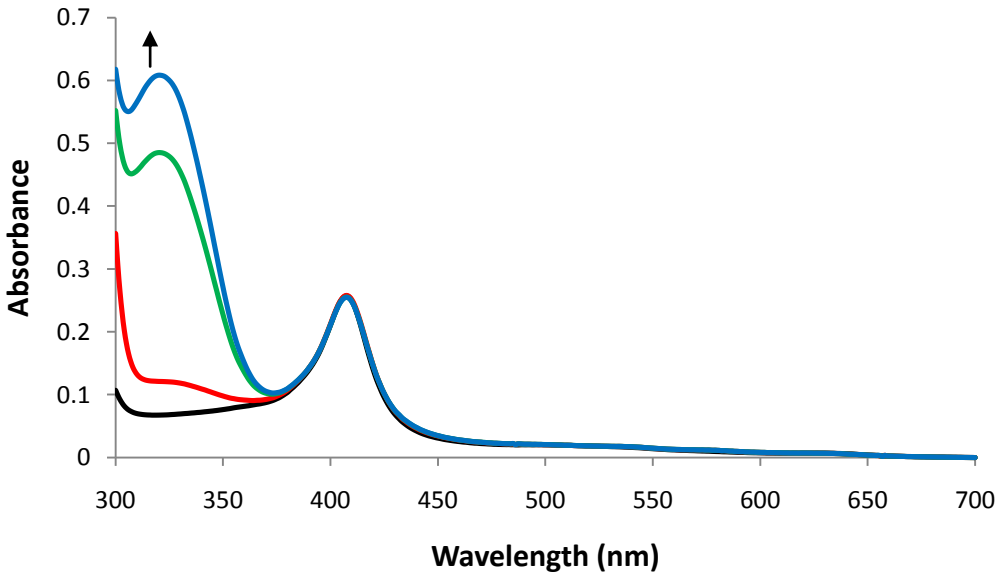

Figure 2.10 Oxidation of L-tryptophan by ferric rhTDO. Spectral changes observed upon reaction ferric rhTDO with 3 mM L-tryptophan. Arrows indicate the direction of absorbance change during the course of the reaction, product formation is observed at 321 nm. Reaction conditions: 50 mM Tris-HCl, pH 8.0, 25.0 ^{o}C.

When the experiments with rhTDO were repeated under anaerobic conditions, there was no significant increase in absorption at 321 nm (Figure 2.11).

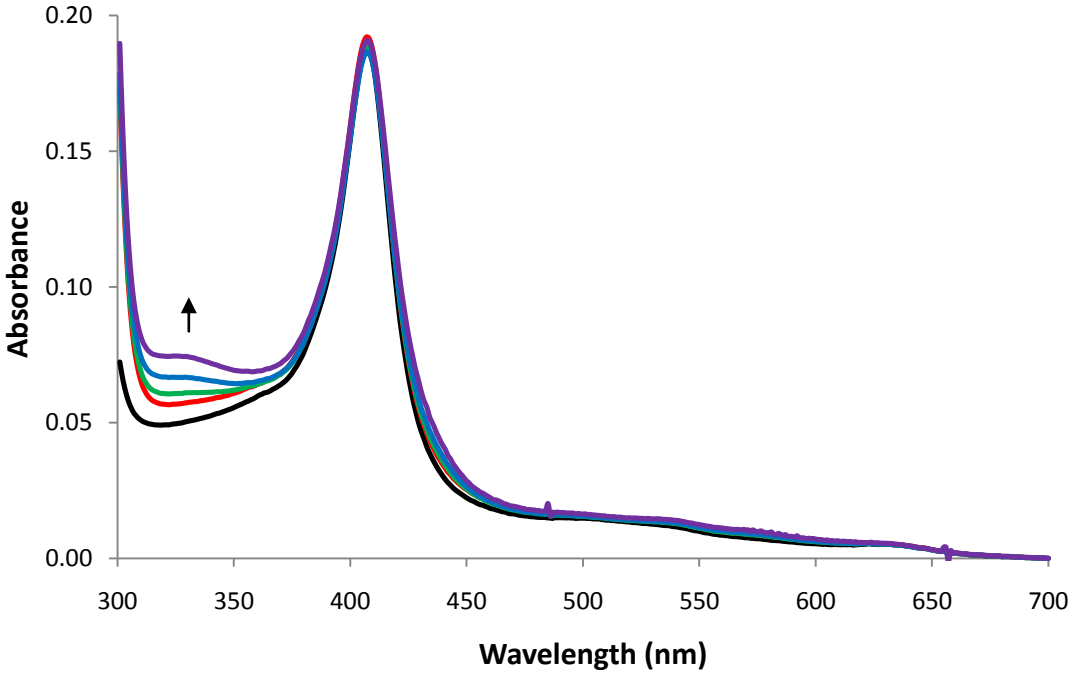

Figure 2.11 Oxidation of L-tryptophan by ferric rhTDO. Spectral changes observed upon reaction of ferric rhTDO with 3 mM L-tryptophan under anaerobic conditions for 30 minutes. Arrows indicate the direction of absorbance change during the course of the reaction, product formation is observed at 321 nm. Reaction conditions: 50 mM Tris-HCl, pH 8.0, 25.0 ^{o}C.

2.9 Binding of O_2 and CO to Ferrous rhTDO

Spectroscopic changes were analysed on reaction of rhTDO with oxygen by directly bubbling O_2 gas into a solution of ferrous rhTDO, which results in the formation of a species that has a Soret band at 412 nm, but there are no sharp peaks in the visible region (expected at ~540 and ~570 nm) that characterise this complex as a ferrous-oxy species (Table 2.1 and Figure 2.12).

To examine whether formation of a ferrous-oxy species was occurring over shorter time scales, the reaction was monitored using photodiode array spectroscopy [3]. There was no evidence for formation of the characteristic ferrous-oxy peaks (expected at ≈540 and ≈570 nm) even when the reaction was observed over an extended period (e.g. 200 s). The spectrum of the final species at 200 seconds is identical to that obtained under equilibrium conditions when a solution of ferrous rhTDO was purged directly with O_2 gas (Figure 2.12).

It was also observed that the ferrous hTDO auto-oxidises through an intermediate, the ferrous-oxy spectrum to ferric obtained with a Soret at 412 nm, which was also seen by the truncated hTDO in the absence of substrate (*18*). However a bacterial TDO *Pseudomonas fluorescens*, which does exhibit the ternary complex at 418, 545 and 580 nm (Table 2.1) does not go through an intermediate in the absence of substrate from ferric to ferrous (*12*). The reason for these differences in the dioxygenase family are unknown.

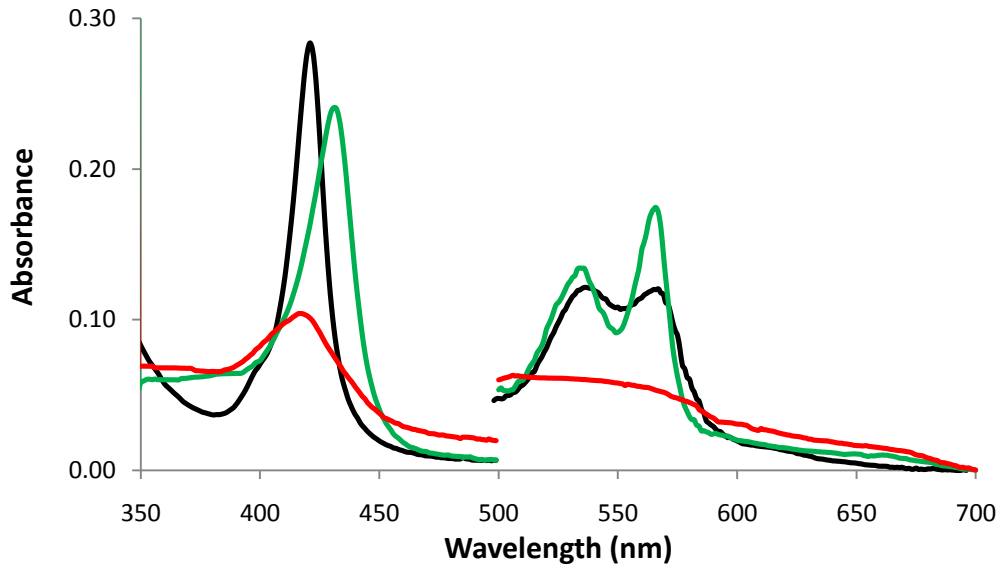

Figure 2.12 Electronic absorption spectra of ferrous derivatives of rhTDO. UV-visible spectra of the ferrous complex in the presence of O_2 (red), CO (black) and cyanide (green). Absorption values in the visible region have been multiplied by a factor of 5. Reaction conditions: 50 mM Tris-HCl, pH 8.0, 25.0 ^{o}C.

[3] By Dr. Basran

In contrast to the reaction with O_2, the ferrous-CO complex of rhTDO is readily isolated (λmax = 420, 539, 565 nm; Table 2.1 and Figure 2.12). Addition of L-tryptophan (3 mM) to the ferrous-CO complex did not result in any further spectral change (Table 2.1). In addition, ferrous rhTDO also binds cyanide, as evidenced by the formation of sharp peaks at 534 and 564 nm in the visible region (Figure 2.12).

2.10 Redox Potentiometry

Reduction potentials for the Fe^{3+}/Fe^{2+} couple of rhTDO were determined using the xanthine/xanthine oxidase assay with simultaneous reduction of a dye of known potential [4]. This method has the advantage over potentiometric titrations in that it allows better equilibria to be obtained because electron exchange occurs in the bulk of the solution: this means that the method is quicker than the potentiometric titration method and does not require the correct choice of mediators. Furthermore it requires less protein than the potentiometric titrations, which is suited for low expressing protein.

Table 2.3 Fe^{2+}/Fe^{3+} Reduction Potentials obtained for various TDOs. Reaction conditions: 100 mM potassium phosphate, pH 7.0, 25.0 ^{o}C.

Enzyme	No L-Trp (mV)	3 mM L-Trp (mV)	Potential Shift (mV)
hTDO	-92 ± 3	-76 ± 3	+16
XcTDO (*20*)	8 ± 5	144 ± 6	+136
rhIDO (*19*)	-30 ± 4	16 ± 3	+46
Rat Liver (*28*)	100	160	+60

[4] Results checked by Dr. Efimov.

The Fe^{3+}/Fe^{2+} couple of rhTDO in the absence (E_{free}) and presence (E_{bound}) of 3 mM L-Tryptophan were found to be -92 ± 3 and -76 ± 3 mV, respectively (Figure 2.13, Table 2.3). The similarity in the two values was unexpected since in other heme dioxygenases a shift in reduction potential is observed on binding of substrate shown in Table 2.3 (*5, 19, 29*). In separate experiments (data not shown), these reduction potentials were confirmed using methylene blue (MB) instead of nile blue chloride (NBC) as the redox dye.

As an independent check on whether the values were correct, these reduction potentials (E_{free} = -92 mV and E_{bound} = -76 mV) were correlated with the binding constants determined for binding of L-tryptophan to the oxidised (K_{OX} = 162 µM) and reduced (K_{RED} = 169 µM) states according to equation 7.7, Chapter 7 (where RT/nF = 25 mV). In this case, a value for K_{OX}/K_{RED} of 0.77 is calculated, which is similar to the value of 0.94 calculated for $\exp[nF(E_{bound} - E_{free})/RT]$. The fact that these reduction potentials correlate with the experimentally determined values for the binding constants in this way is evidence that the measured reduction potentials in the absence and presence of substrate are indeed correct and are a true reflection of the binding thermodynamics. Furthermore the redox potential was measured using the potentiometric titration method at the University of Edinburgh[5], which also confirmed that the redox potentials were correct.

[5] By Dr. Thackray (University of Edinburgh)

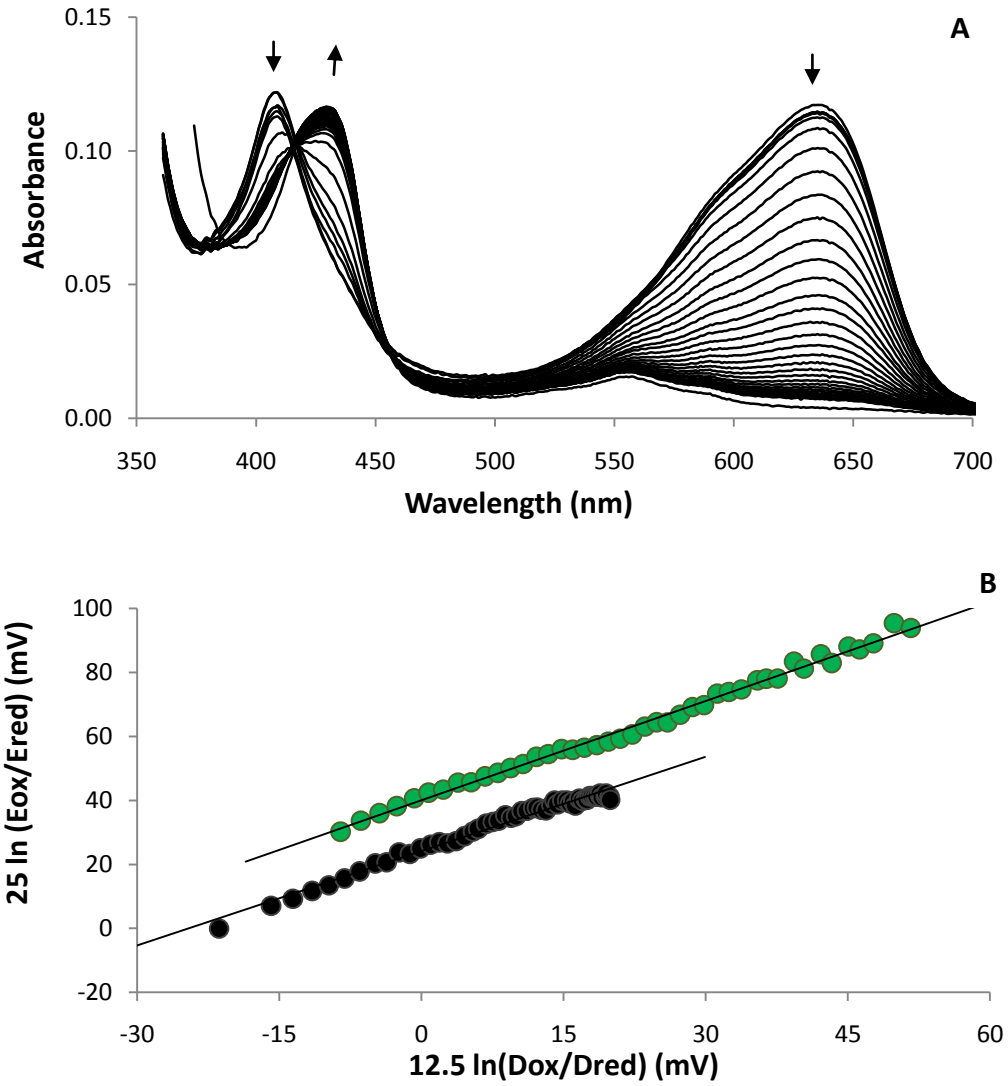

Figure 2.13 Redox potentiometry of rhTDO. (**A**) Spectral changes observed during determination of Fe^{3+}/Fe^{2+} reduction potential with the dye nile blue chloride. Arrows indicate the direction of absorption change during the reductive titration. (**B**) Nernst plots for the data shown in (A) in the absence (black) and presence of 3 mM substrate (green). Reaction conditions: 100 mM potassium phosphate, pH 7.0, 25.0 °C.

2.11 TDO crystal screens

The purity of rhTDO samples used in the crystallisation experiments were determined by measuring Reinheitzahl (R_Z) values (the ratio of the absorbance of the Soret peak at 409 nm and that of the protein peak at 280 nm) and by SDS-PAGE. The protein was then further purified on a 16/60 200 pg gel filtration column using FPLC. All screens were prepared as described in Chapter 7 (Section 7.4.5).

Crystallisation screens of ferric rhTDO were based around the conditions used to crystallise the bacterial TDOs (*5, 6*). Zhang's crystal (PDB 2N0X) was crystallised by vapour diffusion at 22 ^{o}C. The protein was at 25 mg/ml and prepared for crystalisation in 20 mM sodium potassium citrate buffer pH 8.0, 200 mM imidazole, 300 mM sodium chloride. The well solution consisted of 0.8-1.2 M tri-sodium citrate dehydrate (pH 6.5) and 1 mM L-tryptophan. Our collaborators in Edinburgh obtained several crystal structures for *X. campestris* TDO, (PDBs 2NW7, 2NW8, 2NW9) and for some TDO variants (*5*). The enzymes were crystallised in an anaerobic environment in a glove box using the sitting drop vapour diffusion method. The well solution had 100 mM sodium MES buffer (pH 6.3), 10-12 % PEG 4K, 60 mM $MnCl_2$, 10 mM sodium dithionite, 2 mM L-tryptophan. Unfortunately all attempts of these conditions proved unsuccessful for rhTDO.

Structure determination for human TDO is a necessity for furthering our understanding. Therefore a wide screen of over 300 conditions using the high-throughput liquid handling robot, Tecan and a high throughput crystallisation platform, Cartesian and crystal screening kits from multiple companies was conducted (Chapter 7 Section 7.6, Appendix V). PEG 8k was a potential key component in the formula and so Dr I. Efimov screened crystal solutions based on the commercial kits, which contain PEG 8K and altering the pH and concentration of the components. There has been limited success so far, however the protein does not precipitate and it maintains a red colour, which is a step forward (Figure 2.14).

Figure 2.14 TDO crystal attempts, they have some shape and maintain a red colour, however they do not diffract. Protein solution: 50 mM Tris pH 9.0, 5 mM 4-phenyl-imidazole. Well solution: 30-50 mM Tris pH 9.0, 8 % PEG 8K, 4 % ethylene-glycol. Cryo protectant 30 % xylitol [6].

2.12 Discussion

In this chapter a bacterial expression system for human TDO was constructed that produced milligram quantities of enzyme. Thus comparisons between mammalian and bacterial heme dioxygenases can be made and the implications of these data can be discussed in terms of our current understanding of the heme dioxygenase structure and function.

Substrate Interactions

The data with the various substrate analogues clearly show that modifications to the carboxylate and/or ammonium groups of the substrate are not tolerated experimentally by rhTDO, which indicates that hydrogen-bonding interactions to these charged groups are important in the substrate-bound complex, as observed in the crystal structure of *X campestris* TDO in complex with L-tryptophan (*5*). The crystal structure indicates that the arginine residue in the active site forms a

[6] Crystal growth by Dr. Efimov

bidentate interaction with tryptophan at the carboxylate and ammonium groups. Other dioxygenases namely, a truncated hTDO, *X campestris* TDO and hIDO, show binding of substrate analogues in a similar fashion to our hTDO suggesting that binding interactions to the substrate across the TDO family are likely to be conserved (*5-8, 14, 18, 30*).

Substrate binding

The binding affinity of the substrate to ferric and ferrous rhTDO is in the same range as that to ferric rhIDO (~200–300 μM) and ~20 fold stronger compared to *X campestris* TDO (~3-4 mM) (*21*). In bacterial TDOs and human IDO, the substrate discriminates between the ferric and ferrous forms of the enzyme. The substrate preferentially binds to the ferrous form, $K_m \approx 10$ μM for hIDO and K_D for ferrous *X. campestris* TDO ~4 μM whereas TDO shows no such discrimination because the K_D (ferric) ~K_m (ferrous) ~170 μM (*19, 20*).

The Fe^{3+}/Fe^{2+} reduction potential for human TDO was determined as -92 mV. The reduction potential for rhTDO does not shift significantly on addition of substrate. This has functional implications, since the reduction potentials of the substrate-bound and substrate-free forms of the enzyme report indirectly on the relative binding affinity of the substrate. Thus, with rhTDO the redox data show that there is no stabilisation of the ferrous derivative upon binding of the substrate, which is consistent with the data for the active ferric enzyme. This is in contrast to *X. campestris* TDO and rhIDO in which the Fe^{3+}/Fe^{2+} reduction potentials increase by ~60–80 mV (*19, 21*) and ~140 mV (*5*), respectively, upon binding of L-tryptophan.

hTDO showed similar substrate binding affinity to the ferrous and ferric forms and *X. campestris* TDO and hIDO favour the ferrous form. An explanation for this occurrence could be due to the physiological location of the dioxygenases. Human TDO is located in the liver and has been located in the skin and brain (*31, 32*), which are oxygen-rich (oxidising) environments, therefore the enzyme would be present in both ferric and ferrous forms. hIDO is ubiquitously expressed in the body apart from the liver and is always located in the cytoplasm, which is an

overall reducing environment. Therefore suggesting that there would be only low concentrations of ferric IDO present so that efficient binding to the ferric enzyme was not necessary *in vivo* (and consequently that the ferrous form binds substrate preferentially). As dictated by the reduction potentials, human amounts of ferric TDO are present physiologically such that binding to the ferric protein needs to be more efficient relative to hIDO.

A reason *X. campestris* TDO favours the ferrous form over the ferric could be due to that bacteria are prokaryotes therefore they are too small to provide an oxygen-rich environment, therefore bacteria would also contain very low concentrations of ferric TDO.

Substrate oxidation

The value of k_{cat} for rhTDO is identical to that for rhIDO (1.4 s^{-1}). These values for the two mammalian enzymes are lower than those found typically for the bacterial enzymes (k_{cat} usually ≈20 s^{-1} (*5, 12, 29*)), although the reason for this difference is not clear at this stage. Most significantly for rhTDO, the data clearly show that oxidation of substrate is not a reaction catalyzed exclusively by the ferrous enzyme since substrate oxidation also occurs with ferric rhTDO under aerobic conditions.

Substrate oxidation by ferric rhTDO is most likely a result of trace amounts of either H_2O_2 and/or superoxide in solution. This is supported by the fact that substrate oxidation does not occur in the absence of O_2 and by separate experiments in which incubation of the reaction mix with either catalase or superoxide dismutase resulted in a 90% reduction in the total amount of product formed[7] .This characteristic ability of ferric rhTDO to catalyze product formation is also seen by other mammalian TDOs, however bacterial TDOs and rhIDO are inactive in the ferric form (*14, 16, 18-20*). The difference most likely relates to the fact that bacterial TDOs and hIDO discriminates against substrate binding to the ferric enzyme, whereas hTDO does not.

[7] By Dr. Basran

Formation of the Catalytic Ferrous-Oxy Complex

The ferrous-oxy complex of rhTDO is unstable and we find no evidence for formation of a stable ferrous–oxy complex of rhTDO. The histidine in the active site of TDOs is not a conserved residue in dioxygenases for example hIDO has a serine in its place. Variants of hIDO have been examined in particular S167H, in which an active site histidine was incorporated in place of serine (*21*). The surprising outcome was that hIDO can form a stable ferrous-oxy complex and the S167H variant had a very unstable ferrous-oxy complex, suggesting that the histidine plays an important role in the TDOs active site (*21*). Furthermore a variant of *X campestris* TDO was created exchanging the active site histidine for a serine, however no ferrous-oxy complex was observed and also the enzyme still functioned therefore suggesting that the histidine is not an essential residue in the active site (*20*). Chapter 3 discusses the role of the histidine residue using hTDO variants H76A/S and other bacterial TDO variants.

To investigate the active site for a reason the ferrous-oxy complex could not be isolated diatomics such as cyanide and carbon monoxide were reacted with the ferrous enzyme and analysed spectroscopically for binding. These experiments examined whether the ferrous heme group was unreactive as a possible reason it would not bind oxygen. However the results showed typical binding indicating that the ferrous heme group was reactive.

2.13 References

1. Allegri, G., Ragazzi, E., Bertazzo, A., Costa, C. V., and Rocchi, R. (2003) Tryptophan metabolism along the kynurenine pathway in rats, *Adv Exp Med Biol 527*, 481-496.
2. Kotake, Y., and Masayama, I. (1936) The Intermediary metabolism of tryptophan. XVIII. The mechanism of formation of kynurenine from tryptophan, Z, *Physiol. Chem. 243*, 237-244.
3. Higuchi, K., and Hayaishi, O. (1967) Enzymic formation of D-kynurenine from D-tryptophan, *Arch Biochem Biophys 120*, 397-403.
4. Knox, W. E., and Auerbach, V. H. (1955) The hormonal control of tryptophan peroxidase in the rat, *J Biol Chem 214*, 307-313.
5. Forouhar, F., Anderson, J. L., Mowat, C. G., Vorobiev, S. M., Hussain, A., Abashidze, M., Bruckmann, C., Thackray, S. J., Seetharaman, J., Tucker, T., Xiao, R., Ma, L. C., Zhao, L., Acton, T. B., Montelione, G. T., Chapman, S. K., and Tong, L. (2007) Molecular insights into substrate recognition and catalysis by tryptophan 2,3-dioxygenase, *PNAS 104*, 473-478.
6. Zhang, Y., Kang, S. A., Mukherjee, T., Bale, S., Crane, B. R., Begley, T. P., and Ealick, S. E. (2007) Crystal structure and mechanism of tryptophan 2,3-dioxygenase, a heme enzyme involved in tryptophan catabolism and in quinolinate biosynthesis, *Biochemistry 46*, 145-155.
7. Manandhar, S. P., Shimada, H., Nagano, S., Egawa, T., and Ishimura, Y. (2002) Subunit structure of recombinant rat liver L-tryptophan 2,3-dioxygenase, *International Congress Series 1233*, 161-169.
8. Watanabe, Y., Fujiwara, M., Yoshida, R., and Hayaishi, O. (1980) Stereospecificity of hepatic L-tryptophan 2,3-dioxygenase, *Biochem J 189*, 393-405.
9. Searles, L. L., Ruth, R. S., Pret, A. M., Fridell, R. A., and Ali, A. J. (1990) Structure and transcription of the Drosophila melanogaster vermilion gene and several mutant alleles, *Mol Cell Biol 10*, 1423-1431.
10. Comings, D. E., Muhleman, D., Dietz, G., Sherman, M., and Forest, G. L. (1995) Sequence of human tryptophan 2,3-dioxygenase (TDO2): presence of a glucocorticoid response-like element composed of a GTT repeat and an intronic CCCCT repeat, *Genomics 29*, 390-396.
11. Mukabayire, O., Cornel, A. J., Dotson, E. M., Collins, F. H., and Besansky, N. J. (1996) The Tryptophan oxygenase gene of Anopheles gambiae, *Insect Biochem Mol Biol 26*, 525-528.
12. Ishimura, Y., Nozaki, M., and Hayaishi, O. (1970) The oxygenated form of L-tryptophan 2,3-dioxygenase as reaction intermediate, *J Biol Chem 245*, 3593-3602.
13. Matsumura, M., Osada, K., and Aiba, S. (1984) L-tryptophan 2,3-dioxygenase of a moderate thermophile, Bacillus brevis. Purification, properties and a substrate-mediated stabilization of the quaternary structure, *Biochim Biophys Acta 786*, 9-17.

14. Basran, J., Rafice, S. A., Chauhan, N., Efimov, I., Cheesman, M. R., Ghamsari, L., and Raven, E. L. (2008) A kinetic, spectroscopic, and redox study of human tryptophan 2,3-dioxygenase, *Biochemistry 47*, 4752-4760.
15. Batabyal, D., and Yeh, S. R. (2007) Human tryptophan dioxygenase: a comparison to indoleamine 2,3-dioxygenase, *J Am Chem Soc 129*, 15690-15701.
16. Fukumura, E., Sugimoto, H., Misumi, Y., Ogura, T., and Shiro, Y. (2009) Cooperative binding of L-trp to human tryptophan 2,3-dioxygenase: resonance Raman spectroscopic analysis, *J Biochem 145*, 505-515.
17. Sugimoto, H., Oda, S., Otsuki, T., Hino, T., Yoshida, T., and Shiro, Y. (2006) Crystal structure of human indoleamine 2,3-dioxygenase: catalytic mechanism of O2 incorporation by a heme-containing dioxygenase, *PNAS 103*, 2611-2616.
18. Batabyal, D., and Yeh, S. R. (2009) Substrate-Protein Interaction in Human Tryptophan Dioxygenase: The Critical Role of H76, *J Am Chem Soc*.
19. Papadopoulou, N. D., Mewies, M., McLean, K. J., Seward, H. E., Svistunenko, D. A., Munro, A. W., and Raven, E. L. (2005) Redox and spectroscopic properties of human indoleamine 2,3-dioxygenase and a His303Ala variant: implications for catalysis, *Biochemistry 44*, 14318-14328.
20. Thackray, S. J., Bruckmann, C., Anderson, J. L., Campbell, L. P., Xiao, R., Zhao, L., Mowat, C. G., Forouhar, F., Tong, L., and Chapman, S. K. (2008) Histidine 55 of tryptophan 2,3-dioxygenase is not an active site base but regulates catalysis by controlling substrate binding, *Biochemistry 47*, 10677-10684.
21. Chauhan, N., Basran, J., Efimov, I., Svistunenko, D. A., Seward, H. E., Moody, P. C., and Raven, E. L. (2008) The role of serine 167 in human indoleamine 2,3-dioxygenase: a comparison with tryptophan 2,3-dioxygenase, *Biochemistry 47*, 4761-4769.
22. Ren, S., Liu, H., Licad, E., and Correia, M. A. (1996) Expression of rat liver tryptophan 2,3-dioxygenase in Escherichia coli: structural and functional characterization of the purified enzyme, *Arch Biochem Biophys 333*, 96-102.
23. Feigelson, P., Ishimura, Y., and Hayaishi, O. (1964) On the activation and catalytic mechanism of microbial tryptophan pyrrolase, *Biochem Biophys Res Commun 14*, 96-101.
24. Feigelson, P., Ishimura, Y., and Hayaishi, O. (1965) Studies on the Role of Hematin in the Catalytic Mechanism of Tryptophan Pyrrolase, *Biochim Biophys Acta 96*, 283-293.
25. Feigelson, P., and Maeno, H. (1966) *Biological and chemical aspects of oxygenases*, Maruzen Company Ltd., Tokyo.
26. Maeno, H., and Feigelson, P. (1967) Spectral studies on the catalytic mechanism and activation of Pseudomonas tryptophan oxygenase (tryptophan pyrrolase), *J Biol Chem 242*, 596-601.
27. Tokuyama, K., and Knox, W. E. (1964) The Resolution and Activa tion of Hematin-free Tryptophan Pyrrolase from Rat Liver, *Biochim Biophys Acta 81*, 201-204.

28. Makino, R., Sakaguchi, K., Iizuka, T., and Ishimura, Y. (1980) *L-tryptophan 2,3-dioxygenase; structure, function an interaction with substrate*, Elsevier, Amsterdam.
29. Makino, R., Sakaguchi, K., Iizuka, T., and Ishimura, Y. (1980) Acid-alkaline transition and thermal spin equilibrium of the heme in ferric L-tryptophan 2,3-dioxygenases, *J Biol Chem 255*, 11883-11891.
30. Hitchcock, M. J., and Katz, E. (1988) Purification and characterization of tryptophan dioxygenase from Streptomyces parvulus, *Archives of Biochemistry and Biophysics 261*, 148-160.
31. Ishiguro, I., Naito, J., Saito, K., and Nagamura, Y. (1993) Skin L-tryptophan-2,3-dioxygenase and rat hair growth, *FEBS Lett 329*, 178-182.
32. Takikawa, O. (2005) Biochemical and medical aspects of the indoleamine 2,3-dioxygenase-initiated L-tryptophan metabolism, *Biochem Biophys Res Commun 338*, 12-19.

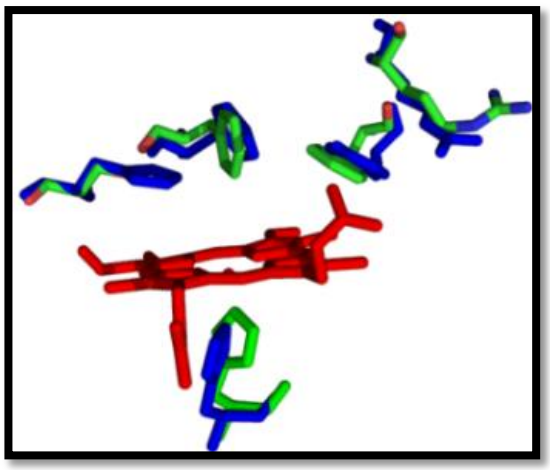

CHAPTER 3

INVESTIGATION OF ACTIVE-SITE INTERACTIONS IN TRYPTOPHAN 2,3-DIOXYGENASE

The hemoproteins tryptophan 2,3-dioxygenase (TDO) and indoleamine 2,3-dioxygenase (IDO) catalyse the initial rate-limiting step in the L-kynurenine pathway, the irreversible degradation of L-tryptophan by insertion of dioxygen into the indole ring of the amino acid to yield *N*-formylkynurenine, (Scheme 3.1).

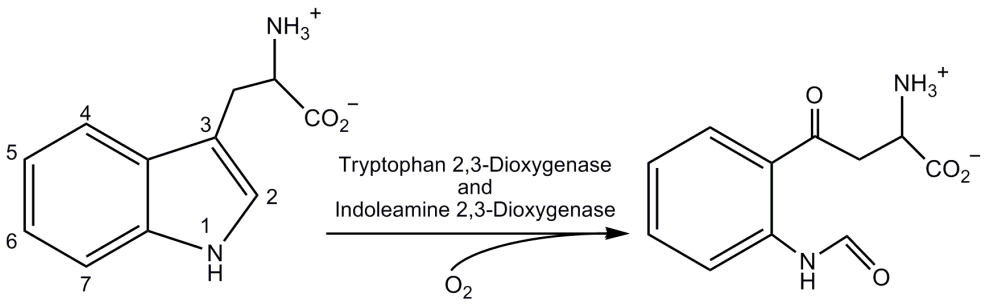

L-Tryptophan N-Formylkynurenine

Scheme 3.1. Reaction catalysed by TDO and IDO, with IUPAC numbering indicated.

TDO is found in both prokaryotes and eukaryotes such as bacteria, insects, yeast and mammals, which are different sizes, varying between 120 kDa to 190 kDa however they share nearly identical residues in each active site (Figure 3.1) (*1-9*).

```
Human TDO    1 ---MSGCPFLGNNFGYTFKK---LPVEGSEEDKSQ---TGVNRASKGGLIYGNYLHLEKVLNAQELQ 58
Mouse TDO    1 ---MSGCPFAGNSVGYTLKN---VSMEDNEEDRAQ---TGVNRASKGGLIYGNYLQLEKILNAQELQ 58
Rat TDO      1 ---MSGCPFSGNSVGYTLKN---LSMEDNEEDGAQ---TGVNRASKGGLIYGDYLQLEKILNAQELQ 58
Bovine TDO   1 ---MSGCPFLGKSFGYAFKP---LSAQGSEEDKSQ---AGVNRASKGGLIYGNYLQLEKVLNAQELQ 58
Xc TDO       1 ------MP-----VDKNLRD---LE-------------PGIHTDLEGRLTYGGYLRLDQLLSAQQPL 40
Rm TDO       1 MSEFKGCP-----MGHGAAP---QNGDGGDSGDTGNGWHGAQMDFARDMSYGDYLGLDQILSAQHPL 59
Human IDO    1 -------------MAHAMENSWTISKEYHIDEEVGFALPNPQENLPDF--YNDWMFIAKHLPDLIES 52

Human TDO   59 SETKGNKIHDEHLFI--ITHQAYELWFKQILWELDSVRE-IFQNGHVRDE--RNMLKVVSRMHRVSV 120
Mouse TDO   59 SEVKGNKIHDEHLFI--ITHQAYELWFKQILWELDSVRE-IFQNGHVRDE--RNMLKVIARMHRVVV 120
Rat TDO     59 SEIKGNKIHDEHLFI--ITHQAYELWFKQILWELDSVRE-IFQNGHVRDE--RNMLKVMTRMHRVVV 120
Bovine TDO  59 SEMKGNKIHDEHLFI--ITHQAYELWFKQILWELDSVRE-IFQNGHVRDE--RNMLKVITRMHRVVV 120
Xc TDO      41 SE---PAHHDEMLFI--IQHQTSELWLKLLAHELRAAIV-HLQRDEVWQC--RKVLA------RSKQ 93
Rm TDO      60 SP-----DHNEMLFI--VQHQTTELWMKLMLHELRAARD-GVKSDQLQPA--FKMLA------RVSR 110
Human IDO   53 GQLRERVEKLNMLSIDHLTDHKSQRLARLVLGCITMAYVWGKGHGDVRKVLPRNIAVPYCQLSKKLE 119

Human TDO  121 ILKLLV------QQFSILETMTALDFNDFREYLSPASGFQSLQFRLLENKIGVLQNMRVPYNRRHYR 181
Mouse TDO  121 IFKLLV------QQFSVLETMTALDFNDFREYLSPASGFQSLQFRLLENKIGVLQSLRVPYNRKHYR 181
Rat TDO    121 IFKLLV------QQFSVLETMTALDFNDFREYLSPASGFQSLQFRLLENKIGVLQSLRVPYNRKHYR 181
Bovine TDO 121 ILKLLV------QQFSVLETMTALDFNDFREYLSPASGFQSLQFRLLENKIGVLQSLRVPYNRRHYR 181
Xc TDO      94 VLRQLT------EQWSVLETLTPSEYMGFRDVLGPSSGFQSLQYRYIEFLLG--------------- 139
Rm TDO     111 IMDQLV------QAWNVLATMTPPEYSAMRPYLGASSGFQSYQYREIEFILG--------------- 156
Human IDO  120 LPPILVYADCVLANWKKKDPNKPLTYENMDVLFSFRDGDCSKGFFLVSLLVEIAAASAIKVIPTVFK 186

Human TDO  182 DNFKGEENELLLKSEQEKTLLELVEAWLERTPG-LEPHGFNFWGKLEKNITRGLEEEFIRIQAKEES 248
Mouse TDO  182 DNFGGDYNELLLKSEQEQTLLQLVEAWLERTPG-LEPNGNFWGKFEKNILKGLEEEFLRIQAKTDSF 248
Rat TDO    182 DNFEGDYNELLLKSEQEQTLLQLVEAWLERTPG-LEPHGFNFWGKFEKNILKGLEEEFLKIQAKKDS 248
Bovine TDO 182 DNFRGKDNELLLKSEQERTLLQLVEAWLERTPG-LEPHGFNFWGKLEKNIVKGLEEEFTKIQAKEES 248
Xc TDO     140 ----NKNPQMLQVFAYDPAGQARLREVLE-APS-LYEEFLRYLARFGHAI---------------PQ 185
Rm TDO     157 ----NKNAAMLRPHAHRPEHLELVETALH-TPS-MYDEAIRLMARRGFQI---------------DP 202
Human IDO  187 AMQMQERDTLLKALLEIASCLEKALQVFHQIHDHVNPKAF-------FSVLRIYLSGWKGNPQLSDG 246

Human TDO  249 EEKEEQVAEFQKQ------KEVLLSLFDEKRHEHLLSKGERRLSYRALQGALMIYFYREEPRFQVPF 309
Mouse TDO  249 EEKEEQMAEFRKQ------KEVLLCLFDEKRHDYLLSKGERRLSYRALQGALMIYFYREEPRFQVPF 309
Rat TDO    249 EEKEEQMAEFRKQ------KEVLLCLFDEKRHDYLLSKGERRLSYRALQGALMIYFYREEPRFQVPF 309
Bovine TDO 249 EEKEEQMAEFQKQ------KEVLLSLFDEKRHEHLLSKGERRLSYKALQGALMIYFYREEPRFQVPF 309
Xc TDO     186 QYQARDWTAAHVA------DDTLRPVFER-------------------------IYENTDRYWREY 220
Rm TDO     203 EVVERDWTQPTQY------NASVEAAWLE-------------------------VYRNPSAHWELY 237
Human IDO  247 LVYEGFWEDPKEFAGGSAGQSSVFQCFDV-----------LLGIQQTAGGGHAAQFLQDMRRYMPP 301

Human TDO  309 QLLTSLMDIDSLMTKWRYNHVCMVHRMLGSKAGTGGSSGY-HYLRSTVSDRYKVFVDLFNLSTYLIP 374
Mouse TDO  309 QLLTSLMDIDTLMTKWRYNHVCMVHRMLGTKAGTGGSSGY-HYLRSTVSDRYKVFVDLFNLSTYLVP 374
Rat TDO    309 QLLTSLMDIDTLMTKWRYNHVCMVHRMLGSKAGTGGSSGY-YYLRSTVSDRYKVFVDLFNLSSYLVP 374
Bovine TDO 309 QLLTFLMDVDSLMTKWRYNHVCLVHRMLGSKAGTGGSSGY-QYLRSTVSDRYKVFVDLFNLSTYLVP 374
Xc TDO     221 SLCEDLVDVETQFQLWRFRHMRTVMRVIGFKRGTGGSSGV-GFLQQALALTF--FPELFDVRTSVGV 284
Rm TDO     238 ELGEKFVDLEDAFRQWRFRHVTTVERVIGFKRGTGGTEGV-SYLRRMLDVVL--FPELWKLRTDL-- 299
Human IDO  302 AHRNFLCSLESN---------PSVREFVLSKGDAGLREAYDACVKALVSLRS--YHLQIVTKYILIP 356

Human TDO  375 RHWIPK----------------MNPTIHKFLYTAEYCDSSYFSSDESD 406
Mouse TDO  375 RHWVPK----------------MNPIIHKFLYTAEYSDSSYFSSDESD 406
Rat TDO    375 RHWIPK----------------MNPIIHKFLYTAEYSDSSYFSSDESD 406
Bovine TDO 375 RHWIPK----------------MNPVIHKFLYTAEYCDSSYFSSDESD 406
Xc TDO     285 DNRPPQ----------------GSADAGKR------------------ 298
Rm TDO         ------------------------------------------------
Human IDO  357 ASQQPKENKTSEDPSKLEAKGTGGTDLMNFLKTVRSTTEKSLLKEG-- 403
```

Figure 3.1 Sequence alignment of human, bovine, mouse, rat, *R. metallidurans* (Rm) and *X. campetris* (Xc) TDO and a comparison with human IDO. Highlighted in blue are active site residues shared between the dioxygenase family residues: F72, H76, F140, R144 and H240 for hTDO. Highlighted in red are the corresponding hIDO residues: F163, S167, F226, R231 and H364.

TDO and IDO catalyse the same reaction but there are a number of differences such as TDO has a tetrameric structure and located primarily in the liver whereas its sister enzyme, IDO, is monomeric in structure and located ubiquitously around the body apart from in the liver. Also the sequence alignment suggests that the important conserved active site residues (highlighted in blue) for different species of TDOs are not shared with IDO in sequence space, whose corresponding residues are shown in red (Figure 3.1).

Table 3.1 Mammalian and bacterial heme-containing dioxygenases, which contain similar active site residues displayed in Figure 3.2.

Species and Enzyme	**Human TDO**	***X. campestris* TDO (*1*)**	***R. metallidurans* TDO (*2*)**	**Human IDO (*10*)**
Residue	H76	H55	H72	S167
	F140	Y113	Y130	F226
	F72	F51	F68	F163
	R144	R117	R134	R231

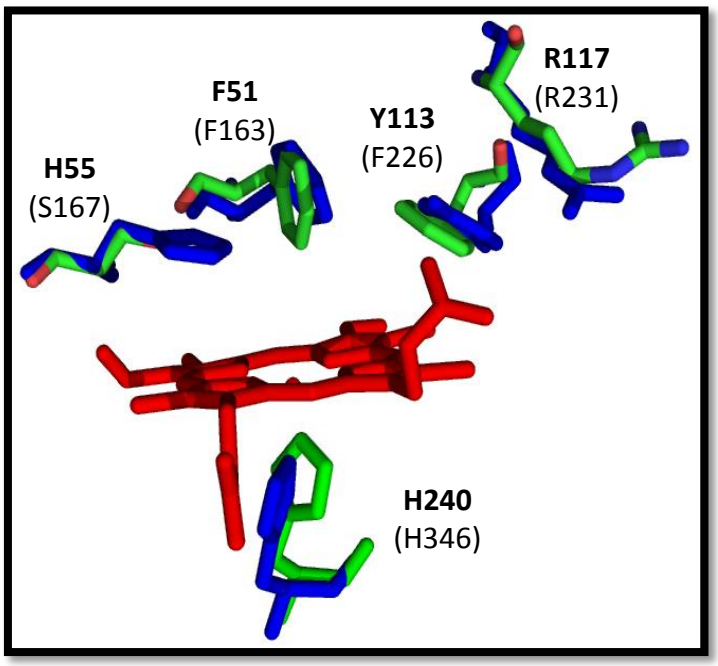

Figure 3.2 Overlaid crystal structures of *X. campestris* TDO (blue, labelled in bold) (*1*) and human IDO (green, labelled in parenthesis) (*10*) showing: histidine (H55), serine (S167), tyrosine (Y113), phenylalanine (F51, F226 and F163) and conserved arginine (R117 and R231) residues.

Since the TDO and IDO crystal structures were solved three to four years ago it was determined that TDO and IDO had very similar active sites as they share many conserved residues, which could not be determined by sequence alignments (Figures 3.1 and 3.2) (*1, 2, 10*). The role and importance of four active site residues were explored in human TDO by making seven variants of TDO. The human TDO residues varied were the distal histidine (residue 76), two phenylalanine residues (72 and 140) and a highly conserved arginine residue (144) (Table 3.1, Figures 3.1, blue residues and 3.2).

Histidine 76

Residue 76 in hTDO is located in the distal pocket of the active site and the variants created to understand this residue were H76A and H76S (Figure 3.2). There are a number of questions regarding the distal histidine which is reported in this chapter:

1) Does the distal histidine have a critical role like that of the distal histidine in the globins?

The distal histidine in the globins acts as a binding site, therefore if the histidine in TDO has a similar role, the variant should be rendered inactive (*11, 12*).

2) Why does IDO have a serine and TDOs have histidine?

The distal histidine is a conserved residue in mammalian and bacterial TDOs but not for IDOs (Table 3.1, Figures 3.1 and 3.2).

3) Why can IDO form a stable ferrous-oxy complex and TDO cannot (*1, 13-15*)?

The role of serine 167 in rhIDO was determined as not essential for oxygen or substrate binding when varied to an alanine residue however, when serine was changed by site-directed mutagenesis to histidine, which is a typical residue for the TDO active site, the ferrous-oxy complex became unstable, which is a TDO characteristic (*16*). The unstable ferrous-oxy complex suggested that the role of serine in IDO was for hydrogen bond stabilisation of the catalytic ferrous-oxy

complex, which involves active site water molecules (*16*). Therefore varying the distal histidine of human TDO to serine would provide useful information for whether TDO could display any IDO characteristics and for determining the role of the distal histidine residue.

4) Is the substrate binding affinity affected, as the histidine residue forms a hydrogen bond which stabilises the substrate (Figure 3.3)?

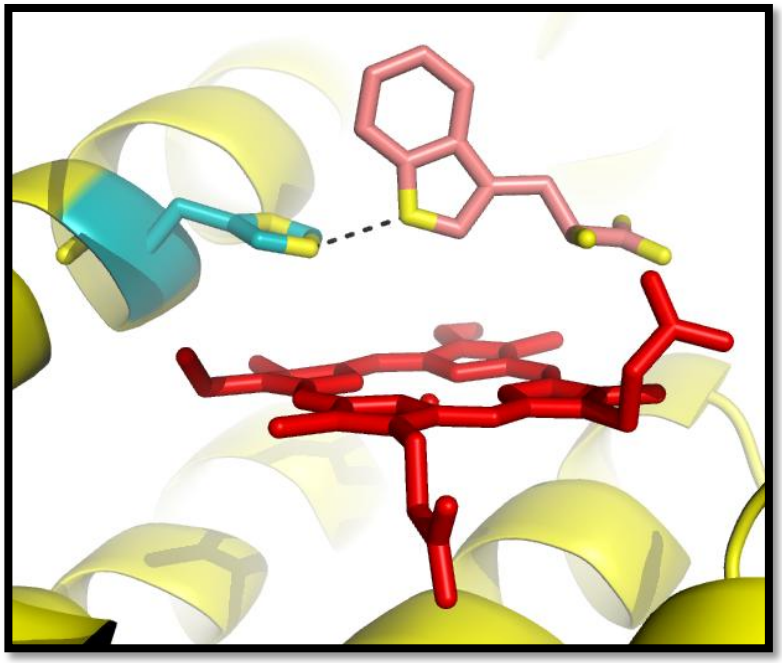

Figure 3.3 X. campestris TDO showing the hydrogen bond between the distal histidine (H55, blue) and L-tryptophan (pink).

Phenylalanine 72

Non-polar hydrophobic residues are in abundance in the active sites of heme containing dioxygenases TDO and IDO (Figure 3.4), so the variant F72A was created to answer two questions:

1) Is hydrophobicity of the active site necessary for the catalytic mechanism, as other heme containing proteins function without such hydrophobic active sites (such as cytochrome P450s and globins (Figure 3.4))?

2) Phenylalanine 72 in human TDO is located in the distal pocket of the active site and when the same conserved residue was changed to alanine in *R. metallidurans* TDO the enzyme was deemed inactive for the substrate L-tryptophan (*2*). Does human TDO produce a similar result (Table 3.1)?

Phenylalanine 140

An interesting phenomenon in the dioxygenase family is that the hydrophobic residues are conserved between TDO and IDO. However ~50 % of heme containing dioxygenases have a phenylalanine whilst the others have a tyrosine at one conserved hydrophobic residue point (Table 3.1, Figures 3.1, 3.2 and 3.4). The variants which were made to further understand this residue in hTDO were F140A and F140Y. The following questions were posed:

1) Is the hydrophobic residue important for the role of the enzyme, (a similar question as for the F72 variant)?

2) Why do some of the dioxygenases have tyrosine and others have phenylalanine? Tyrosine was changed by site-directed mutagenesis in *R. metallidurans* TDO to the amino acid phenylalanine and the Y113F variant of *R. metallidurans* TDO showed a 15-fold increase in activity compared to wild type TDO using L-tryptophan as a substrate (*2*).

3) What is the role of phenylalanine and the role of tyrosine in the active site, does it have structural importance and/or during evolution did it not matter which hydrophobic aromatic residue was used?

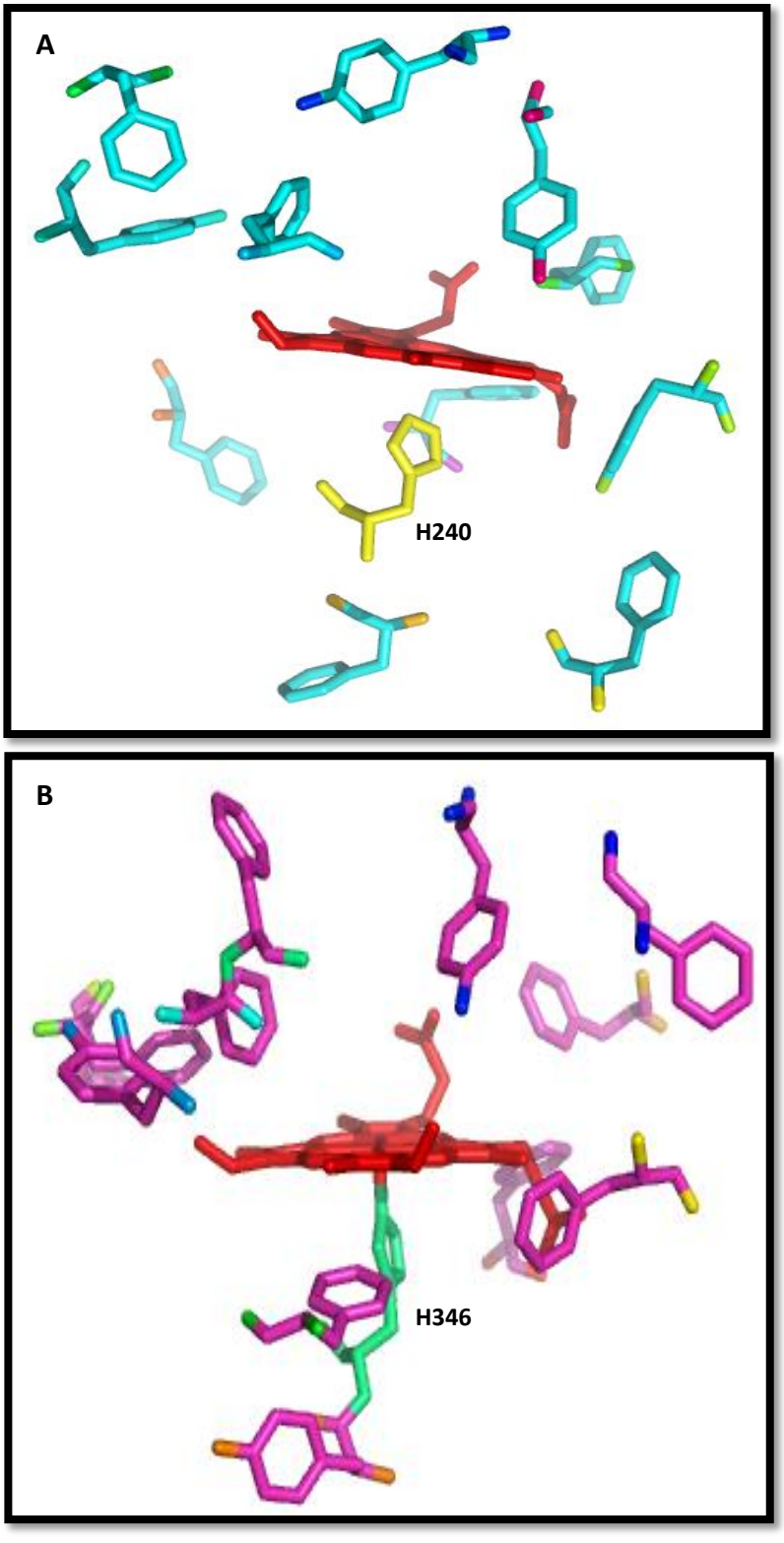

Figure 3.4 Crystal structures of the hydrophobic phenylalanine and tyrosine residues in the active sites of (A) *X. campestris* TDO (blue) (*1*) and (B) rhIDO (purple) (*10*).

Arginine 144

The amino acid arginine is highly conserved in all heme containing dioxygenase enzymes (Table 3.1, Figure 3.2) and in the last three years the crystal structures of *X. campestris* TDO for ferric and ferrous with L-tryptophan bound were solved (Figure 3.5) (*1*). The structures showed that in the absence of L-tryptophan the arginine is in a different position to when TDO has tryptophan bound, with bidentate ion-pair interaction in the distal pocket of the active site with the guanidinim group side chains of the residue R117 interacting with the carboxylate group of L-tryptophan (Figure 3.5) (*1*). The arginine variants made were R144A and R144K to answer the following questions:

1) The arginine residue is highly conserved and appears to hold one side of the tryptophan in place in the active site, when it is removed can the enzyme still bind and turnover substrate?

R134 in *R. metallidurans* TDO was changed by site-directed mutagenesis to alanine and the enzyme was no longer active (*2*).

2) Can the enzyme still turnover substrate by a single interaction with lysine instead of two interactions as observed with arginine?

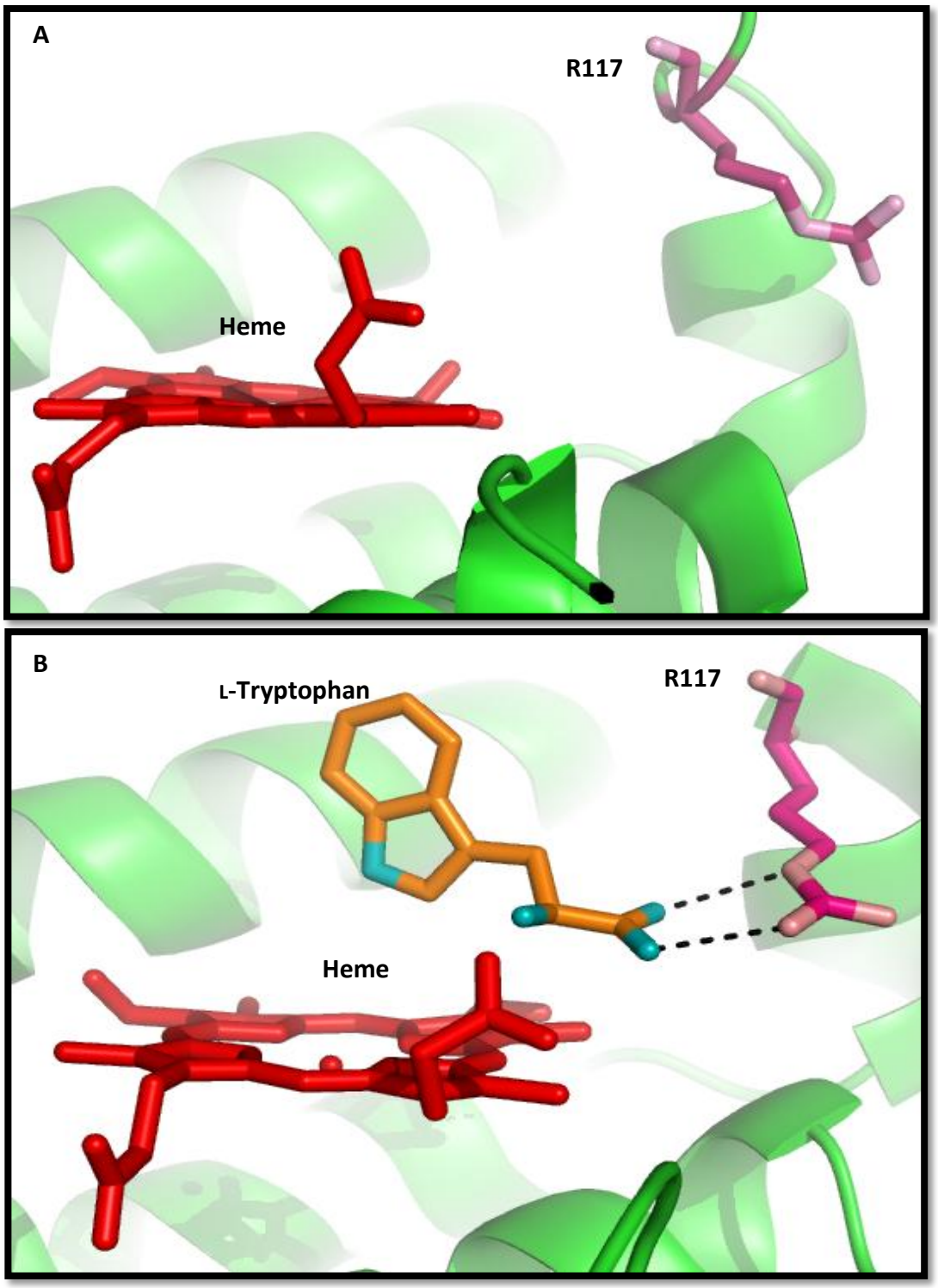

Figure 3.5 The crystal structures of (**A**) substrate-free ferric *X. campestris* TDO and (**B**) ferrous *X. campestris* TDO in complex with L-tryptophan (orange), showing the active site residues R117 (pink) in different positions and the hydrogen bond interactions (black).

3.1 Mutagenesis

The polymerase chain reaction was employed on the human TDO cDNA (contained in the vector pET28a, Figure 3.6) to create seven variants of TDO by site directed mutagenesis. The variants created were H76A, H76S, F72A, F140A, F140Y, R144A and R144K by the PROTEX laboratory[1] using primers which were designed with reference to the nucleic acid sequence and the expression vector pLEICS5 (University of Leicester) (Figure 3.6 and Chapter 7, Table 7.1).

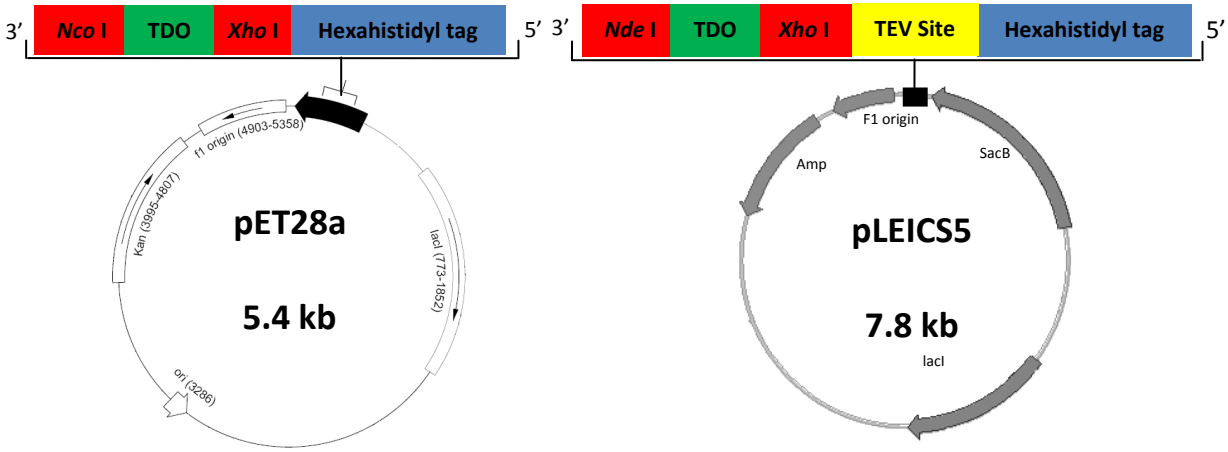

Figure 3.6 The expression vectors pET28a (Novagen) and pLEICS5 (University of Leicester), with the gene sequence TDO (green) inserted in the multiple cloning site of pLEICS5 between two restriction sites (red), with a C-terminal hexahistidyl tag (blue), a TEV cleavage site (yellow) and ampicillin resistance.

The pLEICS5 vector was selected as it was similar to the pET28a vector as both vectors have a C-terminal hexahistidyl tag and restriction sites on either site of the TDO sequence however, the pLEICS5 vector also has a Tobacco Etch Virus (TEV) protease cleavage site for removal of a C-terminal hexahistidyl tag using TEV protease (*17*) (Chapter 7, Section 7.4.4). There are a variety of methods incorporated in vectors for cleaving a hexahistidyl tag after purification including

[1] Mutagenesis carried out by Dr. X. Yang

factor Xa, thrombin or enterokinase, however a vector with a TEV site (amino acid sequence ENLYFQS) cleavable by TEV protease was selected due to its high sequence specificity and stringency (*17*) (Chapter 7, Section 7.4.4). Sequencing of each TDO variant by the Protein and Nucleic Acid Chemistry Laboratory (PNACL) confirmed that no spurious mutations occurred during PCR (Appendix II, Figures A2.2- A2.9, Chapter 7, Section 7.2.2).

3.2 Expression and Purification

The variants were expressed, isolated and purified according to experimental section 7.4, Chapter 7, which were exactly the same methods for rhTDO presented in Chapter 2. After purification an SDS-PAGE gel was run to determine the purity of the protein (Figure 3.7) and trypsin digestion of each sample of the variants of rhTDO enzyme were carried out, followed by MALDI-ToF mass spectrometry which gave clear indications that the protein bands at ~47 kDa were the correct enzymes and size, (Appendix III, Figures A3.2-A3.9, Chapter 7, section 7.4.8).

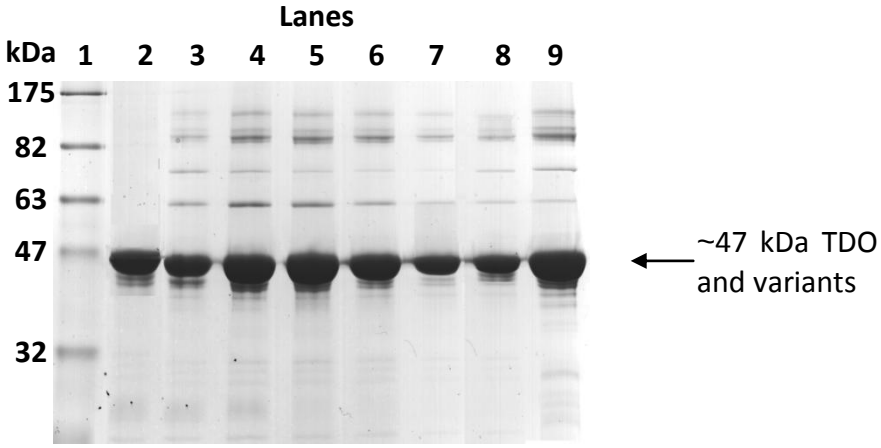

Figure 3.7 SDS-PAGE gel (12%) showing: Lane 1 broad stain protein marker; Lane 2 wild type TDO; Lane 3 H76A; Lane 4 H76S; Lane 5 F72A; Lane 6 F140A; Lane 7 F140Y; Lane 8 R144A; Lane 9 R144K.

The H76S and R144A variants of rhTDO were found to exist as a mixture of apo- and holo-enzyme forms, therefore reconstitution was necessary by addition of

appropriate volumes of hemin (Chapter 7, Section 7.4.6). The concentration of each protein was calculated using absorption coefficients determined by the pyridine hemochromagen method (Appendix IV Table A4.1, Chapter 7, Section 7.5.3). Purified proteins (~1.0 mg/L) were obtained with $R_Z > 0.7$.

3.3 Electronic Absorption Spectroscopy

The UV-visible spectra of ferric and ferrous rhTDO, H76A, H76S, F72A, F140A, F140Y, R144A and R144K are presented in Figure 3.8. Analysis of the electronic spectra of H76S and F140A ferric rhTDO variants revealed wavelength maxima that are similar to those for rhTDO (Table 3.2); the ferric form of rhTDO has maxima at 409, 531, and 630 nm (Table 3.2 and Figure 3.8, black spectra), consistent with there being a mixture of high- and low-spin heme species (*13*). H76A, F72A, F140Y R144A, and R144K TDO variants were slightly different as they consist of a higher proportion of low-spin species, which were indicated by peaks around 535 and 565 nm.

The electronic spectra of the ferrous derivatives of H76A, H76S, F72A, F140A, F140Y, R144A and R144K are essentially identical to that of rhTDO (Figure 3.8 (green spectra), Table 3.2). Reduction of ferric rhTDO resulted in a red shift in the Soret band and the formation of a sharp peak in the visible region (556 nm), which is consistent with the formation of a five-coordinate high-spin species observed by all TDOs; therefore, a similar coordination geometry can be assumed to exist in the ferrous derivatives of the variants.

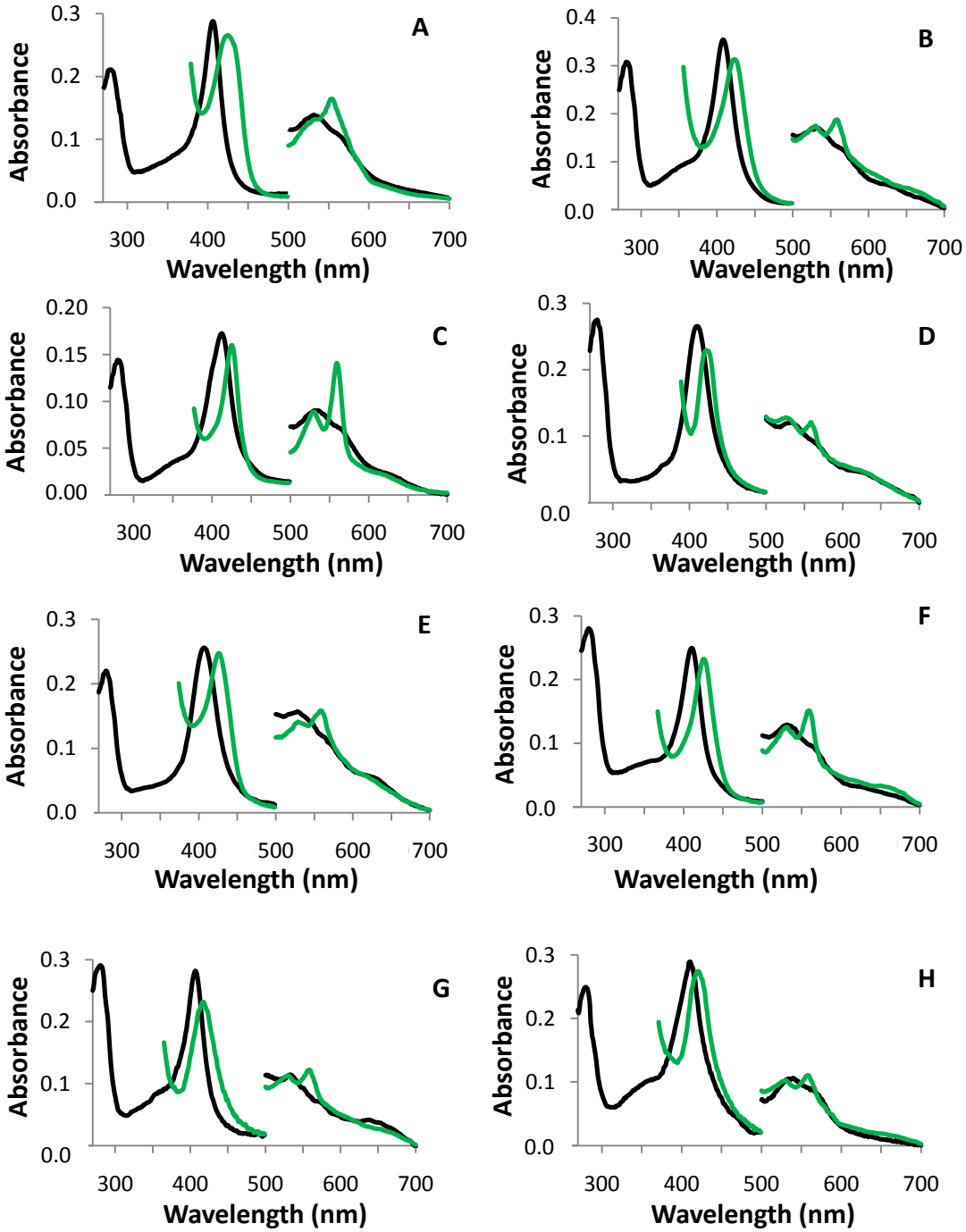

Figure 3.8. UV-visible spectra of ferric (black) and ferrous (green) (**A**) rhTDO, (**B**) F72A, (**C**) H76A, (**D**) H76S, (**E**) F140A, (**F**) F140Y, (**G**) R144A and (**H**) R144K. Absorbance values in the visible region have been multiplied by a factor of 5. Conditions: 50 mM Tris, pH 8.0.

Table 3.2 Absorption maxima for various ferric and ferrous derivatives of rhTDO and the H76A, H76S, F72A, F140A, F140Y, R144A and R144K variants of rhTDO (Chapter 7, section 7.5). Conditions: 50 mM Tris, pH 8.0.

Derivative	λ_{max} (nm)							
	rhTDO	**H76A**	**H76S**	**F140A**	**F140Y**	**F72A**	**R144A**	**R144K**
Ferric	406, 531, 630^{sh}	410, 532, 565^{sh} 631	407, 530, 632^{sh}	410, 531, 660^{sh}	407, 532, 566^{sh}, 660^{sh}	412, 535, 571^{sh}, 635^{sh}	412, 539, 571^{sh}	407, 533, 570^{sh}
Ferrous	425, 531, 554	423, 527, 558	426, 531, 559	426, 532, 560	423, 531, 559	426, 530, 560	422, 530, 557	426, 530, 560
Ferrous-Oxy	413	414	413	418	412	415	412	411
Ferrous + L-Tryptophan	422, 556	418, 531, 554	426, 530, 559	427, 530, 559	424, 530, 559	426, 531, 560	424, 539, 558	426, 558,
Ferrous-Cyanide	431, 535, 566	428, 535, 564	429, 535, 563	428, 532, 562	428, 532, 563	429, 533, 562	430, 535, 562	431, 534, 565, 668
Ferrous-CO	420, 533, 564	419, 532, 562	419, 534, 563	419, 535, 563	420, 533, 559	420, 534, 563	419, 535, 563	420, 534. 563
Ferrous-CO + L-Tryptophan	420, 533, 564	419, 532, 562	419, 533, 564	420, 534, 563	421, 531, 561	420, 533, 563	420, 536, 564	421, 533, 561
Ferric + L-Tryptophan	408, 535, 568^{sh}	410, 534, 564^{sh}	410, 530, 565^{sh}	411, 532, 564^{sh}	410, 533, 562^{sh}	412, 533, 562	412, 530, 563^{sh}	410, 531, 566^{sh}
Ferric-Azide	407, 535, 563^{sh}	411, 535, 565^{sh}	407, 532, 563^{sh}	409, 531, 562^{sh}	408, 533, 564^{sh}	411, 532, 564^{sh}	412, 535, 563^{sh}	408, 533, 564^{sh}
Ferric-Fluoride	406, 528, 626	409	406, 530, 630	-	-	-	-	-
Ferric-Cyanide	419, 540, 565	417, 540, 563	417, 536, 564	417, 541, 575^{sh}	417, 540, 565	416, 540, 565	419, 545, 566	419, 540, 563^{sh}

^{Sh}=shoulder

3.4 EPR Spectroscopy

EPR spectroscopy was carried out at the University of Leicester with Dr. Harriet Seward and with the technical assistance of Dr. Gerry Griffith and was used as a means of providing further information on the heme coordination geometry in rhTDO variants in comparison to rhTDO (*18, 19*). All rhTDO variants; H76A, H76S, F72A, F140A, F140Y, R144A and R144K were analysed by low-temperature X-band EPR. Their spectra were essentially the same for all variants apart from R144A, and therefore the H76A spectra are shown as a representative example and the rest are presented in Appendix VI, Section 6.3.

The rhTDO variant spectra contain an axial species (g_{xy} = 5.96, g_z = 1.99) typical of high-spin ferric heme (Figure 3.9, black spectra), which was also observed for wild type TDO. There is also a trace of rhombic high-spin heme, which is shown by the breadth of the high-spin signal and any structure at $g > 6$. The presence of a majority low-spin form is evident (g values = 2.94, 2.3 and 1.5, Figure 3.9). This species accounts for 80 μM of a 150 μM sample in H76A, for example (*20*). These high- and low-spin species correlate with those observed for rhTDO (g = 5.71, 2.10 and g = 2.89, 2.30, 1.62 respectively (*13*)) and rhIDO (g = 5.82, 1.99 and g = 2.85, 2.27, 1.62, respectively (*16*)) and are likely to arise from bis-nitrogeneous axial heme ligation. There is a high proportion of high-spin heme for the rhTDO variants, which was also observed for ferric rhTDO, which is not typical compared to other dioxygenases such as rhIDO (*14*). The signal observed at g = 4.23 arises from adventitious tetrahedral high-spin ferric iron present in the sample or buffers and is a common contaminant in heme containing enzymes.

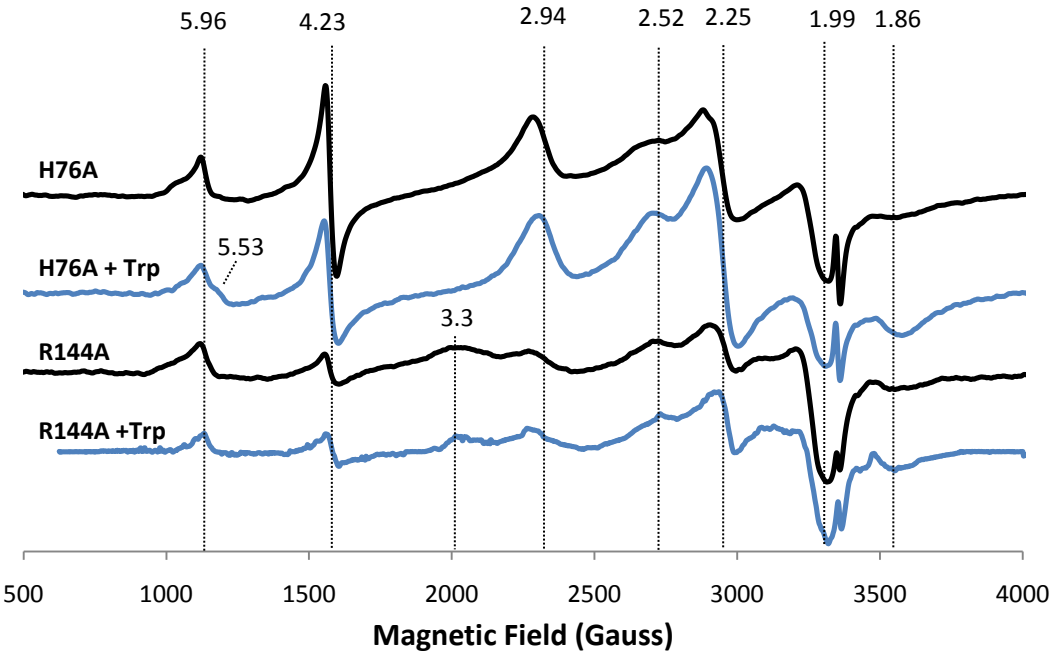

Figure 3.9 X-band EPR spectra of two rhTDO variants, H76A and R144A in the absence (black) and presence (blue) of 3 mM L-tryptophan as a representation for the other variants. Conditions: 11 K, 2.0 mW microwave power, frequency 9.51 GHz, modulation amplitude 1 mT.

On addition of substrate (Figure 3.9, blue spectra), there is a slight decrease in the level of the high-spin species coupled with the increase of a new low-spin form with *g*-values of 2.52, (2.18, obscured) and 1.86, which are likely to arise from hydroxide-bound heme, which is in agreement with the UV–visible data presented above and was also seen for rhTDO and rhIDO (*14*). An additional low-spin species was observed only in the spectrum of the R144A rhTDO variant at g_z =3.3, which is in the range expected for bis-nitrogeneous ligation. In the case of bis-histidine ligation it would indicate an increase in the angle between imidazole group planes from co-planarity (*18*).

3.5 Binding of Non-Catalytic Ligands

As mentioned in Chapter 2, the analysis of exogenous ligands bound at the heme iron provides further information about the distal coordination environment. The representative spectra for the ferric anionic ligand-bound derivatives of rhTDO are presented in Figure 3.10 and the absorption maxima for rhTDO and its variants are presented in Table 3.2. The absorption maxima for the cyanide derivatives of rhTDO and variants are consistent with the formation of a six-coordinate, low-spin species with a red-shift of the Soret band, the disappearance of the CT_1 band and the distinctive peaks at 540 and 565 nm in the visible region (Figure 3.10, blue spectrum). A predominantly low-spin species containing small amounts of high-spin character was observed upon azide binding to rhTDO and its variants, whilst binding of fluoride results in a high-spin six-coordinate species (Figure 3.10, pink and green spectra).

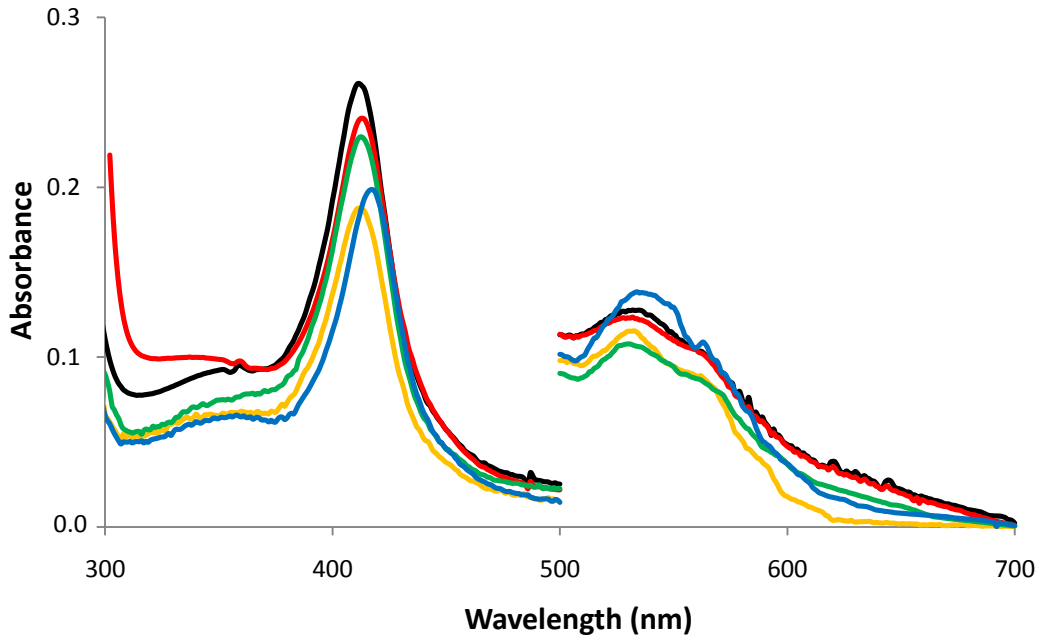

Figure 3.10 Representative data set for the absorption spectra of ferric anionic ligand-bound derivatives of the rhTDO variant F140Y: ferric F140Y (black), ferric-tryptophan (red) ferric-cyanide (blue), ferric-azide (yellow) and ferric-fluoride (green). Absorbance values in the visible region have been multiplied by a factor of 5. Conditions: 50 mM Tris-HCl, pH 8.0, 25.0 ˚C.

L-Tryptophan is classified as a non-catalytic ligand in this chapter because unlike wild type TDO the ferric variants are inactive with the substrate L-tryptophan in an aerobic environment, which is discussed later in the chapter. On addition of 1 mM L-tryptophan to all ferric rhTDO variants a red shift of the Soret band, increases in the low-spin signatures at 535 and 568 nm, and decreases in absorbance at 630 nm is observed. All of which were consistent with the formation of a low-spin heme species on addition of substrate as observed for other human TDOs (Figure 3.10 red spectrum and Appendix VI, Section 6.2 shows UV-visible spectra in the absence and presence of L-tryptophan for the other rhTDO variants) (*13, 21*).

3.6 Binding of Cyanide and L-Tryptophan to Ferric rhTDO

The TDO variants with mutations at H76, F72, F140 and R144 were found to bind cyanide with a similar affinity to rhTDO (K_D of 31 ± 1 μM), which was determined by equilibrium binding measurements, which are in agreement with the spectroscopic data (Table 5.3) (*13*). Figure 3.11 shows a representative family of spectra collected for the TDO variant F140A during the titration of the exogenous ligand cyanide, all other variants including wild type TDO had similar absorption changes. This titration and section 3.5 of this chapter, regarding binding of non-catalytic ligands, suggests that wild type and the variants of TDO have the ability to bind exogenous ligands and furthermore that there are no internal ligands ligated to the sixth coordination site, which has previously occurred after creating a heme peroxidase variant (*22*).

Table 3.3 Thermodynamic parameters for the binding of cyanide and L-tryptophan to ferric rhTDO and the variants. Conditions: 50 mM Tris buffer, pH 8.0, 25.0 ^{o}C.

	WT TDO	H76A	H76S	F140A	F140Y	F72A	R144A	R144K
Cyanide K_D (μM)	31 ± 1	11± 1	48 ± 3	65 ± 7	51 ± 3	24 ± 2	65 ± 3	15 ± 1
Tryptophan K_D (μM)	162 ± 19	234 ± 14	267 ± 26	544 ± 60	558 ± 61	221 ± 22	1884 ± 228	519 ± 57

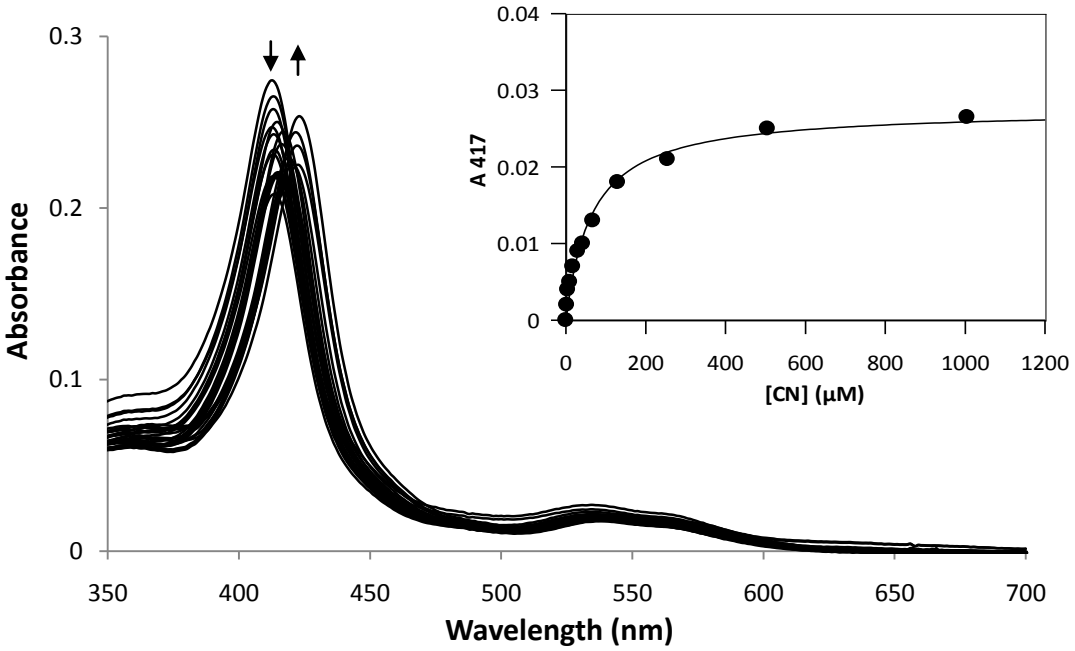

Figure 3.11 Representative data set for the determination of K_D for binding of cyanide to ferric F140A (2 μM). The arrows indicate the direction of changes in absorbance upon successive additions of cyanide. Inset: Fit of data at 417 nm to Equation 7.4, Chapter 7. Conditions: 50 mM Tris-HCl, pH 8.0, 25.0 ^{o}C.

Wild type TDO exhibited characteristic spectroscopic changes upon binding of L-tryptophan (λ_{max} = 408, 535, 568^{sh}) which were consistent with the loss of high-spin heme and the formation of a low-spin, hydroxide-bound species also shown by EPR (Table 3.2, Figures 3.9 and 3.10). Similarly the rhTDO variants H76A, H76S and F72A showed similar absorption changes during the L-tryptophan titrations. This data indicates that the TDO variants bind substrate in a similar mechanism to wild type TDO. The following TDO variants: F140A, F140Y, R144A, R144K had very slightly greater K_D values compared to wild type TDO suggesting that residues F140 and R144 could play important roles in L-tryptophan binding. Figure 3.12 shows the representative family of spectra for H76A during L-tryptophan titrations, which were similar to the absorbance changes observed by the rhTDO and the other TDO variants.

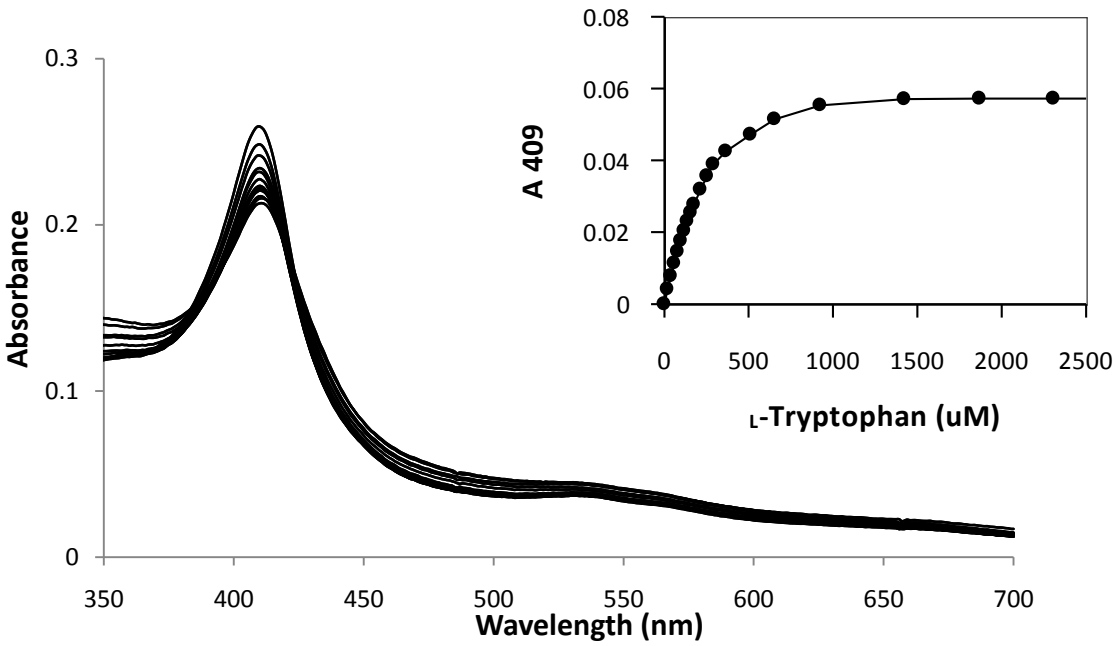

Figure 3.12 Representative data set for the determination of K_D for binding of L-tryptophan to the ferric variant H76A of rhTDO (2 μM). The arrow indicates the direction of change in absorbance upon successive additions of L-tryptophan. Inset: Absorbance change at 409 nm upon successive additions of L-tryptophan and fit of the data (Chapter 7, Equation 7.4). Reaction conditions: 50 mM Tris-HCl, pH 8.0, 25.0 °C.

3.7 Binding of O_2 and CO to ferrous TDO variants

Wild type hTDO could not form a stable ferrous-oxy complex and the TDO variants showed similar spectroscopic changes upon direct bubbling of O_2 gas into a solution of ferrous enzyme (Table 3.2 and Figure 3.13, blue spectrum). The resulting spectra for the TDO variants were all similar, the Soret band was slightly red-shifted and there were no sharp peaks in the visible region (expected at ≈540 and ≈570 nm) that are characteristic of a ferrous-oxy species (Table 3.2 and Figure 3.13, blue spectrum).

As in Chapter 2 the ferrous TDO variants were analysed to observe whether the ferrous heme group was reactive by observing whether the ferrous variants could bind other diatomics such as carbon monoxide and cyanide. All TDO variants

showed a red-shift in the Soret band to approximately 421 nm and distinctive peaks at around 532 and 562 nm appeared as observed for rhTDO (Table 3.2 and Figure 3.13, green spectra) (*13*). Furthermore upon addition of the substrate L-tryptophan (3 mM) to the ferrous-CO complex of the TDO variants, no further spectral changes were observed, which suggests typical binding (Table 3.2). The ferrous rhTDO variants also bound cyanide with similar spectral changes to rhTDO with the formation of sharp peaks at 535 and 564 nm in the visible region (Table 3.2 and Figure 3.13, red spectrum).

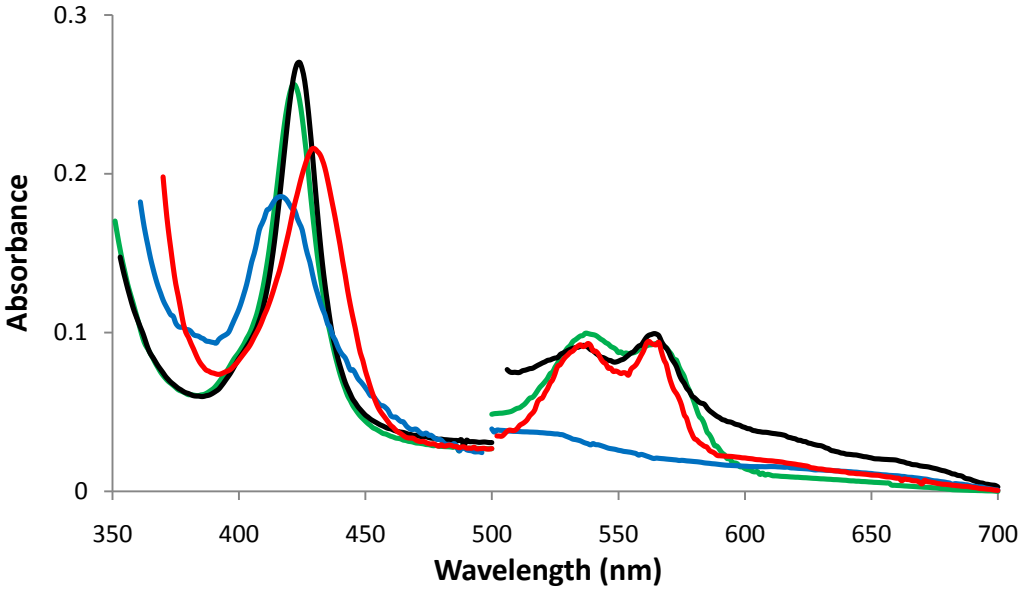

Figure 3.13 Representative electronic absorption spectra of the ferrous R144A variant of rhTDO. UV-visible spectra of the R144A ferrous complex (black) in the presence of O_2 (blue), carbon monoxide (green) and cyanide (red). Absorption values in the visible region have been multiplied by a factor of 5. Reaction conditions: 50 mM Tris-HCl, pH 8.0, 25.0 ^{o}C.

3.8 Steady-state Oxidation of L-Tryptophan and Other Tryptophan Analogues

Steady-state kinetics for the rhTDO variants were carried out with L-tryptophan and its analogues to determine the effect of each mutation on the catalytic properties of rhTDO.

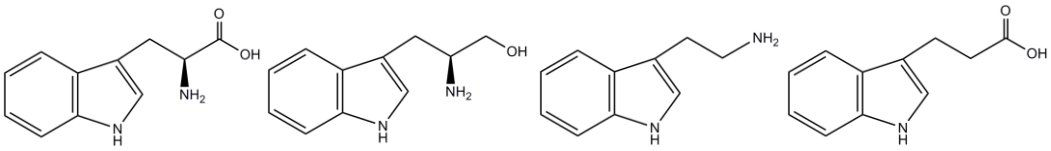

L-Tryptophan **Tryptophanol** **Tryptamine** **Indole-3-propionic Acid**

Scheme 3.2 Structures of L-tryptophan derivatives used in steady-state experiments.

The steady-state data were fitted to the Michaelis-Menten equation (Chapter 7, equation 7.5) and the Michaelis constants (k_{cat} and K_m) are reported in Table 3.4. A representative data set for F140A is presented in Figure 3.14. All variants of TDO had lower affinities for substrate binding and catalysed the oxidation of L-tryptophan at a slower rate in comparison to rhTDO.

The histidine variants of TDO which remained active, which suggests that the histidine residue may not be as crucial to catalytic activity as the phenylalanine and arginine residues. The histidine variants have similar slightly slower rates of turnover and decrease in affinity for substrate binding, which was also observed by the variants of other human TDOs (*23, 24*).

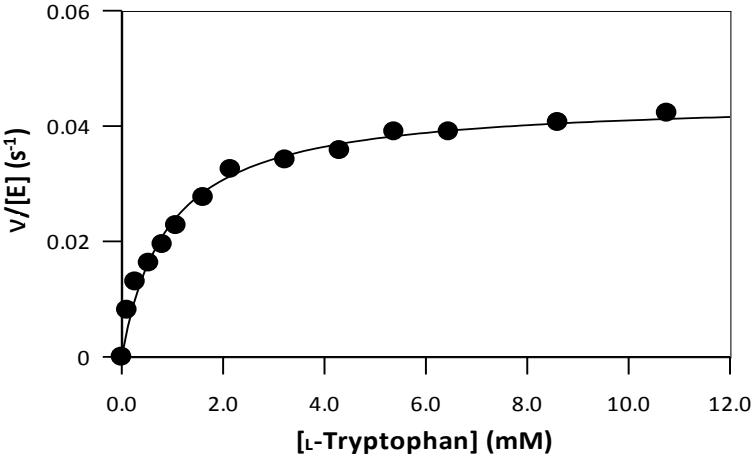

Figure 3.14 A representative data set for the steady-state oxidation of L-tryptophan by the F140A variant of rhTDO. Solid line shows a fit of the data to the Michaelis-Menten Equation (Chapter 7, Equation 7.5)

The F140Y variant had the addition of a hydroxyl group, which caused the rate to reduce by half and had a slightly lower affinity for substrate binding, when the residue F140 was changed with alanine the rate dropped by a factor of ~35 and the substrate binding affinity decreased by a factor of ~5. Also the F72A residue was inactive suggesting that the hydrophobic residues, F140 and F72 play an important role in the catalytic mechanism and substrate recognition.

The rhTDO variant R144A was inactive suggesting that it is a crucial catalytic mechanism residue. Interestingly the R144K was active and had similar turnover rates as the H76S variant, however the affinity for substrate binding was significantly lower for R144K suggesting that the mutation from arginine to lysine was disruptive to substrate binding.

Table 3.4 Steady-state kinetic data for oxidation of L-tryptophan by rhTDO and variants. All data were fitted using the Michaelis-Menten equation (Chapter 7, Equation 7.5) where, each value was an average of at least three independent measurements. Reaction conditions: 50 mM Tris-HCl, pH 8.0, 25.0 ^{o}C

	L-Tryptophan	
Enzyme	k_{cat} (s^{-1})	K_m (μM)
rhTDO	1.40 ± 0.01	169 ± 18
H76A	0.30 ± 0.01	478 ± 52
H76S	0.10 ± 0.01	599 ± 66
F140A	0.040 ± 0.001	917 ± 87
F140Y	0.80 ± 0.02	455 ± 40
F72A	inactive	
R144A	inactive	
R144K	0.16 ± 0.01	828 ± 58

The steady-state parameters for rhTDO variants with L-tryptophanol, tryptamine and indole-3-propionic acid (Scheme 3.2), were determined to analyse substrate-protein interactions in the distal pocket of the variants. No activity was detected for the TDO variants with the tryptophan analogues with modified amino and carboxylate groups, which was the same result as observed for rhTDO (Scheme 3.2) (*13*).

In Chapter 2 rhTDO was shown to be able to turnover substrate in the ferric form in an aerobic environment however, the variants were all inactive in the ferric form.

3.9 Redox Potentiometry

Reduction potentials for the Fe^{3+}/Fe^{2+} couple of rhTDO and the variants were determined using the xanthine/xanthine oxidase assay with simultaneous reduction of a dye of known potential, which was discussed in Chapter 2 [2]. The measured reduction potentials are displayed in Table 3.5 and Figure 3.15 shows a representative family of spectra collected during the Fe^{3+}/Fe^{2+} redox potential for the H76A variant of rhTDO with the dye methylene blue and the corresponding nerst plots (Appendix VI, section A6.1 shows the nerst plots for the other variants of TDO).

Table 3.5 Fe^{2+}/Fe^{3+} Reduction Potentials obtained for rhTDO and the variants. Reaction conditions: 0.1 M potassium phosphate, pH 7.0, 25.0 ^{o}C.

Enzyme	No L-Trp (mV)	+ L-Trp (mV)	Shift
rhTDO	-92 ± 3	-76 ± 3	+16
H76A	-52 ± 2	+2 ± 3	+54
H76S	-119 ± 4	-113 ± 3	+6
F140A	-129 ± 5	-116 ± 3	+13
F140Y	-156 ± 2	-129 ± 4	+27
F72A	-140 ± 1	-139 ± 1	+1
R144A	-133 ± 3	-112 ± 3	+21
R144K	-143 ± 3	-116 ± 2	+27

[2] Results checked by Dr. Igor Efimov.

Reduction potentials for the Fe^{3+}/Fe^{2+} couple of the H76A variant of rhTDO in the absence and presence of L-tryptophan were found to be -52 ± 3 and +2 ± 3 mV, respectively (Figure 3.15). In comparison to rhTDO, the shift of 54 mV in reduction potential is significantly larger on binding of substrate and more positive, which is similar to other heme dioxygenases such as rhIDO which have potential shifts of 46 – 75 mV and 135 mV for *X. campestris* TDO (*1, 13, 14, 16*). The H76A variant is more positive than rhTDO and the rest of the variants which suggests that the enzyme is easier to reduce and hence, there is stabilisation of the ferrous derivative upon binding of substrate.

Reduction potentials for the Fe^{3+}/Fe^{2+} couple of the H76S and F72A variants were significantly smaller compared to rhTDO and other heme dioxygenases (*1, 15, 16*). The minimal shift in redox potential upon binding of substrate and the very negative potentials suggests that H76S and F72A variants have no stabilisation of the ferrous derivative upon binding of substrate and a shift of 1 mV upon addition of substrate, suggests that F72A does not bind the substrate tryptophan.

The reduction potentials for the Fe^{3+}/Fe^{2+} couple of the F140A, F140Y, R144A and R144K variants of rhTDO were found to have similar shifts of redox potential to rhTDO. However, the values in the absence and presence of tryptophan are both more negative compared to rhTDO, which suggests that the variants have not only no stabilisation of the ferrous derivative but they are also harder to reduce, which is significant because they have a lower affinity for binding substrate compared to wild type (*13*).

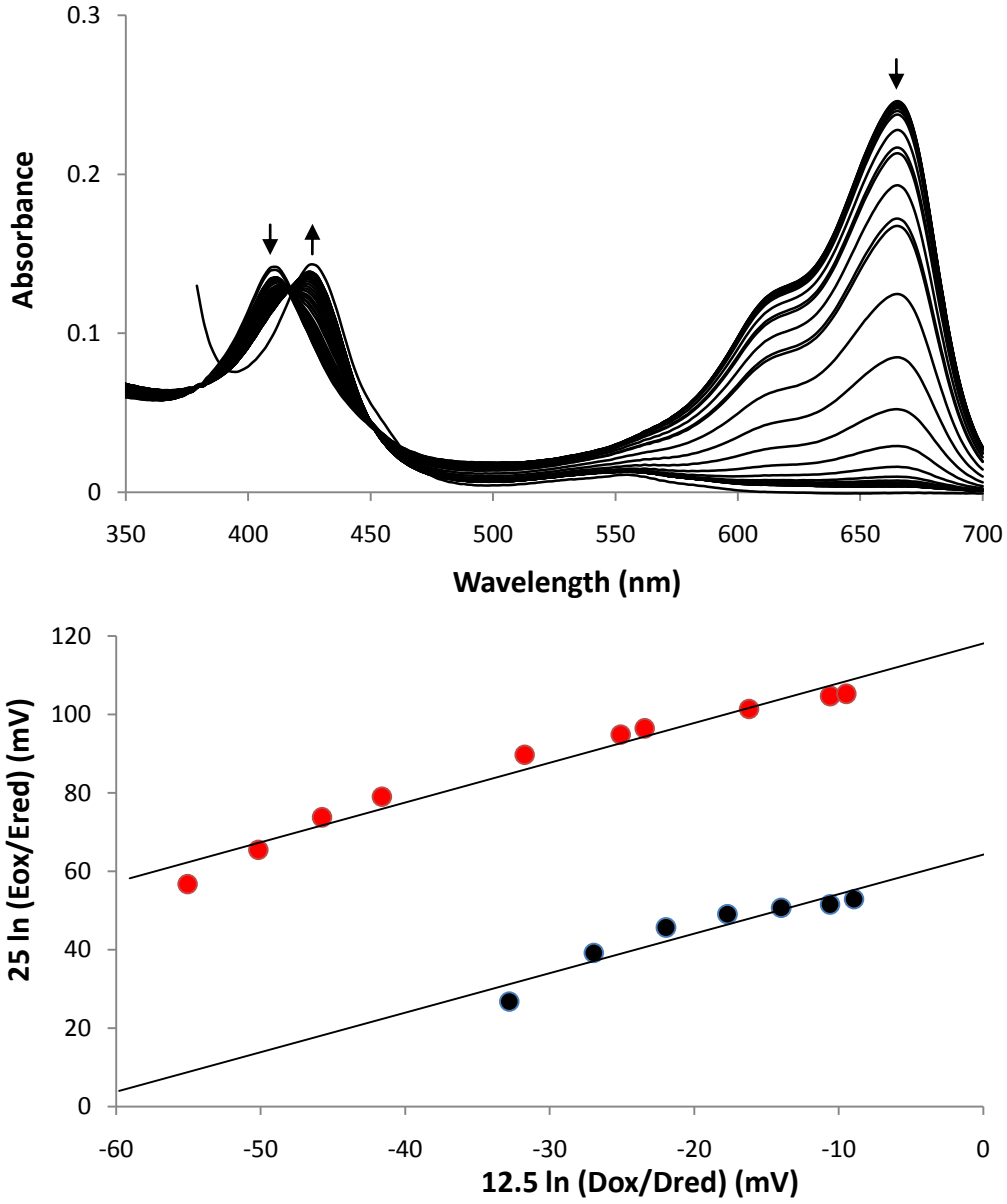

Figure 3.15 Redox potentiometry of the H76A variant of rhTDO. (A) Spectral changes observed during determination of Fe^{3+}/Fe^{2+} reduction potential with the dye methylene blue. Arrows indicate the direction of absorption change during the reductive titration. (B) Nernst plots for the data shown in (A) in the absence (black) and presence of 3 mM substrate (red). Reaction conditions: 100 mM potassium phosphate, pH 7.0, 25.0 °C.

3.10 Discussion

The variants of histidine and serine residues for TDO and IDO respectively were made by site-directed mutagenesis for other dioxygenase constructs, however there is only limited published data regarding variants of other active site residues apart from in Dr. Chauhan's thesis, which focused on rhIDO variants (*1, 2, 15, 16, 23-25*). The crystal structures of bacterial TDO and human IDO provided important information about the active site by structural and sequence alignments (*1, 2, 10*). For this reason, several bacterial expression systems were developed for variants of rhTDO. This work has allowed exploration of the heme-iron coordination environment and provided detailed spectroscopic, kinetic and electrochemical information. The properties of human TDO in comparison with other variants of TDO enzymes will be discussed together with the implications of these data in reference to the current understanding of heme dioxygenase substrate binding, catalytic activity and mechanism.

Histidine Variants

Stability of the Ferrous-Oxy Complex

Interestingly, the rhIDO variant S167H showed destabilisation of the ferrous-oxy complex compared to wild type and variants of rhIDO, which demonstrated that S167H replicated the behaviour observed by rhTDO (*16*). Therefore, suggesting that the distal histidine was a reason that TDOs could not form a stable ferrous-oxy complex. However the rhTDO variant H76S did not show any peaks in the visible region for the ferrous-oxy complex.

S167H had a very low redox potential (-203 mV), and the H76S rhTDO variant had a similarly low redox potential (-119 mV), which showed there would be no stabilisation of the ferrous-oxy complex, however both S167H variant of rhIDO and H76S of rhTDO were still active and bound L-tryptophan normally as evidenced by K_M (*16*). So the unsolved problem is that the formation of the ferrous-oxy complex

is a necessary intermediate in the overall dioxygenase mechanism and it has to be stable enough to interact with the substrate so that product formation can occur, therefore as both S167H and H76S turnover L-tryptophan, a ferrous-oxy complex must be present at some point, which stopped-flow cannot detect (*13, 16*).

None of the full length rhTDO variants formed a stable ferrous-oxy derivative which, is similar to the data presented in Chapter 2 however, a truncated rhTDO with 17 residues removed from both the N- and C-terminals and their H76A and H76S variants could form a ferrous-oxy complex with peaks at 412 and 556 nm observed by UV-visible spectroscopy (*23*). A reason that the truncated TDO could form the ferrous-oxy complex and a ternary complex and rhTDO, H76A and H76S presented in this paper could not, might be due to the removal of C4 and C395, which are conserved residues in mammalian TDOs shown in the sequence alignment (Figure 3.1). The cysteine residues could form disulphide bonds of structural importance which typically prevent mammalian TDOs from forming the ferrous-oxy complex. The Batabyal truncated TDO paper states that the reason both sections were removed from hTDO was to prevent aggregation and the sections were chosen as they are not present in bacterial TDOs, *X. campestris* TDO and *P. aeruginosa* TDO, however only the C-terminus was missing from a different bacterial TDO (*R. metallidurans* TDO) and it does contain the N-terminus cysteine, therefore the conserved N-terminus cysteine residue, which was removed from the truncated TDO could have structurally altered the enzyme to allow ferrous-oxy formation (Figure 3.1) (*23*).

Substrate Binding

Both histidine mutants bound L-tryptophan in the ferric form, determined by the K_D, compared to rhTDO, however the variants have an approximately 3-fold decrease in affinity for substrate (K_m) and a 5- to 14- fold decrease in k_{cat} in the ferrous form. The decrease in K_m and rate of turnover was suggested to be caused by the change in position of L-tryptophan in the active site of the variants compared to wild type, which was determined by comparison of *X. campestris* TDO crystal structures for wild type, H55A and H55S (*15*). These data therefore support

the hypothesis that the role of the histidine residue in TDOs is for controlling binding affinity of the active site substrate and that the hydrogen bond to the substrate holds L-tryptophan in the optimum position for turnover (Figure 3.3) (*15*).

Activity Analysis

Before the structures of hTDO and hIDO were solved by crystallography, site-directed mutagenesis papers focused on determining which histidine residue was in the proximal pocket and their importance in heme binding (*14, 25*). Two approaches were used. For hIDO, sequence alignments were used to locate the most likely histidines that could be in the proximal pocket, thus only a few histidine mutants were made (*14*). The alternative method used was to make 12 mutants for each of the 12 histidines in rat TDO and substitute them with alanines (*25*). The latter publication provided the first insight into the role of histidines in TDOs and it was discovered that the rat H76A variant had decreased activity but remained active, which was observed for all the rhTDO histidine variants including the results presented in this chapter and *X. campestris* TDO. Therefore, the histidine is not essential for catalysis as the enzymes were not rendered inactive as observed by the globins (*11, 12, 15, 23-25*). The 2001 paper also concluded from size exclusion analyses that specifically the H76A variant retained little or no heme, however all the rhTDO variants either contained heme or had the ability to be reconstituted in this work (*25*).

The rhTDO variants were inactive in the ferric form unlike the wild type enzyme and a similar observation was reported for two truncated rhTDOs, which could suggest that the histidine residue is important mechanistically for the active ferric form (*21, 23, 24*). Unlike the rhTDOs, *X. campestris* TDO was inactive in both the wild type and histidine mutant forms (*15*).

Histidine Variant Conclusions

Several conclusions can be drawn in answer to the questions posed at the beginning of the chapter. The distal histidine is not a conserved residue in dioxygenases therefore the long standing mechanism that the histidine acts as an

active site base is unlikely as the S167 in rhIDO was shown not to affect the catalytic properties of the mechanism and serine was the only polar residue located close enough to the heme to act as an active site base. Also the rhTDO histidine variants could turn over substrate which confirms that the histidine is not involved in the catalytic mechanism as a base. Therefore the role of the histidine in dioxygenases is different to the role of the distal histidine in globins, which is located directly above the iron and is poised to hydrogen bond to the bound dioxygen (*11, 12*).

Phenylalanine Variants

The active sites of dioxygenases are abundant in phenylalanine and tyrosine residues (Figure 3.4). The only published data for hydrophobic aromatic residues was Y42F for rhTDO, F68A and Y130F for *R. metallidurans* TDO (*2, 24*). Dr. Chauhan and Dr. Basran made and studied several phenylalanine variants for rhIDO: F163A, F164A, F226A and F226Y, of which three out of four of the corresponding variants (F163A, F226A and F226Y) were made and analysed in this chapter for rhTDO (Table 3.1)[3]. The F72A variant for rhTDO was chosen because it is the closest aromatic residue to the substrate L-tryptophan and also to the heme iron determined from a structural alignment between the substrate-bound *X. campestris* TDO and rhIDO (Figure 3.2).

TDO is a tetramer and the N-terminal located tyrosine is a highly conserved residue in dioxygenases (the corresponding residue of rhTDO Y42 is Y27 in *X. campestris* TDO). It is located on one of the four arms which join each of the subunits together and also the tyrosine residue participates in the active site of the adjacent subunit, which was not chosen as a variant to study in this chapter as the two closest most likely to be interesting residues to the active site were chosen (F72 and F140).

[3] Data published in Dr. Chauhan's thesis 2009 University of Leicester.

Substrate Binding for the F72A Variant

The UV-visible spectrum of both F72A for rhTDO and F163 for rhIDO had very similar characteristics compared to their wild type enzymes, and the variants were able to bind numerous typical exogenous ligands. The F72A variant for rhTDO and F163A variant for rhIDO had similar affinities to bind substrate in the ferric form compared to each wild type (K_D = 221 ± 22 μM and 450 ± 30 μM respectively). However, there was a significant decrease in binding of substrate to the ferrous form indicated by the K_m. F72A for rhTDO and F68A for *R. metallidurans* TDO were inactive and upon addition of substrate to F72A during the redox potential, a shift of only 1 ± 1 mV was observed, which suggested no binding or stabilisation of the ferrous form (*2*). Similar results were observed for the F163A variant of rhIDO, steady-state analysis showed that the variant had lost a large proportion of its activity (k_{cat} = 0.030 ± 0.001 s^{-1}), the K_m increased by a factor of 7 compared to the wild type (47 ± 5 mM) and the redox potential in the absence and presence of substrate was -119 ± 3 mV and -113 ± 4 mV respectively, which also supports in hypothesis that there was no stabilisation of the ferrous derivative. Collectively, this information suggests that this phenylalanine residue is important for orientating the substrate L-tryptophan to the optimum position for catalysis and thus has a similar role to the distal histidine in the active site of rhTDO. Removal of the residue creates space in the pocket which allows the L-tryptophan to move, however the phenylalanine residue unlike the histidine is not bonded to the substrate.

Substrate Binding for the F140 Variant

The variants of the residue F140 for rhTDO and F226 for rhIDO are compared to the Y130F for *R. metallidurans* TDO to determine the importance of the residue and to determine a reason for some dioxygenases containing phenylalanine and others containing tyrosine in the active site (*2*).

The F140A variant of rhTDO and the F226A variant of rhIDO both catalysed oxidation of L-tryptophan with a slightly slower turnover number than the wild

type enzymes (k_{cat} = 0.040 ± 0.001 s^{-1} and 0.39 ± 0.01 s^{-1} respectively), however the binding affinity for substrate was very high (K_m = 917 ± 87 μM and 940 ± 69 μM respectively). This suggests that the role of this particular phenylalanine residue in the active site provides π-π stacking interactions with the benzene ring of L-tryptophan and is important in maintaining the overall hydrophobicity of the substrate binding pocket.

The F140Y and F226Y variants for rhTDO and rhIDO had no significant effect on substrate binding or catalytic mechanism, suggesting that the addition of the hydroxyl group did not alter the structure or function of the enzyme. In contrast changing tyrosine to phenylalanine in *R. metallidurans* TDO (Y130F) altered the catalytic activity of the enzyme significantly, evidenced by a 15-fold increase in activity with L-tryptophan compared to wild type (data not provided in publication) (*2*), which suggests that removal of the hydroxyl group removes a hydrogen bond, which allows more flexibility in the active site for optimum positioning of the substrate, which requires lower activation energy to oxidise into product. Overall the TDO and IDO wild type enzymes both catalyse substrate oxidation and there is no obvious reason as to why some dioxygenase have phenylalanine and others have tyrosine.

Phenylalanine Variant Conclusion

The phenylalanine and tyrosine variants affect the structure and function of dioxygenases when changed to an alanine in the active site, which implies that the highly conserved residues making the hydrophobic pocket are significant for the catalytic mechanism and positioning of the substrate. The hydrophobic pocket is made up of phenylanine and tyrosine residues. The data suggest that swapping the residues by addition or removal of a hydroxyl group has minimal effect on the function or the structure of the enzyme. Furthermore the Y42F variant of a truncated rhTDO appeared to have even less of an effect on the active site because as mentioned earlier none of the ferric forms of the rhTDO variants were active however, the Y42F variant for a truncated rhTDO retained 3 % of its activity suggesting that the mutation did not change the enzyme significantly compared to

the other phenylalanine and tyrosine variants (*24*). During evolution the phenylalanine and tyrosine residues could have interchanged with no consequence on the enzyme, therefore giving neither the tyrosine or phenylalanine dioxygenases a selective survival advantage.

Arginine Variants

The crystal structure of *X. campestris* TDO showed that in the absence and presence of substrate that the arginine changed position, so two variants were made to explore this residue R144A and R144K of rhTDO (Figure 3.5) (*1*). R231K was also constructed for rhIDO by Dr. Chauhan[4] and R134A was made for studying the effects on *R. metallidurans* TDO (*2*).

As expected, changing arginine to alanine renders the enzyme inactive for R144A and R134A. Interestingly the EPR data obtained for R144A showed an atypical signal compared to wild type and the other variants upon addition of substate, indicating an additional low-spin species at g_z = 3.3, which indicated that due to the missing arginine the substrate had changed position so the angles between the histidine imidazole planes are perpendicular to the heme. In bis-histidine axial ligation the angles can twist from parallel (g = 2.95, 2.26, 1.5) to perpendicular (g = 4, 0, 0), making g_z = 3.3 somewhere in between (*19*).

Replacement of highly conserved arginine with lysine to explore the interactions with substrate provided interesting information. Both R144K for rhTDO and R231K for rhIDO remained active and reduced the turnover rate slightly (k_{cat} = 0.10 ± 0.01 s^{-1} and 0.31 ± 0.013 s^{-1} respectively) but did significantly alter the binding affinity compared to wild type (K_m = 828 ± 58 µM and 3.3 ± 0.4 mM respectively). This information suggests that the bidenate ion pair interaction could be required for

[4] Data published in Dr. Chauhan's thesis

relatively good binding between the carboxylate group of the substrate and the arginine residue in dioxygenases (Figure 3.5).

Overall Conclusion

In summary of the information presented in this chapter, the site-directed mutagenesis of active site variants in dioxygenases have shown that the dioxygenase class of enzymes do not follow consistent patterns which are seen in the peroxidase and globin enzymes. Furthermore that the highly conserved phenylalanine and arginine residues allow optimum positioning of the substrate in the active site which is required for catalysis. Future work could involve solving crystal structures of the variants which, would aid in further understanding the structure of the enzymes and making some cysteine variants of rhTDO to observe whether they can form a stable ferrous-oxy complex.

3.11 References

1. Forouhar, F., Anderson, J. L., Mowat, C. G., Vorobiev, S. M., Hussain, A., Abashidze, M., Bruckmann, C., Thackray, S. J., Seetharaman, J., Tucker, T., Xiao, R., Ma, L. C., Zhao, L., Acton, T. B., Montelione, G. T., Chapman, S. K., and Tong, L. (2007) Molecular insights into substrate recognition and catalysis by tryptophan 2,3-dioxygenase, *PNAS 104*, 473-478.
2. Zhang, Y., Kang, S. A., Mukherjee, T., Bale, S., Crane, B. R., Begley, T. P., and Ealick, S. E. (2007) Crystal structure and mechanism of tryptophan 2,3-dioxygenase, a heme enzyme involved in tryptophan catabolism and in quinolinate biosynthesis, *Biochemistry 46*, 145-155.
3. Manandhar, S. P., Shimada, H., Nagano, S., Egawa, T., and Ishimura, Y. (2002) Subunit structure of recombinant rat liver L-tryptophan 2,3-dioxygenase, *International Congress Series 1233*, 161-169.
4. Watanabe, Y., Fujiwara, M., Yoshida, R., and Hayaishi, O. (1980) Stereospecificity of hepatic L-tryptophan 2,3-dioxygenase, *Biochem J 189*, 393-405.

5. Searles, L. L., Ruth, R. S., Pret, A. M., Fridell, R. A., and Ali, A. J. (1990) Structure and transcription of the Drosophila melanogaster vermilion gene and several mutant alleles, *Mol Cell Biol 10*, 1423-1431.

6. Comings, D. E., Muhleman, D., Dietz, G., Sherman, M., and Forest, G. L. (1995) Sequence of human tryptophan 2,3-dioxygenase (TDO2): presence of a glucocorticoid response-like element composed of a GTT repeat and an intronic CCCCT repeat, *Genomics 29*, 390-396.

7. Mukabayire, O., Cornel, A. J., Dotson, E. M., Collins, F. H., and Besansky, N. J. (1996) The Tryptophan oxygenase gene of Anopheles gambiae, *Insect Biochem Mol Biol 26*, 525-528.

8. Ishimura, Y., Nozaki, M., and Hayaishi, O. (1970) The oxygenated form of L-tryptophan 2,3-dioxygenase as reaction intermediate, *J Biol Chem 245*, 3593-3602.

9. Matsumura, M., Osada, K., and Aiba, S. (1984) L-tryptophan 2,3-dioxygenase of a moderate thermophile, Bacillus brevis. Purification, properties and a substrate-mediated stabilization of the quaternary structure, *Biochim Biophys Acta 786*, 9-17.

10. Sugimoto, H., Oda, S., Otsuki, T., Hino, T., Yoshida, T., and Shiro, Y. (2006) Crystal structure of human indoleamine 2,3-dioxygenase: catalytic mechanism of O2 incorporation by a heme-containing dioxygenase, *PNAS 103*, 2611-2616.

11. Patel, N., Jones, D. K., and Raven, E. L. (2000) Investigation of the haem-nicotinate interaction in leghaemoglobin. Role of hydrogen bonding, *Eur J Biochem 267*, 2581-2587.

12. Patel, N., Seward, H. E., Svensson, A., Gurman, S. J., Thomson, A. J., and Raven, E. L. (2003) Exploiting the conformational flexibility of leghemoglobin: a framework for examination of heme protein axial ligation, *Arch Biochem Biophys 418*, 197-204.

13. Basran, J., Rafice, S. A., Chauhan, N., Efimov, I., Cheesman, M. R., Ghamsari, L., and Raven, E. L. (2008) A kinetic, spectroscopic, and redox study of human tryptophan 2,3-dioxygenase, *Biochemistry 47*, 4752-4760.

14. Papadopoulou, N. D., Mewies, M., McLean, K. J., Seward, H. E., Svistunenko, D. A., Munro, A. W., and Raven, E. L. (2005) Redox and spectroscopic properties of human indoleamine 2,3-dioxygenase and a His303Ala variant: implications for catalysis, *Biochemistry 44*, 14318-14328.

15. Thackray, S. J., Bruckmann, C., Anderson, J. L., Campbell, L. P., Xiao, R., Zhao, L., Mowat, C. G., Forouhar, F., Tong, L., and Chapman, S. K. (2008) Histidine

55 of tryptophan 2,3-dioxygenase is not an active site base but regulates catalysis by controlling substrate binding, *Biochemistry 47*, 10677-10684.

16. Chauhan, N., Basran, J., Efimov, I., Svistunenko, D. A., Seward, H. E., Moody, P. C., and Raven, E. L. (2008) The role of serine 167 in human indoleamine 2,3-dioxygenase: a comparison with tryptophan 2,3-dioxygenase, *Biochemistry 47*, 4761-4769.
17. Carrington, J. C., and Dougherty, W. G. (1988) A viral cleavage site cassette: identification of amino acid sequences required for tobacco etch virus polyprotein processing, *Proc Natl Acad Sci U S A 85*, 3391-3395.
18. More, C., Belle, V., Asso, M., Fournel, A., Roger, G., Guigliarelli, B., and Bertrand, P. (1999) *Biospectroscopy S5*, S3-S18.
19. Thomson, A. J., and Gadsby, P. M. (1990) A theoretical model of the intensity of the near-infrared porphyrin-to-iron charge-transfer transitions in low-spin iron(III) haemoproteins. A correlation between the intensity of the magnetic circular dichroism bands and the rhombic distortion parameter of iron, *J. Chem. Soc., Dalton Trans 6*, 1921 - 1928.
20. Aasa, R., and Vanngard, T. (1975) EPR Signal Intensity and Powder Shapes: A Reexamination, *J Magn. Reson. 19*, 308-315.
21. Batabyal, D., and Yeh, S. R. (2007) Human tryptophan dioxygenase: a comparison to indoleamine 2,3-dioxygenase, *J Am Chem Soc 129*, 15690-15701.
22. Badyal, S. K., Joyce, M. G., Sharp, K. H., Seward, H. E., Mewies, M., Basran, J., Macdonald, I. K., Moody, P. C., and Raven, E. L. (2006) Conformational mobility in the active site of a heme peroxidase, *J Biol Chem 281*, 24512-24520.
23. Batabyal, D., and Yeh, S. R. (2009) Substrate-Protein Interaction in Human Tryptophan Dioxygenase: The Critical Role of H76, *J Am Chem Soc*.
24. Fukumura, E., Sugimoto, H., Misumi, Y., Ogura, T., and Shiro, Y. (2009) Cooperative binding of L-trp to human tryptophan 2,3-dioxygenase: resonance Raman spectroscopic analysis, *J Biochem 145*, 505-515.
25. Dick, R., Murray, B. P., Reid, M. J., and Correia, M. A. (2001) Structure--function relationships of rat hepatic tryptophan 2,3-dioxygenase: identification of the putative heme-ligating histidine residues, *Archives of Biochemistry and Biophysics 392*, 71-78.

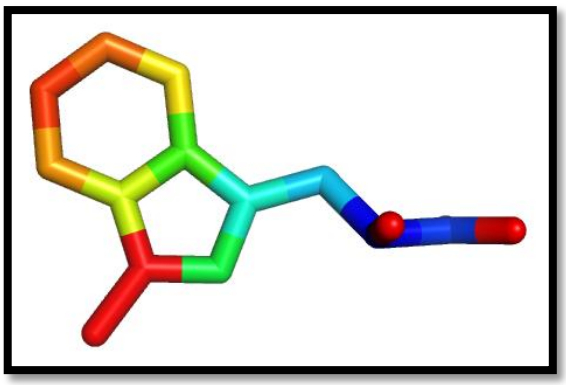

CHAPTER 4

REASSESSMENT OF THE HEME MECHANISM

Tryptophan 2,3-dioxygenase and indoleamine-2,3 dioxygenase are heme containing enzymes which catalyse the oxidation of a substrate, such as L-tryptophan to form the product *N*-formylkynurenine by addition of dioxygen across the C_2-C_3 bond of the substrate (Scheme 4.1).

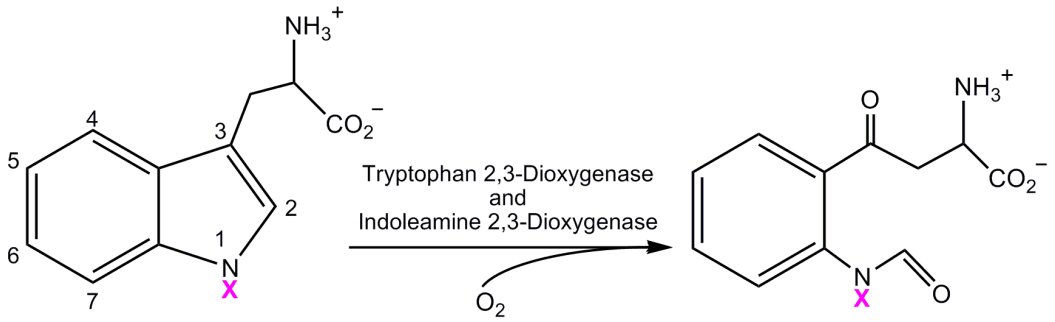

Scheme 4.1 Reaction catalysed by TDO and IDO, with IUPAC numbering indicated, where **X** = H: the substrate is L-tryptophan and the product is *N*-formylkynurenine and **X** = Me: the substrate is 1-methyl-L-tryptophan and the product is *N*-formyl-methylkynurenine

The detailed catalytic mechanism of the dioxygenases has been a matter of debate for 40 years (2009). Hamilton in 1969 proposed that base-catalysed deprotonation of the indole N_1 of the ternary complex (Fe^{2+}-O_2-substrate) was the most probable initiation step (Scheme 4.2A) (*1*). Hamilton based his theory on the observation that 1-methyl-L-tryptophan was an inhibitor to TDO and IDO, and base-catalysed abstraction is not possible with a methylated compound (*2*).

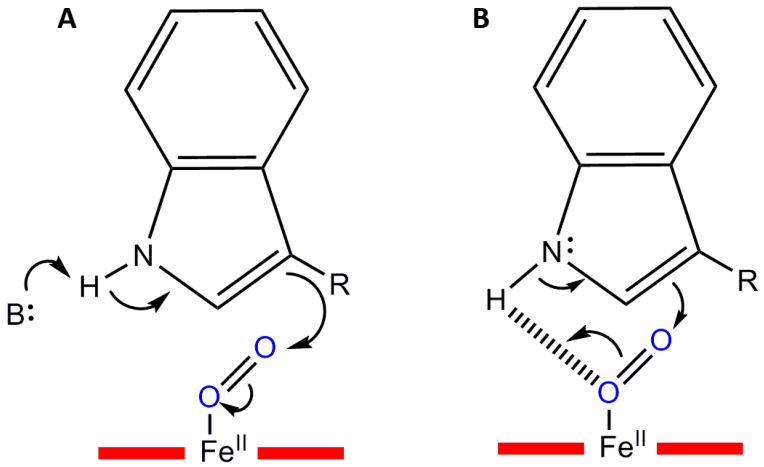

Scheme 4.2 Mechanisms for oxidation of L-tryptophan. (**A**) Abstraction of the indole proton by an active site base. (**B**) Abstraction of the indole proton by the heme-bound dioxygen.

The information presented in this thesis and other publications suggest a number of problems with this mechanism. First, indoles typically react by electrophilic addition across the C_3 position, forming a cation at N_1 (*3*). Also the variant work presented in this thesis for hTDO and hIDO, together with the crystal structures for *X. campestris* TDO and hIDO, revealed that hIDO does not have an active-site base located close enough to the heme iron for abstraction of the indole protein (*4*). In addition, variants of hIDO (S167), hTDO (H76) and *X. campestris* TDO (H55) have shown that they are not essential in the catalytic mechanism as each enzyme remained active when the residue was removed (Chapter 3, (*5-9*)). Therefore if the mechanism was base-catalysed deprotonation of the indole N_1 then the variants would have been inactive.

This information suggested that the bound dioxygen could act as the active-site base without any involvement from the active-site residues (Scheme 4.2B) This chapter discusses further problems associated with the mechanism and suggests an alternative mechanism based on the chemistry of indoles. This work was published in the Journal of the American Chemical Society (*10*).

4.1 Preparation of Materials and Enzymes

Wild type rhTDO and the variant samples were prepared, purified and characterised by spectroscopy as described in Chapters 2, 3 and 7. The compound 1-methyl-L-tryptophan was bought commercially and contained an impurity of 5 %, which needed to be removed, as it was likely to be L-tryptophan which could act as a substrate. The 1-methyl-L-tryptophan was purified by HPLC and the sample was checked by H_1 NMR to confirm that the sample was pure[1].

4.2 Oxidation of 1-Methyl-L-Tryptophan by the TDO and the H76S variant of rhTDO

UV-visible spectroscopy was used to determine that 1-methyl-L-tryptophan could act as a substrate and produce a methylated product, *N*-formyl-methylkynurenine, which is contrary to all published data for the compound 1-methyl-L-tryptophan, which was considered strictly an inhibitor (Scheme 4.1, where X = Me) (*2*). Absorbance changes for oxidation of the substrate L-tryptophan were analysed, which shows formation of the product *N*-formyl-kynurenine (yellow in colour), observed by a peak at 321 nm with the H76S variant of rhTDO (Figure 4.1, blue spectrum). Upon addition of 1-methyl-L-tryptophan in the presence of H76S, a peak at the same wavelength as *N*-formyl-kynurenine was observed indicating formation of *N*-formyl-methylkynurenine (Figure 4.1, green spectrum) and in the absence of H76S no product formation was observed (Figure 4.1, black spectrum), confirming that product formation was due to enzymatic oxidation of the substrate 1-methyl-L-

[1] LC-MS and H_1 NMR was carried out by Dr Chauhan.

tryptophan. Also, upon addition of 1-methyl-L-tryptophan to wild type rhTDO no product was detected suggesting that the wild type enzyme does not oxidise 1-methyl-L-tryptophan (Figure 4.1, red spectrum).

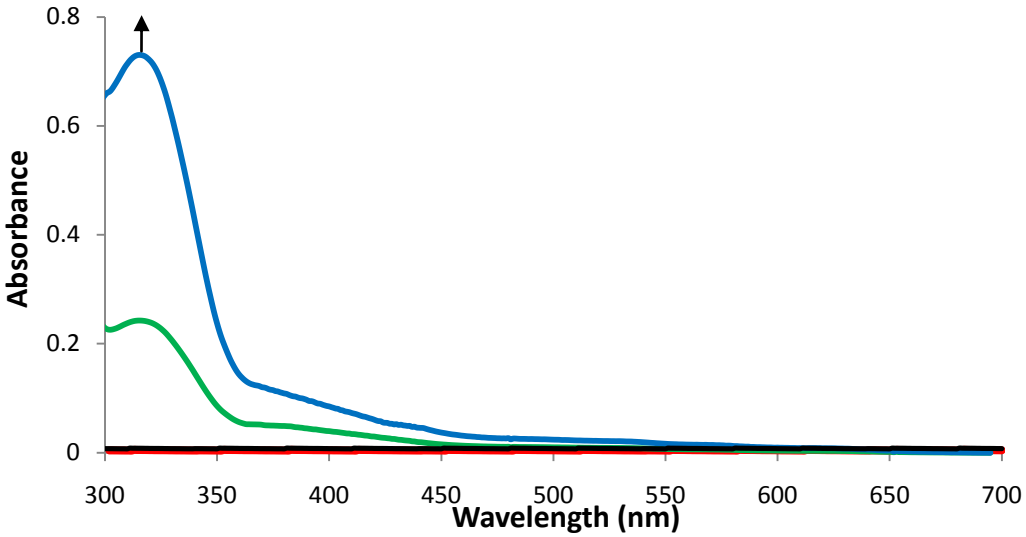

Figure 4.1 Oxidation of L-tryptophan by the rhTDO variant H76S (blue spectrum). Oxidation of 1-methyl-L-tryptophan in the absence (black spectrum) and presence of the rhTDO variant H76S (green spectrum). No product observed for 1-methyl-L-tryptophan in the presence of wild type TDO (red spectrum). Spectra were obtained after purification of 1-methyl-L-tryptophan. The arrow indicates the direction of absorbance change during the course of the reaction, product formation is observed at 321 nm. Reaction conditions: 50 mM Tris-HCl, pH 8.0, 25.0 ^{o}C.

4.3 LC-MS analysis of the Reaction Products Catalysed by H76S

LC-MS analysis using selected ion monitoring was used to determine whether the identity of the product for oxidation of 1-methyl-L-tryptophan by H76S TDO and to confirm that wild type rhTDO does not use 1-methyl-L-tryptophan as a substrate (Figure 4.1, blue spectrum) [2]. A control reaction for oxidation of L-tryptophan by H76S produced *N*-formylkynurenine which had an ion with *m/z* = 237 detected

[2] LC-MS analysis was carried out by Dr. Chauhan.

which corresponds to a mass of *m/z* = 236 (Scheme 4.1, where X = H, Figure 4.2 A) and oxidation of 1-methyl-L-tryptophan generated an ion with *m/z* = 251, which was expected for *N*-formyl-methylkynurenine (*m/z* = 250) (Scheme 4.1, where X = Me, Figure 4.2 B)[3].

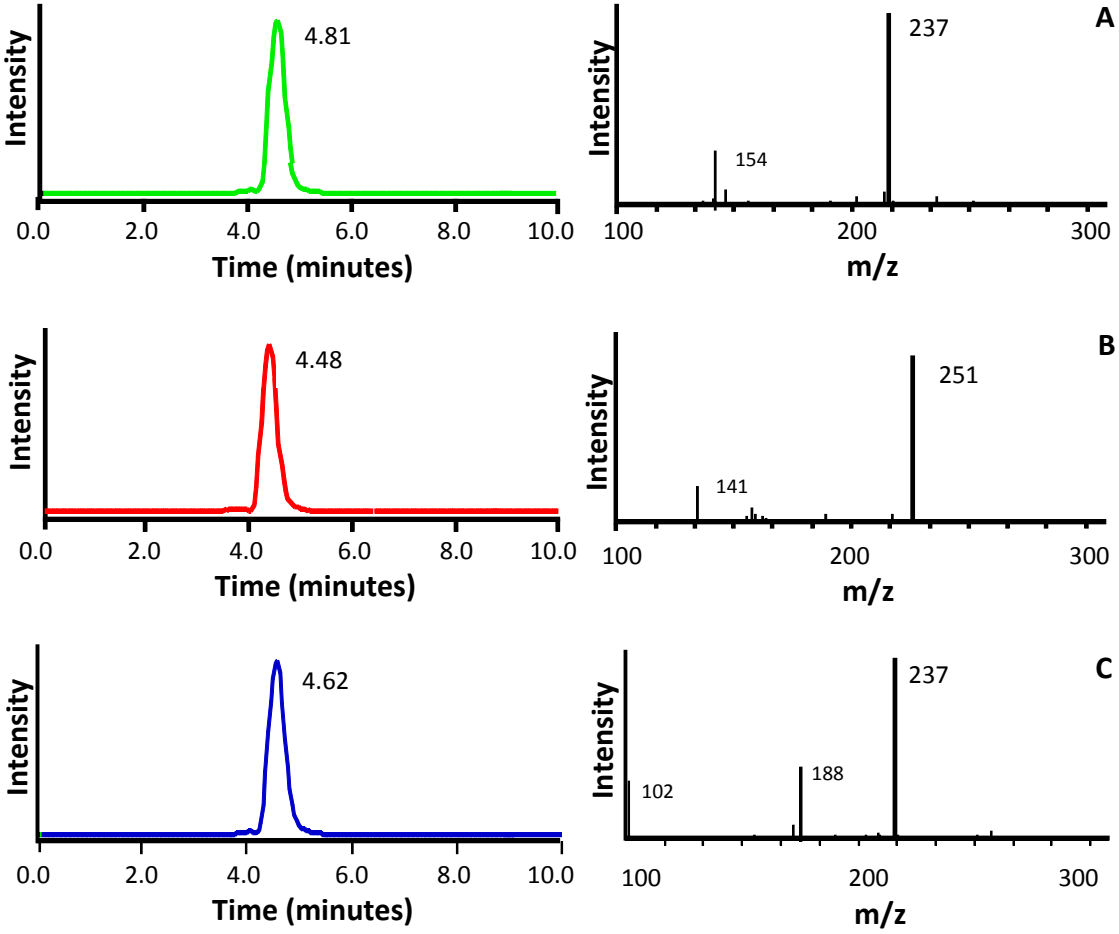

Figure 4.2 LC-MS analysis of product obtained on reaction of (**A**) H76S with L-tryptophan, the selected ion chromatogram with m/z of 237 (right plot A) and the corresponding positive ESI mass spectrum for the product eluted at 4.81 minutes (green). (**B**) H76S with 1-methyl-L-tryptophan, the selected ion chromatogram with m/z of 251 (right plot B) and the corresponding positive ESI mass spectrum for the product eluted at 4.48 minutes (red). (**C**) rhTDO with L-tryptophan, the selected ion chromatogram with m/z of 237 (right plot C) and the corresponding positive ESI mass spectrum for the product eluted at 4.62 minutes (blue).

[3] Reported in Dr. Chauhan's thesis 2009 University of Leicester.

LC-MS analysis carried out for rhTDO with L-tryptophan, which showed a typical ion with m/z 237 detected which corresponds the mass of *N*-formylkynurenine (m/z = 236) (Scheme 4.1, where X = H, Figure 4.2 C), however upon reaction with 1-methyl-L-tryptophan there were no ions with m/z 251 which supports that rhTDO does not utilise 1-methyl-L-tryptophan as a substrate.

LC-MS and UV-visible spectroscopy experiments were carried out by Dr Chauhan for rhIDO and the variant S167A and by Dr S. Thackray for *X. campestris* TDO and the variants H55A and H55S which confirmed similar results, that *X. campestris* TDO variants and wild type rhIDO and variants could utilise 1-methyl-L-tryptophan as a substrate and wild type *X. campestris* TDO could not (*10*).

4.4 Steady-state Oxidation of 1-Methyl-L-Tryptophan

A comparison of the Michaelis constants (k_{cat} and K_m) obtained in this chapter with all available published data is shown in Table 4.1. Wild type rhTDO had no measurable activity with 1-methyl-L-tryptophan, which was expected from the electronic absorption spectroscopy and LC-MS analyses. Wild type *X. campestris* TDO showed similar results (*10*).

A plot of the initial rate of dioxygenase activity (v/[E] s^{-1}), where v is the initial rate and [E] is the enzyme concentration in the reaction mixture versus substrate concentration (mM) (Figure 4.3, L-tryptophan (black) and 1-methyl-L-tryptophan (blue)) shows hyperbolic responses. The data were fitted to the Michaelis-Menten equation (Chapter 7, Equation 7.5)[4].

[4] Analysis checked by Dr. I. Efimov and Mr G. Pantouris (University of Edinburgh).

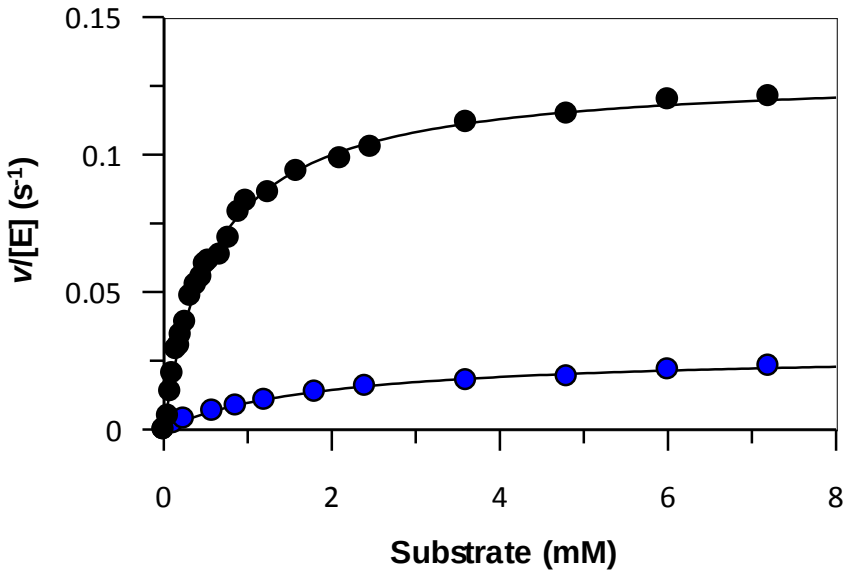

Figure 4.3 Steady-state oxidation of L-tryptophan showing *N*-formylkynurenine formation (black) and steady-state oxidation of 1-methyl-L-tryptophan showing *N*-formyl-methylkynurenine formation (blue) by the TDO variant H76S. Solid line shows a fit of the data to the Michaelis-Menten equation (Chapter 7, Equation 7.5).

The turnover of 1-methyl-L-tryptophan is significantly lower compared to turnover for L-tryptophan for the H76S variant of rhTDO (k_{cat} is 0.10 ± 0.01, Figure 4.3 and Table 4.1), which was also observed for the variants of *X. campestris* TDO, wild type rhIDO and the variants (*7, 10*). The affinity for substrate for all the dioxygenase enzymes, which could utilise 1-methyl-L-tryptophan as a substrate also had significantly lower affinity for substrate in comparison to L-tryptophan as substrate (K_m is 599 ± 35 in the presence of L-tryptophan and 1940 ± 150 in the presence of 1-methyl-L-tryptophan, Figure 4.3 and Table 4.1) (*7, 10, 11*).

Table 4.1 Steady-state data for L-tryptophan and steady-state and inhibition data for 1-methyl-L-tryptophan, dash indicates no measurable activity. Reaction conditions: 50 mM Tris, pH 8.0, 25.0 ^{o}C.

Enzyme	L-Tryptophan		1-Methyl-L-Tryptophan		K_i (μM)	Reference
	k_{cat} (s^{-1})	K_m (μM)	k_{cat} (s^{-1})	K_m (μM)		
hTDO	1.40 ± 0.01[a]	169 ± 18[a]	-	-	364 ± 11	This work
H76S	0.10 ± 0.01[b]	599 ± 66[b]	0.028 ± 0.008	1940 ± 150	-	This work
H76S	0.10 ± 0.01[b]	599 ± 66[b]	0.023 ± 0.001	2300 ± 230	-	(*10*)
XcTDO	19.5 ± 1.2	114 ± 1	-	-	-	(*7, 10*)
H55A	2.9 ± 0.1	133 ± 7	0.048 ± 0.011	59 ± 16	146 ± 9[c]	(*7, 10*)
H55S	2.6 ± 0.1	197 ± 2	0.052 ± 0.009	70 ± 11	398 ± 49[c]	(*7, 10*)
hIDO	1.4 ± 0.1	7 ± 1	0.027 ± 0.001	150 ± 11	-	(*10*)
S167A	1.6 ± 0.1	21 ± 2	0.032 ± 0.002	31 ± 5	-	(*10*)
hIDO	3.1 ± 0.2	15 ± 2	0.064 ± 0.003	62 ± 9	32 ± 0.8	(*11*)

[a] Data presented in Chapter 2. [b] Data presented in Chapter 3. [c] K_i results determined by Dr. Thackray (not published).

4.5 Inhibition Analysis for 1-Methyl-L-Tryptophan

Inhibition information is important for drug development as enzyme inhibition is the typical desired biological effect for a majority of drugs (*12*). The dissociation constant for the enzyme-inhibitor complex is (K_i) which was calculated to characterise the inhibitor 1-methyl-L-tryptophan for rhTDO for the first time and to determine the effect of 1-methyl- L-tryptophan as an inhibitor in the presence of L-tryptophan. The dioxygenases can utilise 1-methyl-L-tryptophan as a substrate, as shown by the spectroscopy, LC-MS and steady-state reactions but it is also an inhibitor in the presence of L-tryptophan as both compounds can form a complex with the enzyme, however they are mutually exclusive because they cannot both form a complex with the enzyme at the same time. Therefore in the presence of both compounds the enzyme-catalysed reaction rate decreases compared to the rate in absence of the inhibitor (Chapter 7, section 7.5.8) (*13*).

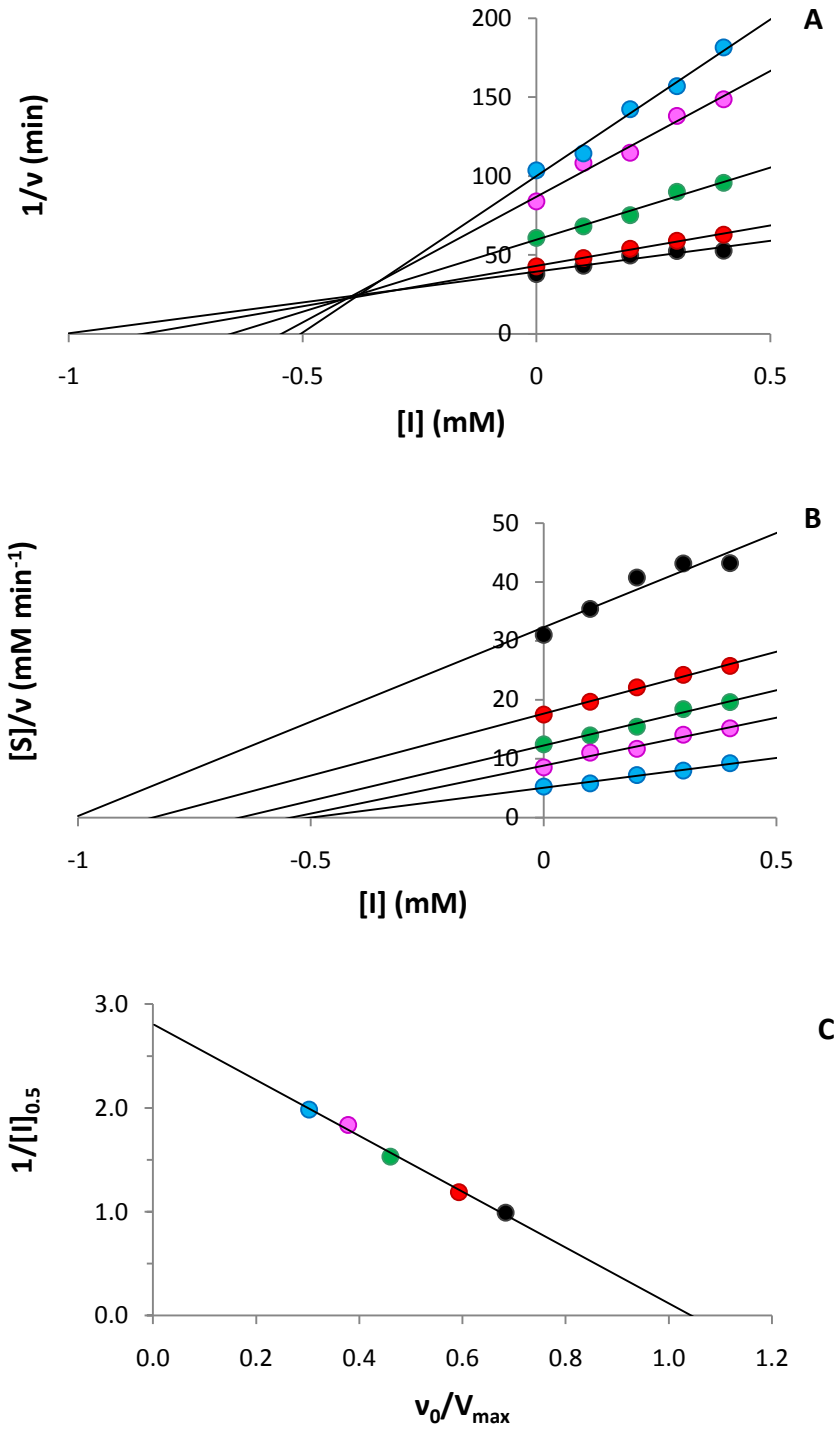

Figure 4.4 Inhibition plots for determining the K_i and characterisation of the inhibitor 1-methyl-L-tryptophan. (**A**) 1/v against [I], where the lines intersect x = K_{ic} and y = $1/V_{max}$. (**B**) [S]/v against [I], where [S] = K_m. (**C**) $1/[I]_{0.5}$ against v_0/V_{max}, where the y intercept is $1/K_{ic}$ and the slope is $-1/K_{ic}$. For all plots A to C the substrate concentration is shown 0.051 µM (blue), 0.102 µM (pink), 0.205 µM (green), 0.41 µM (red) and 0.82 µM (black).

The data indicates that 1-methyl-L-tryptophan is a competitive inhibitor for rhTDO, as the V_{max} is constant for all concentrations of inhibitor as all lines intersect for Figure 4.4A, where V_{max} is 0.035 min^{-1}, and the K_m increases with inhibitor concentration (Figure 4.4B, where [S] = K_m). The data presented in Figure 4.4 A and B are confirmed by plot C (*12, 14-16*).

1-Methyl-L-tryptophan has been well defined in the literature as a competitive inhibitor for human and rabbit IDO, with similar values for K_i ~30 - 60 μM (*2, 11, 17, 18*). However, the value of K_i for rhTDO and the *X. campestris* TDO variant are much larger (K_i ~150 - 400 μM), which indicates that 1-methyl-L-tryptophan is a more potent inhibitor for IDOs compared to TDOs.

4.6 Redox Potentiometry

The redox potential of the Fe^{2+}/Fe^{3+} couple for rhTDO in the absence and presence of 1-methyl-L-tryptophan was -92 and -101 mV respectively, which shows a negative shift of -9 mV compared to in the presence of L-tryptophan, which had a positive shift of +16 mV (Table 4.2, Figure 4.5). The data for rhTDO shows no stabilisation of the ferrous form upon addition of the 1-methyl-L-tryptophan. The redox data are supported by the kinetic parameters, which show no oxidation of 1-methyl-L-tryptophan.

The rhTDO variant H76S had a positive shift in potential for both L-tryptophan and 1-methyl-L-tryptophan, which supports the idea that there was stabilisation of the ferrous form, allowing reduction of the protein. These data support the spectroscopic, LC-MS and steady-state data presented in this chapter, which shows that the H76S variant of rhTDO can oxidise 1-methyl-L-tryptophan to produce a methylated product *N*-formyl-methylkynurenine (scheme 4.1, where X = Me).

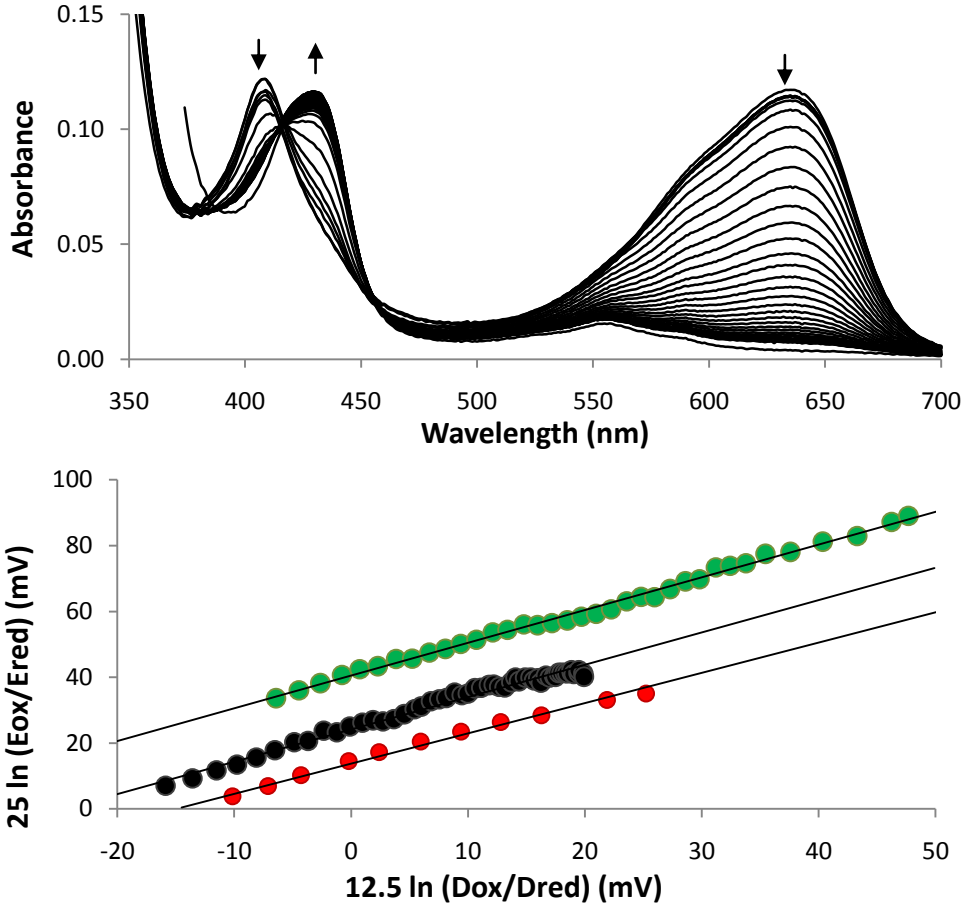

Figure 4.5 A representative family of spectra observed during the redox of the Fe^{2+}/Fe^{3+} couple of rhTDO. Nernst plots showing in the absence (black) and presence of L-tryptophan (red) or 1-methyl-L-tryptophan (green). Arrows indicate the direction of absorption change during the reductive titration.

Table 4.2 Fe^{2+}/Fe^{3+} reduction potentials obtained for rhTDO and the variant H76S in the absence and presence of either L-tryptophan or 1-methyl-L-tryptophan. Reaction conditions: 100 mM potassium phosphate, pH 7.0, 25.0 ^{o}C.

Enzyme	WT TDO	H76S
No Substrate (mV)	-92 ± 3	-119 ± 4
+ L-Tryptophan (mV)	-76 ± 3	-113 ± 3
+ 1-Methyl-L-tryptophan (mV)	-101 ± 4	-100 ± 3
Potential Shift for L-tryptophan (mV)	+16	+6
Potential Shift for 1-Methyl-L-tryptophan (mV)	-9	+19

4.7 Discussion

Catalytic Mechanism

The catalytic mechanism for the dioxygenases is still unclear, however several proposals have been made such as base-catalysed abstraction of the indole N_1 (scheme 4.2 A), however since the crystal structure for mammalian IDO was solved, the mechanism was questioned as hIDO does not contain a suitable active-site base (*1, 2, 4*). A new mechanism was proposed still using the deprotonation mechanism as the crystal structure of *X. campestris* showed that TDOs had a distal histidine which could act as an active-site base, therefore the new suggestion was abstraction of the indole N_1 by dioxygen for IDOs (Scheme 4.2B) (*6*).

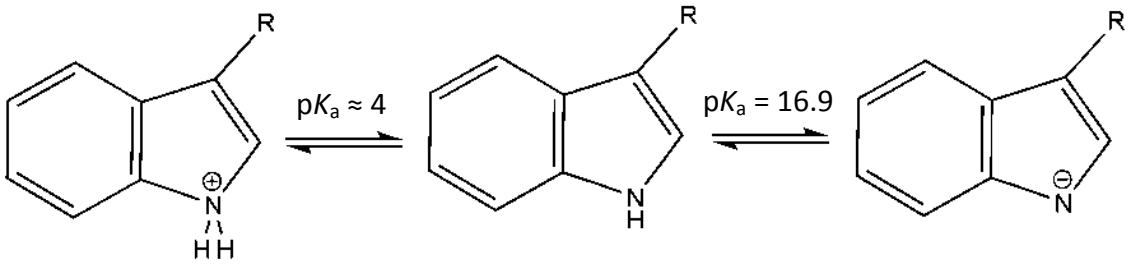

Figure 4.6 pH-dependent properties of L-tryptophan. Deprotonation of indole N_1 occurs at a pK_a of 16.9 (*19*).

The information presented in this Chapter shows that a mechanism involving deprotonation for any dioxygenase is not possible, as 1-methyl-L-tryptophan acts as a substrate (*3*). Deprotonation of the indole N^1 is also unlikely as the pK_a for deprotonation is 16.9, which is out of range for a biological system, although the pK_a could change in the enzyme active site (Figure 4.6) (*19*).

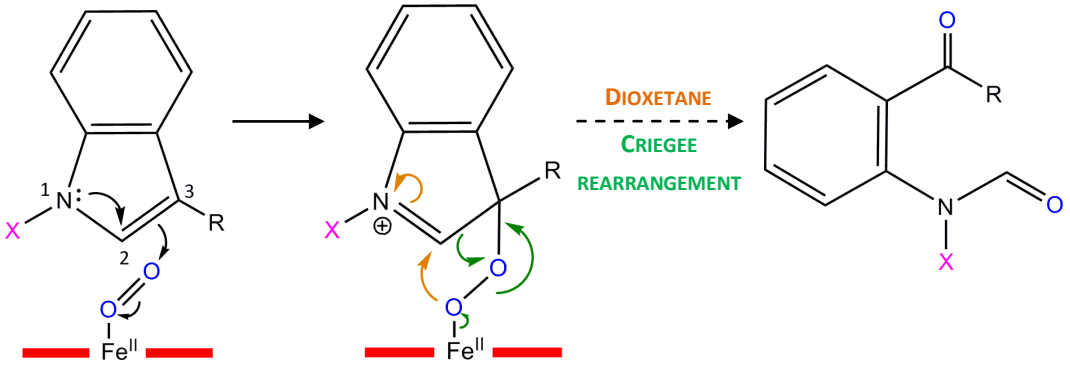

Scheme 4.3 Proposal of a new mechanism for the initial catalytic step for product formation in both TDO and IDO, where X = H or Me. Following formation of the first intermediate the dioxetane or Criegee rearrangement pathways were proposed to complete conversion to product (*1, 21, 22*).

A recent density functional theory (DFT) paper provided theoretical calculations for the previous deprotonation mechanisms and the proposed electrophilic addition mechanism and found that deprotonation was unfavourable because the indole N_1 would have a bent conformation to interact with dioxygen, which creates steric strain (Scheme 4.2) (*20*). They also proposed electrophilic addition and found that it required low activation energy. Together it seems that deprotonation is unlikely and that the initial step for conversion to product in heme containing dioxygenases occurs by electrophilic addition (Scheme 4.3) (*20*).

Direct electrophilic addition could occur for heme containing dioxygenases where the lone pair on the indole N_1 initiates the reaction with dioxygen, the electrophile in this case, allowing dioxygen to be attached at either C_2 or C_3 (Scheme 4.4). The DFT paper that suggested dioxygen would attached to the C^2 position, which is atypical for indole chemistry (C_3 is more favourable) because a positive charge would be generated on C_3 which would be stabilised by the benzene ring, which is not as effective in comparison to attaching to the C^3 position which generates a positive charge on C_2, which is stabilised by the lone pair on the indole N_1 (Scheme 4.4) (*3, 20*).

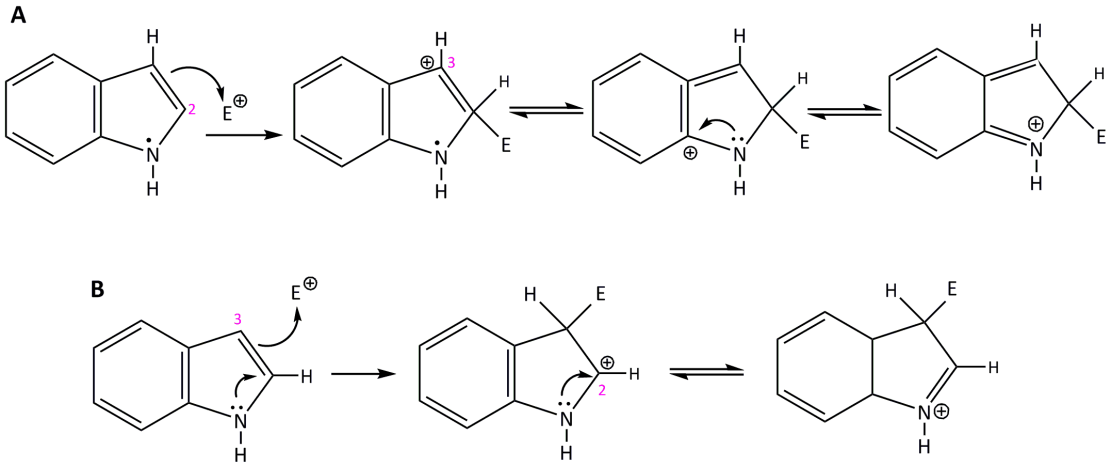

Scheme 4.4 Direct electrophilic addition to (**A**) the C_2 position or (**B**) the C_3 position on the indole ring (*3, 20*).

Another advantage to the direct electrophilic addition mechanism is not only that it follows indole chemistry but the mechanism would work for both substrates L-tryptophan and 1-methyl-L-tryptophan. A distal active site residue is not necessary for electrophilic addition, therefore both dioxygenases regardless of having different active site residues could use this mechanism (Scheme 4.3, where X = H for L-tryptophan and Me for 1-methyl-L-tryptophan).

Wild Type TDOs Are Catalytically Inactive with 1-methyl-L-tryptophan

Wild type TDO for both human and bacterial TDO were inactive with 1-methyl-L-tryptophan. However, wild type IDO and the variants of IDO and TDO were catalytically active with 1-methyl-L-tryptophan. As discussed in Chapter 3, the distal histidine in TDOs stabilises the substrate with a hydrogen bond, for optimum positioning in the heme pocket for catalysis; this was concluded from the ferrous crystal structure of *X. campestris* TDO with L-tryptophan bound in the active site (Figure 4.7 A) (*6*).

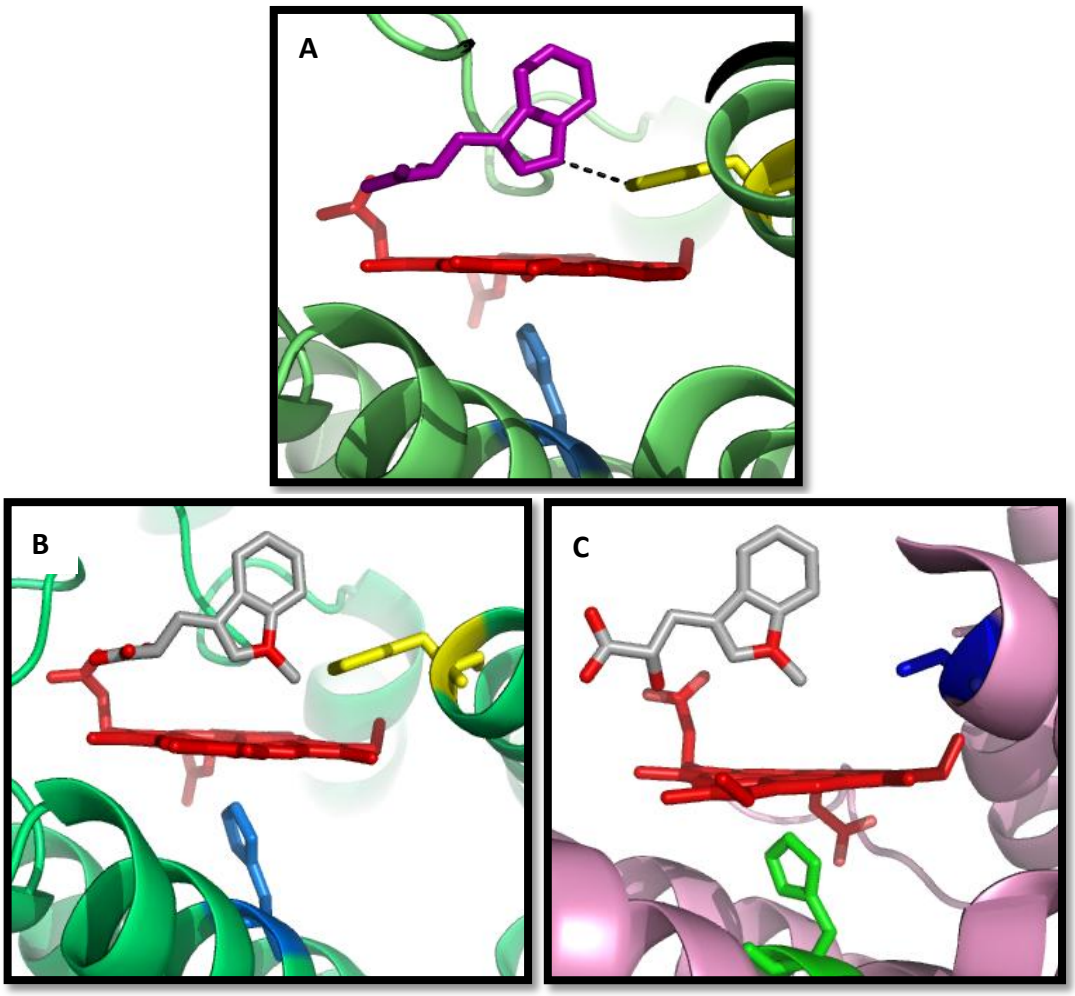

Figure 4.7 Crystal structures of *X. campestris* TDO (green) in complex with (**A**) L-tryptophan (purple) and (**B**) modelled with 1-methy-L-tryptophan (silver). The active site residues H55 (yellow), H240 (blue) (*6*). (**C**) Crystal structure of hIDO (pink) modelled with 1-methyl-L-tryptophan (silver) and the active site residues S167 (blue) and H346 (green) (*4*) [5].

1-Methyl-L-tryptophan was modelled into the active site of *X. campestris* TDO and a potential steric clash of the histidine and the methyl group was identified, which would be also expected in mammalian TDOs (Figure 4.7 B) (*6*) [5]. Furthermore, 1-methyl-L-tryptophan was modelled into the active site of rhIDO for a comparison

[5] By Dr Thackray (University of Edinburgh)

with TDO, and there was clearly enough space in the heme pocket to incorporate 1-methyl-L-tryptophan as IDOs do not have a distal histidine (Figure 4.7 C)(*4*).

This information indicates that wild type TDOs are inactive because they do not have enough space to accommodate the 1-methyl-L-tryptophan due to the distal histidine, whereas IDO does. Also the *X. campestris* TDO variants and the H76S variant of rhTDO were able to utilise 1-methyl-L-tryptophan because substitution of the histidine residue in the distal cavity created enough space to position the compound in the active site for catalysis, which was the reason activity was detected (Table 4.1). These data also support that histidine is not a critical active site residue as the variants which have a substituted histidine can turnover L-tryptophan and 1-methyl-L-tryptophan (Chapter 3) (*7*).

The Use of 1-Methyl-L-Tryptophan as an Inhibitory Drug

Deficient IDO has been found to cause immunomodulatory, neurological and pathophysiological disorders and more specifically, cancer, diabetes and schizophrenia (*23-29*). A recent review of the literature for IDO inhibitors refers to using 1-methyl-L-tryptophan in several trials however, it did not block IDO as they expected (*30*). For example the Opinion article discusses reasons for and against using IDO inhibitors as a therapeutic strategy for tumour therapy (it is thought that tumour growth is caused by increased IDO activity (*31*)). These questions were raised because 1-methyl-L-tryptophan was used to block IDO in the trials and it was not completely effective as it only retarded the growth of the tumour, it did not prevent progression of the tumour (*24, 26, 31, 32*).

The overall conclusion was that better understanding of IDO biology was required to understand how the IDO inhibitors would interact with the protein and that more potent inhibitors were required (*30, 33*). As previously mentioned until the publication from our lab this year no one in the dioxygenase field from chemists through to pharmacologists observed 1-methyl-L-tryptophan as a substrate, it was strictly considered an inhibitor (*1, 2, 10*). Therefore our findings provide essential

information that 1-methyl-L-tryptophan is a weak substrate which provides a possible reason for why the trials failed. Therefore drug trials using alternative inhibitory drugs for IDO could still be considered.

Ferryl-Based Mechanism

An alternative mechanism was recently proposed whereby the mechanism goes through a ferryl intermediate typically observed by peroxidases and cytochrome P450 enzymes called compound I (Scheme 4.5) (*21, 34-38*). The difference between peroxidases and cytochrome P450 enzymes compared with the heme dioxygenases is that the first two enzymes require activation by 2-electrons for dioxygen reduction, however the heme dioxygenases do not use any further electrons after the initial reduction to ferrous heme (*21*). Instead of simultaneous dioxygen addition to tryptophan, it was proposed that dioxygen is added using a 2-step mechanism (*38*).

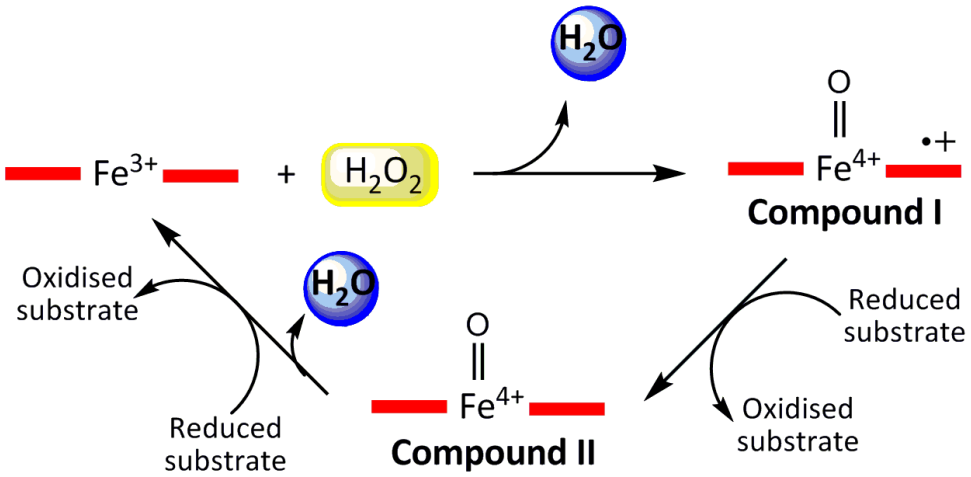

Scheme 4.5 The catalytic cycle of a peroxidase (*39*).

Resonance Raman data confirmed the presence of a heme-bound dioxygen which exhibited superoxide characteristics, in contrast to the previously proposed mechanisms which suggested neutral dioxygen bound to iron, as well as a compound II ferryl derivative with histidine as a proximal ligand (Scheme 4.5) (*21,*

40, 41). These experimental data indicate that the first dioxygen atom is added to the superoxo intermediate (A) to form the peroxo intermediate (B), without the need for deprotonation, which spontaneously converts to the ferryl intermediate (C) via a homolytic O-O bond cleavage (Scheme 4.6). The second oxygen is then inserted after the ferryl intermediate (C) to yield the product *N*-formylkynurenine (D) (Scheme 4.6).

Computational calculations were conducted by the same group using the TDO and IDO crystal structures, which supported their mechanistic proposal (*4, 6*). The ferryl intermediate of hTDO was not found in experimental trials, however it was proposed to either still go through the ferryl intermediate which is a faster step than for IDO or that TDO follows an alternate mechanism (*38*).

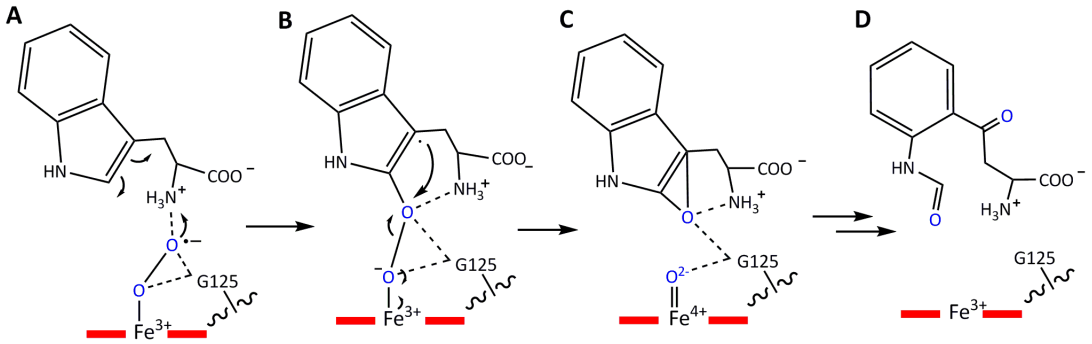

Scheme 4.6 Proposed ferryl-based dioxygenase mechanism (*38*). The reaction for *X. campestris* TDO, which is applicable for hIDO however the G125 residue is replaced by A264 and the bond between G125 and the heme bound oxygen for the ferryl intermediate is absent. Intermediates (**A**) superoxo, (**B**) peroxo, (**C**) ferryl and the product (**D**) *N*-formykynurenine.

A reason that the ferryl intermediate of TDO was not detected could be due to the structural differences between the dioxygenases. TDO enzymes contain a distal histidine residue (H55) which, constrains movement of the substrate by hydrogen bonding to the indole NH group, whereas IDO has a serine residue (S167) which, does not bind to the substrate allowing mobility. Therefore it was suggested that the substrate flexibility in the catalytic IDO pocket reduces the reaction rate, as the

substrate could be in a variety of positions, allowing enough of the intermediate to accumulate and be detected, however in TDO as the substrate is tightly held in the optimum position for the reaction, hence the reaction is too fast for accumulation of the intermediate, therefore it could not be detected (*38*).

Overall Conclusion

Despite years of investigation going back to the 1930s, the reaction mechanism of the heme dioxygenase is still not clarified (*42*). But recently it has become clear that mechanisms are beginning to unravel as new information emerges. Initial concerns were raised regarding the idea of base-catalysed abstraction (Scheme 4.2). This proposal originated from studies on 1-methyl-L-tryptophan, which was thought to be an inhibitor (*2*). Our computational, mass spectrometry and mutagenesis work, showed that 1-methyl-L-tryptophan is actually a slow substrate for wild type IDO and variants of TDO and IDO, therefore base-catalysed abstraction is not possible (*10*). This would be consistent with structural data since some dioxygenases (e.g. human IDO) have no active site base (*4*).

A recent paper cited our observation that 1-methy-L-tryptophan was a substrate and provided their own experimental data showing that their human truncated TDO had a 50-fold lower k_{cat} for 1-methyl-L-tryptophan compared to the turnover with L-tryptophan however there is not complete agreement (*9, 11*). We proposed direct electrophilic addition instead, which fits with the chemistry of indoles, whereby the indole N_1 initiates electrophilic addition of dioxygen to the C_3 position. The information presented in this chapter and our paper will be used for understanding the structure and function of proteins and it will be used more widely by pharmacologists in drug design for a number of diseases which affect millions each year.

4.8 References

1. Hamilton, G. A. (1969) Mechanisms of two- and four-electron oxidations catalyzed by some metalloenzymes, *Adv Enzymol Relat Areas Mol Biol 32*, 55-96.
2. Cady, S. G., and Sono, M. (1991) 1-Methyl-DL-tryptophan, beta-(3-benzofuranyl)-DL-alanine (the oxygen analog of tryptophan), and beta-[3-benzo(b)thienyl]-DL-alanine (the sulfur analog of tryptophan) are competitive inhibitors for indoleamine 2,3-dioxygenase, *Arch Biochem Biophys 291*, 326-333.
3. Joule, J. A., and Mills, K. (2000) *Heterocyclic Chemistry* Fourth ed., Blackwell Publishing.
4. Sugimoto, H., Oda, S., Otsuki, T., Hino, T., Yoshida, T., and Shiro, Y. (2006) Crystal structure of human indoleamine 2,3-dioxygenase: catalytic mechanism of O2 incorporation by a heme-containing dioxygenase, *PNAS 103*, 2611-2616.
5. Chauhan, N., Basran, J., Efimov, I., Svistunenko, D. A., Seward, H. E., Moody, P. C., and Raven, E. L. (2008) The role of serine 167 in human indoleamine 2,3-dioxygenase: a comparison with tryptophan 2,3-dioxygenase, *Biochemistry 47*, 4761-4769.
6. Forouhar, F., Anderson, J. L., Mowat, C. G., Vorobiev, S. M., Hussain, A., Abashidze, M., Bruckmann, C., Thackray, S. J., Seetharaman, J., Tucker, T., Xiao, R., Ma, L. C., Zhao, L., Acton, T. B., Montelione, G. T., Chapman, S. K., and Tong, L. (2007) Molecular insights into substrate recognition and catalysis by tryptophan 2,3-dioxygenase, *PNAS 104*, 473-478.
7. Thackray, S. J., Bruckmann, C., Anderson, J. L., Campbell, L. P., Xiao, R., Zhao, L., Mowat, C. G., Forouhar, F., Tong, L., and Chapman, S. K. (2008) Histidine 55 of tryptophan 2,3-dioxygenase is not an active site base but regulates catalysis by controlling substrate binding, *Biochemistry 47*, 10677-10684.
8. Fukumura, E., Sugimoto, H., Misumi, Y., Ogura, T., and Shiro, Y. (2009) Cooperative binding of L-trp to human tryptophan 2,3-dioxygenase: resonance Raman spectroscopic analysis, *J Biochem 145*, 505-515.
9. Batabyal, D., and Yeh, S. R. (2009) Substrate-Protein Interaction in Human Tryptophan Dioxygenase: The Critical Role of H76, *J Am Chem Soc*.
10. Chauhan, N., Thackray, S. J., Rafice, S. A., Eaton, G., Lee, M., Efimov, I., Basran, J., Jenkins, P. R., Mowat, C. G., Chapman, S. K., and Raven, E. L. (2009) Reassessment of the reaction mechanism in the heme dioxygenases, *J Am Chem Soc 131*, 4186-4187.
11. Lu, C., Lin, Y., and Yeh, S. R. (2009) Inhibitory substrate binding site of human indoleamine 2,3-dioxygenase, *J Am Chem Soc 131*, 12866-12867.
12. Cortes, A., Cascante, M., Cardenas, M. L., and Cornish-Bowden, A. (2001) Relationships between inhibition constants, inhibitor concentrations for 50% inhibition and types of inhibition: new ways of analysing data, *Biochem J 357*, 263-268.
13. Engel, P. C. (1981) *Enzyme kinetics : the steady-state approach*, 2nd ed. ed., Chapman and Hall, London.

14. Dixon, M. (1953) The determination of enzyme inhibitor constants, *Biochem J 55*, 170-171.
15. Cornish-Bowden, A. (1974) A simple graphical method for determining the inhibition constants of mixed, uncompetitive and non-competitive inhibitors, *Biochem J 137*, 143-144.
16. Carr, G., Chung, M. K., Mauk, A. G., and Andersen, R. J. (2008) Synthesis of indoleamine 2,3-dioxygenase inhibitory analogues of the sponge alkaloid exiguamine A, *J Med Chem 51*, 2634-2637.
17. Austin, C. J., Astelbauer, F., Kosim-Satyaputra, P., Ball, H. J., Willows, R. D., Jamie, J. F., and Hunt, N. H. (2009) Mouse and human indoleamine 2,3-dioxygenase display some distinct biochemical and structural properties, *Amino Acids 36*, 99-106.
18. Hou, D. Y., Muller, A. J., Sharma, M. D., DuHadaway, J., Banerjee, T., Johnson, M., Mellor, A. L., Prendergast, G. C., and Munn, D. H. (2007) Inhibition of indoleamine 2,3-dioxygenase in dendritic cells by stereoisomers of 1-methyl-tryptophan correlates with antitumor responses, *Cancer Res 67*, 792-801.
19. Yagil, G. (1967) The proton dissociation constant of pyrrole, indole and related compounds, *Tetrahedron 23*, 2855-2861.
20. Chung, L. W., Li, X., Sugimoto, H., Shiro, Y., and Morokuma, K. (2008) Density functional theory study on a missing piece in understanding of heme chemistry: the reaction mechanism for indoleamine 2,3-dioxygenase and tryptophan 2,3-dioxygenase, *J Am Chem Soc 130*, 12299-12309.
21. Sono, M., Roach, M. P., Coulter, E. D., and Dawson, J. H. (1996) Heme-Containing Oxygenases, *Chem Rev 96*, 2841-2888.
22. Leeds, J. M., Brown, P. J., McGeehan, G. M., Brown, F. K., and Wiseman, J. S. (1993) Isotope effects and alternative substrate reactivities for tryptophan 2,3-dioxygenase, *J Biol Chem 268*, 17781-17786.
23. Munn, D. H., Zhou, M., Attwood, J. T., Bondarev, I., Conway, S. J., Marshall, B., Brown, C., and Mellor, A. L. (1998) Prevention of allogeneic fetal rejection by tryptophan catabolism, *Science 281*, 1191-1193.
24. Munn, D. H., and Mellor, A. L. (2007) Indoleamine 2,3-dioxygenase and tumor-induced tolerance, *J Clin Invest 117*, 1147-1154.
25. Frumento, G., Rotondo, R., Tonetti, M., Damonte, G., Benatti, U., and Ferrara, G. B. (2002) Tryptophan-derived catabolites are responsible for inhibition of T and natural killer cell proliferation induced by indoleamine 2,3-dioxygenase, *J Exp Med 196*, 459-468.
26. Uyttenhove, C., Pilotte, L., Theate, I., Stroobant, V., Colau, D., Parmentier, N., Boon, T., and Van den Eynde, B. J. (2003) Evidence for a tumoral immune resistance mechanism based on tryptophan degradation by indoleamine 2,3-dioxygenase, *Nat Med 9*, 1269-1274.
27. Lob, S., Konigsrainer, A., Zieker, D., Brucher, B. L., Rammensee, H. G., Opelz, G., and Terness, P. (2009) IDO1 and IDO2 are expressed in human tumors: levo- but not dextro-1-methyl tryptophan inhibits tryptophan catabolism, *Cancer Immunol Immunother 58*, 153-157.

28. Takikawa, O. (2005) Biochemical and medical aspects of the indoleamine 2,3-dioxygenase-initiated L-tryptophan metabolism, *Biochem Biophys Res Commun 338*, 12-19.
29. Miller, C. L., Llenos, I. C., Dulay, J. R., Barillo, M. M., Yolken, R. H., and Weis, S. (2004) Expression of the kynurenine pathway enzyme tryptophan 2,3-dioxygenase is increased in the frontal cortex of individuals with schizophrenia, *Neurobiol Dis 15*, 618-629.
30. Lob, S., Konigsrainer, A., Rammensee, H. G., Opelz, G., and Terness, P. (2009) Inhibitors of indoleamine-2,3-dioxygenase for cancer therapy: can we see the wood for the trees?, *Nat Rev Cancer 9*, 445-452.
31. Muller, A. J., DuHadaway, J. B., Donover, P. S., Sutanto-Ward, E., and Prendergast, G. C. (2005) Inhibition of indoleamine 2,3-dioxygenase, an immunoregulatory target of the cancer suppression gene Bin1, potentiates cancer chemotherapy, *Nat Med 11*, 312-319.
32. Zou, W. (2005) Immunosuppressive networks in the tumour environment and their therapeutic relevance, *Nat Rev Cancer 5*, 263-274.
33. Zheng, X., Koropatnick, J., Li, M., Zhang, X., Ling, F., Ren, X., Hao, X., Sun, H., Vladau, C., Franek, J. A., Feng, B., Urquhart, B. L., Zhong, R., Freeman, D. J., Garcia, B., and Min, W. P. (2006) Reinstalling antitumor immunity by inhibiting tumor-derived immunosuppressive molecule IDO through RNA interference, *J Immunol 177*, 5639-5646.
34. English, A. M., and Tsaprailis, G. (1995) Catalytic and structure-function relationships in heme peroxidases, *Adv. Inorg. Chem. 43*, 79 - 125.
35. Wong, L. L. (1998) Cytochrome P450 monooxygenases, *Curr Opin Chem Biol 2*, 263-268.
36. Groves, J. T. (2005) *Cytochrome P450 : structure, mechanism, and biochemistry*, 3rd ed. ed., Kluwer Academic/Plenum Publishers, New York.
37. Makris, T. M., von Koenig, K., Schlichting, I., and Sligar, S. G. (2006) The status of high-valent metal oxo complexes in the P450 cytochromes, *J Inorg Biochem 100*, 507-518.
38. Lewis-Ballester, A., Batabyal, D., Egawa, T., Lu, C., Lin, Y., Marti, M. A., Capece, L., Estrin, D. A., and Yeh, S. R. (2009) Evidence for a ferryl intermediate in a heme-based dioxygenase, *Proc Natl Acad Sci U S A 106*, 17371-17376.
39. Hiner, A. N., Raven, E. L., Thorneley, R. N., Garcia-Canovas, F., and Rodriguez-Lopez, J. N. (2002) Mechanisms of compound I formation in heme peroxidases, *J Inorg Biochem 91*, 27-34.
40. Drago, R. S., and Corden, B. B. (1980) Spin-pairing model of dioxygen binding and its application to various transition-metal systems as well as hemoglobin cooperativity, *Acc. Chem. Res 13*, 353–360.
41. Terner, J., Palaniappan, V., Gold, A., Weiss, R., Fitzgerald, M. M., Sullivan, A. M., and Hosten, C. M. (2006) Resonance Raman spectroscopy of oxoiron(IV) porphyrin pi-cation radical and oxoiron(IV) hemes in peroxidase intermediates, *J Inorg Biochem 100*, 480-501.

42. Kotake, Y., and Masayama, I. (1936) The Intermediary metabolism of tryptophan. XVIII. The mechanism of formation of kynurenine from tryptophan, Z, *Physiol. Chem. 243*, 237-244.

CHAPTER 5

CHARACTERISATION OF A CLEAVABLE HEXAHISTIDYL TAG EXPRESSION SYSTEM FOR HUMAN INDOLEAMINE 2,3-DIOXYGENASE

Human indoleamine 2,3-dioxygenase (hIDO) and its sister enzyme tryptophan 2,3-dioxygenase both catalyse the first rate limiting step in the kynurenine pathway, breaking the C_2-C_3 bond of the indole ring of L-tryptophan to form *N*-formylkynurenine (Scheme 5.1) (*1-3*). Although the two dioxygenases catalyse the same reaction, they are otherwise distinct.

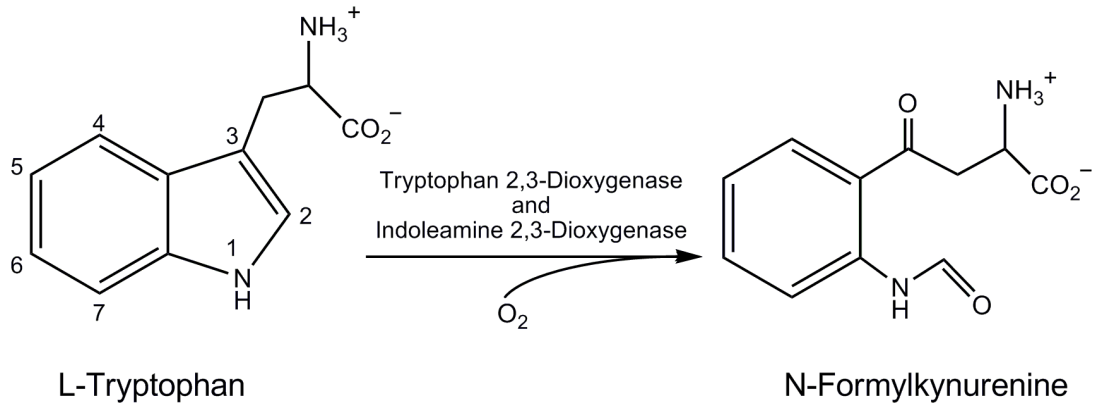

Scheme 5.1. Reaction Catalysed by IDO and TDO, with IUPAC Numbering Indicated

IDO is a monomeric (~45 kDa), heme-containing enzyme that was first isolated by Hayaishi (*4, 5*). HUman IDO is ubiquitously located throughout the body apart from in the liver and human IDO has a broader substrate specificity including both stereoisomers of tryptophan, 5-hydroxy-tryptophan, tryptamine and serotonin. Human IDO induction and the kynurenine pathway metabolites have been linked to various physiological and pathophysiological conditions, including antimicrobibal, antiviral, antiparasitic and antitumor activity, renal allograft rejection and various neurological disorders (*5-9*).

Several bacterial expression systems for rhIDO have been reported (*10-13*) however only Sugimoto's construct has been crystallised and the structure solved (PDBs 2D0T and 2D0U)(*10*). Ferric rhIDO crystalised with the inhibitor 4-phenylimidazole in the active site (Figure 5.1a) of two IDO monomers in each asymmetric unit (Figure 5.1b), which is joined together by a disulphide bridge at the cysteine residue 308 of each monomer at the N-terminal (Figure 5.1c) (*10*). Although this structure has provided insight into the molecular details of the active site architecture, a crystal structure of the enzyme in the presence of a substrate or dioxygen would aid in understanding whether hydrogen-bonding stabilisation of the ferrous-oxy species is required during IDO catalysis and as a comparison to TDO.

Papadopoulou's construct was the first to provide EPR, kinetic and redox potentiometric data about hIDO to the dioxygenase field (*12*). Papadopoulou's

rhIDO was expressed in our lab in the vector pQE30, which has a non-cleavable hexa-histidyl tag at the N-terminus. Subsequently all crystal screening attempts proved unsuccessful (*12*). It was presumed that crystallisation attempts with rhIDO in the pQE30 vector failed because the floppy N-terminal hexa-histidyl tag could be preventing the IDO monomers from aligning into a dimer to form the crystal (Figure 5.1 B and C).

This chapter will focus on constructing a new recombinant human IDO (rhIDO) vector which has the option of removing the hexa-histidyl tag after purification, with the aim of producing diffraction quality rhIDO crystals. Expression, purification, kinetic, spectroscopic and electrochemical data are reported here. This work was used as a basis upon which crystallographic studies on rhIDO could be carried out.

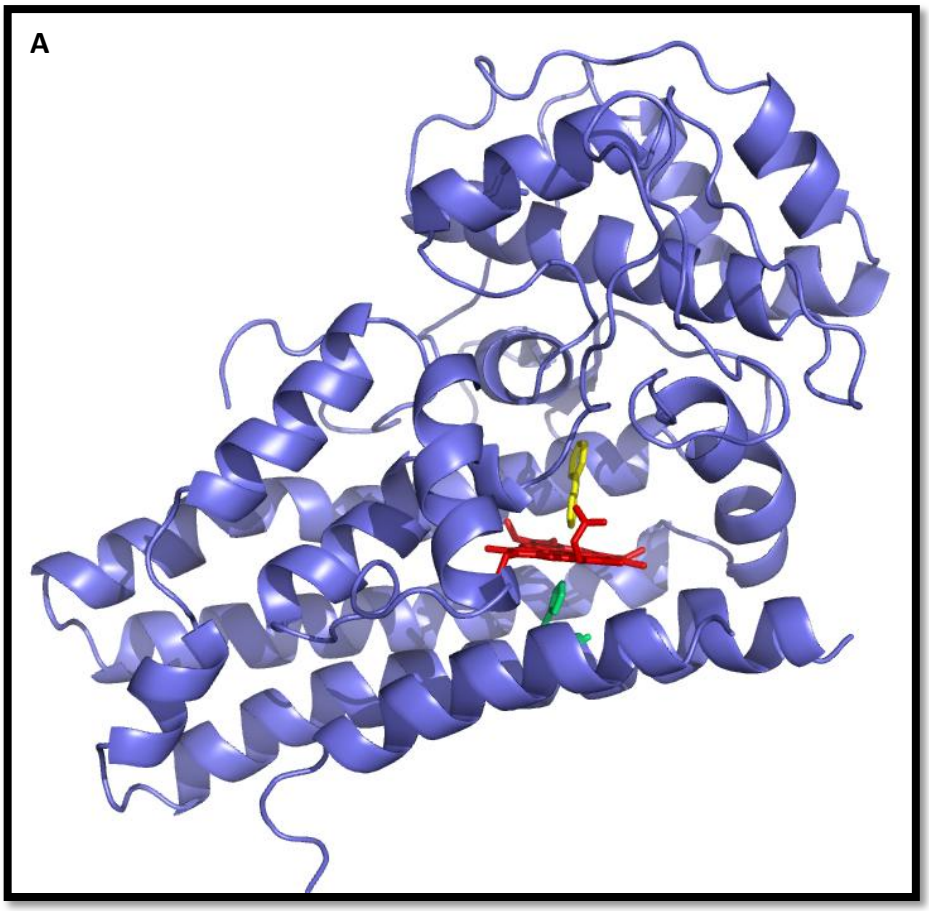

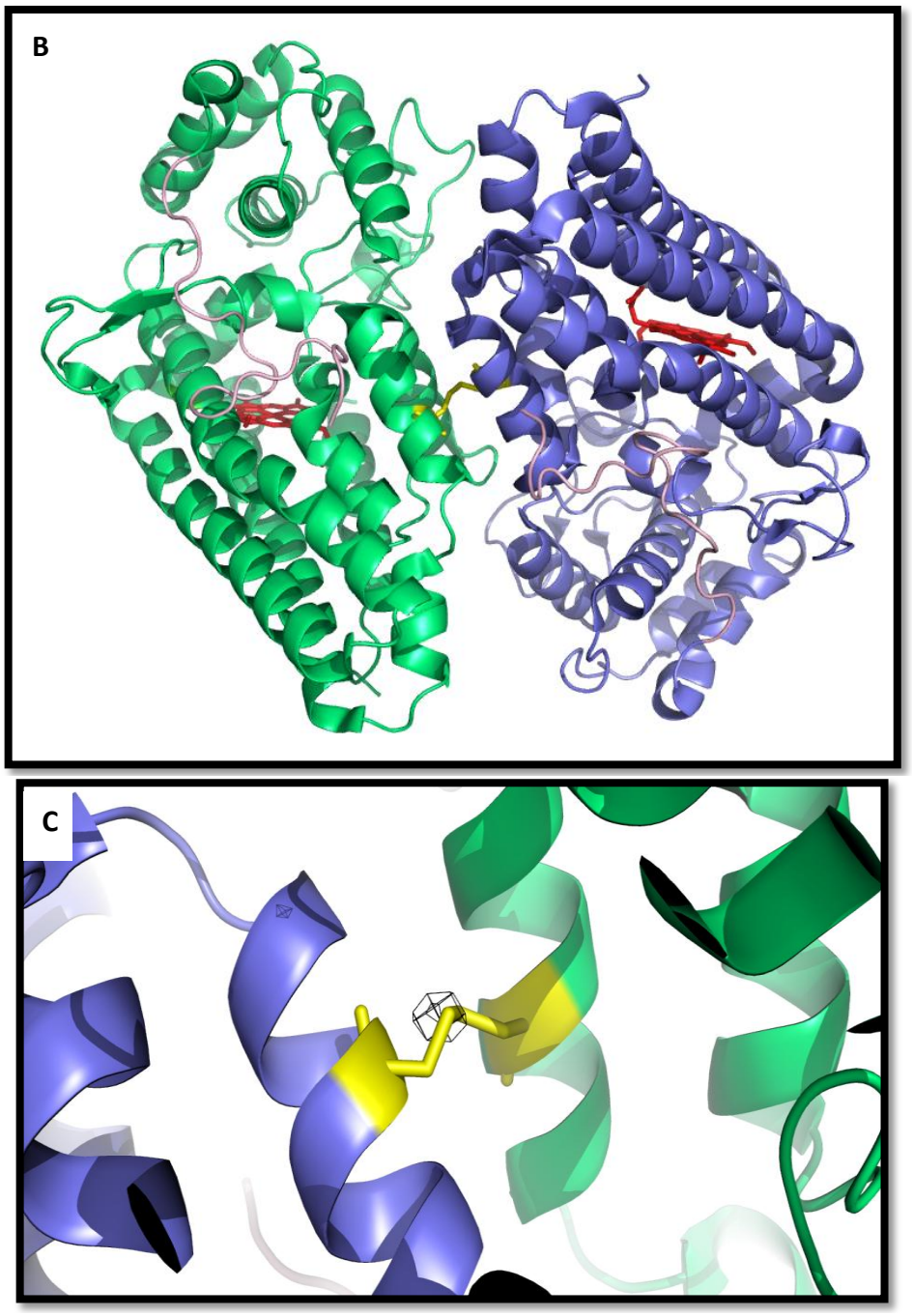

Figure 5.1. Crystal structure PDB 2D0T. (A) rhIDO with 4-phenylimidazole (yellow) in the active site, heme (red), proximal histidine (H346 green). (B) The two monomers of IDO shown in green and blue, the heme is indicated in red and the N-terminal regions where the hexa-histidyl tag is located shown in pink. (C) The two monomers of IDO shown in green and blue, residues C308 on each monomer (yellow) forming a disulphide bridge between the monomers (shown by positive electron density in black).

5.1 Construct of rhIDO

The polymerase chain reaction was employed to create an overhang on the 5' end of the human IDO cDNA (contained in the vector pQE30, Qiagen)[1] by addition of four bases (CACC), which is complementary to the sticky end (GTGG) on the pET151/d TOPO vector (Invitrogen), for in-frame directional cloning (Figure 5.2) (Chapter 7, Table 7.1). The pET151/d TOPO vector was selected for its Tobacco Etch Virus (TEV) protease cleavage site for removal of a N-terminal hexa-histidyl tag using TEV protease (Chapter 7, Section 7.4.4), which the current vector, pQE30, does not contain (*14*) (Figure 5.2). pET151/d TOPO-IDO was sequenced by the Protein and Nucleic Acid Chemistry Laboratory (PNACL), University of Leicester, which confirmed that no spurious mutations occurred during PCR (Appendix II, Figure A2.10, Chapter 7, Section 7.2.2).

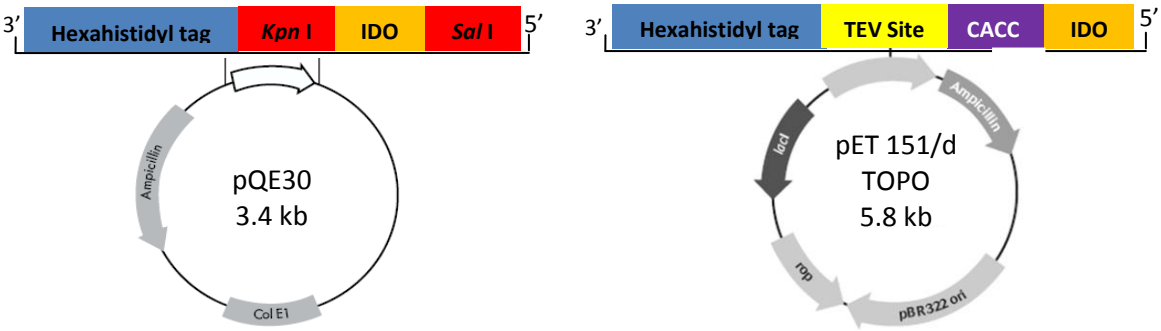

Figure 5.2 Vector maps of pQE30-IDO (Qiagen) and pET151/d TOPO-IDO (Invitrogen), both encoding the human IDO cDNA (black box). IDO cDNA is in-frame directionally cloned into the vector pET151/d TOPO which contains a N-terminal hexa-histidyl tag and TEV recognition site.

The pET151/d TOPO vector is 5760 bp and has a number of important features including a T7 promoter which allows IPTG-inducible expression of the recombinant

[1] pQE30 vector with hIDO was made by Dr. Papadopoulou

protein (Figure 5.2). Another feature of the vector is that it confers ampicillin resistance, allowing selection of the plasmid in *E. coli*. pET151d/TOPO has an N-terminal hexa-histidyl tag allowing metal-ion affinity chromatography to purify the protein. A significant feature of the vector is the TOPO® directional cloning site which allows rapid cloning of the PCR product as the PCR product can directional anneal to the pET151/d TOPO vector characterised by four bases (CACC) and its complementary sequence on the vector (GTGG). The rhIDO was transformed into an expression cell line *E. coli* BL21 (DE3) and positive colonies containing pET151/d TOPO-IDO were selected from 100 μg/ml ampicillin LB plates as the bacterial colonies conferred resistance to ampicillin.

5.2 Expression and Purification of rhIDO

The previous method for expression of the pQE30 vector was optimised for the new vector by reducing the induction temperature from 27.0 ^{o}C to 25.0 ^{o}C, which stopped inclusion bodies forming (Chapter 7, section 7.3.1) (*12*). rhIDO was purified using the same method as pQE30-IDO described in Chapter 7, section 7.4, with the addition of a second metal-ion affinity column to separate the hexa-histidyl tag cleaved and bound rhIDO after incubation with TEV protease and a gel filtration step using a FPLC, to further separate contaminants because for crystal formation pure protein is required. The FPLC trace shows two distinct peaks, the eluent between 40.0 and 60.0 ml was collected and run on a SDS gel to determine which peak the desired protein was in and it's purity (Figure 5.3). The first peak was a contaminant and the second at the tail was the desired pure protein rhIDO (Figure 5.3).

The concentration of the protein was calculated using an absorption coefficient determined by the pyridine hemochromagen method (Appendix IV Table A4.1, Chapter 7 Section 7.5.3). After purification, an SDS-gel was run and trypsin digestion of a sample of rhIDO enzyme was carried out, followed by MALDI-ToF mass spectrometry, 35 % of the total protein sequence was identified, which gave a

clear indication that the protein band was indeed rhIDO, (Appendix III, Figure A3.10. Chapter 7, section 7.4.8).

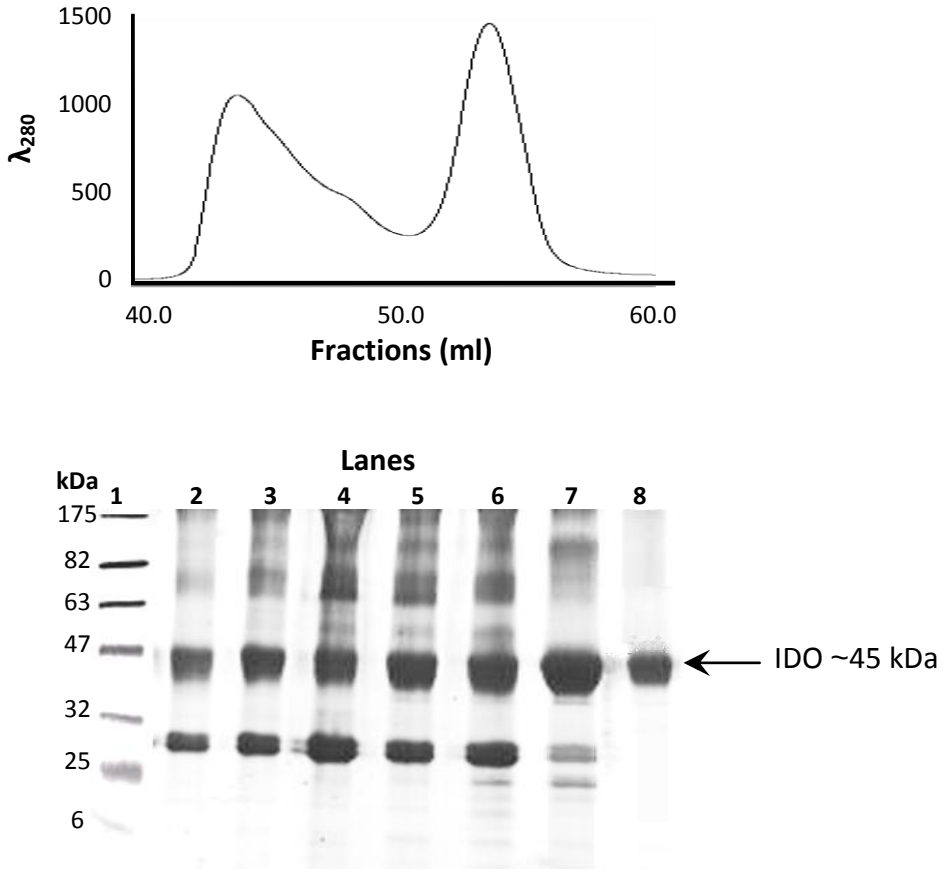

Figure 5.3. An FPLC trace of rhIDO separated by gel filtration. Reaction conditions: 50 mM Tris, pH 8.0, 4 ^{o}C. A 12 % SDS-PAGE gel showing the eluted fractions from the gel filtration column using the FPLC between 40.0 and 60.0 ml. Lane 1: 6 - 175 kDa broad range protein marker; Lane 2 - 7: IDO protein with contaminants (fractions from 40.0 – 54.0 ml); Lane 8: the tail end of the FPLC trace showing pure protein (Fractions from 54.0 – 60.0 ml).

5.3 Electronic Absorption Spectra of rhIDO

The absorption maxima for ferric and ferrous derivatives of rhIDO has maxima at 404, 500, 542 and 634 nm, which are consistent with a mixture of high-spin water bound heme and a minority contribution of low-spin nitrogenous ligated heme (Figure 5.4A). Comparison to previously published maxima for human IDO in Table 5.1 and Figure 5.4B shows that the published spectrum has more low-spin heme. The spectrum presented in this chapter is similar compared to early published literature (Figure 5.4) (*12, 15-18*). The reasons for this difference is outlined in the discussion. Reduction of rhIDO shows distinct low-spin heme peaks and a red shift in the Soret peak (from 404 to 427) which is consistent with the presence of a 5-coordinate heme species observed in all published data (Figure 5.4, Table 5.1) (*12*).

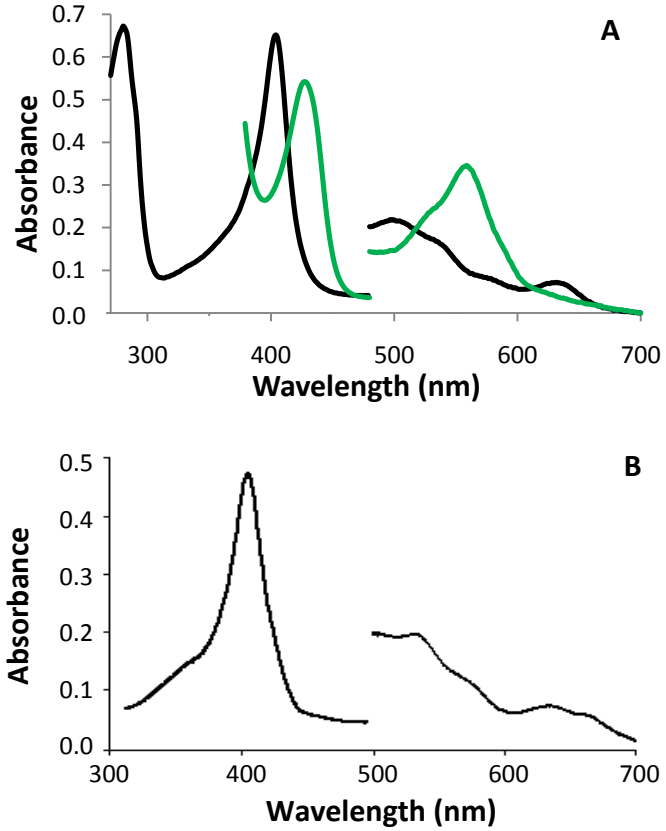

Figure 5.4. (**A**) UV-visible spectra of ferric rhIDO (black) and ferrous rhIDO (green). Conditions: 50 mM Tris, pH 8.0, 25.0 ^{o}C. (**B**) UV-visible spectra of ferric rhIDO reference (*12*), Conditions: 50 mM Tris, pH 8.1, 25.0 ^{o}C. Absorbance values in the visible region have been multiplied by a factor of 5.

On addition of 1 mM L-tryptophan to ferric rhIDO, formation of a low-spin species (λ_{max} = 411, 542 and 578 nm Figure 5.5B) occurs, the visible region at 540 and 570 nm, which is typical for rhIDO (Figure 5.5A, as indicated by Table 5.1). Values are consistent with other rhIDO reported values, which also support that the spectrum for rhIDO arises from formation of a low-spin, hydroxide bound heme (*12*). Formation of a stable ferrous-oxy complex is determined by characteristic peaks at approximately 540 and 570 nm in the visible region, which is observed in rhIDO (Figure 5.5B, Table 5.1).

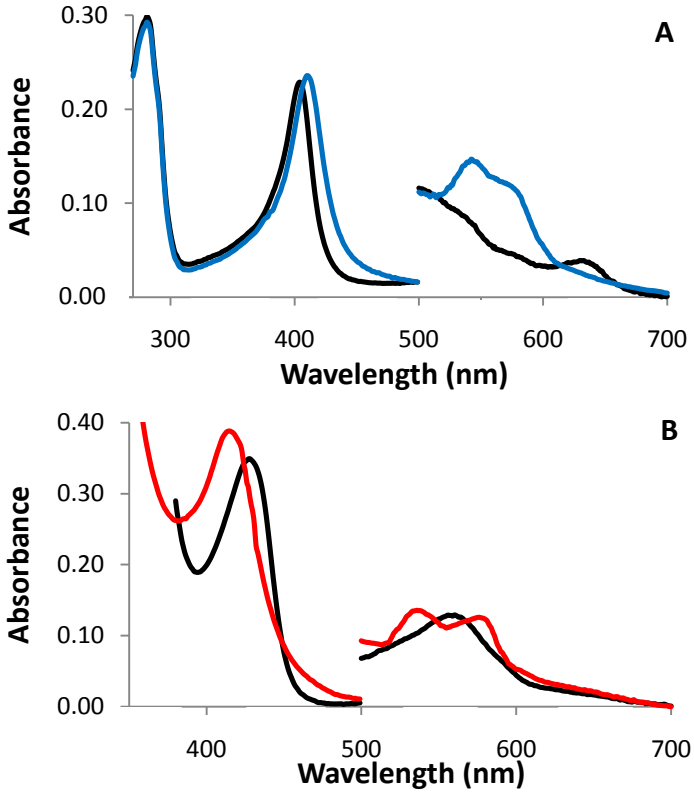

Figure 5.5. (A) UV-visible spectra of ferric rhIDO in the absence (black) and presence (blue) of 1 mM L-tryptophan. (B) UV-visible spectra of ferrous rhIDO (black) and ferrous-oxy rhIDO (red). Absorbance values in the visible region have been multiplied by a factor of 5. Reaction conditions: 50 mM Tris, pH 8.0, 25.0 ^{o}C.

Table 5.1. Absorption maxima for various ferric and ferrous derivatives of mammalian and rabbit IDO.

Derivative	λ_{max} (nm)				
	rhIDO[a]	rhIDO[b] (*12*)	rhIDO[c] (*15*)	Rabbit IDO[d] (*18*)	Rabbit IDO[e] (*17*) (*16*)
Ferric	404, 503, 536, 576, 634	404, 500, 533, 635	404, 500, 533, 635	405, 500, 534, 570, 632	404, 504, 536, 573, 634
Ferrous	427, 528[sh], 559	425, 527[sh], 558	425, 527[sh], 558	-	-
Ferrous-oxy	416, 540, 576	416, 539, 576	416, 539, 576	-	415, 544, 577
Ferric + L-tryptophan	411, 542, 578	410, 540, 576	410, 540, 576	411, 542, 572	530, 548, 562
Ferric azide	405, 536, 572, 632	413, 535, 572, 643	413, 535, 572, 643	415, 540, 572	-
Ferric fluoride	404, 497, 536, 631	404, 502, 532, 635	404, 502, 532, 635	403, 488, 528, 580, 608	-
Ferric cyanide	419, 540, 569[sh]	419, 538, 569[sh]	419, 538, 569[sh]	418, 540	420, 543, 575[sh]

[Sh] = shoulder. Conditions: [a] this work and [c] 50 mM Tris pH 8.0, 25.0 [o]C; [b] 0.5 M sodium phosphate, pH 7.0, 25.0 [o]C; [d] 0.1 M Potassium phosphate buffer, pH 5.5-8.5, 25.0 [o]C; [e] 0.1 M Potassium phosphate buffer, pH 7.3, 4.0 [o]C.

5.4 Binding of Non-Catalytic Ligands

The binding of various non-catalytic ligands to ferric enzyme is informative because it provides further information on the coordination environment of the heme. The representative spectra for the ferric anionic ligand-bound derivatives of rhIDO are presented in Figure 5.6 and the absorption maxima for rhIDO is presented in Table 5.1. Wavelength maxima for rhIDO found in this work are consistent with those previously published for rhIDO (*12, 16, 18, 19*).

The spectrum for the cyanide derivative of rhIDO is consistent with the formation of a six-coordinate, low-spin species with a red-shift of the Soret band and disappearance of the CT_1 band in the visible region. The binding constant (K_D) for the rhIDO-cyanide complex was calculated to be 3.6 ± 0.2 μM (Figure 5.7 and inset), which is in agreement with the spectroscopic data. Binding of azide was consistent with the formation of low- and high-spin species. Binding of fluoride resulted in the formation of a six-coordinate high-spin species which is characteristic of ligand binding to the sixth coordination site (Table 5.1).

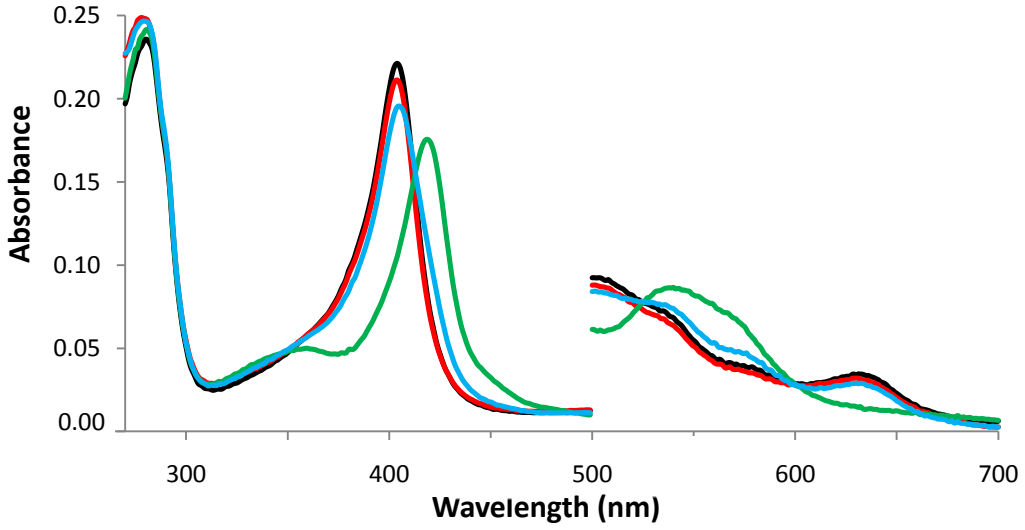

Figure 5.6. UV-visible spectra of ferric anionic ligand-bound derivatives of rhIDO: ferric (black), ferric-cyanide (green), ferric-azide (blue) and ferric-fluoride (red). Absorbance values in the visible region have been multiplied by a factor of 5. Reaction conditions: 50 mM Tris buffer, pH 8.0, 25.0 ˚C.

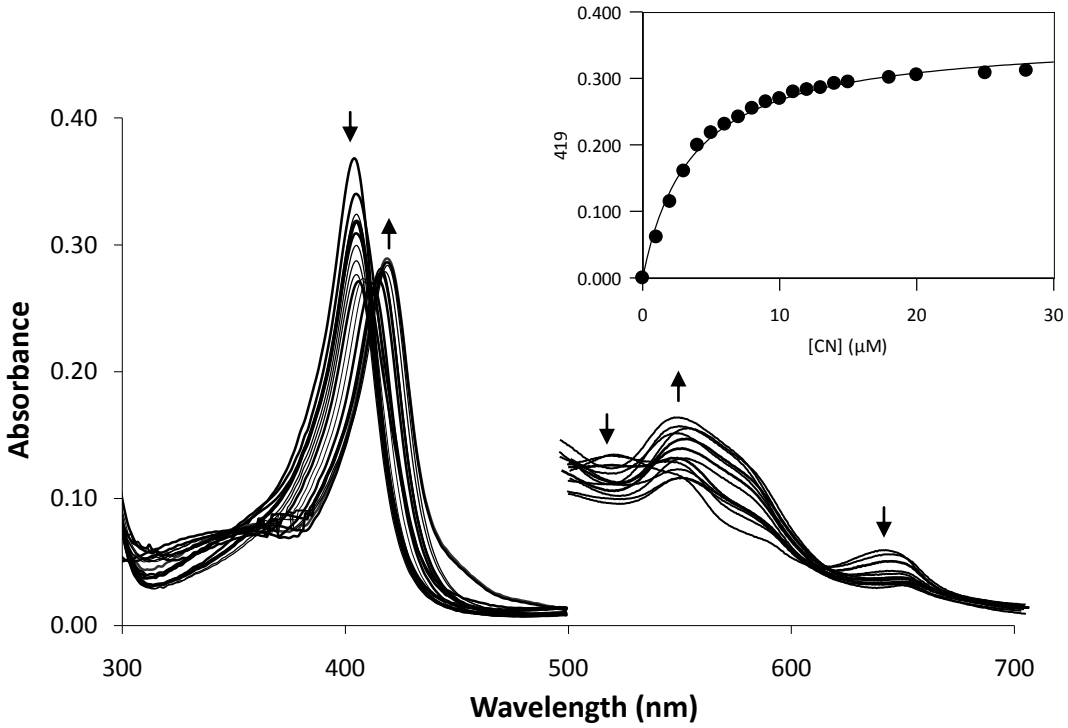

Figure 5.7. Representative data set for the determination of K_D for binding of cyanide to rhIDO. The arrows indicate the direction of change in absorbance upon successive additions of cyanide. Absorbance values in the visible region have been multiplied by a factor of 5. (Inset) Fit of data at 419 nm to Equation 7.4, Chapter 7. Reaction conditions: 50 mM Tris buffer, pH 8.0, 25.0 ˚C

5.5 Substrate Binding

Table 5.2. Binding of cyanide and L-tryptophan to ferric rhIDO. Reaction conditions: 50 mM Tris-HCl Buffer, pH 8.0, 25.0 °C

	K_D	
	L-Trp (μM)	**Cyanide (μM)**
rhIDO	238 ± 16	3.6 ± 0.2
rhIDO (*15*)	285 ± 6	3.6 ± 0.4
rhIDO (*10*)	320 ± 30	-

The new rhIDO construct exhibited characteristic spectroscopic changes upon binding of L-tryptophan at pH 8.0 (Table 5.1): the Soret band shifts to 411 nm which is consistent with the loss of high-spin heme and the formation of a low-spin, hydroxide-bound species on binding of L-tryptophan, most likely as a consequence of deprotonation of a water molecule in the active site (*12*). Binding constants, K_D, for binding of L-tryptophan to rhIDO were determined from the above data as 238 ± 16 at pH 8.0, which was consistent with published data (Figure 5.8, Table 5.2).

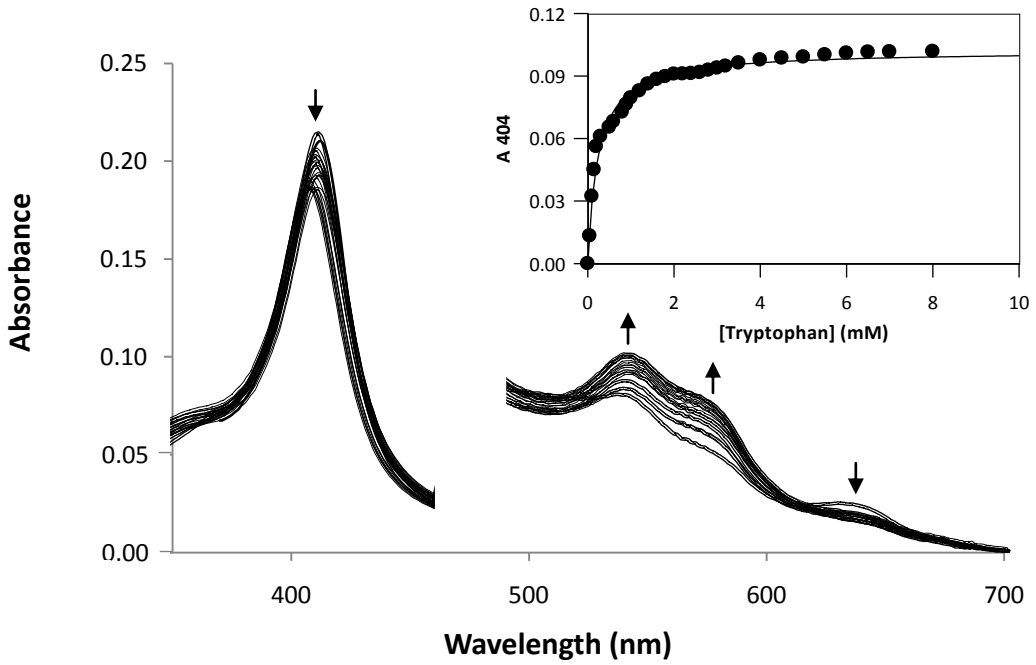

Figure 5.8. Representative data set for the determination of K_D for binding of L-tryptophan to rhIDO. The arrows indicate the direction of change in absorbance upon successive additions of L-tryptophan. Absorbance values in the visible region have been multiplied by a factor of 5. (Inset) Fit of data at 404 nm to Equation 7.4, Chapter 7. Reaction conditions: 50 mM Tris buffer, pH 8.0, 25.0 ˚C.

5.6 Steady-State Oxidation of L-tryptophan

A plot of the initial rate of dioxygenase activity (v/[E] s^{-1}), where v is the initial rate and [E] is the enzyme concentration in the reaction mixture *versus* L-tryptophan concentration (μM) shows a hyperbolic response. The data were fitted to the Michaelis-Menten equation (Chapter 7, Equation 7.5) and a representative plot for rhIDO is presented in Figure 5.9. Steady-state oxidation of L-tryptophan at pH 8.0 gave values for k_{cat} and K_m 1.4 ± 0.1 s^{-1} and 7.0 ± 0.4 μM respectively, which is consistent with published data for rhIDO compared in Table 5.3.

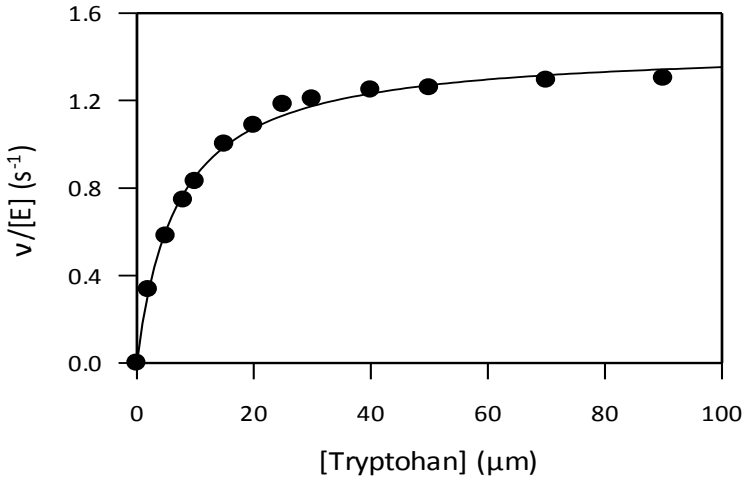

Figure 5.9. Steady-State oxidation of L-tryptophan by rhIDO. Reaction conditions: 50 mM Tris-HCl, pH 8.0, 25.0 °C.

Table 5.3 Steady-state oxidation of L-tryptophan by rhIDO. All data were fitted using the Michaelis-Menten equation (Chapter 7, Equation 7.5) where each value is an average of at least three independent measurements. Reaction conditions: 50 mM Tris-HCl, pH 8.0, 25.0 °C

	k_{cat} (s^{-1})	K_m (μM)
rhIDO	1.4 ± 0.1	7.0 ± 0.4
rhIDO (*12*)	5.2 ± 0.2	7.1 ± 1.1
rhIDO (*20*)	1.4 ± 0.1	7.0 ± 0.8
rhIDO (*21*)	3.1 ± 0.2	15.0 ± 2.0

5.7 Redox Potentiometry

The Fe^{3+}/Fe^{2+} reduction potentials for rhIDO were determined using the xanthine/xanthine oxidase assay with simultaneous reduction of a dye of known potential [2] (Chapter 7, Section 7.5.9). Reduction potentials for the Fe^{3+}/Fe^{2+} couple of rhIDO in the absence and presence of L-tryptophan were found to be -75 ± 3 mV and +11 ± 3 mV respectively (Figure 5.10, Table 5.4). A shift of approximately 40-80 mV was observed upon binding of L-tryptophan across all human IDO enzymes indicating that the enzyme binds substrate the same regardless of expression vector. The reduction potentials were calculated using two dyes; nile blue chloride (NBC) ($E^{o\prime}$ = -116 mV (*22*)) and toluene blue O (TBO) ($E^{o\prime}$ = +34 mV (*22*)) (Chapter 7, Section 7.5.9).

Table 5.4. Redox potentiometry values in the absence and presence of the substrate **L**-tryptophan for several expressed human IDO enzymes. Reaction conditions: 100 mM potassium phosphate, pH 7.0, 25.0 ^{o}C.

	No L-Trp (mV)	**3 mM L-Trp (mV)**
rhIDO	-75 ± 3	11 ± 3
rhIDO (*12*)	-30 ± 4	16 ± 4
rhIDO (*20*)	-63 ± 3	18 ± 3

[2] Results were checked by Dr. Igor Efimov.

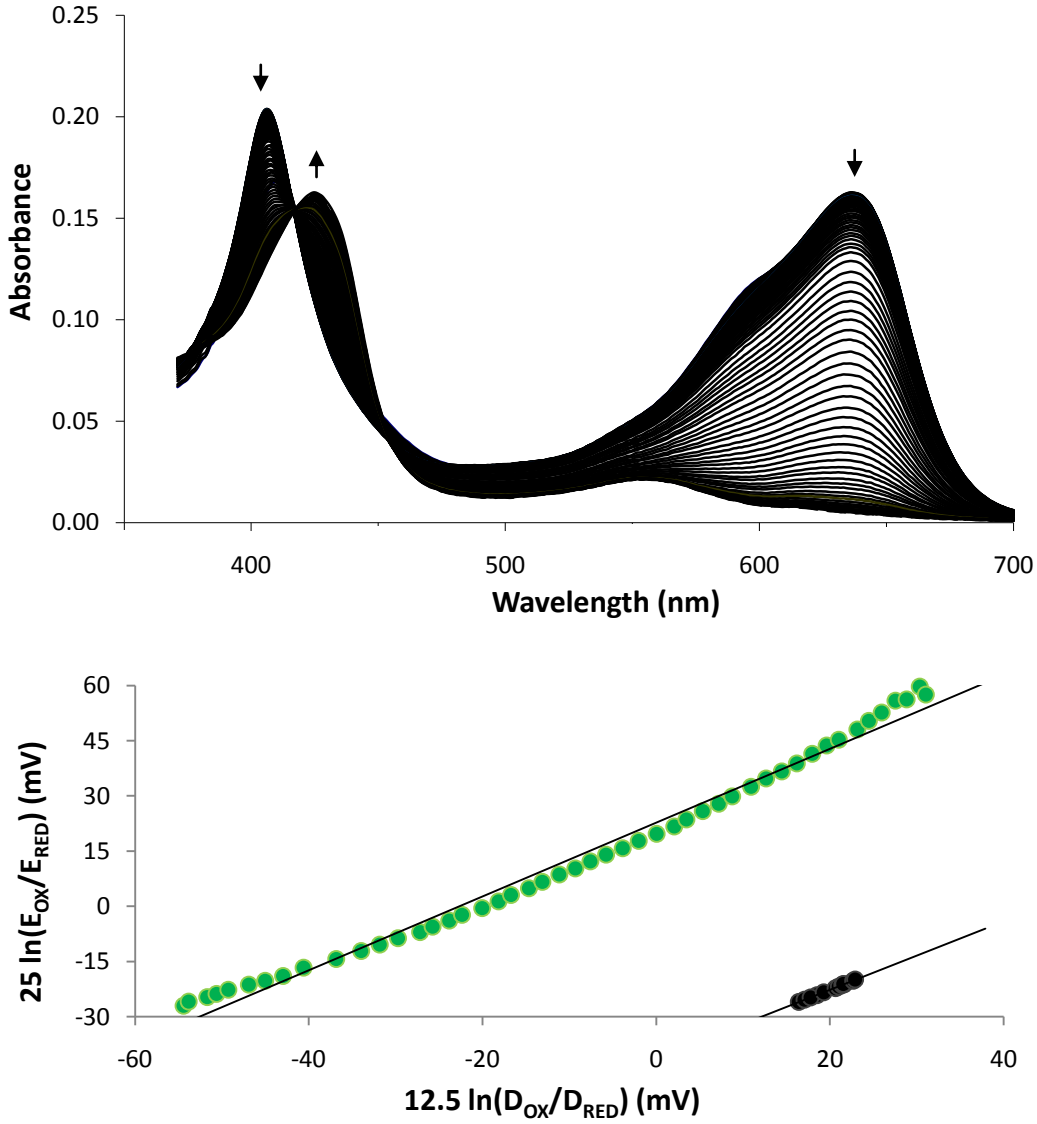

Figure 5.10. Redox potentiometry of rhIDO. (**A**) Spectral changes observed during determination of Fe^{3+}/Fe^{2+} reduction potential for rhIDO with the dye nile blue chloride. (**B**) Nernst plots for the data shown in (A) for the data collected in the absence (black) and presence of 3 mM L-tryptophan (green). Reaction conditions: 100 mM potassium phosphate, pH 7.0, 25.0 ^{o}C.

5.8 Crystallography

Pure rhIDO enzyme with the hexa-histidyl tag cleaved using TEV protease was used for crystal screens. Only two structures of rhIDO exist produced using the hanging drop vapour diffusion method, with 40 mg/ml rhIDO, protein solution: 10 mM MES buffer (pH 6.5) 25 mM NaCl, 1 mM 4-phyneylimidazol or 5 mM potassium cyanide and well solution: 100 mM CHES buffer (pH 9.0), 200 mM ammonium acetate, 10 % PEG 8K, which took 3 months to grow (*10*). Therefore initial crystal screen attempts were made by preparing the protein in a similar fashion. All of these were unsuccessful.

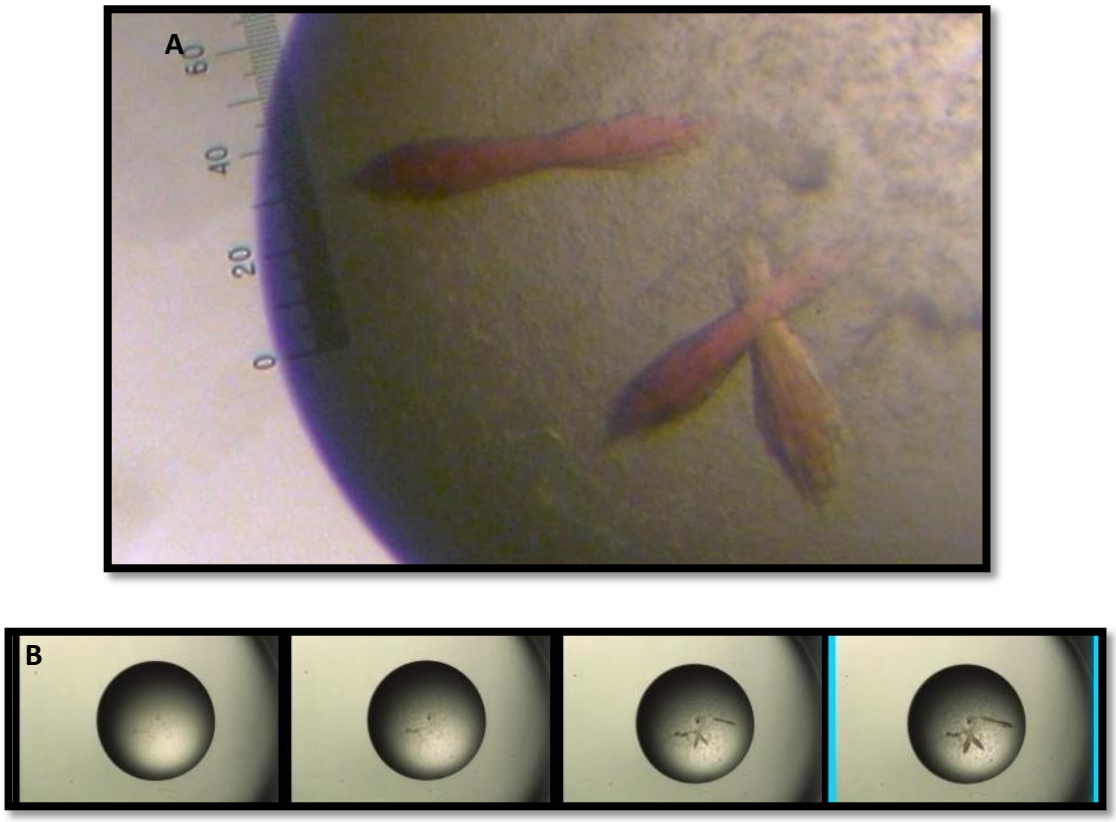

Figure 5.11. Pictures of the successful micro-crystal growth from the Emerald Cryo kit I and II well solution 20 % (v/v) PEG-300, Tris pH 8.5, 5% (w/v) PEG-8K and 10 % (v/v) glycerol at room temperature in the CrystalPro® HT (TriTek) a self contained plate storage hotel and imaging robot. (A) Microscope view of the crystal, 0.05 mm wide, 0.3 mm long, a single fibre is 0.005 mm wide. (B) The growth of the crystals over a 5 day period.

The robots TECAN and Cartesian were also used to screen solutions from the Emerald Wizard kit I and II and the Emerald Cryo Wizard Kit I and II at room temperature and at 6 ^{o}C using the sitting drop method (Chapter 7, section 7.6 and Appendix V). Two micro-crystals grew from the Emerald Cryo Kit using well conditions: 10 % (w/v) PEG-8K, Tris pH 7.0, 0.2 M $MgCl_2$ at 6 ^{o}C and promising crystals grew in a second well solution: 20 % (v/v) PEG-300, Tris pH 8.5, 5% (w/v) PEG-8K, 10 % (v/v) glycerol at room temperature (Figure 5.11). Attempts of regrowing these crystals were unsuccessful.

New crystal screens were attempted using the sitting drop method with over 300 crystal formulations from multiple companies, which produce kits including Molecular dimensions, Hampton research and Emerald biosciences (Appendix V) [3]. Formulations which contained similar components to the first micro-crystals grew successfully, they contained PEG-8K and Tris pH 7.5 - 9.0. A formulation from Hampton Research (Tris pH 8.5, 8% PEG 8K) produced diffracting crystals without need to refine the conditions (Figure 5.12a). The cryo protectant used was 30 % xylitol, which was also used by Sugimoto with their IDO crystals for cryo diffraction (*10*). The diffraction results obtained from the in-house Rigaku RU2HB x-ray generator were in the region of 5 - 6 Å therefore the crystals need to be taken to a synchrotron for higher resolution (Figure 5.12b, Chapter 7, section 7.6.2).

[3] Dr. I. Efimov and Andrea Gumiero aided in crystal screening attempts.

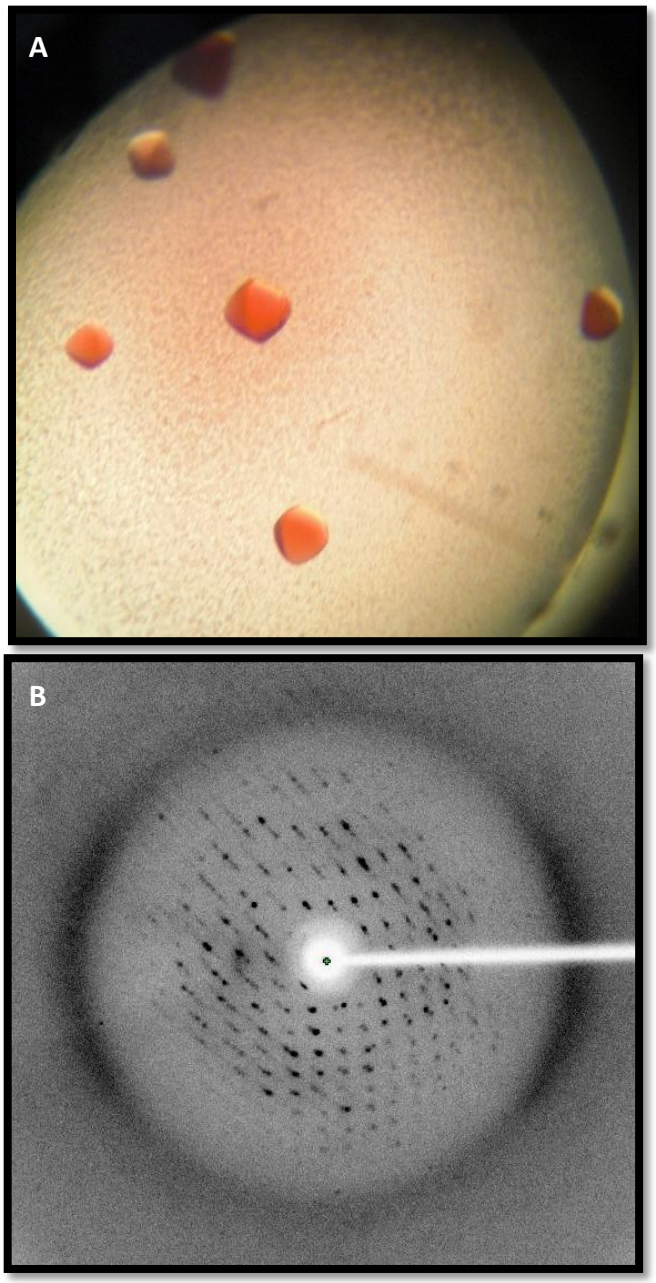

Figure 5.12. rhIDO diffracting crystals. A) Protein solution: 0.5 M Tris pH 8.0, 5 mM 4-phenylimidazol. Well Solution: 0.1 M Tris pH 8.5, 8 % PEG 8K. B) Cryo protectant for diffraction: 30 % Xylitol, the reflections show the diffracting crystal and the resolution was 5 - 6 Å. Diffraction was controlled and the data was collected using the Rigaku Structure Studio Suite and the diffraction data was analysed using the computer software Imosfilm (Collaborative Computational Project 4) [4].

[4] Crystal data collect with Dr. P. Moody and Andrea Gumiero's help.

5.9 Discussion

The intention in this Chapter was to make characteristic comparisons between IDO in a new vector compared to other rhIDOs, to determine whether changing the vector affected the structure and/or function of the enzyme and to use this as a basis for growing IDO crystals to further understand dioxgenases in terms of their mechanism. IDO cDNA was cloned into a new vector pET151/d TOPO, which had the capability of hexa-histidyl tag cleavage, which could have previously potentially prevented crystal formation [5]. IDO was expressed and purified using similar methods to previous rhIDOs with the addition of a couple purification steps and then checked spectroscopically, electrochemically and kinetically to ensure that the protein had not been altered by the process.

Expression and Purification

The enzyme was ~45 kDa in size which was the same as all other hIDOs expressed in the field. Purification of the enzyme rhIDO via a FPLC on a gel filtration column proved quite important as a significant impurity was removed. The additional step of hexa-histidyl tag removal and running the protein down the metal-ion affinity column to separate cleaved and non-cleaved protein seemed to be key in allowing crystal formation as all previous attempts without this step in the past did not successfully lead to crystal formation anf.

Heme Coordination Environment

The electronic absorption spectra at pH 8.0 for ferric wild type rhIDO had two distinct species in solution: a high- and low-spin heme species, which was similar to previously published data, however the spectra indicated that the protein had more high-spin (*12, 15-18*). In the 1980s ferric IDO was obtained from rabbit mucosa and it was observed that the enzyme had more high-spin species indicated by the peaks at approximately 500, 630 nm, which the data presented in this

[5] Previous crystal trials were performed by Dr N. Papadopoulou and Dr. N. Chauhan.

chapter fits with (*16-18*). Reduced high-spin species were observed for recent bacterial expression systems for mammalian IDO enzymes and a reason for this discrepancy could be due to improvements in protein purification methods and perhaps the speed of protein preparations, might be influential here (*12, 15*). Production of high-spin protein is reproducible and preparations of rhIDO from the Mauk laboratory in Vancouver also exhibit higher contributions from high-spin heme than have been reported previously [6] (*12, 15*).

Ferrous wild type rhIDO was consistent with the typical spectra observed by other rhIDOs, indicated by a change from a mixed-spin species as a ferric enzyme to low-spin 5-coordinate species when reduced (*12*). The ferrous-oxy derivative of the enzyme formed normally with the typical peaks at 540 and 570 nm in the visible region for IDOs, which is atypical for TDOs (*12, 15-17, 20, 23-26*).

Substrate binding

Upon binding of substrate the predominant species present is hydroxide-bound heme which is consistent with other rhIDO data reported in Table 5.1 (*12, 18, 27*). The binding affinity to ferric rhIDO is in the same range as that to ferric and ferrous rhTDO ≈ 200 - 300 µM (*20*), however unlike TDO, IDO discriminates between the ferric and ferrous forms of the enzyme, so that the substrate preferentially binds to the ferrous form (Table 5.3). This data supports that the new rhIDO binds substrate in the same fashion as all other IDOs. Upon binding of non catalytic ligands similar binding to other rhIDOs was observed (*12*).

Redox Properties

Table 5.4 collates the redox data available in the field for IDO and as a comparison to the data obtained in this work. The redox potentiometric data was similar to previous data for IDO in other vectors supporting that changing the vector to pET151/d TOPO did not affect the structure and function of rhIDO (*12, 15, 20*). The

[6] A personal communication from Professor G. Mauk to Professor E. Raven

observed potential in the absence of substrate was -75 ± 3 mV which was similarly located to other dioxygenases, between the potentials observed in myoglobins (E^o ~+50 mV (*28*)) and the heme peroxidases (E^o between -100 to -250 mV (*29-35*)). Upon substrate binding there was a 64 mV increase in reduction potential as observed by all dioxygenases, however the shift upon binding of substrate to mammalian TDOs is smaller, which confirms that the new IDO has stabilisation of the ferrous derivative as other rhIDOs (*12, 15, 20*). The shift upon substrate binding in dioxygenases is small compared to cytochrome P450s which is ≈130 - 140 mV (*36, 37*).

Oxidation of Substrate

Turnover of substrate for rhIDO is identical to that for rhTDO and similar to all other IDOs (k_{cat} = 1.4 s^{-1}) (Table 5.3) (*20*). The ferric form of rhIDO was inactive as are all other IDOs, which is in contrast to TDOs which can oxidise substrate in the ferric form in aerobic conditions (*20*). The steady state data indicate that rhIDO binds substrate as evidenced by K_m as all other IDOs, therefore supporting that different vectors do not affect the activity of the enzyme (*12, 15, 20*). The reason different vectors could affect the activity of the enzyme is that if the vector has additional tags for example, they could influence the structure of the protein thus affect the catalytic binding site.

Crystallography and Summary

Currently the rhIDO used for growing crystals has been shown to be similar to all other IDOs and crystal growth of rhIDO crystals is reproducible. The expectation of future work will involve binding other inhibitors to rhIDO and attempt to crystallise them. An important inhibitor to use would be 1-methyl-L-tryptophan as recently it has been shown to have some activity with rhIDO and 1-methyl-L-tryptophan is being used in drug trials, so the structure with the inhibitor bound would be globally and medically important (*21, 38*). Also a ferrous structure of the enzyme does not currently exist, which would also be helpful in understanding the mechanism better.

5.10 References

1. Sono, M., Roach, M. P., Coulter, E. D., and Dawson, J. H. (1996) Heme-Containing Oxygenases, *Chem Rev 96*, 2841-2888.
2. Hayaishi, O., and Yoshida, R. (1990) Indoleamine 2,3-dioxygenase: Properties and functions of a superoxide utilising enzyme, *Prog. Inorg. Chem. 38*, 75-94.
3. Thomas, S. R., and Stocker, R. (1999) Redox reactions related to indoleamine 2,3-dioxygenase and tryptophan metabolism along the kynurenine pathway, *Redox Rep 4*, 199-200.
4. Higuchi, K., and Hayaishi, O. (1967) Enzymic formation of D-kynurenine from D-tryptophan, *Arch Biochem Biophys 120*, 397-403.
5. Yamamoto, S., and Hayaishi, O. (1967) Tryptophan pyrrolase of rabbit intestine. D- and L-tryptophan-cleaving enzyme or enzymes, *J Biol Chem 242*, 5260-5266.
6. Kerr, S. J., Armati, P. J., Pemberton, L. A., Smythe, G., Tattam, B., and Brew, B. J. (1997) Kynurenine pathway inhibition reduces neurotoxicity of HIV-1infected macrophages, *Neurology 49*, 1671-1681.
7. Grohmann, U., Fallarino, F., and Puccetti, P. (2003) Tolerance, DCs and tryptophan: much ado about IDO, *Trends Immunol 24*, 242-248.
8. Aquilina, J. A., Carver, J. A., and Truscott, R. J. (1997) Oxidation products of 3-hydroxykynurenine bind to lens proteins: relevance for nuclear cataract, *Exp Eye Res 64*, 727-735.
9. Munn, D. H., Zhou, M., Attwood, J. T., Bondarev, I., Conway, S. J., Marshall, B., Brown, C., and Mellor, A. L. (1998) Prevention of allogeneic fetal rejection by tryptophan catabolism, *Science 281*, 1191-1193.
10. Sugimoto, H., Oda, S., Otsuki, T., Hino, T., Yoshida, T., and Shiro, Y. (2006) Crystal structure of human indoleamine 2,3-dioxygenase: catalytic mechanism of O2 incorporation by a heme-containing dioxygenase, *PNAS 103*, 2611-2616.
11. Littlejohn, T. K., Takikawa, O., Skylas, D., Jamie, J. F., Walker, M. J., and Truscott, R. J. (2000) Expression and purification of recombinant human indoleamine 2, 3-dioxygenase, *Protein Expr Purif 19*, 22-29.
12. Papadopoulou, N. D., Mewies, M., McLean, K. J., Seward, H. E., Svistunenko, D. A., Munro, A. W., and Raven, E. L. (2005) Redox and spectroscopic properties of human indoleamine 2,3-dioxygenase and a His303Ala variant: implications for catalysis, *Biochemistry 44*, 14318-14328.
13. Vottero, E., Mitchell, D. A., Page, M. J., MacGillivray, R. T., Sadowski, I. J., Roberge, M., and Mauk, A. G. (2006) Cytochrome b(5) is a major reductant in vivo of human indoleamine 2,3-dioxygenase expressed in yeast, *FEBS Lett 580*, 2265-2268.
14. Carrington, J. C., and Dougherty, W. G. (1988) A viral cleavage site cassette: identification of amino acid sequences required for tobacco etch virus polyprotein processing, *Proc Natl Acad Sci U S A 85*, 3391-3395.
15. Chauhan, N., Basran, J., Efimov, I., Svistunenko, D. A., Seward, H. E., Moody, P. C., and Raven, E. L. (2008) The role of serine 167 in human indoleamine

2,3-dioxygenase: a comparison with tryptophan 2,3-dioxygenase, *Biochemistry 47*, 4761-4769.

16. Uchida, K., Shimizu, T., Makino, R., Sakaguchi, K., Iizuka, T., Ishimura, Y., Nozawa, T., and Hatano, M. (1983) Magnetic and natural circular dichroism of L-tryptophan 2,3-dioxygenases and indoleamine 2,3-dioxygenase. II. Spectra of their ferric cyanide and ferrous carbon monoxide complexes and an oxygenated form, *J Biol Chem 258*, 2526-2533.
17. Uchida, K., Shimizu, T., Makino, R., Sakaguchi, K., Iizuka, T., Ishimura, Y., Nozawa, T., and Hatano, M. (1983) Magnetic and natural circular dichroism of L-tryptophan 2,3-dioxygenases and indoleamine 2,3-dioxygenase. I. Spectra of ferric and ferrous high spin forms, *J Biol Chem 258*, 2519-2525.
18. Sono, M., and Dawson, J. H. (1984) Extensive studies of the heme coordination structure of indoleamine 2,3-dioxygenase and of tryptophan binding with magnetic and natural circular dichroism and electron paramagnetic resonance spectroscopy, *Biochim Biophys Acta 789*, 170-187.
19. Sono, M., Taniguchi, T., Watanabe, Y., and Hayaishi, O. (1980) Indoleamine 2,3-dioxygenase. Equilibrium studies of the tryptophan binding to the ferric, ferrous, and CO-bound enzymes, *J Biol Chem 255*, 1339-1345.
20. Basran, J., Rafice, S. A., Chauhan, N., Efimov, I., Cheesman, M. R., Ghamsari, L., and Raven, E. L. (2008) A kinetic, spectroscopic, and redox study of human tryptophan 2,3-dioxygenase, *Biochemistry 47*, 4752-4760.
21. Lu, C., Lin, Y., and Yeh, S. R. (2009) Inhibitory substrate binding site of human indoleamine 2,3-dioxygenase, *J Am Chem Soc 131*, 12866-12867.
22. Clark, M. W. (1972) *Oxidation-Reduction Potentials of Organic Systems*, Robert E. Kreiger Publishing Co., Huntington, NY.
23. Batabyal, D., and Yeh, S. R. (2007) Human tryptophan dioxygenase: a comparison to indoleamine 2,3-dioxygenase, *J Am Chem Soc 129*, 15690-15701.
24. Batabyal, D., and Yeh, S. R. (2009) Substrate-Protein Interaction in Human Tryptophan Dioxygenase: The Critical Role of H76, *J Am Chem Soc*.
25. Forouhar, F., Anderson, J. L., Mowat, C. G., Vorobiev, S. M., Hussain, A., Abashidze, M., Bruckmann, C., Thackray, S. J., Seetharaman, J., Tucker, T., Xiao, R., Ma, L. C., Zhao, L., Acton, T. B., Montelione, G. T., Chapman, S. K., and Tong, L. (2007) Molecular insights into substrate recognition and catalysis by tryptophan 2,3-dioxygenase, *PNAS 104*, 473-478.
26. Fukumura, E., Sugimoto, H., Misumi, Y., Ogura, T., and Shiro, Y. (2009) Cooperative binding of L-trp to human tryptophan 2,3-dioxygenase: resonance Raman spectroscopic analysis, *J Biochem 145*, 505-515.
27. Terentis, A. C., Thomas, S. R., Takikawa, O., Littlejohn, T. K., Truscott, R. J., Armstrong, R. S., Yeh, S. R., and Stocker, R. (2002) The heme environment of recombinant human indoleamine 2,3-dioxygenase. Structural properties and substrate-ligand interactions, *J Biol Chem 277*, 15788-15794.
28. Raven, E. L., and Mauk, A. G. (2001) Chemical reactivity of the active site of myoglobin, *Adv. Inorg. Chem. 51*, 1-49.
29. Conroy, C. W., Tyma, P., Daum, P. H., and Erman, J. E. (1978) Oxidation-reduction potential measurements of cytochrome c peroxidase and pH

dependent spectral transitions in the ferrous enzyme, *Biochim Biophys Acta 537*, 62-69.

30. Goodin, D. B., and McRee, D. E. (1993) The Asp-His-Fe triad of cytochrome c peroxidase controls the reduction potential, electronic structure, and coupling of the tryptophan free radical to the heme, *Biochemistry 32*, 3313-3324.
31. Harbury, H. A. (1957) Oxidation-reduction potentials of horseradish peroxidase, *J Biol Chem 225*, 1009-1024.
32. Jones, D. K., Dalton, D. A., Rosell, F. I., and Raven, E. L. (1998) Class I heme peroxidases: characterization of soybean ascorbate peroxidase, *Arch Biochem Biophys 360*, 173-178.
33. Millis, C. D., Cai, D. Y., Stankovich, M. T., and Tien, M. (1989) Oxidation-reduction potentials and ionization states of extracellular peroxidases from the lignin-degrading fungus Phanerochaete chrysosporium, *Biochemistry 28*, 8484-8489.
34. Tanaka, M., Ishimori, K., and Morishima, I. (1998) Structural roles of the highly conserved glu residue in the heme distal site of peroxidases, *Biochemistry 37*, 2629-2638.
35. Yamada, H., Makino, R., and Yamazaki, I. (1975) Effects of 2,4-substituents of deuteropheme upon redox potentials of horseradish peroxidases, *Arch Biochem Biophys 169*, 344-353.
36. Daff, S. N., Chapman, S. K., Turner, K. L., Holt, R. A., Govindaraj, S., Poulos, T. L., and Munro, A. W. (1997) Redox control of the catalytic cycle of flavocytochrome P-450 BM3, *Biochemistry 36*, 13816-13823.
37. Sligar, S. G. (1976) Coupling of spin, substrate, and redox equilibria in cytochrome P450, *Biochemistry 15*, 5399-5406.
38. Chauhan, N., Thackray, S. J., Rafice, S. A., Eaton, G., Lee, M., Efimov, I., Basran, J., Jenkins, P. R., Mowat, C. G., Chapman, S. K., and Raven, E. L. (2009) Reassessment of the reaction mechanism in the heme dioxygenases, *J Am Chem Soc 131*, 4186-4187.

CHAPTER 6

THE PAST, PRESENT AND FUTURE OF THE HUMAN HEME DIOXYGENASES

The dioxygenases were discovered over 70 years ago however there is very little information about them compared to other heme containing enzymes such as peroxidases, cytochrome P450 and the globins. Before I started my PhD in 2006 there were only expression systems for rat TDO in comparison to IDO, which had several expression systems for human IDO (Chapter 1, Table 1.1). Information regarding the dioxygenases increased immensely after 2005 for both TDO and IDO, which has answered a few questions, corrected some facts and left still more questions. In this chapter some of the misconceptions in the early literature and open questions are discussed.

6.1 Human TDO

Human TDO was discovered in the liver in 1955 and the only information gathered for human TDO was in 1980, which determined that the L-isomer of tryptophan was preferred over the D-isomer as a substrate (*1, 2*). There was nearly a 30 year gap before the mammalian TDO information boom, which was largely due to the development of three expression systems, two of which were truncated forms of human TDO and the other was full length human TDO presented in Chapter 2 (*3-5*). The basic characterisation of hTDO was highly important in the field as both TDO and IDO are immunologically active and cause physiological, pathophysiological and neurological problems.

A number of similarities were found within the dioxygenase family such as a positive shift in the Fe^{2+}/Fe^{3+} redox couple in the absence and presence of substrate suggesting stabilisation of the ferrous form, though hTDO has a smaller shift than hIDO, bacterial and rat TDO (Chapter 2). There were some significant differences though, such as the fact that all the dioxygenases are only active in the ferrous form apart from hTDO which is active as both the ferric and ferrous form (Chapter 2). This was significant as mechanisms have been based around the fact that dioxygenases were only active in the ferrous form, which was assumed to be made from the ferrous form of the enzyme whereby the substrates L-tryptophan and dioxygen bind.

In addition there was some dissimilarity between the rhTDO data presented in the three papers. The truncated forms of rhTDO could form a stable ferrous-oxy complex however full length rhTDO could not, which is discussed in detail later.

6.2 The Subunit Structure of TDO

Many errors were initially presented in the dioxygenase literature regarding the structure of the dioxygenase enzymes, which were solved after the crystal structures were published. The subunit structure of TDO was discussed briefly in the literature whereby the subunits were determined by gel filtration and confirmed by SDS gels using other proteins as standards (*2*). The molecular weight of the tetramer was determined as ≈160 kDa, which was ascribed to different subunits (α and β) in the enzyme as two identical dimers combining to form the TDO tetramer ($\alpha_2\beta_2$) (≈40 and ≈50 kDa) (*2, 6, 7*). Also the enzyme contained two moles of protoheme IX per mole of tetramer, therefore it was assumed that each dimer had an active site (*2, 6, 7*).

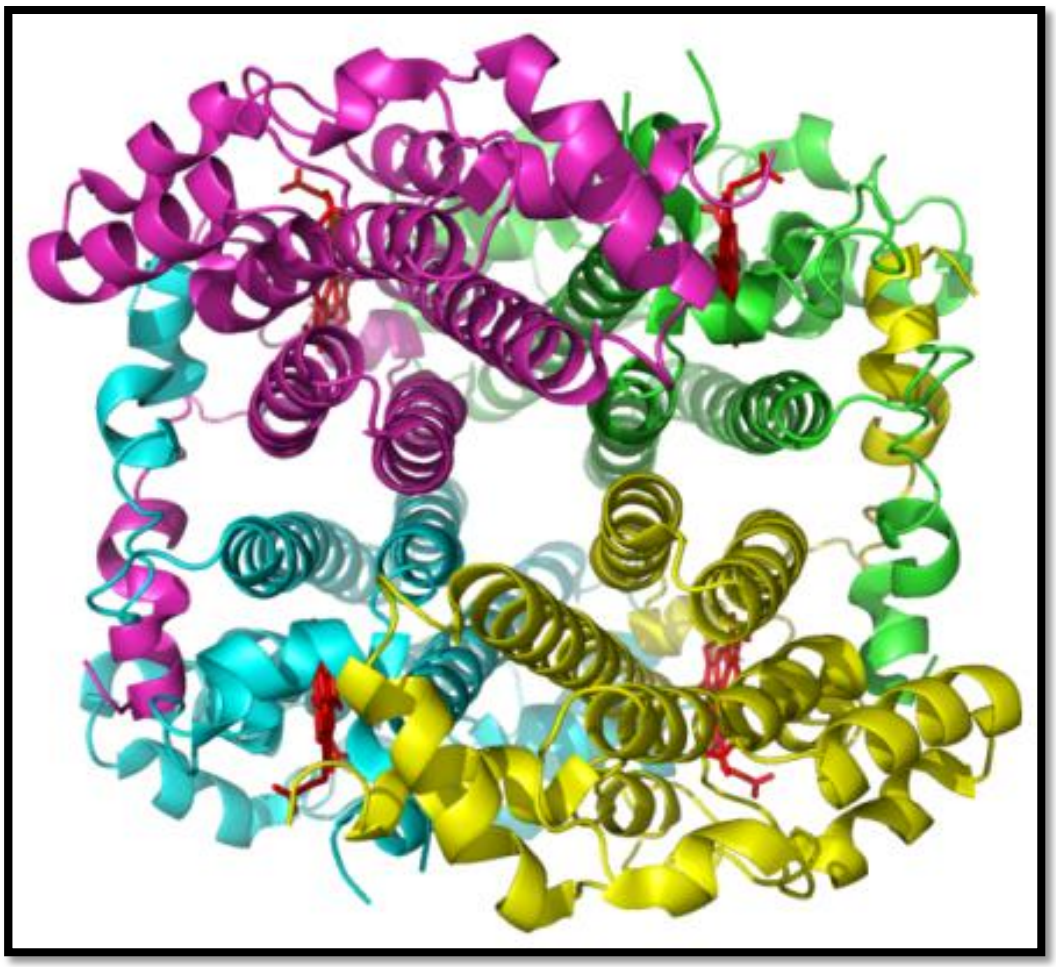

Figure 6.1 *X. campestris* TDO crystal structure showing four subunits, α_4 (pink, green, yellow and cyan), with four prosthetic heme groups (red) (*8*).

The crystal structure for *X. campestris* TDO was solved in 2006, which not only showed that all four subunits were the same (α_4) but that each subunit had a catalytic pocket with a heme prosthetic group, therefore there is a total of four heme prosthetic groups (Figure 6.1) (*8*).

The two bands observed on the TDO gels was determined to be the full length protein and a cleaved form of the dioxygenase enzyme, whereby the N-terminus was cleaved as opposed to the two bands corresponding to two different subunits. Several groups showed that the truncated TDO and the full length enzyme had the same properties (*2, 6, 7, 9*)[1]. Furthermore, the reason for the truncation of both enzymes is still unknown.

To further our knowledge about TDO, a crystal structure of the mammalian form is required to make a comparison with the bacteria crystal structure, as the bacterial TDO enzymes have a molecular weight of ~120 kDa whereas mammalian TDO is much larger, ~190 kDa. The hTDO structure would also help with determining the reaction mechanism and be utilised by the pharmaceutical industry because TDO is a target for drug discovery.

6.3 The Presence and Role of a Distal Histidine in TDO and IDO

The heme coordination structure was a major part of the dioxygenase literature and as discussed in Chapter 1, the electron-paramagnetic resonance data (EPR) and magnetic circular dichroism (MCD) data indicated that both TDO and IDO had a distal histidine in the catalytic pocket. The distal histidine was proposed to have a dual purpose; it was assumed to stabilise the heme-bound dioxygen, as observed in the globins, particularly as IDO and mollusc IDO-like myoglobins shared 37 % sequence identity (*10*). Also it was assumed that the distal histidine had an integral role in the catalytic mechanism by initiating the deprotonation of the indole N_1 (*11*).

[1] Dr. Papadopoulou's thesis, 2005, University of Leicester.

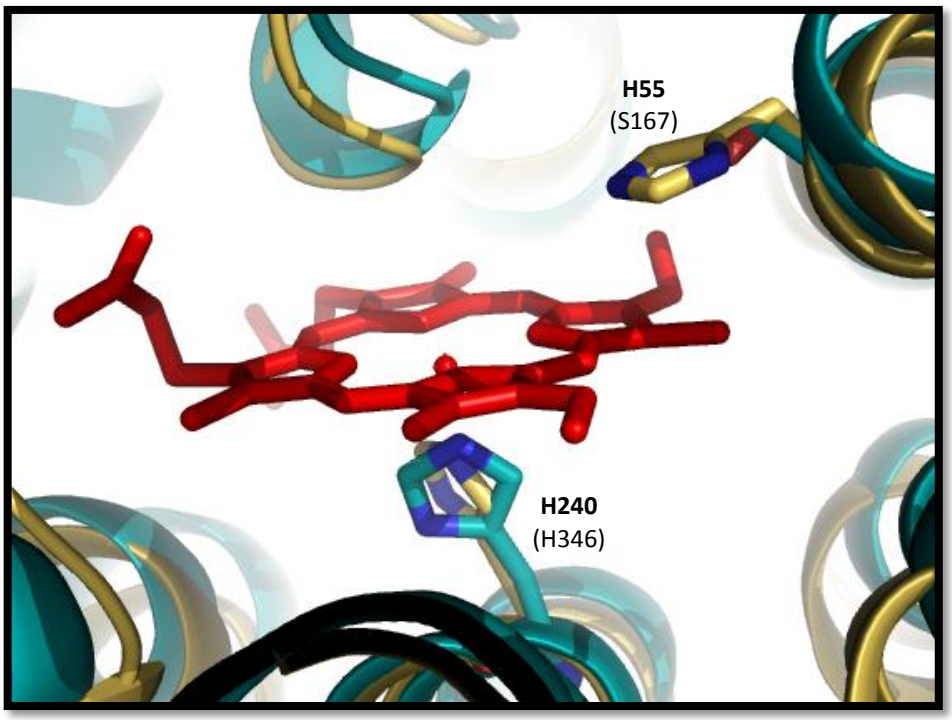

Figure 6.2 TDO (yellow, bold label) and IDO (blue, label in parenthesis) crystal structure overlaid showing the proximal histidine for both enzymes, the TDO distal histidine and the IDO distal serine (*8, 12*).

In 2005 the mammalian IDO crystal structure was solved, which surprised the community as no histidine was found in the distal pocket and a serine residue (S167) was in the place of the assumed distal histidine (Figure 6.2) (*12*). In 2007 when the crystal structure of bacterial TDO was published a distal histidine was found located in the distal pocket (H55) (Figure 6.2) (*8*). Since the heme coordination environment was clarified, new mechanisms have been proposed.

More detailed structural information for IDO is required to determine the full role of the serine residue and other active site residues in the reaction mechanism and substrate binding, which is the reason in Chapter 4 a new expression system was created for mammalian IDO to reproduce and grow other crystals.

Initially, mutagenesis investigations were used to search for the proximal and distal histidine residues by observing whether removal of the histidine would inactivate the enzyme, thus it could be assumed to be a potential catalytic residue (*13-19*).

However after the IDO crystal structure was published, mutagenesis studies were used to determine the role the S167 residue in the active site (*20*). The S167 residue was shown to not be catalytically active, or involved in dioxygen binding (*20*).

As mentioned previously, full length mammalian TDO and others including *X. campestris* TDO cannot form a stable ferrous-oxy complex (*4, 8, 21*). Mutagenesis experiments involving switching S167 with a histidine resulted in a destabilised ferrous-oxy complex, a TDO characteristic, which has not been observed in hemoprotein literature previously (*20*). Therefore the distal histidine in TDOs could be a reason they cannot form a stable ferrous-oxy complex, which is contrary to the situation in the globins where the distal histidine has an essential role in stabilising heme-bound dioxygen. In Chapter 3 H76 was switched to a serine in rhTDO to observe whether there would be any IDO characteristics; however there were none and the ferrous-oxy complex remained unstable.

In Chapters 2 and 3 wild type TDO and the variants were shown to react with carbon monoxide and other diatomics, which confirmed that the ferrous heme group was reactive and meant that the ferrous enzyme is capable of binding oxygen, but it could not form a stable complex (*4*). In contrast, the truncated TDO enzymes and the histidine variants could form stable ferrous-oxy complexes, which suggested that there was a significant difference between the full length enzyme and the truncated forms (*5, 22*). The truncation was discussed in Chapter 3 as a possible reason for the stability of the ferrous-oxy complex. The curious dissimilarity between the TDO enzymes, which do not form a stable ferrous-oxy complex (apart from the truncated form) and the IDO enzyme which can bind dioxygen, and the physiological importance still remains to be resolved.

6.4 How Many Binding Sites Do the Dioxygenases Have?

Another complication in the literature includes substrate binding in the dioxygenases. The dioxygenase literature has recently raised an old question

regarding whether the dioxygenases have one or two binding sites. During the 1970s and 80s several papers in the literature suggested that TDO (*23*) and IDO (*24-28*) had two binding sites, the catalytic pocket and a secondary binding site (Scheme 6.1). Recently a few papers have revived the debate, renaming the two sites the catalytic pocket and the inhibitory substrate binding site (Scheme 6.1) (*29, 30*).

The data were based on photodissociation experiments of carbon monoxide (CO) and tryptophan (*30, 31*). CO has been used extensively as a local probe of heme protein conformation and dynamics. The observation that the photodissociation reaction of CO allows the substrate to be released from the catalytic binding site, which requires large conformational changes, followed by CO rebinding very slowly suggested that substrate bound at the secondary binding site prevented the CO from rebinding, thus confirming the presence of a secondary site (*30*). Other data which support the presence of two binding sites is also provided as a solution for the observation of substrate-inhibition behaviour in IDO, which is discussed later (Scheme 6.1).

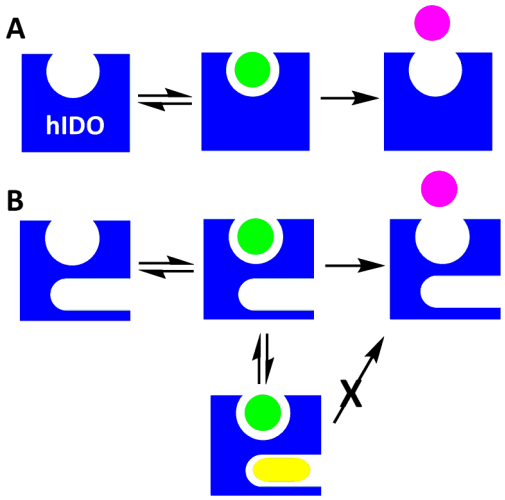

Scheme 6.1 A schematic illustration of (**A**) the typical mechanism with one binding site where the substrate (green) reversibly binds to the catalytic pocket to form the product *N*-formylkynurenine (pink) or (**B**) the mechanism with two binding pockets, whereby the reaction proceeds the same as the single binding pocket or if a substrate/inhibitor (yellow) reversibly binds the inhibitory substrate-binding pocket, it inhibits the enzyme from producing product.

The current mammalian IDO crystal structure has the inhibitor 4-phenylimidazole (PIM) bound, however there is no second PIM molecule bound at the proposed inhibitory substrate binding site. It is claimed that the inhibitory binding site binds substrates (L-tryptophan and 1-methyl-L-tryptophan), an effector (3-indole ethanol) and an uncompetitive inhibitor (Mitomycin C) (*12, 25, 29, 30*).

The main problem regarding whether there is more than one binding site is that the papers say that the secondary binding site is spectroscopically silent and the available crystallographic data doesn't show the other binding site (*8, 12*). Therefore the new expression system for mammalian IDO constructed and characterised in Chapter 4 would be very useful once a crystal structure has been obtained to further investigate the possibility of a secondary binding site.

Also the crystal structures do not show another region in the enzyme which would be suitable for another binding site. The current binding pockets are quite small, the literature suggests by computation calculations using the IDO crystal structure that the pocket is flexible enough to accommodate L-tryptophan and another indole derivative however without the support of any real structural data to firmly support their findings showing a substrate or inhibitor bound at both sites, the debate will continue (*12, 29, 32*).

6.5 What is the Cause of the Substrate-Inhibition Behaviour Observed in IDO?

The binding site information has provided alternative explantions for the cause of substrate-inhibition behaviour in IDO. At high concentrations of substrate with IDO, decreases in activity are observed, indicative of substrate-inhibition behaviour, which is a confirmed dioxygenase fact (Figure 6.3) (*33, 34*). Substrate-inhibition behaviour has not been observed for TDO. Several proposals for the cause of inhibition have been discussed in the literature. The ferric form of IDO was confirmed to be inactive so it was suggested that as the enzyme can exist in both ferric and ferrous forms, inhibition at high concentrations of enzyme could be due to substrate binding to the ferric form, thus enzyme turnover is retarded because

the ferric enzyme is prevented from being reduced to the active ferrous form (*28, 33, 34*).

Recently a new theory was produced in association with the theory that there are two binding sites (F 6.3, Scheme 6.1) (*29, 30*). It was suggested that inhibition occurs because at high substrate concentration, the substrate would bind to both sites thus rendering the enzyme inactive (Scheme 6.1) (*29, 30*). Also the Fe^{3+}/Fe^{2+} redox couple for mammalian IDO in the absence and presence of substrate had a positive shift of 46 mV, it was suggested this was evidence that the ferric enzyme could still be reduced in the presence of substrate therefore excluding the previous inhibition proposal (*14, 29*). Other evidence against the initial suggestions for substrate-behaviour was that it was unlikely that substrate would bind to the ferric form, followed by reduction to the ferrous form as the binding constant for the ferric form (K_d = 0.9 mM) is weaker than binding to the ferrous form (K_m = 15 μM) (*29, 34*).

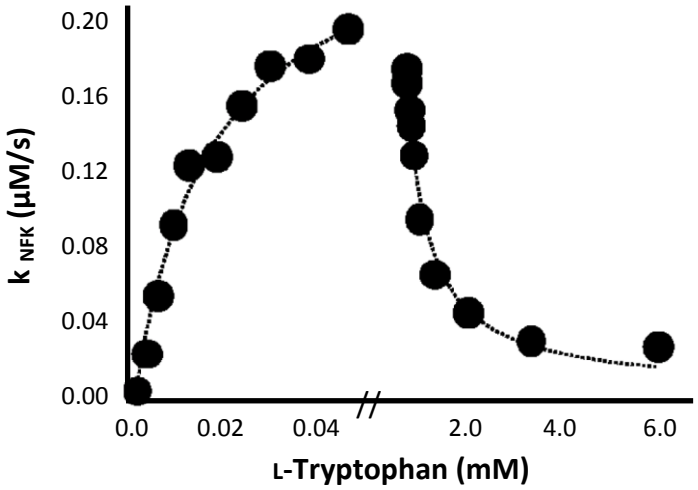

Figure 6.3 Michaelis-Menten plot of hIDO with respect to an increasing concentration of L-tryptophan, showing substrate-inhibition behaviour at high concentrations of substrate, from reference (*29*).

The two proposals for the substrate-inhibition behaviour require more experimental evidence for a better understanding of the cause. TDO does not show

substrate-inhibition behaviour however, it has also been suggested that TDO has two binding sites, therefore theoretically a similar mechanism to IDO could apply for inhibiting TDO at high concentrations of substrate. In addition, substrate-inhibition for IDO is not observed with D-tryptophan and the reason substrate-inhibition is stereospecific was suggested to be because IDO preferentially binds the L-isomer. There is no answer yet for why certain substrates and particular enzymes show substrate-inhibition behaviour, there are still many unanswered questions (*29, 35*).

6.6 What is the Substrate Binding Order?

The substrate binding order has not been resolved in the literature, however many papers have concentrated on providing experimental evidence for proposals of a mechanism for formation of the ternary complex. There was some confusion in the literature regarding the substrate binding order of tryptophan and oxygen to form the ternary structure which was discovered in 1972 (Scheme 6.2) (*36*). The ternary complex is made up of the ferrous form of the enzyme plus the two substrates dioxygen and L-tryptophan (Fe^{2+}-O_2-substrate) (Scheme 6.2). Table 6.1 presents the divide in the literature for the substrate binding order for each enzyme. A majority of the literature favours tryptophan binding first followed by oxygen for TDO and IDO, with a minority of the groups presenting the alternative binding order combination for TDO.

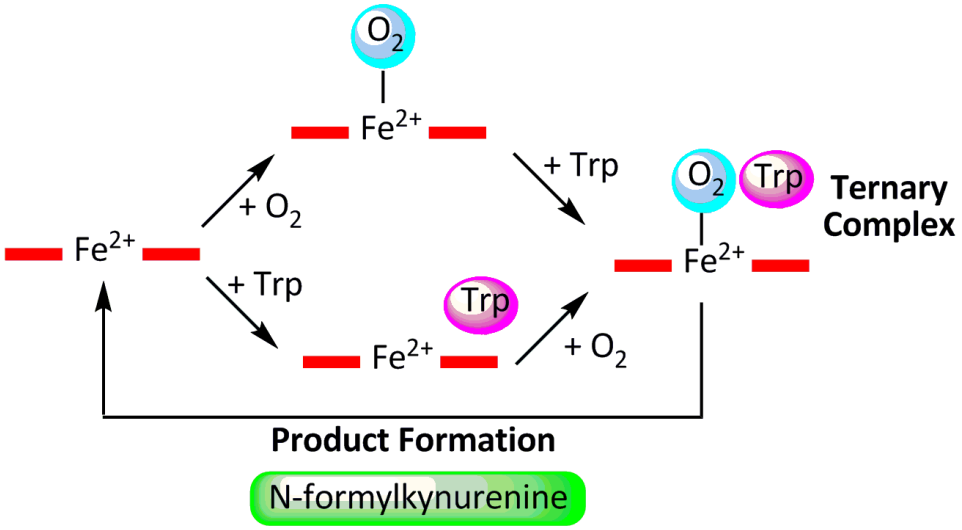

Scheme 6.2 Substrate binding order for formation of the ternary complex, which then follows a mechanism for product formation.

There have been numerous observations to support the idea that tryptophan binds first followed by dioxygen. However, there is no suggestion in the literature that the substrate binding order could be random. The arguments which have been presented are that as a ferrous-oxy complex is observed for IDO but not for TDO, it is suspected that TDO must bind tryptophan first, as that is a stable complex, which was discussed in the previous section (Table 6.1, Scheme 6.2) (*3, 8, 37*). Also upon additions of substrate to both dioxygenases there are changes in the UV-visible, CD and MCD spectra, in the absence and presence of oxygen, and decomposition of the oxygenated form of the enzyme is independent of tryptophan concentration thus suggesting that tryptophan bound first and oxygen second (Table 6.1, Scheme 6.2) (*18, 24, 36, 38-42*).

Table 6.1 Substrate binding order to ferrous enzyme to form the ternary complex (Fe^{2+}-O_2-substrate).

Enzyme	Binds First	Binds Second	Reference
IDO	Tryptophan	Oxygen	(*15, 16, 18, 24, 34, 43-47*)
TDO	Tryptophan	Oxygen	(*3, 8, 17, 23, 36-42, 48-50*)
TDO	Oxygen	Tryptophan	(*51-53*)

There are only three papers in the literature which presented evidence for dioxygen binding first followed by tryptophan, one of which was based on a hypothetical reaction mechanism after presenting evidence that the ferric form of the TDO enzyme was inactive but could be reduced to the active ferrous form (Table 6.1, Scheme 6.2) (*51-53*).

The ternary complex for TDOs could potentially be obtained by using a slower substrate than L-tryptophan, therefore ternary complex formation might be slower. Tryptophan analogues could be used such as 5-fluoro-tryptophan, 5-methyl-tryptophan or 5-hydroxy-tryptophan and reacted with ferrous enzyme and dioxygen on the milli-second time scale using stopped-flow.

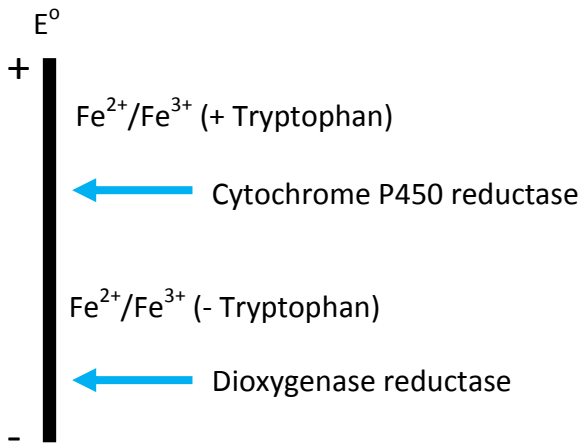

Figure 6.4 An illustration of redox potentials for cytochrome P450s, dioxygenases in the absence and presence of substrate and reductases for both enzymes (blue arrows).

Substrate binding order could be less important in the dioxygenases then in the cytochrome P450s. Order of binding is essential because the P450s can only be reduced by the reductase when substrate is bound. This means that substrate binding must precede reduction because the reduction potential of the cytochrome P450 reductase lies in between that of the substrate free and substrate bound enzyme (Figure 6.4). In the dioxygenases, this is not necessarily the case because the reduction potential of the reductase is not known as the reductase is not known either and could well be below the potential of both substrate-free and substrate-bound enzymes (Figure 6.4). If this were the case, the reductase would reduce the enzymes in both cases and the order of binding becomes less important.

In summary, even though all the literature for IDO and a majority of the literature for TDO suggests that tryptophan binds first followed by dioxygen, the dioxygenase community is still unclear whether to accept that mechanism for both enzymes and more information regarding the mechanism is required, especially as Chapter 2 presented that the ferric form of rhTDO was also active, which implies there could be an alternative mechanism.

6.7 The Substrate 1-Methyl-L-Tryptophan and Dioxygenase Reaction Mechansims

The original dioxygenase mechanisms were based on the observation that 1-methyl-L-tryptophan was an inhibitor. However Chapter 4 presented contrasting results, which have now been supported in the literature that 1-methyl-L-tryptophan is actually a slow-substrate for wild type IDO and variants of IDO and TDO (*11, 29, 54*). However wild type mammalian and bacterial TDO were inactive with 1-methyl-L-tryptophan. The reason for this unexpected result is due to the lack of space in the TDO catalytic pocket to incorporate 1-methyl-L-tryptophan, in comparison to IDO which has a larger pocket. Also as mentioned in several chapters, TDO has a distal histidine in contrast to IDO which has a distal serine. The histidine in TDO was found to form hydrogen bonds with the substrate in the *X. campestris* TDO structure, therefore it is expected to cause a steric crash with the

methyl group of 1-methyl-L-tryptophan upon binding. The histidine variants of TDO could utilise 1-methyl-L-tryptophan as a substrate suggesting that removal of the histidine residue allows accommodation of the additional methyl group in the catalytic site, which was not a problem for IDO as serine is a much smaller residue, which does not form any known interactions with the substrate.

Due to the observation that 1-methyl-L-tryptophan was a substrate, the abstraction of the indole N_1 group mechanism was excluded and an alternate reaction mechanism was proposed in Chapter 4, taking into account the chemistry of indoles. The mechanism involved direct electrophilic addition to dioxygen, facilitated by the lone pair on the indole N_1 (*54*).

There is very little information with regards to the reaction mechanism for dioxygenases available in the literature, however computational analysis of proposed mechanisms has helped to favour some mechanisms over others. A comparison of the abstraction and electrophilic addition mechanisms was made in a density functional theory (DFT) paper, which found that the latter mechanism was favourable, as it had a lower activation energy (*55*). The computational studies also supported the conclusion that deprotonation of the indole N_1 group by dioxygen was unlikely as the hydrogen bond from the NH group to the heme-bound dioxygen would be significantly bent (*55*).

Another mechanism which was analysed by DFT calculations was the Criegee-type rearrangement pathway, which was found to require a high activation barrier for formation of the neutral indole intermediate. So, an alternative reaction pathway was proposed involving zwitterionic and diradical products formed from direct addition pathways, which were suggested to be followed by charge or radical recombination to form a dioxetane intermediate. The diradical product was also proposed to undergo homolytic O-O bond cleavage followed by oxo-attack and C_2-C_3 bond cleavage.

Recently another mechanism was proposed, which goes through a ferryl intermediate, whereby the molecules of oxygen are added using a 2-step

mechanism (*29, 30*). The mechanism involves addition of one molecule of oxygen, which spontaneously converts to the ferryl intermediate followed by homolytic O-O bond cleavage, whereby the second oxygen molecule is added to form the product.

Overall, there has been no direct experimental evidence to confirm any of the mechanistic routes, after initial addition of the distal oxygen to L-tryptophan *i.e.* dioxetane versus Criegee rearrangement, and further investigations will be necessary before the molecular details that occur further down the mechanism are understood.

6.8 References

1. Knox, W. E. (1955) *Tryptophan oxidation. A tryptophan peroxidase from liver*, Vol. 2, Aacademic Press, New York.
2. Watanabe, Y., Fujiwara, M., Yoshida, R., and Hayaishi, O. (1980) Stereospecificity of hepatic L-tryptophan 2,3-dioxygenase, *Biochem J 189*, 393-405.
3. Batabyal, D., and Yeh, S. R. (2007) Human tryptophan dioxygenase: a comparison to indoleamine 2,3-dioxygenase, *J Am Chem Soc 129*, 15690-15701.
4. Basran, J., Rafice, S. A., Chauhan, N., Efimov, I., Cheesman, M. R., Ghamsari, L., and Raven, E. L. (2008) A kinetic, spectroscopic, and redox study of human tryptophan 2,3-dioxygenase, *Biochemistry 47*, 4752-4760.
5. Fukumura, E., Sugimoto, H., Misumi, Y., Ogura, T., and Shiro, Y. (2009) Cooperative binding of L-trp to human tryptophan 2,3-dioxygenase: resonance Raman spectroscopic analysis, *J Biochem 145*, 505-515.
6. Schutz, G., and Feigelson, P. (1972) Purification and properties of rat liver tryptophan oxygenase, *J Biol Chem 247*, 5327-5332.
7. Manandhar, S. P., Shimada, H., Nagano, S., Egawa, T., and Ishimura, Y. (2002) Subunit structure of recombinant rat liver L-tryptophan 2,3-dioxygenase, *International Congress Series 1233*, 161-169.
8. Forouhar, F., Anderson, J. L., Mowat, C. G., Vorobiev, S. M., Hussain, A., Abashidze, M., Bruckmann, C., Thackray, S. J., Seetharaman, J., Tucker, T., Xiao, R., Ma, L. C., Zhao, L., Acton, T. B., Montelione, G. T., Chapman, S. K., and Tong, L. (2007) Molecular insights into substrate recognition and catalysis by tryptophan 2,3-dioxygenase, *PNAS 104*, 473-478.
9. Hitchcock, M. J., and Katz, E. (1988) Purification and characterization of tryptophan dioxygenase from Streptomyces parvulus, *Archives of Biochemistry and Biophysics 261*, 148-160.
10. Suzuki, T., Kawamichi, H., and Imai, K. (1998) A myoglobin evolved from indoleamine 2,3-dioxygenase, a tryptophan-degrading enzyme, *Comp Biochem Physiol B Biochem Mol Biol 121*, 117-128.

11. Hamilton, G. A. (1969) Mechanisms of two- and four-electron oxidations catalyzed by some metalloenzymes, *Adv Enzymol Relat Areas Mol Biol 32*, 55-96.
12. Sugimoto, H., Oda, S., Otsuki, T., Hino, T., Yoshida, T., and Shiro, Y. (2006) Crystal structure of human indoleamine 2,3-dioxygenase: catalytic mechanism of O2 incorporation by a heme-containing dioxygenase, *PNAS 103*, 2611-2616.
13. Dick, R., Murray, B. P., Reid, M. J., and Correia, M. A. (2001) Structure--function relationships of rat hepatic tryptophan 2,3-dioxygenase: identification of the putative heme-ligating histidine residues, *Archives of Biochemistry and Biophysics 392*, 71-78.
14. Papadopoulou, N. D., Mewies, M., McLean, K. J., Seward, H. E., Svistunenko, D. A., Munro, A. W., and Raven, E. L. (2005) Redox and spectroscopic properties of human indoleamine 2,3-dioxygenase and a His303Ala variant: implications for catalysis, *Biochemistry 44*, 14318-14328.
15. Sono, M., and Dawson, J. H. (1984) Extensive studies of the heme coordination structure of indoleamine 2,3-dioxygenase and of tryptophan binding with magnetic and natural circular dichroism and electron paramagnetic resonance spectroscopy, *Biochim Biophys Acta 789*, 170-187.
16. Terentis, A. C., Thomas, S. R., Takikawa, O., Littlejohn, T. K., Truscott, R. J., Armstrong, R. S., Yeh, S. R., and Stocker, R. (2002) The heme environment of recombinant human indoleamine 2,3-dioxygenase. Structural properties and substrate-ligand interactions, *J Biol Chem 277*, 15788-15794.
17. Makino, R., Sakaguchi, K., Iizuka, T., and Ishimura, Y. (1980) Acid-alkaline transition and thermal spin equilibrium of the heme in ferric L-tryptophan 2,3-dioxygenases, *J Biol Chem 255*, 11883-11891.
18. Uchida, K., Shimizu, T., Makino, R., Sakaguchi, K., Iizuka, T., Ishimura, Y., Nozawa, T., and Hatano, M. (1983) Magnetic and natural circular dichroism of L-tryptophan 2,3-dioxygenases and indoleamine 2,3-dioxygenase. II. Spectra of their ferric cyanide and ferrous carbon monoxide complexes and an oxygenated form, *J Biol Chem 258*, 2526-2533.
19. Suzuki, T., Watanabe, Y. H., Nagasawa, M., Matsuoka, A., and Shikama, K. (2000) Dual nature of the distal histidine residue in the autoxidation reaction of myoglobin and hemoglobin comparison of the H64 mutants, *Eur J Biochem 267*, 6166-6174.
20. Chauhan, N., Basran, J., Efimov, I., Svistunenko, D. A., Seward, H. E., Moody, P. C., and Raven, E. L. (2008) The role of serine 167 in human indoleamine 2,3-dioxygenase: a comparison with tryptophan 2,3-dioxygenase, *Biochemistry 47*, 4761-4769.
21. Thackray, S. J., Bruckmann, C., Anderson, J. L., Campbell, L. P., Xiao, R., Zhao, L., Mowat, C. G., Forouhar, F., Tong, L., and Chapman, S. K. (2008) Histidine 55 of tryptophan 2,3-dioxygenase is not an active site base but regulates catalysis by controlling substrate binding, *Biochemistry 47*, 10677-10684.
22. Batabyal, D., and Yeh, S. R. (2009) Substrate-Protein Interaction in Human Tryptophan Dioxygenase: The Critical Role of H76, *J Am Chem Soc*.

23. Henry, Y., Ishimura, Y., and Peisach, J. (1976) Binding of nitric oxide to reduced L-tryptophan-2,3-dioxygenase as studied by electron paramagnetic resonance, *J Biol Chem 251*, 1578-1581.
24. Uchida, K., Bandow, H., Makino, R., Sakaguchi, K., Iizuka, T., and Ishimura, Y. (1985) Infrared spectra of carbon monoxide complexes of indoleamine 2,3-dioxygenase and L-tryptophan 2,3-dioxygenases. Effects of substrates on the CO-stretching frequencies, *J Biol Chem 260*, 1400-1406.
25. Sono, M. (1989) Enzyme kinetic and spectroscopic studies of inhibitor and effector interactions with indoleamine 2,3-dioxygenase. 2. Evidence for the existence of another binding site in the enzyme for indole derivative effectors, *Biochemistry 28*, 5400-5407.
26. Feigelson, P., and Brady, F. O. (1974) *Molecular Mechanisms of Oxygen Activation*, Academic, New York.
27. Eguchi, N., Watanabe, Y., Kawanishi, K., Hashimoto, Y., and Hayaishi, O. (1984) Inhibition of indoleamine 2,3-dioxygenase and tryptophan 2,3-dioxygenase by beta-carboline and indole derivatives, *Arch Biochem Biophys 232*, 602-609.
28. Kobayashi, K., Hayashi, K., and Sono, M. (1989) Effects of tryptophan and pH on the kinetics of superoxide radical binding to indoleamine 2,3-dioxygenase studied by pulse radiolysis, *J Biol Chem 264*, 15280-15283.
29. Lu, C., Lin, Y., and Yeh, S. R. (2009) Inhibitory substrate binding site of human indoleamine 2,3-dioxygenase, *J Am Chem Soc 131*, 12866-12867.
30. Nickel, E., Nienhaus, K., Lu, C., Yeh, S. R., and Nienhaus, G. U. (2009) Ligand and substrate migration in human indoleamine 2,3-dioxygenase, *J Biol Chem*.
31. Nienhaus, K., Deng, P., Kriegl, J. M., and Nienhaus, G. U. (2003) Structural dynamics of myoglobin: effect of internal cavities on ligand migration and binding, *Biochemistry 42*, 9647-9658.
32. Macchiarulo, A., Nuti, R., Bellocchi, D., Camaioni, E., and Pellicciari, R. (2007) Molecular docking and spatial coarse graining simulations as tools to investigate substrate recognition, enhancer binding and conformational transitions in indoleamine-2,3-dioxygenase (IDO), *Biochim Biophys Acta 1774*, 1058-1068.
33. Muller, A. J., DuHadaway, J. B., Donover, P. S., Sutanto-Ward, E., and Prendergast, G. C. (2005) Inhibition of indoleamine 2,3-dioxygenase, an immunoregulatory target of the cancer suppression gene Bin1, potentiates cancer chemotherapy, *Nat Med 11*, 312-319.
34. Sono, M., Taniguchi, T., Watanabe, Y., and Hayaishi, O. (1980) Indoleamine 2,3-dioxygenase. Equilibrium studies of the tryptophan binding to the ferric, ferrous, and CO-bound enzymes, *J Biol Chem 255*, 1339-1345.
35. Yamamoto, S., and Hayaishi, O. (1967) Tryptophan pyrrolase of rabbit intestine. D- and L-tryptophan-cleaving enzyme or enzymes, *J Biol Chem 242*, 5260-5266.
36. Ishimura, Y., Nozaki, M., and Hayaishi, O. (1970) The oxygenated form of L-tryptophan 2,3-dioxygenase as reaction intermediate, *J Biol Chem 245*, 3593-3602.

37. Li, J. S., Han, Q., Fang, J., Rizzi, M., James, A. A., and Li, J. (2007) Biochemical mechanisms leading to tryptophan 2,3-dioxygenase activation, *Archives of Insect Biochemistry and Physiology 64*, 74-87.
38. Feigelson, P., Ishimura, Y., and Hayaishi, O. (1964) On the activation and catalytic mechanism of microbial tryptophan pyrrolase, *Biochem Biophys Res Commun 14*, 96-101.
39. Feigelson, P., Ishimura, Y., and Hayaishi, O. (1965) Studies on the Role of Hematin in the Catalytic Mechanism of Tryptophan Pyrrolase, *Biochim Biophys Acta 96*, 283-293.
40. Feigelson, P., and Maeno, H. (1966) *Biological and chemical aspects of oxygenases*, Maruzen Company Ltd., Tokyo.
41. Maeno, H., and Feigelson, P. (1967) Spectral studies on the catalytic mechanism and activation of Pseudomonas tryptophan oxygenase (tryptophan pyrrolase), *J Biol Chem 242*, 596-601.
42. Ishimura, Y., Nozaki, M., and Hayaishi, O. (1967) Evidence for an oxygenated intermediate in the tryptophan pyrrolase reaction, *J Biol Chem 242*, 2574-2576.
43. Sono, M. (1986) Spectroscopic and equilibrium properties of the indoleamine 2,3-dioxygenase-tryptophan-O2 ternary complex and of analogous enzyme derivatives. Tryptophan binding to ferrous enzyme adducts with dioxygen, nitric oxide, and carbon monoxide, *Biochemistry 25*, 6089-6097.
44. Sono, M. (1989) The roles of superoxide anion and methylene blue in the reductive activation of indoleamine 2,3-dioxygenase by ascorbic acid or by xanthine oxidase-hypoxanthine, *J Biol Chem 264*, 1616-1622.
45. Hirata, F., Ohnishi, T., and Hayaishi, O. (1977) Indoleamine 2,3-dioxygenase. Characterization and properties of enzyme. O2- complex, *J Biol Chem 252*, 4637-4642.
46. King, N. J., and Thomas, S. R. (2007) Molecules in focus: indoleamine 2,3-dioxygenase, *Int J Biochem Cell Biol 39*, 2167-2172.
47. Thomas, S. R., Terentis, A. C., Cai, H., Takikawa, O., Levina, A., Lay, P. A., Freewan, M., and Stocker, R. (2007) Post-translational regulation of human indoleamine 2,3-dioxygenase activity by nitric oxide, *J Biol Chem 282*, 23778-23787.
48. Koike, K., and Feigelson, P. (1971) Studies on the catalytic and allosteric sites in modulating the reactivity of tryptophan oxygenase with heme ligands. II. Carbon monoxide derivatives, *Biochemistry 10*, 3385-3390.
49. Koike, K., and Feigelson, P. (1971) Studies on the roles of the catalytic and allosteric sites in modulating the reactivity of tryptophan oxygenase with heme ligands. I. Cyanide derivatives, *Biochemistry 10*, 3378-3384.
50. Brady, F. O., and Feigelson, P. (1975) The oxygenated complexes of the two catalytically active oxidation-reduction states of L-tryptophan-2,3-dioxygenase, *J Biol Chem 250*, 5041-5048.
51. Tanaka, T., and Knox, W. E. (1959) The nature and mechanism of the tryptophan pyrrolase (peroxidase-oxidase) reaction of Pseudomonas and of rat liver, *J Biol Chem 234*, 1162-1170.

52. Leeds, J. M., Brown, P. J., McGeehan, G. M., Brown, F. K., and Wiseman, J. S. (1993) Isotope effects and alternative substrate reactivities for tryptophan 2,3-dioxygenase, *J Biol Chem 268*, 17781-17786.
53. Tokuyama, K., and Knox, W. E. (1964) The Resolution and Activa tion of Hematin-free Tryptophan Pyrrolase from Rat Liver, *Biochim Biophys Acta 81*, 201-204.
54. Chauhan, N., Thackray, S. J., Rafice, S. A., Eaton, G., Lee, M., Efimov, I., Basran, J., Jenkins, P. R., Mowat, C. G., Chapman, S. K., and Raven, E. L. (2009) Reassessment of the reaction mechanism in the heme dioxygenases, *J Am Chem Soc 131*, 4186-4187.
55. Chung, L. W., Li, X., Sugimoto, H., Shiro, Y., and Morokuma, K. (2008) Density functional theory study on a missing piece in understanding of heme chemistry: the reaction mechanism for indoleamine 2,3-dioxygenase and tryptophan 2,3-dioxygenase, *J Am Chem Soc 130*, 12299-12309.

CHAPTER 7

EXPERIMENTAL

This Chapter describes the experimental methods and techniques used throughout this thesis.

7.1 Materials and Stock Solutions

All molecular biology was conducted under aseptic conditions and all glycerol was sterilised. All chemicals were obtained from commercial sources unless otherwise stated and were used without further purification. All chemicals were of the highest analytical grade. All buffers and solutions were made using double deionised water drawn from an Elga PureLab option (DV35) water purifier and listed in Appendix I. All buffers and solutions which required a certain pH were determined using a PHM 220 pH meter (Radiometer analytical) with a Glass electrode (Thermo scientific), which was calibrated with pH 4.0, pH 7.0 and pH 10.0 solutions (Thermo scientific).

7.2 Recombinant DNA Techniques

7.2.1 Oligonucleotides

The polymerase chain reaction (PCR) was employed for amplification of wild type TDO from the human liver IMAGE clone ID 4071714 [1], amplification of wild type TDO for insertion into the vector pLEICS5, formation of TDO variants and amplification of hIDO for insertion from the vector pQE30 to pET151/d TOPO.

Equation 7.1- Primer Annealing Temperatures

$$\mathrm{Tm} = \left(81.5 \times \left(16.6 \times (\log_{10}[\mathrm{J}^+]) + 0.41\,(\%\mathrm{GC}) - \left(\frac{600}{\mathrm{l}}\right)\right)\right) - 5$$

Where J is concentration of monovalent cations (M), l the length of oligo (bp).

Primers were designed to be complementary to the original sequence, up to 30-36 bp in length with a high G and C ratio compared to A and T (Table 7.1). Some primers were designed with a homology region, which allows direct annealing of the PCR product to the desired vector using ligase. Other primers were designed with restriction sites which could be cut by restriction enzymes creating sticky ends which could anneal using ligase to a vector which has been cut with the same restriction enzymes for directional cloning. The primer annealing temperatures were calculated using Equation 7.1.

Equation 7.2- DNA concentration

$$\text{Concentration}\ (\mu\text{g/ml}) = (\mathrm{A}_{260} - \mathrm{A}_{320}) \times \text{dilution factor} \times 50\ (\mu\text{g/ml})$$

The preordered oligos (Invitrogen) were prepared by addition of 300 µl TE buffer (Appendix I) and resuspended at 13,000 rpm for 1 min. The DNA concentration was calculated using a spectrophotometer and analysing the absorbance. The OD_{260} was measured and the DNA concentration was calculated using Equation 7.2 using the relationship that A_{260} of 1.0 is 50 µg/ml pure DNA.

[1] By Dr Basran

Table 7.1 Forward (F) and reverse (R) primers for cloning: TDO into pET28a (pET28a TDO F/R), TDO from pET28a to pLEICS5 (pLEICS TDO F/R and TDO variant primers pLEICS H76A/S, F72A, F140A/Y & R144A/K F/R) and IDO from pQE30 to pET151/d TOPO (pET151/d TOPO IDO F/R).

Oligonucleotides	Sequence 5' to 3'	Underlined
pET28a TDO F[2]	GCCTTTTCACCATGGCGGGGTGCCCATTTTTAGG	Nco I site
pET28a TDO R[2]	CATAGATTTTGCAGACGCTCGAGATCTGATTCATCA	Xho I site
pLEICS5 TDO F	AGGAGATATACATATGGCGGGGTGCCCATTTTTAGG	Nde I site and homology region
pLEICS5 TDO R	GAAGTACAGGTTCTCATCTGATTCATCACTGCTGAA	Homology region
pLEICS5 H76A TDO F	CTTTTTATCATAACTGCGCAAGCTTATGAACTCT	H to A
pLEICS5 H76A TDO R	AGAGTTCATAAGCTTGCGCAGTTATGATAAAAAG	H to A
pLEICS5 H76S TDO F	CTTTTTATCATAACTAGCCAAGCTTATGAACTCT	H to S
pLEICS5 H76S TDO R	AGAGTTCATAAGCTTGTCGAGTTATGATAAAAAG	H to S
pLEICS5 F72A TDO F	ATCCATGATGAACATCTTGCGATCATAACTCATCAAGCT	F to A
pLEICS5 F72A TDO R	AGCTTGATGAGTTATGATCGCAAGATGTTCATCATGGAT	F to A
pLEICS5 F140A TDO F	GATGACAGCCTTGGACGCGAATGACTTCAGAGAGTA	F to A
pLEICS5 F140A TDO R	TACTCTCTGAAGTCATTCGCGTCCAAGGCTGTCATC	F to A
pLEICS5 F140Y TDO F	GATGACAGCCTTGGACTATAATGACTTCAGAGAGTA	F to Y
pLEICS5 F140Y TDO R	TACTCTCTGAAGTCATTATAGTCCAAGGCTGTCATC	F to Y
pLEICS5 R144A TDO F	TTGGACTTCAATGACTTCGCGGAGTACTTATCTCCAGCA	R to A
pLEICS5 R144A TDO R	TGCTGGAGATAAGTACTCCGCGAAGTCATTGAAGTCCAA	R to A
pLEICS5 R144K TDO F	TTGGACTTCAATGACTTCAAAGAGTACTTATCTCCAGCA	R to K
pLEICS5 R144K TDO R	TGCTGGAGATAAGTACTCTTTGAAGTCATTGAAGTCCAA	R to K
pET151/d TOPO IDO F	CACCATGACCGCACACGCTATGGAAAACTCC	Homology region
pET151/d TOPO IDO R	TTAACCTTCCTTCAAAAGGGATTTCTCAGTTG	

The PCR reaction involved denaturing the DNA at a high temperature to separate the double strands of DNA, so that the forward and reverse primers could anneal to their complementary sequence. After annealing, elongation takes place which was the synthesis of a new strand of DNA (Table 7.2). There was an exponential increase in the number of new DNA strands produced per each cycle.

[2] Primers designed by Dr Basran

Table 7.2 Thermocycler program for the PCR reaction.

	Temperature (°C)	Time	Number of Cycles
	94.0	30 seconds	1
Denaturation	94.0	30 seconds	
Annealing	56.0	30 seconds	25
Elongation	72.0	1 minute	
	72.0	8 minutes	1
	4.0	∞	∞

The mixture added to the thermocycler consisted of (30 µl) ddH_2O, (5 µl) 10 × buffer, (5 µl) dNTPs, (2 µl) $MgSO_4$, (1 µl) DNA, (4 µl) each of the forward and reverse primer (Table 7.1) and 1 µl KOD which initiated the reaction. The PCR product was analysed by running on a 1 % agarose gel.

PCR for wild type TDO and site directed mutagenesis of TDO variants was carried out by the Dr X. Yang at the Protein and Expression Laboratory (PROTEX), University of Leicester, with the oligonucleotides that I designed. The PROTEX lab inserted my TDO PCR products into one of their own vectors called pLEICS5.

7.2.2 DNA Sequencing

Sequencing of rhTDO, TDO variants and rhIDO coding genes was performed to ensure there were no spurious mutations by The Protein and Nucleic Acid Chemistry Laboratory (PNACL at the University of Leicester carried out all DNA sequencing) (Appendix II). An Applied Biosystems 3730-DNA Analyser machine generated the sequence by automated fluorescence using the primers T7 promoter and T7 terminator. The sequence was analysed using the program SeqED (Applied Biosystems).

7.2.3 Isolation of DNA

A single colony of cells from an LB plate was grown overnight 37.0 ^{o}C in LB media with the appropriate antibiotics. DNA was extracted from the cell culture using a QIAprep® Spin Miniprep kit (Qiagen catalogue number 27104). Bacterial cells (3 ml) were pelleted and resuspended in P1 buffer (250 µl, alkaline buffer with RNase stored at 4.0 ^{o}C, Appendix I). The cells were lysed by P2 buffer (250 µl, contains sodium hydroxide, Appendix I) was added and inverted 4-6 times. The solution was neutralised by addition of N3 buffer (350 µl, contains guanidine hydrochloride, acetic acid, Appendix I) and mixed immediately and centrifuged at 13,000 rpm for 10 minute. The supernatant was decanted into QIAprep® spin column and centrifuged again for 1 minute and the flow-through discarded. The QIAprep® spin column was washed with PB buffer (0.5 ml, containing guanidine hydrochloride and isopropanol, Appendix I), centrifuged for 1 minute and the flow-through discarded. The QIAprep® spin column was washed by addition of PE buffer (0.75ml, containing ethanol, Appendix I), centrifuged for 1 minute and the flow-through discarded. The residual of PE buffer was removed by centrifugation for 1 minute and DNA eluted by addition of ddH_2O (50 µl) and centrifuged for 1 minute and stored at -20.0 ^{o}C.

The DNA was checked by double digesting with two restriction enzymes which cut the vector at two restriction sites creating three sections of linear DNA. The double digestion mixture consisted of DNA (10 µl) with each of the two restriction enzymes (0.5 µl), buffer tango (2 µl, Appendix I) and addition of ddH_2O (up to a total of 20 µl). The mixture was incubated for 1 hour at 37.0 ^{o}C and analysed by agarose gel electrophoresis.

7.2.4 Agarose Gel Electrophoresis

Agarose gel electrophoresis is used to determine the purity and the size of DNA with respect to a marker with known sizes. Agarose gels (1 % w/v) were cast with ethidium bromide (6 µl), which binds DNA. Ethidum bromide has an intense fluorescence therefore the DNA is visible in the gel under UV light. The gel was placed into a tank of 1 × TAE buffer (Appendix I). Isolated DNA samples (8 µl) were mixed with loading buffer (2 µl, Fermentas) and loaded into the gel wells. A Quick-Load® 1 kb DNA Ladder (New England BioLabs) was loaded on to the gel to identify the size of the DNA bands. The ladder consisted of DNA strands which were 10.0, 8.0, 6.0, 5.0, 4.0, 3.0, 2.0, 1.5, 1.0 and 0.5 kb in size. An electric current is applied to the gel and after 1 hour the DNA was visualised under UV light on a transilluminator.

7.2.5 Qiaquick® Gel Extraction Kit

DNA bands were excised from the agarose gel and dissolved in buffer QG (Appendix I) at 60.0 ^{o}C for 5 minutes and the supernatant was decanted into a Qiaquick® spin column and centrifuged for 1 minute, allowing DNA to bind to the column. The flow-through was discarded and the column was washed in QG buffer (0.5 ml, Appendix I) and centrifuged for 1 minute. The column was washed again in buffer PE (0.75 ml, Appendix I) and centrifuged for 1 minute and the bound DNA was eluted into a microcentrifuge tube (1.5 ml) after addition of ddH_2O (50 µl) and centrifuged for 1 minute and stored at -20.0 ^{o}C.

7.2.6 Transformation of DNA into Competent *E. coli* Cells

The competent cells Rosetta pLysS (DE3) (Novagen) *E. coli* and DH5α (Invitrogen) (50 µl) were thawed and sequenced recombinant DNA (2 µl) was added, swirled to mix and left for 30 minutes on ice. The sample was heat shocked at 42.0 ^{o}C for 45 seconds and incubated on ice for 2 minutes. SOC media (500 µl, Appendix I) was added to the reactions and incubated at 37.0 ^{o}C for 1 hour shaking at 240 rpm. The reaction (100 µl) was streaked on antibiotic LB agar plates and the remaining solution was made ten times concentrated by pelleting and resuspension in fresh SOC media (100 µl, Appendix I) and streaked on to another antibiotic LB agar plate. The plates were left inverted at 37.0 ^{o}C overnight.

Successfully transformed cells will grow to form colonies as they express the antibiotic resistance gene, a single colony was selected and incubated in LB media (5 ml, Appendix I) containing antibiotics at 37.0 ^{o}C, shaking at 225 rpm, overnight. The DNA was checked by isolation using Qiagen® mini-prep kit and analysed by restriction digestion and agarose gel electrophoresis.

7.2.7 Glycerol Stocks

For isolation of DNA or grow ups of cells a sample of the glycerol stock was taken from hTDO in vector pET28a (kanamycin resistance), hTDO and variants in vector pLEICS5 (ampicillin resistance) and hIDO in vector pET151d/TOPO (ampicillin resistance) and streaked on to a LB plate with the appropriate antibiotic (50 µg/ml kanamycin, 100 µg/ml ampicilin), which the cells of interest have resistance to and a single colony was used for growth. Bacterial cells containing the recombinant vector were grown at 37.0 ^{o}C, overnight with an appropriate antibiotic and the cells were stored at -80.0 ^{o}C as glycerol stocks (500 µl cell culture, 250 µl 50 % sterile glycerol).

7.3 Protein Expression of rhTDO and variants

Figure 7.1 From left to right a picture two sterilins (5 ml) from an overnight growth of a colony from the petri dish, a petri dish with *E. coli* colonies of TDO, on top of the petri dish is purified protein, a metal-ion affinity chromatography column, a flask (500 ml) with 2× YT media (150 ml) and a flask (2 L) with 2× YT media (1 L).

Expression for both rhTDO and the variants in vectors pET28a, which carries antibiotic resistance for kanamycin and pLEICS5, which carries resistance for ampicillin, were prepared in the bacterial strain Rosetta (DE3) pLysS. The cells from a glycerol stock for each of the enzymes were streaked on to their respective ampicillin (100 μg/ml) or kanamycin (50 μg/ml) antibiotic LB agar plates and incubated overnight at 37.0 ^{o}C (Figure 7.1). A starter culture was made by inoculating a single colony from the plate in 2×YT media (5 ml) supplemented with the respective antibiotics for each enzyme, overnight 37.0 ^{o}C with shaking (Figure 7.1).

The starter culture (5 ml) grown overnight at 37.0 ^{o}C with shaking at 200 rpm was used to inoculate fresh sterile 2 × YT media (150 ml). The overnight culture (150 ml) was then used to inoculate 2 × YT media (10 L, Appendix I) supplemented with filtered ampicillin (100 μg/ml) or filtered kanamycin (50 μg/ml) for hTDO growth depending on the vector. There was 2 × YT media (1 L) in baffled flasks (2 L) for aeration. The bacterial cells were induced at OD_{600} = 0.6 - 1.0 with IPTG (100 μM)

and hemin (4.6 mg/L, 0.046 g, 10mM NaOH, make up to 20 ml with ddH_2O), overnight 22.0 ^oC. The cells were pelleted by centrifugation at 5000 rpm for 15 minutes at 4.0 ^oC and the pellets were stored at -80.0 ^oC until they were needed.

7.3.1 Expression of rhIDO

Expression of rhIDO was the same as previously described for rhTDO and the TDO variants (Section 7.3). However, when the rhIDO cells were induced with IPTG and hemin they were incubated at 25.0 ^oC as a higher temperature was tolerated for protein expression and without the formation of inclusion bodies.

7.4 Isolation and Purification of rhIDO, rhTDO and variants

7.4.1 Preparation of Cell-free Extract

All purification methods followed the same method for preparation of the cell free extract. Filtered sonication buffer A (60-80 ml, Appendix I) for rhTDO and the variants or sonication buffer B (Appendix I) for rhIDO was added to the frozen bacterial cell pellets and thawed slowly. Once thawed, two EDTA-free Complete^{TM} tablets (Roche), PMSF (2 ml (0.05 g /5 ml isopropanol)), a protease inhibitor, $MgCl_2$ (20 mM), lysozyme (5 mg) and DNase I (5 mg), were added to the cell suspension whilst stirring at room temperature for 25 minutes. The mixture was then sonicated on ice for 6 × 30 second bursts, and lysozyme, DNase I and $MgCl_2$ were added again to ensure that the cells were completely lysed. The cell-free extract was obtained by centrifugation for 1 hour at 19000 rpm and 4.0 ^oC, which pelleted the cell debris leaving the supernatant containing the cell free extract, which was kept at 4.0 ^oC for the rest of the purification process.

7.4.2 Immobilised Metal Ion Affinity Chromatography: purification with an imidazole gradient

A nickel-nitrilotracetic acid (Ni-NTA) agarose column (Qiagen) (10 ml) was used to isolate hexahistidyl tagged proteins from the cell-free extract. The Ni-NTA column was flushed with ddH_2O (250 ml) and then equilibrated with sonication buffer A (200 ml, Appendix I), and the cell free extract was loaded on slowly by gravity and the tagged protein binds to the resin (Figure 7.2). After protein loading, the column was washed for a second time with sonication buffer A (250 ml, Appendix I), to ensure all the cell-free extract had loaded on to the column. The column was then washed with wash buffer A (2 L, Appendix I) to ensure that all the non-tagged proteins from *E. coli* were removed from the column. Imidazole has an absorbance around 280 nm therefore complete protein removal from the column could not be verified by UV-visble spectroscopy however eluted fractions were checked by SDS-PAGE.

Figure 7.2 rhTDO bound to the Ni-NTA column with imidazole present in the buffers.

A gradient maker was used to create the imidazole gradient for elution of the bound protein with 300 ml wash buffer A (Appendix I) and 300 ml elution buffer A (Appendix I) to generate a continuous gradient.

The imidazole gradient was determined using a FPLC with a Ni-NTA column, which followed the 280 nm peak and the imidazole gradient so that the concentration of imidazole could be calculated for removal of bound TDO.

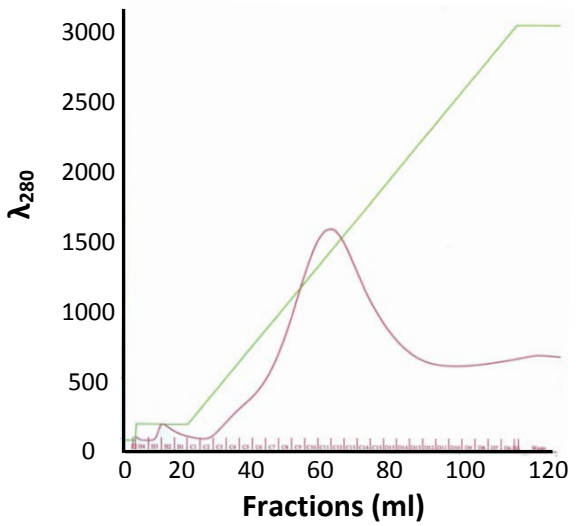

Figure 7.3 FPLC trace of TDO eluting from a Ni-NTA column on the FPLC (red) by an imidazole gradient (green).

The protein eluted at ≈ 200 mM imidazole and 5 ml fractions were collected from the column(Figure 7.3). The most concentrated fractions were pooled together and dialysed in storage buffer (Appendix I) at 4 ^{o}C overnight stirring to remove imidazole from the protein. The protein was checked by UV-visible spectroscopy to ensure all imidazole w as removed as imidazole has a peak at 280 nm.

7.4.3 Immobilised Metal Ion Affinity Chromatography, eluting with EDTA

A similar purification method as above was used for elution with EDTA for rhIDO. The Ni-NTA column was washed with ddH_2O, equilibrated with 200 ml sonication buffer B (Appendix I), and cell free extract was loaded slowly. The protein bound to the column was washed with 200 ml sonication buffer B (Appendix I) again to remove any contaminants and then washed with 2 L filtered wash buffer B (Appendix I) rapidly. The protein was then eluted from the column with elution buffer B (Appendix I) and 5 ml samples were collected and the most concentrated sampled were pooled and dialysed in storage buffer (Appendix I) at 4 ^{o}C overnight stirring to remove EDTA (Figure 7.4).

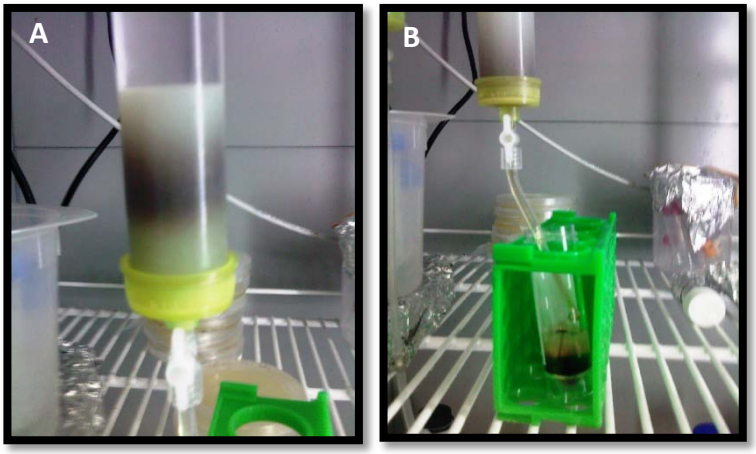

Figure 7.4 Purification using EDTA. (**A**) rhIDO bound to the Ni-NTA column. (**B**) rhIDO eluting from the column into a fractions (5 ml).

7.4.4 Purification by Hexahistidyl Tag Removal for rhTDO in pLEICS5 and rhIDO

Tobacco Etch Virus (TEV) nuclear inclusion a (NIa) proteinase has a 27 kDa catalytic domain, which specifically cleaves at a TEV site (ENLYFQS), which is incorporated in the pLEICS5 and pET151/d TOPO vectors. One unit of TEV cuts 100 µg protein at 4 ^{o}C overnight. This purification step was only employed for wild type TDO in pLEICS5 and wild type IDO in pET151/d TOPO as an extra purification step for crystallisation.

After enzymatic treatment, the hexahistidyl tag, cleaved and non-cleaved protein were separated by firstly exchanging the storage buffer (Appendix I) for separation

buffer (Appendix I), the NaCl prevents non-specific binding of proteins. The protein was then run through a Ni-NTA column with 1 ml of resin, which had been pre-equilibrated with separation buffer (Appendix I). The cleaved protein ran straight through the column, the hexahistidyl tag non-cleaved protein bound to the column.

The protein which was not cleaved was eluted with Elution buffer B (Appendix I), dialysed in Storage buffer (Appendix I), concentrated and incubated again with TEV protease and the purification procedure was repeated.

7.4.5 Purification of the Proteins rhTDO and rhIDO by FPLC with a Gel Filtration Column

Fast Performance Liquid Chromatography (FPLC) with a gel filtration column was used to purify rhTDO and rhIDO, to obtain pure samples of protein for crystallisation. A HiLoad^{TM} 16/60 Superdex 200 prep grade gel filtration column (GE Healthcare) was used to purify rhTDO (Figure 7.5). A HiLoad^{TM} 16/60 Superdex 30 prep grade gel (GE Healthcare) filtration column was used to polish rhIDO. Polishing the protein would remove any other contaminants present in the sample and TEV protease by size.

The FPLC, gel filtration column and other significant parts used in the purification procedure below are labelled in Figure 7.5. The columns for both proteins were washed with 500 ml degassed ddH_2O and equilibrated with 250 ml filtered, degassed separation buffer (Appendix I) before loading 1.0 – 2.5 ml concentrated protein with a syringe and needle, which was centrifuged for 1 minute at 13,000 rpm to remove any precipitated protein. Following injection of the protein into the system, the FPLC was controlled using the Unicorn software version 4.0 (GE Healthcare). The column was run at its lowest flow rate 0.1 ml per minute to obtain the highest resolution.

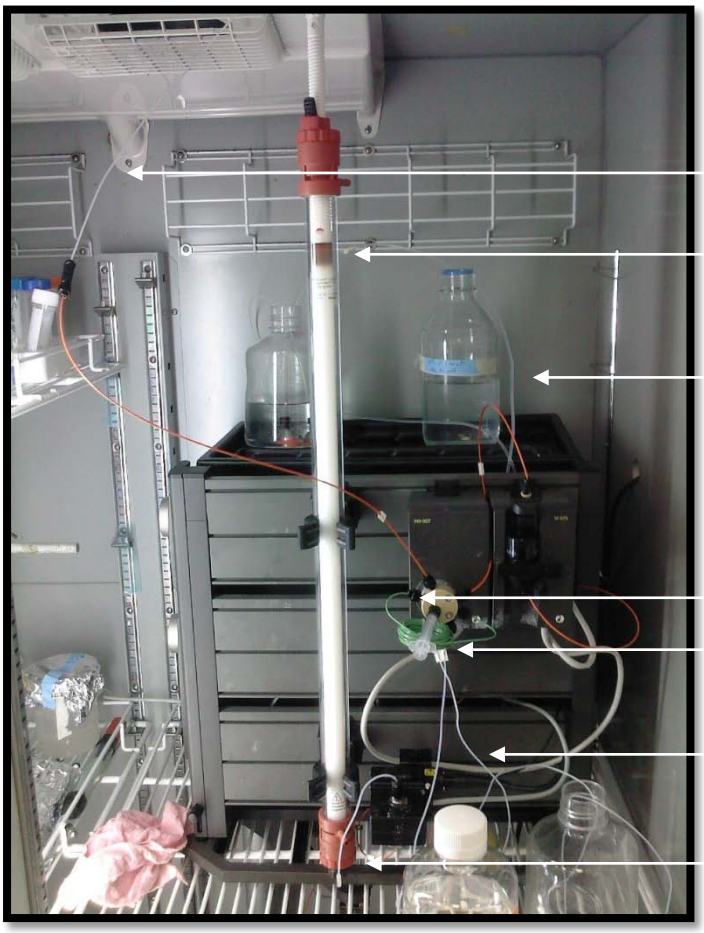

Figure 7.5 A FPLC system by GE Healthcare with a HiLoad™ 16/60 Superdex 200 preperative grade gel filtration column and hTDO loaded at the top.

The software was set to monitor the wavelength at 280 nm, to observe when the protein is eluting and controlled the fraction collector, which was set to discard all flow through until there was an absorbance at 280 nm. The fraction collector was set to collect fractions of 10 ml until an absorbance at 280 nm was reached and 1 ml samples were collected (Figure 7.6).

The pure protein determined from the FPLC trace (Figure 7.6, second peak) was pooled and concentrated in a 100 MW Amicon (Millipore) for rhTDO and a 30 MW Amicon (Millipore) for rhIDO and was used for crystallisation.

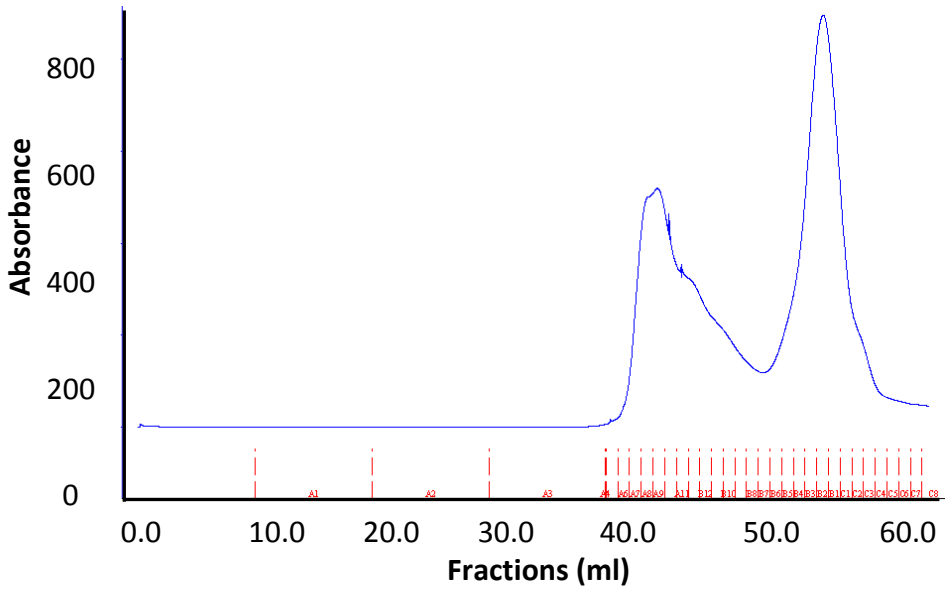

Figure 7.6 A typical FPLC trace of rhIDO eluted from a 16/60 30 pg superdex gel filtration column followed by the Unicorn software monitoring elution from the column at 280 nm (blue). The fractions in red (10 ml fractions at low 280 nm absorbance and 1 ml fractions at high 280 nm absorbance) collected by the fraction collector during the procedure.

7.4.6 Reconstitution of rhTDO and variants

rhTDO and the variants required reconstituting so 5 µl of 3 mM hemin in storage buffer (Appendix I) was added to 100 µl/100 µM protein for 2 hours at 4.0 ^{o}C. The excess hemin was removed by separation in a 3 ml pre-packed gel filtration column (Bio-Rad 10 DG). The eluted protein was then checked by UV – visible spectroscopy: if excess hemin was still in the sample, a shoulder at 340 – 380 nm was visible on the heme Soret peak, and the protein was concentrated in a 100 MW Amicon (Millipore).

7.4.7 SDS -PAGE

Electrophoresis was used to confirm the purity of the protein, check the size of the protein against a marker and determine what the protein was by peptide mass fingerprint analysis, if a protein band was unknown. After assembling the mini-Protean SDS gel apparatus (Bio-Rad), the lower gel was made from stacking buffer (Appendix I) and left to polymerise with water-n-butanol which levels the gel. The water-butanol was decanted after the bottom gel had set and the top layer of the gel was made from resolving buffer (Appendix I) and left to set with combs. The combs were removed and the gel was placed into a tank with tank buffer (Appendix I). The protein samples (10 µl) were mixed with sample buffer (2 µl, Appendix I) and ddH_2O (8 µl) were boiled for 2-3 minutes and loaded onto the gel with GelWell® tips (Rainin). The gel was run at 150 V and afterwards the apparatus was disassembled and the gel stained with staining buffer (Appendix I), which contained the dye Coomassie Brilliant Blue R250 for 10 minutes and washed with ddH_2O and destained overnight in destain (Appendix I). The protein bands were identified using a prestained protein marker, broad range 6-175 kDa (New England BioLabs), it consisted of 8 bands of protein, 175, 80, 58, 46, 30, 25, 17 and 7 kDa.

7.4.8 Peptide Mass Fingerprinting

Bands of interest were excised from the SDS gel and subjected to in-gel trypsin digestion, which cuts at arginine and lysine residues (*1*). Proteolytic peptides were analysed by MALDI-ToF mass spectrometry; the sample was mixed 1:1 with α-cyano-4-hydroxycinnamic acid (5 mg/ml in 0.1 % TFA 50 % acetonitrile in H_2O), spotted onto a stainless steel MALDI target plate and analysed using a Voyager DE-STR MALDI-ToF mass spectrometer (Applied Biosystems). The resulting peptide masses were searched against the NCBInr protein database using the MASCOT search algorithm (Matrix Science, London, UK) (*2*). A 95 % significance threshold was used for validating statistically significant identifications (Appendix III). MALDI was performed by The Protein Nucleic Acid Chemistry Laboratory (PNACL), University of Leicester.

7.5 Spectroscopic and Analytical Techniques

7.5.1 EPR

Electron Paramagnetic Resonance spectroscopy was conducted for rhTDO and variants in the absence and presence of 3 mM L-tryptophan for ferric enzyme. rhTDO EPR spectra were recorded by Dr. Myles Cheeseman using a Bruker ER300D spectrophotometer fitted with a dual-mode cavity, type ER4116M, interfaced to an ELEXYS computer control system (Bruker Analytische Messtechnik GmBH) and equipped with a variable temperature cryostat and liquid helium transfer line (Oxford Instruments) at the Univeristy of East Anglia. EPR simulations were performed using the Bruker program WINEPR Simfonia (v1.25).

EPR of the TDO variants were carried out by Dr Harriet Seward and Dr Gerry Griffith at the University of Leicester using a Bruker ELEXSYS E500 computer control system and spectrophotometer, fitted with a SHQE (super high Q) cavity and equipped with a variable temperature cryostat and a liquid helium transfer line (Oxford Instruments). The cryostat was an ESR-900 low temperature cavity (Oxford Instruments). EPR simulations were performed using the Bruker program xEPR (Bruker).

Determination of low-spin heme concentrations was achieved by simulation and double integration of spectra recorded under nonsaturating conditions at 9 K using 1 mM Cu(II)-EDTA as a spin standard (*3*). rhTDO and variant samples were prepared in 50 mM potassium phosphate, pH 8.0. For samples in the presence of L-tryptophan, the substrate (50 mM stock solution in buffer) was added to a final concentration of 3 mM and then frozen immediately to prevent oxidation of the substrate. Final concentrations of enzyme were 60 μM.

7.5.2 UV-visible Spectroscopy

Absorption measurements and spectra were conducted using a variable-slit Perkin-Elmer Lambda 35 (1 mm slit width) UV-visible spectrophotometer. A peltier temperature control accessory was used to maintain 25.0 ± 0.1 ^{o}C temperature of

the cell holder which was internally thermally-jacketed. Quartz cuvettes were used for UV measurements and baseline corrections were made against the buffers and solutions used.

7.5.3 Determination of Absorption Coefficients

The pyridine haemochromagen method was used to determine the absorption coefficient of rhIDO, rhTDO and the variants according to the protocol of Antonini and Brunori (*4*). A protein solution (1 ml), with an absorbance at the heme soret peak between 0.3- 0.9 was mixed with pyridine solution in NaOH (3 ml, (pyridine 100 ml, 1M NaOH 30 ml, H_2O to 300 ml)) to form the pyridine-heme complex. After 5 minutes (to allow complete conversion to hemochromagen), the absorption spectrum of the resulting solution (800 μl) of oxidised hemochromagen (yellow in colour) was recorded. Addition of a single crystal of sodium dithionite to the oxidised pyridine haemochromagen, formed an unstable reduced haemochromogen which was recorded between the wavelength range 450 – 650 nm (*5*).

The complete transfer of heme from the protein to the pyridine was checked by determining the maximum (λ = 557 nm) and minimum (λ = 450 nm) wavelengths; a ratio of A_{557}/A_{540} = 3.5 was found for protoheme. The pyridine-protoheme complex has a known absorption coefficient (32 $mM^{-1}cm^{-1}$), therefore using the Beer-Lambert law (Equation 7.3), the absorption coefficients for the proteins could be calculated. The absorption coefficients for each protein are in Appendix IV.

Equation 7.3

$$A = \varepsilon c l$$

where A is the absorbance of the stock solution, ε is the molar absorption coefficient ($mM^{-1}cm^{-1}$), c is the concentration of the protein (mM) and l is the pathlength of the cuvette (cm).

7.5.4 Ligand-Bound Derivative Spectra

Potassium cyanide, sodium fluoride and sodium azide (Sigma, analytical grade) were used without any further purification and were dissolved in storage buffer (Appendix I). Small additions of excess ligand (1 M potassium cyanide, sodium fluoride and sodium azide stock solutions) were made to a solution of ferric rhIDO, rhTDO and variants separately.

The ferrous form of rhIDO, rhTDO and variants were prepared and carried out in an anaerobic cuvette by the addition of fresh sodium dithionite solution (1-2 μl) to the ferric enzyme (Figure 7.6). Storage buffer (1 ml, Appendix I) was initially put into the cuvette and the air was evacuated for 30 minutes by a vacuum pump, so the storage buffer was purged of oxygen, then the protein, sodium dithionite and the ligands were added using the arm under the flow of nitrogen (Figure 7.7). The concentration of the sodium dithionite stock was not determined directly, but was used to provide qualitative reduction of the protein samples.

7.5.5 Ligand Binding Equilibria

Equilibrium binding parameters were determined by addition of the appropriately diluted ligand (1-2 μL, cyanide or L-tryptophan) solutions made in storage buffer (Appendix I) using a Hamilton syringe to the anaerobic cuvette containing ferric ≈2-5 μM protein, which was mixed by inversion and allowed to equilibrate (Figure 7.7). The UV-visible spectra were recorded after each addition of ligand. The ligand binding affinity was monitored spectroscopically using the absorption at 419 nm (rhTDO, H76A and H76S) and 416 nm (F72A, F140A F140Y R144A, R144K) for cyanide binding and 409 nm (rhTDO, H76A, H76S, F72A, R144A, R144K) and 412 nm (F140A and F140Y) for L-tryptophan binding.

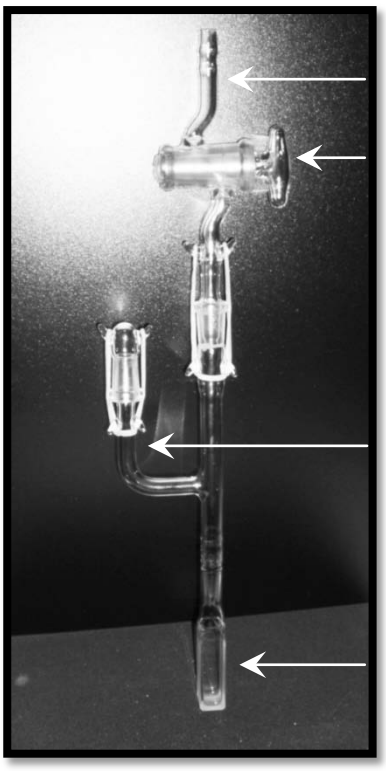

Figure 7.7 An adapted cuvette for anaerobic measurements. The inlet allows evacuation of air by a vacuum pump

Equilibrium dissociation constants for binding of cyanide and L-tryptophan to ferric enzyme were calculated using Equation 7.4 in the Grafit 5 software package version 5.0.3, Erithacus Software Ltd (*6*).

Equation 7.4

$$\Delta A = \frac{\Delta A_{\infty}\,[\mathrm{Free}]}{K_d + [\mathrm{Free}]}$$

Where ΔA and ΔA_{∞} are the absorbance changes corresponding to the intermediate and saturating ligand concentrations, [Free] is the total free concentration of unbound ligand and K_D is the equilibrium dissociation constant.

7.5.6 Steady-state Kinetics

Steady-state reactions were carried out at 25.0 ^{o}C and monitored for 5 minutes in a 1 ml cuvette at λ = 321 nm. The samples consisted of between 0.08 - 0.2 μM enzyme, 10 μM methylene blue (Sigma), 20 mM ascorbate (Sigma), 100 μg catalase (bovine liver, Sigma), different concentrations of L-tryptophan which were all soluble in storage buffer (*7*).

Reduction of heme iron is required to facilitate catalytic activity. Ascorbate and methylene blue are reducing agents, but also react with dioxygen to form superoxide and peroxide by-products, which can bleach the heme and destroy catalytic activity. Catalase is present in catalytic amounts to remove any superoxide or peroxide in solution and hence allows an efficient turnover of substrate.

The reaction was initiated by addition of the protein (0.3 μM). The rate of activity for the enzymes rhIDO, rhTDO and variants was determined by dividing the change in absorbance from product *N*-formylkynurenine (NFK) formation at 321 nm by the absorbance coefficient of NFK (ε_{321} = 3.75 mM^{-1} cm^{-1}) (*8*).

Values for k_{cat} were obtained directly from rate (μM s^{-1})/[enzyme concentration used in the assay] (μM) versus substrate concentration plots of the assay data. All kinetic parameters reported are averages of at least three separate experiments, unless stated otherwise. All kinetic profiles were fitted to the Michaelis-Menten, Equation 7.5.

Equation 7.5

$$v = \frac{V_{max}[S]}{K_m + [S]}$$

Where, v is the rate, V_{max} is the maximal rate, K_m, the Michaelis constant is the concentration at which the reaction rate is half its maximal value and [S] is the substrate concentration. Steady-state reactions were conducted for rhTDO, H76A and H76S TDO variants, using the same method as above was applied for measuring product formation, with 1.5 mM 1-methyl-L-tryptophan as the substrate.

7.5.7 Tryptophan Concentration

Concentration of tryptophan stock in storage buffer (Appendix I) was determined using the absorption coefficient ε_{278} = 5.5 $mM^{-1}cm^{-1}$ and Equation 7.3.

7.5.8 Inhibition Studies

L-Tryptophan activity was measured in 50 mM Tris, pH 8.0, at 25.0 ^{o}C, in the presence and absence of variable concentrations (0.0 - 0.5 mM) of the inhibitor, 1-methyl-L-tryptophan. Initial reaction rates were determined by monitoring the change in absorbance at 321 nm due to formation of the product, *N*-formylkynurenine, (ε_{321} = 3.75 mM^{-1} cm^{-1}) in a Perkin Elmer Perkin-Elmer Lambda 35 (1 mm slit width) UV-visible spectrophotometer or an Agilent 8453 diode array UV/visible spectrophotometer (*8*). A peltier temperature control accessory was used to maintain 25.0 ± 0.1 ^{o}C temperature of the cell holder which was internally thermally-jacketed. A typical kinetic experiment consisted of 20 to 25 steady-state rates at different combinations of substrate and inhibitor concentrations, as indicated in the Figures, which were measured in triplicate.

The rate v depends on the concentrations of substrate [S] and of inhibitor [I], in accordance with the following equation 7.6:

Equation 7.6

$$v = \frac{V_{max}\,[S]}{K_m\left(1 + \frac{[I]}{K_{ic}}\right) + [S]\left(1 + \frac{[I]}{K_{iu}}\right)}$$

In which V_{max} is the limiting rate, K_m is the Michaelis constant, K_{ic} is the competitive inhibition constant and K_{iu} is the uncompetitive inhibition constant. In competitive inhibition, [I]/K_{iu} is negligible, in uncompetitive inhibition [I]/K_{ic} is negligible, and in pure noncompetitive inhibition the two inhibition constants are equal, $K_{ic} = K_{iu}$ (*9*).

The values for the competitive inhibition constant K_{ic}, can be directly obtained from plots of 1/v against [I] at different [S] values which, generates a series of straight lines that intersect at a point, where [I] is K_{ic} (Figure 7.8, left side plots) (*10*). The values for the uncompetitive inhibition constant K_{iu}, can be directly

obtained from plots of [S]/v against [I], where the intersecting point of the straight lines is K_{iu} (Figure 7.8, middle plots) (*11*). Plotting both graphs (1/v against [I] and [S]/v against [I]) will determine which type of inhibitor 1-methyl-L-tryptophan is; pure competitive, pure uncompetitive, mixed-competitive or mixed-uncompetitive (Figure 7.8, left and middle plots).

A plot of v_0/V_{max} against $1/[I]_{0.5}$ (where $[I]_{0.5}$ is where the lines intercept the x axis after 0.5 which indicates where the inhibitor concentration inhibits the enzyme by 50 % at a particular substrate concentration) allows confirmation of the inhibition type and the inhibition constants K_{ic} or K_{iu} (Figure 7.8, right side plots). Comparison of the V_{max} and K_m of uninhibited reaction with the V_{max} and K_m of the inhibited reactions shows the type of inhibition; for competitive inhibition the K_m increases and the V_{max} is the same for the inhibited reaction; for non-competitive inhibition the K_m does not change but V_{max} decreases; for a mixed-type inhibition the K_m increases and V_{max} decreases; for uncompetitive inhibition both the V_{max} and K_m decrease (Figure 7.8).

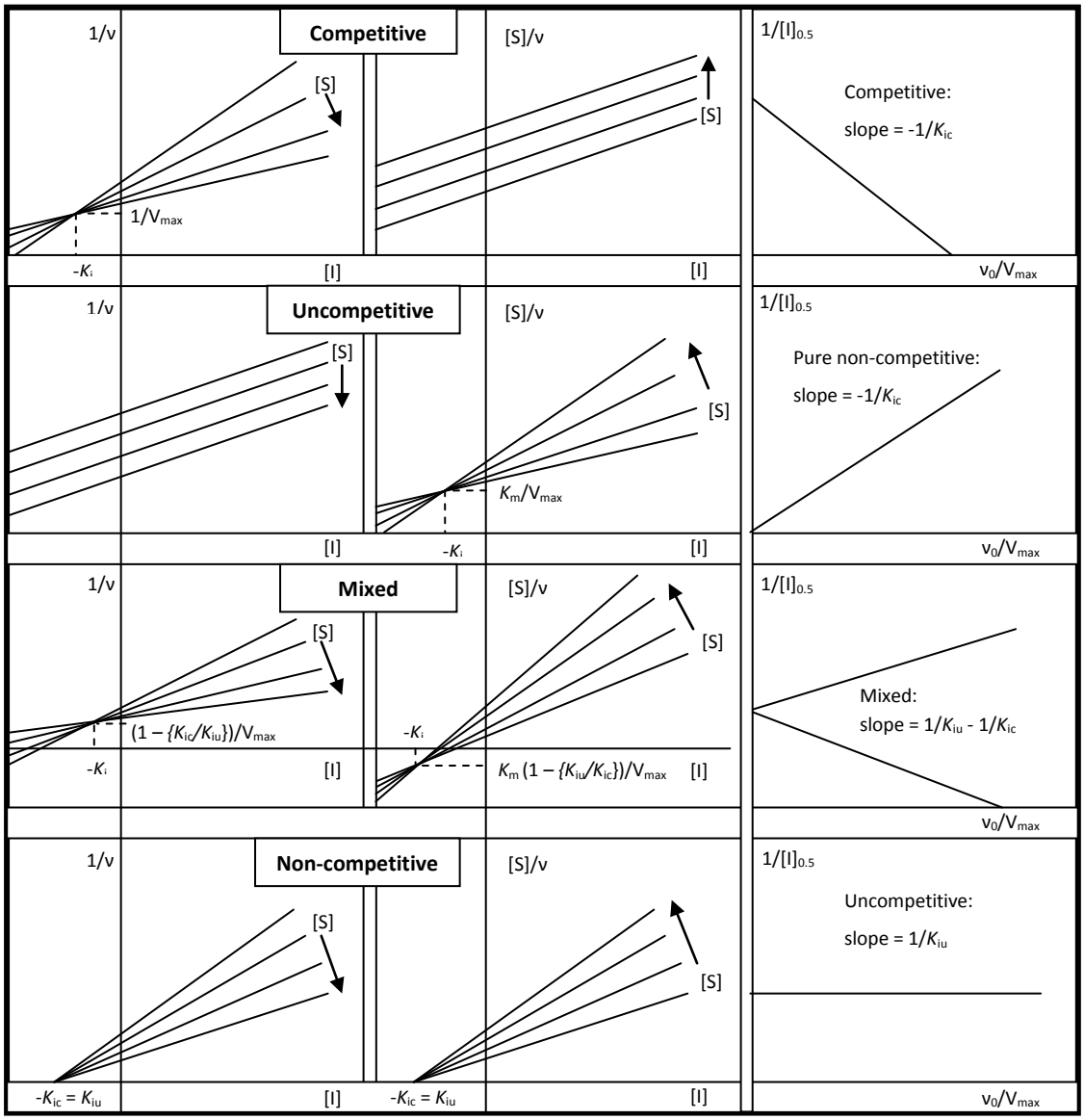

Figure 7.8 Plots for determining inhibition constants and types of inhibition. Plots on the left column are 1/v against [I], the middle plots are [S]/v against [I] and the right hand plots are $1/[I]_{0.5}$ against v_0/V_{max}. The three sets of plots in combination show four types of inhibition. $[I]_{0.5}$ is indicated where the lines intercept the x axis for a particular substrate concentration. The direction in which the substrate concentration increases/decreases is indicated on each plot by an arrow (*9, 11*).

7.5.9 Redox Potentiometry

Reduction potentials for Fe^{3+}/Fe^{2+} of rhIDO, rhTDO and the variants were determined by the reduction of a dye with a known potential (*12*). The assay solution contained potassium phosphate buffer (0.1 M, KPi pH 7.0), glucose (5 mM), xanthine (16 μM), xanthine oxidase (5 mM), glucose oxidase (50 μg/ ml) catalase (5 μg/ ml) (Sigma), enzyme (2 μM) and several dyes were required for different enzymes: nile blue chloride (NBC) ($E^{o'}$ = -116 mV (*13*)), methylene blue (MB) ($E^{o'}$ = -11 mV (*13*)), toluene blue O (TBO) ($E^{o'}$ = +34 mV (*13*)). The components glucose, glucose oxidase and catalase generated an oxygen-free environment. The absorbance change for the heme peak was measured at the isobestic point for the dye at 409 nm and the absorbance change for the dye was measured at the isobestic point for the heme peak at 635 nm for NBC, 665 nm for methylene blue and 635 for toluidene blue O; at these wavelengths there was no absorption from the other components of the reaction solution.

The results were analysed using the Nernst equations (25 mV $\ln(E_{ox}/E_{red})$) and (12.5 mV $\ln(E_{ox}/E_{red})$), where E_{ox}/E_{red} and D_{ox}/D_{red} are the oxidised and reduced forms of the enzyme and dye respectively, thus producing a linear graph, with a gradient of 1 across a wide potential range. The intercept gives a reliable value for $E^{o'}$. UV-visible spectra obtained in all experiments were analysed using SPECFIT (*14*) for singular value decomposition based on factor analysis. All potentials reported in this thesis are given versus the normal hydrogen electrode (NHE).

Determination of the relationship between equilibrium binding constants for oxidised, K_{ox}, and reduced, K_{red}, proteins and the reduction potential was according to Equation 7.7:

Equation 7.7

$$\frac{K_{\mathrm{ox}}}{K_{\mathrm{red}}} = exp\left(\frac{nF\left(E_{bound} - E_{free}\right)}{RT}\right)$$

$$\begin{array}{ccc} \boldsymbol{Fe^{3+}} & \overset{\boldsymbol{E_{free}}}{\Longleftrightarrow} & \boldsymbol{Fe^{2+}} \\ \boldsymbol{K_{ox}} \Updownarrow & & \Updownarrow \boldsymbol{K_{red}} \end{array}$$

$$\boldsymbol{Fe^{3+} + Trp \underset{E_{bound}}{\Longleftrightarrow} Fe^{2+} + Trp}$$

where K_{ox} and K_{red} are equilibrium binding constants for oxidised and reduced rhTDO, respectively, E^{bound} and E^{free} are the redox potentials of rhTDO bound to L-tryptophan and free protein respectively, R = 8.314 J/K mol the gas constant, T is the temperature (K) and F = 96487 C/mol the Faraday constant.

7.6 Crystallisation

Crystallisation of the enzymes TDO and IDO were carried out in collaboration with Dr. Peter Moody and the help from Dr Igor Efimov and Andrea Gumiero.

7.6.1 Screening Conditions

Crystal structures of rhIDO and bacterial TDOs have been solved so the conditions for those crystals were first tried with rhIDO and rhTDO but were unsuccessful. Therefore high-throughput screening of crystal solutions was required to find crystallisation conditions for our enzymes using the sitting drop technique. The robots called Tecan and Cartesian were used for the screening process (Figure 7.9).

The Tecan Freedom Evo 75 is a high-throughput liquid handling robot that is equipped with a robotic arm that is capable of simultaneous 2-syringe/position, controlled by Evoware (Figure 7.9A). The tecan transferred solutions from the crystal kits into the wells of the nano-drop plates.

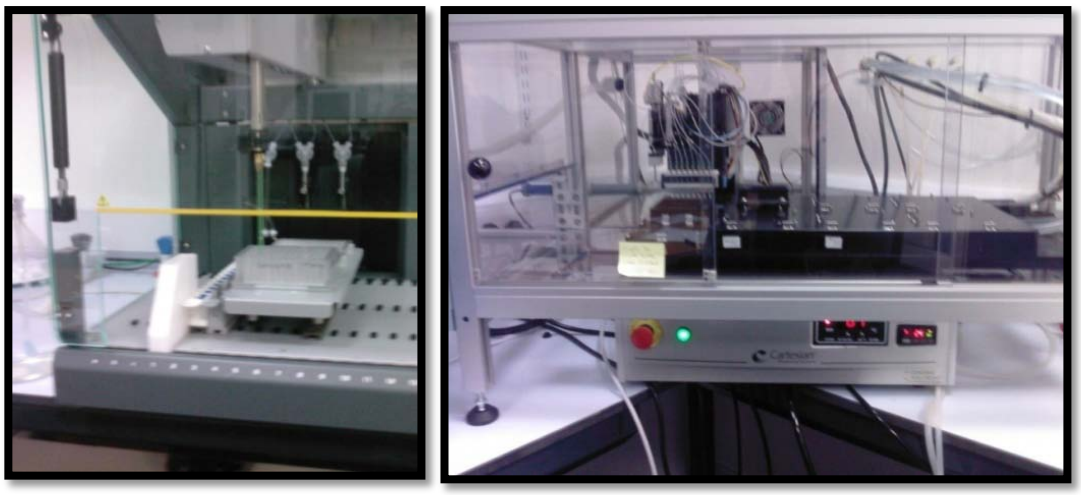

Figure 7.9 Crystal screening robots. A) The Tecan is a robotic multipipette which transfers crystal solutions from a large volume in a deep well plate to the well of a nano drop plate. B) The Cartesian moves on all three axis, x, y and z to transfer 100 nl of the well solution and protein to the sitting drop section of the plate.

The Cartesian Dispensing Systems (Genomic Solutions) is a high-throughput crystallisation platform, which has a multi-pipette for dispensing crystal formulations from 96 wells to 192 sitting drop shelves very rapidly. The robot transfers 100 nL therefore minimising protein requirements for crystal screening, which was a benefit with rhTDO which has relatively low expression (Figure 7.9B).

Commercially available kits were used to screen a wide range of conditions (Wizard I and II and Cryo I and II (Emerald Biosciences), Crystal screen I (Hampton Research) and JCSG Crystal screen (Molecular Dimensions) Appendix V). In total 336 conditions were tested for both ferric rhTDO and ferric rhIDO using the sitting drop method. For rhIDO screens were conducted in the absence and presence of 5 mM 4-Phenylimidazole (PIM), as this inhibitor was bound to the rhIDO in the published crystal structure (*15*).

Two nano-drop plates were set up for each screen, one would be stored at 6.0 ^{o}C and the other at room temperature in a TriTek CrystalPro™ HT after they had been sealed with crystal clear sealing film. The hotel is controlled by CrystalLIMS™ software (TriTek), which schedules scanning of the plates using an imaging robot

which consists of a microscope, a motorised sub-micron resolution focus, cold-light illumination system and a patented optical configuration, high-resolution digital camera.

Figure 7.10 CrystalPro® HT (TriTek) a self contained plate storage hotel and imaging robot.

Crystals typically form in 1-2 weeks and once a micro crystal is observed using the CrystalLIMS™ software (TriTek) another crystal screen is conducted on a larger scale (Figure 7.10). A 24 well plate (4 × 6 Cryschem plates with 1 ml wells, Hampton Research) was used with protein (1 µl) and then sealed with crystal clear tape and left for 1-2 weeks at either 6.0 ^{o}C or room temperature depending on the optimum growth conditions of the micro-crystals. A microscope was used to observe whether there was formation of any crystals. The successful crystal formula consisted of 50 mM Tris pH 8.5 and 8 % PEG 8K for rhIDO.

Once a crystal has grown the conditions were systematically altered by changing the pH and/or the concentration of the crystal formulation so that optimum-sized crystals could be grown.

7.6.2 Determination of Diffraction for Crystals

Once the crystals were a reasonable size (0.01 – 1 mm) the crystals needed to be tested for whether they diffracted. We used two different diffraction methods, one conducted at room temperature and the other at 100 K. An advantage of diffraction at room temperature is that the protein does not need to be coated with a protecting solution, the disadvantage is that the crystals become rapidly denatured from the effects of the X-rays. Cryo diffraction is preferred, the advantage being that the crystals are protected from damage by X-rays and the cryo environment by being encapsulated by a cryo solution, the disadvantage is that a suitable cryo solution to protect the crystal has to be determined through trial and error.

For room temperature diffraction a MicroRT^{TM} room temperature mounting kit (Mitegen) was used which has a polyester sock over the crystal, with some of the crystal formulation inside to create an internal environment, which stops the crystal from drying out and denaturing. For cryo diffraction a cryo solution was required which has the same concentration as the well solution with the addition of a cryo protectant. The cryo protectant for rhIDO crystals was 30 % Xylitol.

Figure 7.11 A Rigaku RU2HB X-ray generator with a copper anode, Xenocs multilayer optics and an R-Axis IV detector.

Diffraction data were collected in house using a Rigaku RU2HB X-ray generator with copper anode, Xenocs multilayer optics, an R-Axis IV detector and a cryo stream 700 (Oxford Cryo Systems) for rhIDO at room temperature and under cryo conditions (Figure 7.11). The cryo solution used to protect the crystal consisted of 50 mM Tris pH 8.5, 8 % PEG 8K, 30 % Xylitol. Diffraction was controlled and the data was collected using the Rigaku Structure Studio Suite and the diffraction data was analysed using the computer software Imosfilm (Collaborative Computational Project 4). The crystals are being taken to the synchrotron for better diffraction.

7.7 References

1. Speicher, K. D., Kolbas, O., Harper, S., and Speicher, D. W. (2000) Systematic Analysis of Peptide Recoveries from In-Gel Digestions for Protein Identifications in Proteome Studies, *J Biomol Tech 11*, 74-86.
2. Perkin, D. N., Pappin, D. J., Creasy, D. M., and Cottrell, J. S. (1999) Probability-based protein identification by searching sequence databases using mass spectrometry data, *Electrophoresis 20*, 3551-3567.
3. Aasa, R., and Vanngard, T. (1975) EPR Signal Intensity and Powder Shapes: A Reexamination, *J Magn. Reson. 19*, 308-315.
4. Antonini, M., and Brunori, E. (1971) *Haemoglobin and Myoglobin and their reactions with ligands*, North Holland Publishers, Amsterdam.
5. De Duve, C. (1948) A spectroscopic method for simultaneous determination o myglobin and hemoglobin in extracts of human muscle, *Acta Chem Scandinavica 2*, 164.
6. Leatherbarrow, R. J. (2001) Grafit Version 5.0 Erithacus Software Ltd Staine UK.
7. Takikawa, O. (2005) Biochemical and medical aspects of the indoleamine 2,3-dioxygenase-initiated L-tryptophan metabolism, *Biochem Biophys Res Commun 338*, 12-19.
8. Shimizu, T., Nomiyama, S., Hirata, F., and Hayaishi, O. (1978) Indoleamine 2,3-dioxygenase. Purification and some properties, *J Biol Chem 253*, 4700-4706.
9. Cortes, A., Cascante, M., Cardenas, M. L., and Cornish-Bowden, A. (2001) Relationships between inhibition constants, inhibitor concentrations for 50% inhibition and types of inhibition: new ways of analysing data, *Biochem J 357*, 263-268.
10. Dixon, M. (1953) The determination of enzyme inhibitor constants, *Biochem J 55*, 170-171.
11. Cornish-Bowden, A. (1974) A simple graphical method for determining the inhibition constants of mixed, uncompetitive and non-competitive inhibitors, *Biochem J 137*, 143-144.
12. Massey, V. (1991) Flavins and Flavoproteins (Curti, B., Ronchi, S., and Zanetti, G., Eds.) pp 59-66, *Walter de Gruyter & Co., New York*.
13. Clark, M. W. (1972) *Oxidation-Reduction Potentials of Organic Systems*, Robert E. Kreiger Publishing Co., Huntington, NY.
14. Binstead, R. A., and Zuberbuehler, A. D. (1994) *SPECFIT*, Spectrum Software Associates, Chapel Hill, NC.
15. Sugimoto, H., Oda, S., Otsuki, T., Hino, T., Yoshida, T., and Shiro, Y. (2006) Crystal structure of human indoleamine 2,3-dioxygenase: catalytic mechanism of O2 incorporation by a heme-containing dioxygenase, *PNAS 103*, 2611-2616.

APPENDIX I

BUFFERS AND MEDIA

TE Buffer
1 mM TE-EDTA
10 mM Tris pH 8.0

P1 Buffer (DNA Isolation)
50 mM Tris-Cl, pH 8.0
10 mM EDTA
100 µg/ml RNase A

P2 Buffer (DNA Isolation)
200 mM NaOH
1% SDS (w/v)

N3 (DNA Isolation)
Composition patented.

Phosphate Buffer (PB) (DNA Isolation)
Composition patented.

PE (DNA Isolation)
Composition patented.

10 ×Tango Buffer (Restriction Digest)
33 mM Tris-acetate (pH 7.9 at 37 ^{o}C)
10 mM Magnesium acetate
66 mM potassium acetate
0.1 mg/ml BSA

1 % Agarose Gel (Agarose gel electrophoresis)
0.6 g Agarose
60 ml 1 × TAE buffer

50 × TAE Buffer (Agarose gel electrophoresis)
242 g Tris base
37.1 g Glacial acetic acid
100 ml of 0.5 M EDTA
900 ml ddH_2O

Buffer QG (DNA gel extraction)
1.0 M NaCl
50 mM MOPS, pH 7.0
15 % Isopropanol

SOC Media (Transformation)
2 g Tryptone
0.5 g Yeast extract
0.05 g Sodium chloride
0.4 g Glucose
Make up to 100 ml with ddH_2O
Autoclave
Add 1ml filter sterilised 1 M magnesium chloride and 1 M magnesium sulphate

Luria-Bertani broth (LB) (Melford)
10 g Tryptone
5 g Yeast Extract
10 g NaCl
2 g Glucose
Make up to 1.0 l with deionised water
Autoclave

2 × Yeast Tryptone Media (2 × YT) (Melford)
16 g Tryptone
10 g Yeast extract
5 g NaCl media
Make up to 1.0 L with autoclaved dH_2O

Sonication Buffer A (For Purification with Imidazole)
50 mM Potassium phosphate buffer pH 8.0
300 mM Potassium chloride
20 mM Imidazole

Sonication Buffer B (For Purification with EDTA)
50 mM Potassium phosphate buffer pH 8.0
300 mM Potassium chloride

Wash Buffer A (For Purification with Imidazole)
50 mM Potassium phosphate buffer pH 8.0
300 mM Potassium chloride
60 mM Imidazole

Wash Buffer B (For purification with EDTA)
50 mM Potassium phosphate buffer pH 8.0
300 mM Potassium chloride

Elution Buffer A (For purification with Imidazole)
50 mM Potassium phosphate buffer pH 8.0
300 mM Potassium chloride
300 mM Imidazole

Elution Buffer B (For purification with EDTA)
50 mM Potassium phosphate buffer pH 8.0
300 mM Potassium chloride
100 mM EDTA

Storage Buffer
50 mM Tris-HCl pH 8.0

Separation Buffer
50 mM Tris-HCl pH 8.0
300 mM Sodium Chloride

Stacking Buffer (SDS-PAGE)
0.5 M Tris base
0.4% SDS
Adjust to pH 6.8

Resolving Buffer (SDS-PAGE)
0.5 M Tris base
0.4% SDS
Adjust to pH 8.8

Tank buffer (SDS-PAGE)
25 mM Tris-HCl
192 mM Glycine
0.1% w/v SDS

Sample Buffer (SDS-PAGE)
125 mM Tris-HCl, pH 6.8
4% SDS
20% w/v Glycerol
0.002% Bromophenol blue

Staining Buffer (SDS-PAGE)
30% v/v Methanol
12% w/v Trichloroacetic acid
0.01% w/v Coomassie Blue R
10% w/v Sulphosalicylic acid

Destain (SDS-PAGE)
7.5 % Acetic acid
5 % Methanol

APPENDIX II

SEQUENCING

Sequencing was carried out by the The Protein Nucleic Acid Chemistry Laboratory (PNACL), University of Leicester (Chapter 7, section 7.2.2).

MAGCPFLGNNFGYTFKKLPVEGSEEDKSQTGVNRASKGGLIYGNYLHLEKVLNAQELQSETKG
NKIHDEHLFIITHQAYELWFKQILWELDSVREIFQNGHVRDERNMLKVVSRMHRVSVILKLLV
QQFSILETMTALDFNDFREYLSPASGFQSLQFRLLENKIGVLQNMRVPYNRRHYRDNFKGEEN
ELLLKSEQEKTLLELVEAWLERTPGLEPHGFNFWGKLEKNITRGLEEEFIRIQAKEESEEKEEQVA
EFQKQKEVLLSLFDEKRHEHLLSKGERRLSYRALQGALMIYFYREEPRFQVPFQLLTSLMDIDSL
MTKWRYNHVCMVHRMLGSKAGTGGSSGYHYLRSTVSDRYKVFVDLFNLSTYLIPRHWIPKM
NPTIHKFLYTAEYCDSSYFSSDESDLEHHHHHH

Figure A2.1. Amino acid sequence of rhTDO in the vector pET28a. Highlighted in blue are the residues which differ from the human TDO sequence after PCR, the TDO/pET28a sequence has a C-terminus hexahistidyl tag and the second residue was mutated from S to A as it is part of the *NcoI* site which anneals to the vector pET28a .

MSGCPFLGNNFGYTFKKLPVEGSEEDKSQTGVNRASKGGLIYGNYLHLEKVLNAQELQSETKG
NKIHDEHLFIITHQAYELWFKQILWELDSVREIFQNGHVRDERNMLKVVSRMHRVSVILKLLV
QQFSILETMTALDFNDFREYLSPASGFQSLQFRLLENKIGVLQNMRVPYNRRHYRDNFKGEEN
ELLLKSEQEKTLLELVEAWLERTPGLEPHGFNFWGKLEKNITRGLEEEFIRIQAKEESEEKEEQVA
EFQKQKEVLLSLFDEKRHEHLLSKGERRLSYRALQGALMIYFYREEPRFQVPFQLLTSLMDIDSL
MTKWRYNHVCMVHRMLGSKAGTGGSSGYHYLRSTVSDRYKVFVDLFNLSTYLIPRHWIPKM
NPTIHKFLYTAEYCDSSYFSSDESDENLYFQSLEHHHHHH

Figure A2.2. Amino acid sequence of rhTDO in the vector pLEICS5. Highlighted in blue are the residues which differ from the human TDO sequence after PCR, the TDO/pLEICS5 sequence has a C-terminus TEV cleavage site followed by a hexa-histidyl tag.

MSGCPFLGNNFGYTFKKLPVEGSEEDKSQTGVNRASKGGLIYGNYLHLEKVLNAQELQSETKG
NKIHDEHLFIIT**A**QAYELWFKQILWELDSVREIFQNGHVRDERNMLKVVSRMHRVSVILKLLV
QQFSILETMTALDFNDFREYLSPASGFQSLQFRLLENKIGVLQNMRVPYNRRHYRDNFKGEEN
ELLLKSEQEKTLLELVEAWLERTPGLEPHGFNFWGKLEKNITRGLEEEFIRIQAKEESEEKEEQVA
EFQKQKEVLLSLFDEKRHEHLLSKGERRLSYRALQGALMIYFYREEPRFQVPFQLLTSLMDIDSL
MTKWRYNHVCMVHRMLGSKAGTGGSSGYHYLRSTVSDRYKVFVDLFNLSTYLIPRHWIPKM
NPTIHKFLYTAEYCDSSYFSSDESD**ENLYFQSLEHHHHHH**

Figure A2.3. Amino acid sequence of the H76A variant of rhTDO. Highlighted in blue are the residues which differ from the human TDO sequence after PCR, the TDO/pLEICS5 sequence has a C-terminus TEV cleavage site followed by a hexa-histidyl tag and residue 76 was mutated from H to A.

MSGCPFLGNNFGYTFKKLPVEGSEEDKSQTGVNRASKGGLIYGNYLHLEKVLNAQELQSETKG
NKIHDEHLFIIT**S**QAYELWFKQILWELDSVREIFQNGHVRDERNMLKVVSRMHRVSVILKLLVQ
QFSILETMTALDFNDFREYLSPASGFQSLQFRLLENKIGVLQNMRVPYNRRHYRDNFKGEENE
LLLKSEQEKTLLELVEAWLERTPGLEPHGFNFWGKLEKNITRGLEEEFIRIQAKEESEEKEEQVAE
FQKQKEVLLSLFDEKRHEHLLSKGERRLSYRALQGALMIYFYREEPRFQVPFQLLTSLMDIDSLM
TKWRYNHVCMVHRMLGSKAGTGGSSGYHYLRSTVSDRYKVFVDLFNLSTYLIPRHWIPKMN
PTIHKFLYTAEYCDSSYFSSDESD**ENLYFQSLEHHHHHH**

Figure A2.4. Amino acid sequence of the H76AS variant of rhTDO. Highlighted in blue are the residues which differ from the human TDO sequence after PCR, the TDO/pLEICS5 sequence has a C-terminus TEV cleavage site followed by a hexa-histidyl tag and residue 76 was mutated from H to S.

MSGCPFLGNNFGYTFKKLPVEGSEEDKSQTGVNRASKGGLIYGNYLHLEKVLNAQELQSETKG
NKIHDEHL**A**IITHQAYELWFKQILWELDSVREIFQNGHVRDERNMLKVVSRMHRVSVILKLLV
QQFSILETMTALDFNDFREYLSPASGFQSLQFRLLENKIGVLQNMRVPYNRRHYRDNFKGEEN
ELLLKSEQEKTLLELVEAWLERTPGLEPHGFNFWGKLEKNITRGLEEEFIRIQAKEESEEKEEQVA
EFQKQKEVLLSLFDEKRHEHLLSKGERRLSYRALQGALMIYFYREEPRFQVPFQLLTSLMDIDSL
MTKWRYNHVCMVHRMLGSKAGTGGSSGYHYLRSTVSDRYKVFVDLFNLSTYLIPRHWIPKM
NPTIHKFLYTAEYCDSSYFSSDESD**ENLYFQSLEHHHHHH**

Figure A2.5. Amino acid sequence of the F72A variant of rhTDO. Highlighted in blue are the residues which differ from the human TDO sequence after PCR, the TDO/pLEICS5 sequence has a C-terminus TEV cleavage site followed by a hexa-histidyl tag and residue 72 was mutated from F to A.

MSGCPFLGNNFGYTFKKLPVEGSEEDKSQTGVNRASKGGLIYGNYLHLEKVLNAQELQSETKG
NKIHDEHLFIITHQAYELWFKQILWELDSVREIFQNGHVRDERNMLKVVSRMHRVSVILKLLV
QQFSILETMTALD**A**NDFREYLSPASGFQSLQFRLLENKIGVLQNMRVPYNRRHYRDNFKGEEN
ELLLKSEQEKTLLELVEAWLERTPGLEPHGFNFWGKLEKNITRGLEEEFIRIQAKEESEEKEEQVA
EFQKQKEVLLSLFDEKRHEHLLSKGERRLSYRALQGALMIYFYREEPRFQVPFQLLTSLMDIDSL
MTKWRYNHVCMVHRMLGSKAGTGGSSGYHYLRSTVSDRYKVFVDLFNLSTYLIPRHWIPKM
NPTIHKFLYTAEYCDSSYFSSDESD**ENLYFQSLEHHHHHH**

Figure A2.6. Amino acid sequence of the F140A variant of rhTDO. Highlighted in blue are the residues which differ from the human TDO sequence after PCR, the TDO/pLEICS5 sequence has a C-terminus TEV cleavage site followed by a hexa-histidyl tag and residue 140 was mutated from F to A.

MSGCPFLGNNFGYTFKKLPVEGSEEDKSQTGVNRASKGGLIYGNYLHLEKVLNAQELQSETKG
NKIHDEHLFIITHQAYELWFKQILWELDSVREIFQNGHVRDERNMLKVVSRMHRVSVILKLLV
QQFSILETMTALD**Y**NDFREYLSPASGFQSLQFRLLENKIGVLQNMRVPYNRRHYRDNFKGEEN
ELLLKSEQEKTLLELVEAWLERTPGLEPHGFNFWGKLEKNITRGLEEEFIRIQAKEESEEKEEQVA
EFQKQKEVLLSLFDEKRHEHLLSKGERRLSYRALQGALMIYFYREEPRFQVPFQLLTSLMDIDSL
MTKWRYNHVCMVHRMLGSKAGTGGSSGYHYLRSTVSDRYKVFVDLFNLSTYLIPRHWIPKM
NPTIHKFLYTAEYCDSSYFSSDESD**ENLYFQSLEHHHHHH**

Figure A2.7. Amino acid sequence of the F140Y variant of rhTDO. Highlighted in blue are the residues which differ from the human TDO sequence after PCR, the TDO/pLEICS5 sequence has a C-terminus TEV cleavage site followed by a hexa-histidyl tag and residue 140 was mutated from F to Y.

MSGCPFLGNNFGYTFKKLPVEGSEEDKSQTGVNRASKGGLIYGNYLHLEKVLNAQELQSETKG
NKIHDEHLFIITHQAYELWFKQILWELDSVREIFQNGHVRDERNMLKVVSRMHRVSVILKLLV
QQFSILETMTALDFNDF**A**EYLSPASGFQSLQFRLLENKIGVLQNMRVPYNRRHYRDNFKGEEN
ELLLKSEQEKTLLELVEAWLERTPGLEPHGFNFWGKLEKNITRGLEEEFIRIQAKEESEEKEEQVA
EFQKQKEVLLSLFDEKRHEHLLSKGERRLSYRALQGALMIYFYREEPRFQVPFQLLTSLMDIDSL
MTKWRYNHVCMVHRMLGSKAGTGGSSGYHYLRSTVSDRYKVFVDLFNLSTYLIPRHWIPKM
NPTIHKFLYTAEYCDSSYFSSDESD**ENLYFQSLEHHHHHH**

Figure A2.8. Amino acid sequence of the R144A variant of rhTDO. Highlighted in blue are the residues which differ from the human TDO sequence after PCR, the TDO/pLEICS5 sequence has a C-terminus TEV cleavage site followed by a hexa-histidyl tag and residue 144 was mutated from R to A.

MSGCPFLGNNFGYTFKKLPVEGSEEDKSQTGVNRASKGGLIYGNYLHLEKVLNAQELQSETKG
NKIHDEHLFIITHQAYELWFKQILWELDSVREIFQNGHVRDERNMLKVVSRMHRVSVILKLLV
QQFSILETMTALDFNDF**K**EYLSPASGFQSLQFRLLENKIGVLQNMRVPYNRRHYRDNFKGEEN
ELLLKSEQEKTLLELVEAWLERTPGLEPHGFNFWGKLEKNITRGLEEEFIRIQAKEESEEKEEQVA
EFQKQKEVLLSLFDEKRHEHLLSKGERRLSYRALQGALMIYFYREEPRFQVPFQLLTSLMDIDSL
MTKWRYNHVCMVHRMLGSKAGTGGSSGYHYLRSTVSDRYKVFVDLFNLSTYLIPRHWIPKM
NPTIHKFLYTAEYCDSSYFSSDESD**ENLYFQSLEHHHHHH**

Figure A2.9. Amino acid sequence of the R144K variant of rhTDO. Highlighted in blue are the residues which differ from the human TDO sequence after PCR, the TDO/pLEICS5 sequence has a C-terminus TEV cleavage site followed by a hexa-histidyl tag and residue 144 was mutated from R to K.

MHHHHHHGKPIPNPLLGLDSTENLYFQGIDPFTMAHAMENSWTISKEYHIDEEVGFALPNP
QENLPDFYNDWMFIAKHLPDLIESGQLRERVEKLNMLSIDHLTDHKSQRLARLVLGCITMAYV
WGKGHGDVRKVLPRNIAVPYCQLSKKLELPPILVYADCVLANWKKKDPNKPLTYENMDVLFSF
RDGDCSKGFFLVSLLVEIAAASAIKVIPTVFKAMQMQERDTLLKALLEIASCLEKALQVFHQIHD
HVNPKAFFSVLRIYLSGWKGNPQLSDGLVYEGFWEDPKEFAGGSAGQSSVFQCFDVLLGIQQ
TAGGGHAAQFLQDMRRYMPPAHRNFLCSLESNPSVREFVLSKGDAGLREAYDACVKALVSLR
SYHLQIVTKYILIPASQQPKENKTSEDPSKLEAKGTGGTDLMNFLKTVRSTTEKSLLKEG

Figure A2.10. Amino acid sequence of rhIDO in the vector pET151/d TOPO. Highlighted in blue are the residues which differ from the human IDO sequence after PCR, the IDO/pET151/d TOPO sequence has a N-terminus start codon, a hexa-histidyl tag, a V5 epitope followed by a TEV cleavage site.

APPENDIX III

PEPTIDE MASS FINGERPRINT RESULTS

Peptide mass fingerprint was carried out by the The Protein Nucleic Acid Chemistry Laboratory (PNACL), University of Leicester (Chapter 7, section 7.4.8).

MSGCPFLGNNFGYTFK**KLPVEGSEEDKSQTGVNRA**S**KGGLIYGNYLHLEKVLNAQELQSETK**
GNKIHDEHLFIITHQAYELWF**KQILWELDSVREIFQNGHVRD**ERNMLKVVSRMHRVSVILKLL
VQQFSILETMTALDFNDF**REYLSPASGFQSLQFRL**LEN**KIGVLQNMRVPYNRRH**Y**RDNFKGE**
ENELLLKSEQEKTLLELVEAWLE**RTPGLEPHGFNFWGKL**EKNIT**RGLEEEFIRI**QA**KEESEEKEE**
QVAEFQKQKEVLLSLFDE**KRHEHLLSKG**ERRLSY**RALQGALMIYFYREEPRF**QVPFQLLTSLM
DIDSLMTKW**RYNHVCMVHRM**LGS**KAGTGGSSGYHYLRS**TVSDRYKVFVDLFNLSTYLIPRH
WIPKMNPTIHKFLYTAEYCDSSYFSSDESDLEHHHHHHHH

Figure A3.1. Amino acid sequence of rhTDO in the vector pET28a. Highlighted in red are the peptides observed by MALDI-ToF after tryptic digest of rhTDO. In this experiment, 45 % of the total protein sequence was identified by mass spectrometry.

MSGCPFLGNNFGYTFK**KLPVEGSEEDKSQTGVNR**ASKGGLIYGNYLHLEK**VLNAQELQSETK**
GNKIHDEHLFIITHQAYELWFK**QILWELDSVREIFQNGHVR**DERNMLKVVSRMHRVSVILKLL
VQQFSILETMTALDFNDFR**EYLSPASGFQSLQFR**LLENK**IGVLQNMR**VPYNRRHYR**DNFKGE**
ENELLLKSEQEKTLLELVEAWLER**TPGLEPHGFNFWGK**LEK**NITRGLEEEFIR**IQAK**EESEEKEE**
QVAEFQKQKEVLLSLFDEKRHEHLLSKGERRLSYR**ALQGALMIYFYR**EEPRFQVPFQLLTSLM
DIDSLMTKWR**YNHVCMVHR**MLGSK**AGTGGSSGYHYLR**STVSDRYK**VFVDLFNLSTYLIPR**H
WIPKMNPTIHKFLYTAEYCDSSYFSSDESD

Figure A3.2. Amino acid sequence of rhTDO in the vector pLEICS5. Highlighted in red are the peptides observed by MALDI-ToF after tryptic digest of rhTDO. In this experiment, 48 % of the total protein sequence was identified by mass spectrometry.

MSGCPFLGNNFGYTFKK**LPVEGSEEDKSQTGVNR**ASKGGLIYGNYLHLEK**VLNAQELQSETK**
GNKIHDEHLFIITHQAYELWFK**QILWELDSVREIFQNGHVR**DERNMLKVVSRMHRVSVILKLL
VQQFSILETMTALDFNDFR**EYLSPASGFQSLQFR**LLENK**IGVLQNMR**VPYNRRHYR**DNFKGE**
ENELLLKSEQEK**TLLELVEAWLERTPGLEPHGFNFWGK**LEK**NITRGLEEEFIR**IQAK**EESEEKEE**
QVAEFQKQKEVLLSLFDEKRHEHLLSKGERRLSYR**ALQGALMIYFYREEPR**FQVPFQLLTSLM
DIDSLMTKWR**YNHVCMVHR**MLGSK**AGTGGSSGYHYLR**STVSDRYK**VFVDLFNLSTYLIPR**H
WIPKMNPTIHKFLYTAEYCDSSYFSSDESD

Figure A3.3. Amino acid sequence of the H76A variant of rhTDO. Highlighted in red are the peptides observed by MALDI-ToF after tryptic digest of rhTDO. In this experiment, 51 % of the total protein sequence was identified by mass spectrometry.

M**SGCPFLGNNFGYTFK**KLPVEGSEEDKSQTGVNRASKGGLIYGNYLHLEK**VLNAQELQSETK**
GNKIHDEHLFIITHQAYELWFK**QILWELDSVREIFQNGHVR**DERNMLKVVSRMHRVSVILKLL
VQQFSILETMTALDFNDFR**EYLSPASGFQSLQFR**LLENKIGVLQNMRVPYNRRHYRDNFKGEE
NELLLKSEQEKTLLELVEAWLERTPGLEPHGFNFWGKLEK**NITRGLEEEFIR**IQAKEESEEKEEQ
VAEFQKQKEVLL**SLFDEKRHEHLLSK**GERRLSYR**ALQGALMIYFYREEPR**FQVPFQLLTSLMDI
DSLMTKWR**YNHVCMVHR**MLGSKAGTGGSSGYHYLRSTVSDRYK**VFVDLFNLSTYLIPR**HWI
PKMNPTIHKFLYTAEYCDSSYFSSDESD

Figure A3.4. Amino acid sequence of the H76S variant of rhTDO. Highlighted in red are the peptides observed by MALDI-ToF after tryptic digest of rhTDO. In this experiment, 31 % of the total protein sequence was identified by mass spectrometry.

M**SGCPFLGNNFGYTFK**K**LPVEGSEEDKSQTGVNR**ASKGGLIYGNYLHLEK**VLNAQELQSETK**
GNKIHDEHLFIITHQAYELWFK**QILWELDSVREIFQNGHVRDER**NMLKVVSRMHRVSVILKLL
VQQFSILETMTALDFNDFR**EYLSPASGFQSLQFR**LLENK**IGVLQNMRVPYNRR**HYR**DNFKGE**
ENELLLKSEQEK**TLLELVEAWLERTPGLEPHGFNFWGK**LEK**NITRGLEEEFIR**IQAK**EESEEKEE**
QVAEFQKQKEVLLSLFDEKRHEHLLSKGERRLSYR**ALQGALMIYFYREEPR**FQVPFQLLTSLM
DIDSLMTKWR**YNHVCMVHR**MLGSK**AGTGGSSGYHYLR**STVSDRYK**VFVDLFNLSTYLIPR**H
WIPKMNPTIHKFLYTAEYCDSSYFSSDESD

Figure A3.5. Amino acid sequence of the F72A variant of rhTDO. Highlighted in red are the peptides observed by MALDI-ToF after tryptic digest of rhTDO. In this experiment, 57 % of the total protein sequence was identified by mass spectrometry.

MSGCPFLGNNFGYTFKKLPVEGSEEDKSQTGVNRASKGGLIYGNYLHLEKVLNAQELQSETK
GNKIHDEHLFIITHQAYELWFKQILWELDSVREIFQNGHVRDERNMLKVVSRMHRVSVILKLL
VQQFSILETMTALDFNDFREYLSPASGFQSLQFRLLENKIGVLQNMRVPYNRRHYRDNFKGE
ENELLLKSEQEKTLLELVEAWLERTPGLEPHGFNFWGKLEKNITRGLEEEFIRIQAKEESEEKEE
QVAEFQKQKEVLLSLFDEKRHEHLLSKGERRLSYRALQGALMIYFYREEPRFQVPFQLLTSLM
DIDSLMTKWRYNHVCMVHRMLGSKAGTGGSSGYHYLRSTVSDRYKVFVDLFNLSTYLIPRH
WIPKMNPTIHKFLYTAEYCDSSYFSSDESD

Figure A3.6. Amino acid sequence of the F140A variant of rhTDO. Highlighted in red are the peptides observed by MALDI-ToF after tryptic digest of rhTDO. In this experiment, 60 % of the total protein sequence was identified by mass spectrometry.

MSGCPFLGNNFGYTFKKLPVEGSEEDKSQTGVNRASKGGLIYGNYLHLEKVLNAQELQSETK
GNKIHDEHLFIITHQAYELWFKQILWELDSVREIFQNGHVRDERNMLKVVSRMHRVSVILKLL
VQQFSILETMTALDFNDFREYLSPASGFQSLQFRLLENKIGVLQNMRVPYNRRHYRDNFKGE
ENELLLKSEQEKTLLELVEAWLERTPGLEPHGFNFWGKLEKNITRGLEEEFIRIQAKEESEEKEE
QVAEFQKQKEVLLSLFDEKRHEHLLSKGERRLSYRALQGALMIYFYREEPRFQVPFQLLTSLM
DIDSLMTKWRYNHVCMVHRMLGSKAGTGGSSGYHYLRSTVSDRYKVFVDLFNLSTYLIPRH
WIPKMNPTIHKFLYTAEYCDSSYFSSDESD

Figure A3.7. Amino acid sequence of the F140Y variant of rhTDO. Highlighted in red are the peptides observed by MALDI-ToF after tryptic digest of rhTDO. In this experiment, 54 % of the total protein sequence was identified by mass spectrometry.

MSGCPFLGNNFGYTFKKLPVEGSEEDKSQTGVNRASKGGLIYGNYLHLEKVLNAQELQSETKG
NKIHDEHLFIITHQAYELWFKQILWELDSVREIFQNGHVRDERNMLKVVSRMHRVSVILKLLV
QQFSILETMTALDFNDFREYLSPASGFQSLQFRLLENKIGVLQNMRVPYNRRHYRDNFKGEEN
ELLLKSEQEKTLLELVEAWLERTPGLEPHGFNFWGKLEKNITRGLEEEFIRIQAKEESEEKEEQVA
EFQKQKEVLLSLFDEKRHEHLLSKGERRLSYRALQGALMIYFYREEPRFQVPFQLLTSLMDIDSL
MTKWRYNHVCMVHRMLGSKAGTGGSSGYHYLRSTVSDRYKVFVDLFNLSTYLIPRHWIPKM
NPTIHKFLYTAEYCDSSYFSSDESD

Figure A3.8. Amino acid sequence of the R144A variant of rhTDO. Highlighted in red are the peptides observed by MALDI-ToF after tryptic digest of rhTDO. In this experiment, 18 % of the total protein sequence was identified by mass spectrometry.

M**SGCPFLGNNFGYTFKKLPVEGSEEDKSQTGVNRASKGGLIYGNYLHLEKVLNAQELQSETK**
GNK**IHDEHLFIITHQAYELWFKQILWELDSVR**EIFQNGHVRDERNMLKVVSRMHRVSVILKLL
VQQFSILETMTALDFNDFR**EYLSPASGFQSLQFR**LLENK**IGVLQNMR**VPYNRRHYR**DNFKGE**
ENELLLKSEQEKTLLELVEAWLER**TPGLEPHGFNFWGK**LEKNITR**GLEEEFIR**IQAK**EESEEKEE**
QVAEFQKQKEVLLSLFDEKRHEHLLSKGERRLSYR**ALQGALMIYFYR**EEPRFQVPFQLLTSLM
DIDSLMTKWRYNHVCMVHRMLGSK**AGTGGSSGYHYLR**STVSDRYKVFVDLFNLSTYLIPRH
WIPKMNPTIHKFLYTAEYCDSSYFSSDESD

Figure A3.9. Amino acid sequence of the R144K variant of rhTDO. Highlighted in red are the peptides observed by MALDI-ToF after tryptic digest of rhTDO. In this experiment, 49 % of the total protein sequence was identified by mass spectrometry.

MAHAMENSWTISKEYHIDEEVGFALPNPQENLPDFYNDWMFIAK**HLPDLIESGQLR**ERVEK**L**
NMLSIDHLTDHKSQRLARLVLGCITMAYVWGKGHGDVRKVLPRNIAVPYCQLSKKLELPPILV
YADCVLANWKK**KDPNKPLTYENMDVLFSFR**DGDCSKGFFLVSLLVEIAAASAIKVIPTVFK**AM**
QMQERDTLLKALLEIASCLEK**ALQVFHQIHDHVNPKAFFSVLRIYLSGWKGNPQLSDGLVYE**
GFWEDPKEFAGGSAGQSSVFQCFDVLLGIQQTAGGGHAAQFLQDMR**RYMPPAHRNFLCSL**
ESNPSVREFVLSKGDAGLREAYDACVKALVSLRSYHLQIVTK**YILIPASQQPK**ENKTSEDPSKLE
AK**GTGGTDLMNFLK**TVRSTTEKSLLKEG

Figure A3.10. Amino acid sequence of rhIDO in the vector pET151/d TOPO. Highlighted in red are the peptides observed by MALDI-ToF after tryptic digest of rhTDO. In this experiment, 35 % of the total protein sequence was identified by mass spectrometry.

APPENDIX IV

ABSORPTION COEFFICIENTS

Table A4.1. Absorption coefficients calculated using the pyridine hemochromagen method (Chapter 7, section 7.5.3).

Enzyme	($mM^{-1}cm^{-1}$)
rhTDO	ε_{408} = 196
rhIDO	ε_{404} = 158
H76A	ε_{410} = 132
H76S	ε_{407} = 105
F140A	ε_{410} = 166
F140Y	ε_{407} = 154
F72A	ε_{412} = 124
R144A	ε_{412} = 117
R144K	ε_{407} = 165

APPENDIX V

CRYSTAL SCREEN FORMULATIONS

A5.1 Emerald Biosystems Wizard I & II

	Crystallant	Buffer (0.1 M)	Salt (0.2 M)
1	20% (w/v) PEG-8K	CHES pH 9.5	None
2	10% (v/v) 2-propanol	HEPES pH 7.5	NaCl
3	15% (v/v) ethanol	CHES pH 9.5	None
4	35% (v/v) 2-methyl-2,4-pentanediol	Imidazole pH 8.0	$MgCl_2$
5	30% (v/v) PEG-400	CAPS pH 10.5	None
6	20% (w/v) PEG-3K	Citrate pH 5.5	None
7	10% (w/v) PEG-8K	MES pH 6.0	$Zn(OAc)_2$
8	2.0 M $(NH_4)_2SO_4$	Citrate pH 5.5	None
9	1.0 M $(NH_4)_2HPO_4$	Acetate pH 4.5	None
10	20% (w/v) PEG-2000 MME	Tris pH 7.0	None
11	20% (v/v) 1,4-butanediol	MES pH 6.0	Li_2SO_4
12	20% (w/v) PEG-1K	Imidazole pH 8.0	$Ca(OAc)_2$
13	1.26 M $(NH_4)_2SO_4$	Cacodylate pH 6.5	None
14	1.0 M sodium Citrate	Cacodylate pH 6.5	None
15	10% (w/v) PEG-3K	Imidazole pH 8.0	Li_2SO_4
16	2.5 M NaCl	Na/K Phosphate pH 6.2	None
17	30% (w/v) PEG-8K	Acetate pH 4.5	Li_2SO_4
18	1.0 M K/Na tartrate	Imidazole pH 8.0	NaCl
19	20% (w/v) PEG-1K	Tris pH 7.0	None
20	0.4 M NaH_2PO_4/1.6 M K_2HPO_4	Imidazole pH 8.0	NaCl
21	20% (w/v) PEG-8K	HEPES pH 7.5	None
22	10% (v/v) 2-propanol	Tris pH 8.5	None
23	15% (v/v) ethanol	Imidazole pH 8.0	$MgCl_2$
24	35% (v/v) 2-methyl-2,4-pentanediol	Tris pH 7.0	NaCl
25	30% (v/v) PEG-400	Tris pH 8.5	$MgCl_2$
26	10% (w/v) PEG-3K	CHES pH 9.5	None
27	1.2 M NaH_2PO_4/0.8 M K_2HPO_4	CAPS pH 10.5	Li_2SO_4
28	20% (w/v) PEG-3K	HEPES pH 7.5	NaCl
29	10% (w/v) PEG-8K	CHES pH 9.5	NaCl
30	1.26 M $(NH_4)_2SO_4$	Acetate pH 4.5	NaCl
31	20% (w/v) PEG-8K	Phosphate-Citrate pH 4.2	NaCl
32	10% (w/v) PEG-3K	Na/K Phosphate pH 6.2	None
33	2.0 M $(NH_4)_2SO_4$	CAPS pH 10.5	Li_2SO_4
34	1.0 M $(NH_4)_2HPO_4$	Imidazole pH 8.0	None
35	20% (v/v) 1,4-butanediol	Acetate pH 4.5	None
36	1.0 M sodium Citrate	Imidazole pH 8.0	None
37	2.5 M NaCl	Imidazole pH 8.0	None

38	1.0 M K/Na tartrate	CHES pH 9.5	Li_2SO_4
39	20% (w/v) PEG-1K	Phosphate-Citrate pH 4.2	Li_2SO_4
40	10% (v/v) 2-propanol	MES pH 6.0	$Ca(OAc)_2$
41	30% (w/v) PEG-3K	CHES pH 9.5	None
42	15% (v/v) ethanol	Tris pH 7.0	None
43	35% (v/v) 2-methyl-2,4-pentanediol	Na/K Phosphate pH 6.2	None
44	30% (v/v) PEG-400	Acetate pH 4.5	$Ca(OAc)_2$
45	20% (w/v) PEG-3K	Acetate pH 4.5	None
46	10% (w/v) PEG-8K	Imidazole pH 8.0	$Ca(OAc)_2$
47	1.26 M $(NH_4)_2SO_4$	Tris pH 8.5	Li_2SO_4
48	20% (w/v) PEG-1K	Acetate pH 4.5	$Zn(OAc)_2$
49	10% (w/v) PEG-3K	Acetate pH 4.5	$Zn(OAc)_2$
50	35% (v/v) 2-methyl-2,4-pentanediol	MES pH 6.0	Li_2SO_4
51	20% (w/v) PEG-8K	Tris pH 8.5	$MgCl_2$
52	2.0 M $(NH_4)_2SO_4$	Cacodylate pH 6.5	NaCl
53	20% (v/v) 1,4-butanediol	HEPES pH 7.5	NaCl
54	10% (v/v) 2-propanol	Phosphate-Citrate pH 4.2	Li_2SO_4
55	30% (w/v) PEG-3K	Tris pH 7.0	NaCl
56	10% (w/v) PEG-8K	Na/K Phosphate pH 6.2	NaCl
57	2.0 M $(NH_4)_2SO_4$	Phosphate-Citrate pH 4.2	None
58	1.0 M $(NH_4)_2HPO_4$	Tris pH 8.5	None
59	10% (v/v) 2-propanol	Cacodylate pH 6.5	$Zn(OAc)_2$
60	30% (v/v) PEG-400	Cacodylate pH 6.5	Li_2SO_4
61	15% (v/v) ethanol	Citrate pH 5.5	Li_2SO_4
62	20% (w/v) PEG-1K	Na/K Phosphate pH 6.2	NaCl
63	1.26 M $(NH_4)_2SO_4$	HEPES pH 7.5	None
64	1.0 M sodium Citrate	CHES pH 9.5	None
65	2.5 M NaCl	Tris pH 7.0	$MgCl_2$
66	20% (w/v) PEG-3K	Tris pH 7.0	$Ca(OAc)_2$
67	1.6 M NaH_2PO_4/0.4 M K_2HPO_4	Phosphate-Citrate pH 4.2	None
68	15% (v/v) ethanol	MES pH 6.0	$Zn(OAc)_2$
69	35% (v/v) 2-methyl-2,4-pentanediol	Acetate pH 4.5	None
70	10% (v/v) 2-propanol	Imidazole pH 8.0	None
71	15% (v/v) ethanol	HEPES pH 7.5	$MgCl_2$
72	30% (w/v) PEG-8K	Imidazole pH 8.0	NaCl
73	35% (v/v) 2-methyl-2,4-pentanediol	HEPES pH 7.5	NaCl
74	30% (v/v) PEG-400	CHES pH 9.5	None
75	10% (w/v) PEG-3K	Cacodylate pH 6.5	$MgCl_2$
76	20% (w/v) PEG-8K	MES pH 6.0	$Ca(OAc)_2$
77	1.26 M $(NH_4)_2SO_4$	CHES pH 9.5	NaCl
78	20% (v/v) 1,4-butanediol	Imidazole pH 8.0	$Zn(OAc)_2$
79	1.0 M sodium Citrate	Tris pH 7.0	NaCl
80	20% (w/v) PEG-1K	Tris pH 8.5	None
81	1.0 M $(NH_4)_2HPO_4$	Citrate pH 5.5	NaCl
82	10% (w/v) PEG-8K	Imidazole pH 8.0	None
83	0.8 M NaH_2PO_4/1.2 M K_2HPO_4	Acetate pH 4.5	None
84	10% (w/v) PEG-3K	Phosphate-Citrate pH 4.2	NaCl
85	1.0 M K/Na tartrate	Tris pH 7.0	Li_2SO_4
86	2.5 M NaCl	Acetate pH 4.5	Li_2SO_4
87	20% (w/v) PEG-8K	CAPS pH 10.5	NaCl

88	20% (w/v) PEG-3K	Imidazole pH 8.0	$Zn(OAc)_2$
89	2.0 M $(NH_4)_2SO_4$	Tris pH 7.0	Li_2SO_4
90	30% (v/v) PEG-400	HEPES pH 7.5	NaCl
91	10% (w/v) PEG-8K	Tris pH 7.0	$MgCl_2$
92	20% (w/v) PEG-1K	Cacodylate pH 6.5	$MgCl_2$
93	1.26 M $(NH_4)_2SO_4$	MES pH 6.0	None
94	1.0 M $(NH_4)_2HPO_4$	Imidazole pH 8.0	NaCl
95	2.5 M NaCl	Imidazole pH 8.0	$Zn(OAc)_2$
96	1.0 M K/Na tartrate	MES pH 6.0	None

A5.2 Emerald Biosystems Cryo I & II

	Crystallant	Buffer (0.1 M)	Additive(s)
1	40% (v/v) 2-methyl-2,4-pentanediol	Phosphate-Citrate pH 4.2	None
2	40% (v/v) ethylene glycol	Acetate pH 4.5	None
3	50% (v/v) PEG-200	Citrate pH 5.5	None
4	40% (v/v) PEG-300	HEPES pH 7.5	0.2 M NaCl
5	40% (v/v) PEG-400	Citrate pH 5.5	0.2 M $MgCl_2$
6	40% (v/v) PEG-600	Cacodylate pH 6.5	0.2 M $Ca(OAc)_2$
7	40% (v/v) ethanol	Tris pH 8.5	0.05 M $MgCl_2$
8	35% (v/v) 2-ethoxyethanol	Cacodylate pH 6.5	None
9	35% (v/v) 2-propanol	Phosphate-Citrate pH 4.2	None
10	45% (v/v) glycerol	Imidazole pH 8.0	None
11	35% (v/v) 2-methyl-2,4-pentanediol	Tris pH 8.5	0.2 M $(NH_4)_2SO_4$
12	50% (v/v) ethylene glycol	Acetate pH 4.5	5% (w/v) PEG-1K
13	30% (v/v) PEG-200	MES pH 6.0	5% (w/v) PEG-3K
14	20% (v/v) PEG-300	Phosphate-Citrate pH 4.2	0.2 M $(NH_4)_2SO_4$, 10% (v/v) glycerol
15	50% (v/v) PEG-400	CHES pH 9.5	0.2 M NaCl
16	30% (v/v) PEG-600	MES pH 6.0	5% (w/v) PEG-1K, 10% (v/v) glycerol
17	40% (v/v) 1, 2-propanediol	HEPES pH 7.5	None
18	35% (v/v) 2-ethoxyethanol	Imidazole pH 8.0	0.05 M $Ca(OAc)_2$
19	35% (v/v) 2-propanol	Tris pH 8.5	None
20	30% (v/v) 1,2-propanediol	Citrate pH 5.5	20% (v/v) 2-methyl-2,4-pentanediol
21	40% (v/v) 1,2-propanediol	Acetate pH 4.5	0.05 M $Ca(OAc)_2$
22	40% (v/v) ethylene glycol	Na/K Phosphate pH 6.2	None
23	40% (v/v) 2-methyl-2,4-pentanediol	Tris pH 7.0	0.2 M $(NH_4)_2SO_4$
24	40% (v/v) PEG-400	Na/K Phosphate pH 6.2	0.2 M NaCl
25	30% (v/v) PEG-200	Tris pH 8.5	0.2 M $(NH_4)_2HPO_4$
26	40% (v/v) PEG-300	CHES pH 9.5	0.2 M NaCl
27	30% (v/v) PEG-400	CAPS pH 10.5	0.5 M $(NH_4)_2SO_4$, 10% (v/v) glycerol
28	30% (v/v) PEG-600	HEPES pH 7.5	0.05 M Li_2SO_4, 10% (v/v) glycerol
29	40% (v/v) PEG-300	CHES pH 9.5	0.2 M sodium Citrate
30	35% (v/v) 2-ethoxyethanol	Citrate pH 5.5	None
31	35% (v/v) 2-propanol	Citrate pH 5.5	5% (w/v) PEG-1K
32	40% (v/v) 1,2-propanediol	CHES pH 9.5	0.2 M sodium Citrate

33	25% (v/v) 1, 2-propanediol	Imidazole pH 8.0	0.2 M $Zn(OAc)_2$, 10% (v/v) glycerol
34	40% (v/v) 2-methyl-2,4-pentanediol	Imidazole pH 8.0	0.2 M $MgCl_2$
35	40% (v/v) ethylene glycol	HEPES pH 7.5	5% (w/v) PEG-3K
36	50% (v/v) PEG-200	Tris pH 7.0	0.05 M Li_2SO_4
37	40% (v/v) PEG-300	Cacodylate pH 6.5	0.2 M $Ca(OAc)_2$
38	40% (v/v) PEG-400	Tris pH 8.5	0.2 M Li_2SO_4
39	40% (v/v) PEG-600	Phosphate-Citrate pH 4.2	None
40	40% (v/v) ethanol	Phosphate-Citrate pH 4.2	5% (w/v) PEG-1K
41	25% (v/v) 1, 2-propanediol	Phosphate-Citrate pH 4.2	5% (w/v) PEG-3K, 10% (v/v) glycerol
42	40% (v/v) ethylene glycol	Tris pH 7.0	None
43	50% (v/v) ethylene glycol	Tris pH 8.5	0.2 M $MgCl_2$
44	50% (v/v) PEG-200	Cacodylate pH 6.5	0.2 M $Zn(OAc)_2$
45	20% (v/v) PEG-300	Tris pH 8.5	5% (w/v) PEG-8K, 10% (v/v) glycerol
46	40% (v/v) PEG-400	MES pH 6.0	5% (w/v) PEG-3K
47	50% (v/v) PEG-400	Acetate pH 4.5	0.2 M Li_2SO_4
48	40% (v/v) PEG-600	Imidazole pH 8.0	0.2 M $Zn(OAc)_2$
49	40% (v/v) 2-methyl-2,4-pentanediol	Cacodylate pH 6.5	5% (w/v) PEG-8K
50	50% (v/v) PEG-200	CHES pH 9.5	None
51	40% (v/v) ethylene glycol	Phosphate-Citrate pH 4.2	0.2 M $(NH4)_2SO_4$
52	40% (v/v) PEG-400	HEPES pH 7.5	0.2 M $Ca(OAc)_2$
53	40% (v/v) PEG-300	Tris pH 7.0	5% (w/v) PEG-1K
54	30% (v/v) PEG-600	Cacodylate pH 6.5	1 M NaCl, 10% (v/v) glycerol
55	40% (v/v) ethanol	Tris pH 7.0	None
56	35% (v/v) 2-ethoxyethanol	Na/K Phosphate pH 6.2	0.2 M NaCl
57	35% (v/v) 2-propanol	Imidazole pH 8.0	0.05 M $Zn(OAc)_2$
58	40% (v/v) 1,2-propanediol	Acetate pH 4.5	None
59	25% (v/v) 1, 2-propanediol	Na/K Phosphate pH 6.2	10% (v/v) glycerol
60	40% (v/v) 1,2-propanediol	Citrate pH 5.5	0.2 M NaCl
61	35% (v/v) 2-methyl-2,4-pentanediol	Cacodylate pH 6.5	0.05 M $Zn(OAc)_2$
62	40% (v/v) ethylene glycol	Imidazole pH 8.0	0.2 M $Ca(OAc)_2$
63	50% (v/v) PEG-200	Na/K Phosphate pH 6.2	0.2 M NaCl
64	20% (v/v) PEG-300	Imidazole pH 8.0	1 M $(NH4)_2SO4$, 10% (v/v) glycerol
65	50% (v/v) PEG-400	MES pH 6.0	None
66	40% (v/v) PEG-300	Phosphate-Citrate pH 4.2	None
67	40% (v/v) PEG-600	Acetate pH 4.5	0.2 M $MgCl_2$
68	50% (v/v) ethylene glycol	CHES pH 9.5	0.5 M K/Na tartrate
69	35% (v/v) 2-ethoxyethanol	Tris pH 8.5	0.2 M Li_2SO4
70	35% (v/v) 2-propanol	Cacodylate pH 6.5	0.2 M $MgCl_2$
71	30% (v/v) 1,2-propanediol	HEPES pH 7.5	20% (v/v) PEG-400
72	25% (v/v) 1, 2-propanediol	Tris pH 8.5	0.2 M $MgCl_2$, 10% (v/v) glycerol
73	40% (v/v) 2-methyl-2,4-pentanediol	CAPS pH 10.5	None
74	40% (v/v) ethylene glycol	MES pH 6.0	0.2 M $Zn(OAc)_2$
75	50% (v/v) PEG-200	Tris pH 7.0	None
76	40% (v/v) PEG-300	Imidazole pH 8.0	0.2 M $Zn(OAc)_2$
77	30% (v/v) PEG-400	HEPES pH 7.5	5% (w/v) PEG-3K, 10% (v/v)

			glycerol
78	40% (v/v) PEG-600	Citrate pH 5.5	None
79	40% (v/v) PEG-600	CHES pH 9.5	None
80	35% (v/v) 2-propanol	Acetate pH 4.5	None
81	45% (v/v) glycerol	Cacodylate pH 6.5	0.2 M $Ca(OAc)_2$
82	25% (v/v) 1, 2-propanediol	Tris pH 7.0	0.2 M (NH4)2SO4, 10% (v/v) glycerol
83	40% (v/v) 2-methyl-2,4-pentanediol	Citrate pH 5.5	None
84	50% (v/v) PEG-200	Cacodylate pH 6.5	0.2 M $MgCl_2$
85	50% (v/v) ethylene glycol	Imidazole pH 8.0	None
86	40% (v/v) PEG-400	Acetate pH 4.5	None
87	30% (v/v) PEG-600	Tris pH 7.0	0.5 M $(NH4)_2SO4$, 10% (v/v) glycerol
88	40% (v/v) 2-methyl-2,4-pentanediol	CHES pH 9.5	None
89	50% (v/v) ethylene glycol	HEPES pH 7.5	0.2 M Li_2SO_4
90	30% (v/v) PEG-200	Acetate pH 4.5	0.1 M NaCl
91	40% (v/v) PEG-400	Imidazole pH 8.0	None
92	35% (v/v) 2-methyl-2,4-pentanediol	Acetate pH 4.5	10% (v/v) glycerol
93	40% (v/v) PEG-300	Acetate pH 4.5	0.2 M NaCl
94	30% (v/v) PEG-200	CAPS pH 10.5	0.2 M $(NH_4)_2SO_4$
95	50% (v/v) PEG-200	HEPES pH 7.5	None
96	50% (v/v) PEG-200	Phosphate-Citrate pH 4.2	0.2 M NaCl

A5.3 Hampton Crystal Screen

	Crystallant	Buffer (0.1 M)	Salt (0.2 M) unless stated
1	30 % v/v (+/-)-2-Methyl-2,4-pentanediol	Sodium Acetate Trihydrate pH 4.6	0.02 M $CaCl_2$ dihydrate
2	0.4 M Potassium Sodium tartrate tetrahydrate	None	None
3	0.4 M Ammonium Phosphate monobasic	None	None
4	2.0 M $(NH_4)_2SO_4$	TRIS hydrochloride pH 8.5	None
5	30 % v/v (+/-)-2-Methyl-2,4-pentanediol	HEPES Sodium pH 7.5	Sodium Citrate Tribasic dihydrate
6	30 % w/v PEG 4K	TRIS hydrochloride pH 8.5	$MgCl_2$ hexahydrate
7	1.4 M Sodium Acetate Trihydrate	Sodium Cacodylate Trihydrate pH 6.5	
8	30 % v/v 2-Propanol	Sodium Cacodylate Trihydrate pH 6.5	Sodium Citrate Tribasic dihydrate
9	30 % w/v PEG 4K	Sodium Citrate Tribasic dehydrate pH 5.6	Ammonium Acetate
10	30 % w/v PEG 4K	Sodium Acetate Trihydrate pH 4.6	Ammonium Acetate
11	1.0 M Ammonium Phosphate monobasic	Sodium Citrate Tribasic dehydrate pH 5.6	None
12	30 % v/v 2-Propanol	HEPES Sodium pH 7.5	$MgCl_2$ hexahydrate
13	30 % v/v PEG 400	TRIS hydrochloride pH 8.5	Sodium Citrate Tribasic dihydrate
14	28 % v/v PEG 400	HEPES Sodium pH 7.5	$CaCl_2$ dihydrate
15	30 % w/v PEG 8K	Sodium Cacodylate Trihydrate pH 6.5	$(NH_4)_2SO_4$

16	1.5 M Li_2SO_4 monohydrate	HEPES Sodium pH7.5	None
17	30 % w/v PEG 4K	TRIS hydrochloride pH 8.5	Li_2SO_4 monohydrate
18	20 % w/v PEG 8K	Sodium Cacodylate Trihydrate pH 6.5	Magnesium Acetate tetrahydrate
19	30 % v/v 2-Propanol	TRIS hydrochloride pH 8.5	Ammonium Acetate
20	25 % w/v PEG 4K	Sodium Acetate Trihydrate pH 4.6	$(NH_4)_2SO_4$
21	30 % v/v (+/-)-2-Methyl-2,4-pentanediol	Sodium Cacodylate Trihydrate pH 6.5	Magnesium Acetate tetrahydrate
22	30 % w/v PEG 4K	TRIS hydrochloride pH 8.5	Sodium Acetate Trihydrate
23	30 % v/v PEG 400	HEPES Sodium pH 7.5	$MgCl_2$ hexahydrate
24	20 % v/v 2-Propanol	Sodium Acetate Trihydrate pH 4.6	$CaCl_2$ dihydrate
25	1.0 M Sodium Acetate Trihydrate	Imidazole pH 6.5	None
26	30 % v/v (+/-)-2-Methyl-2,4-pentanediol	Sodium Citrate Tribasic dehydrate pH 5.6	Ammonium Acetate
27	20 % v/v 2-Propanol	HEPES Sodium pH 7.5	Sodium Citrate Tribasic dihydrate
28	30 % w/v PEG 8K	Sodium Cacodylate Trihydrate pH 6.5	Sodium Acetate Trihydrate
29	0.8 M Potassium Sodium tartrate tetrahydrate	HEPES Sodium pH 7.5	None
30	30 % w/v PEG 8K	None	$(NH_4)_2SO_4$
31	30 % w/v PEG 4K	None	$(NH_4)_2SO_4$
32	2.0 M $(NH_4)_2SO_4$	None	None
33	4.0 M Sodium formate	None	None
34	2.0 M Sodium formate	Sodium Acetate Trihydrate pH 4.6	None
35	0.8 M Sodium Phosphate monobasic monohydrate, 0.8 M Potassium Phosphate monobasic	HEPES Sodium pH 7.5	None
36	8 % w/v PEG 8K	TRIS hydrochloride pH 8.5	None
37	8 % w/v PEG 4K	Sodium Acetate Trihydrate pH 4.6	None
38	1.4 M Sodium Citrate Tribasic dihydrate	HEPES Sodium pH 7.5	None
39	2 % v/v PEG 400, 2.0 M $(NH_4)_2SO_4$	HEPES Sodium pH 7.5	None
40	20 % v/v 2-Propanol, 20 % w/v PEG 4K	Sodium Citrate Tribasic dehydrate pH 5.6	None
41	10 % v/v 2-Propanol, 20 % w/v PEG 4K	HEPES Sodium pH 7.5	None
42	20 % w/v PEG 8K	None	0.05 M Potassium Phosphate monobasic
43	30 % w/v PEG 1,500	None	None
44	0.2 M Magnesium formate dihydrate	None	None
45	18 % w/v PEG 8K	Sodium Cacodylate Trihydrate pH 6.5	$Zn(OAc)_2$ dihydrate
46	18 % w/v PEG 8K	Sodium Cacodylate Trihydrate pH 6.5	$Ca(OAc)_2$ hydrate
47	2.0 M $(NH_4)_2SO_4$	Sodium Acetate Trihydrate pH 4.6	None
48	2.0 M Ammonium Phosphate monobasic	TRIS hydrochloride pH 8.5	None
49	2 % w/v PEG 8K	None	1.0 M Li_2SO_4 monohydrate
50	15 % w/v PEG 8K	None	0.5 M Li_2SO_4 monohydrate

A5.4 Molecular Dimensions JCSG Screen

	Crystallant	Buffer (0.1 M) unless stated	Salt (0.2 M) unless stated
A1	50 % v/v PEG 400	Sodium Acetate pH 4.5	Li_2SO_4
A2	20 % w/v PEG 3K	Citrate pH 5.5	
A3	20 % w/v PEG 3350	None	di-Ammonium hydrogen Citrate
A4	30 % v/v MPD	Sodium Acetate pH 4.6	0.02 M $CaCl_2$
A5	20 % w/v PEG 3350	None	Magnesium formate
A6	20 % w/v PEG 1K	Phosphate, Citrate pH 4.2	Li_2SO_4
A7	20 % w/v PEG 8K	CHES pH 9.5	
A8	20 % w/v PEG 3350	None	Ammonium formate
A9	20 % w/v PEG 3350	None	Ammonium chloride
A10	20 % w/v PEG 3350	None	Potassium formate
A11	50 % v/v MPD	Tris pH 8.5	Ammonium dihydrogen Phosphate
A12	20 % w/v PEG 3350		Potassium nitrate
B1	0.8 M $(NH_4)_2SO_4$	Sodium Citrate pH 4.0	None
B2	20 % w/v PEG 3350		Sodium thiocyanate
B3	20 % w/v PEG 6K	Bicine pH 9.0	
B4	10 % w/v PEG 8K, 8 % v/v Ethylene glycol	HEPES pH 7.5	None
B5	40 % v/v MPD, 5 % w/v PEG 8K	Sodium Cacodylate pH 6.5	None
B6	40 % v/v Ethanol, 5 % w/v PEG 1K	Phosphate, Citrate pH 4.2	None
B7	8 % w/v PEG 4K	Sodium Acetate pH 4.6	None
B8	10 % w/v PEG 8K	Tris pH 7	$MgCl_2$
B9	20 % w/v PEG 6K	Sodium Citrate pH 5.0	
B10	50 % v/v PEG 200	Sodium Cacodylate pH 6.5	$MgCl_2$
B11	1.6 M Tri-Sodium Citrate pH 6.5	None	None
B12	20 % w/v PEG 3350	None	Tri-Potassium Citrate
C1	20 % w/v PEG 8K	Phosphate, Citrate pH 4.2	NaCl
C2	20 % w/v PEG 6K	Na Citrate pH 4.0	1 M Lithium chloride
C3	20 % w/v PEG 3350	None	Ammonium nitrate
C4	10 % w/v PEG 6K	HEPES pH 7.0	None
C5	0.8 M Sodium dihydrogen Phosphate	Sodium HEPES pH 7.5	None
C6	0.8 M Potassium dihydrogen Phosphate	Phosphate, Citrate pH 4.2	None
C7	40 % v/v PEG 300	Sodium Acetate pH 4.5	$Zn(OAc)_2$
C8	10 % w/v PEG 3K	Tris pH 8.5	None
C9	20 % v/v Ethanol	Sodium Phosphate, Potassium Phosphate pH 6.2	None
C10	25 % v/v 1,2-propanediol	Bicine pH 9.5	None
C11	10 % v/v Glycerol	Sodium Acetate pH 4.6	None
C12	10 % w/v PEG 20K, 2 % v/v Dioxane	None	None
D1	2M $(NH_4)_2SO_4$	None	None
D2	10 % w/v PEG 1K, 10 % w/v PEG 8K	Sodium HEPES pH 7.5	$MgCl_2$

D3	24 % w/v PEG 1.5K, 20 % v/v Glycerol	Sodium Phosphate, Potassium Phosphate pH 6.2	NaCl
D4	30 % v/v PEG 400	Sodium Acetate pH 4.5	Li_2SO_4
D5	50 % v/v PEG 200	HEPES pH 7.5	
D6	30 % w/v PEG 8K	Tris pH 8.5	$MgCl_2$
D7	70 % v/v MPD	Tris pH 8.5	Li_2SO_4
D8	20 % w/v PEG 8K	Tris pH 8.0	
D9	40 % v/v PEG 400	None	0.17 M $(NH_4)_2SO_4$
D10	40 % v/v MPD	Sodium Cacodylate pH 6.5	$Ca(OAc)_2$
D11	25.5 % w/v PEG 4K, 15 % v/v Glycerol	Sodium Acetate pH 4.6	0.14 M $CaCl_2$
D12	40 % v/v PEG 300	None	0.04 M Potassium dihydrogen Phosphate
E1	14 % v/v 2-propanol, 30 % v/v Glycerol	Sodium Cacodylate pH 6.5	None
E2	16 % w/v PEG 8K, 20 % v/v Glycerol	Sodium Cacodylate pH 6.5	NaCl
E3	1 M Tri-Sodium Citrate	HEPES pH 7.5	NaCl
E4	2 M $(NH_4)_2SO_4$	Tris pH 8.5	Li_2SO_4
E5	10 % v/v 2-propanol	CAPS pH 10.5	None
E6	1.26 M $(NH_4)_2SO_4$	Imidazole pH 8.0	$Zn(OAc)_2$
E7	40 % v/v MPD	Sodium Cacodylate pH 6.5	$Zn(OAc)_2$
E8	20 % w/v PEG 3K	Sodium Acetate pH 4.5	None
E9	10 % v/v 2-propanol	MES pH 6.5	None
E10	1 M di-Ammonium hydrogen Phosphate	Bicine pH 9.0	None
E11	1.6 M Magnesium sulfate	0.08 M Sodium Cacodylate pH 6.5	0.16 M $Ca(OAc)_2$
E12	10 % w/v PEG 6K	Imidazole pH 8.0	None
F1	14.4 % w/v PEG 8K, 20 % v/v glycerol	MES pH 6.5	Caesium chloride
F2	10 % w/v PEG 8K	Sodium Citrate pH 5.0	None
F3	30 % v/v Jeffamine M-600	Tris pH 8.0	None
F4	3.2 M $(NH_4)_2SO_4$	HEPES pH 7.5	None
F5	20 % v/v MPD	Tris pH 8.5	$MgCl_2$
F6	20 % v/v Jeffamine M-600	Bicine pH 9.0	None
F7	50 % v/v Ethylene glycol pH 7	None	None
F8	10 % v/v MPD pH 7	None	None
F9	0.8 M Succinic acid pH 7	None	None
F10	2.1 M DL-Malic acid	HEPES pH 7.0	1.1 M Sodium malonate
F11	2.4 M Sodium malonate	HEPES pH 7.0	1 M Succinic acid
F12	0.5 % v/v Jeffamine ED-2001	HEPES pH 7.0	None
G1	1 % w/v PEG 2K MME	HEPES pH 7.0	None
G2	30 % v/v Jeffamine M-600	HEPES pH 7.5	0.02 M $MgCl_2$
G3	30 % v/v Jeffamine ED-2001	Tris pH 8.5	0.01 M Cobalt chloride
G4	22 % w/v Polyacrylic acid 5100 Sodium salt	Tris pH 8.5	Tri-methylamine N-oxide
G5	20 % w/v Polyvinylpyrrolidone K15	HEPES pH 7.5	0.005 M Cobalt chloride, cadmium chloride, $MgCl_2$, nickel chloride
G6	20 % w/v PEG 2K MME pH 7	None	Sodium malonate
G7	12 % w/v PEG 3350 pH 7	None	0.1 M Succinic acid
G8	20 % w/v PEG 3350 pH 7	None	0.15 M DL- malic acid
G9	15 % w/v PEG 3350	None	0.1 M Potassium

			thiocyanate
G10	20 % w/v PEG 3350	None	0.15 M Potassium bromide
G11	30 % w/v PEG 2K MME	Bis Tris pH 5.5	None
G12	30 % w/v PEG 2K MME	Bis Tris pH 5.5	None
H1	2 M $(NH_4)_2SO_4$	Bis Tris pH 5.5	None
H2	3 M NaCl	Bis Tris pH 5.5	1 M $(NH_4)_2SO_4$
H3	0.3 M Magnesium formate	Bis Tris pH 5.5	None
H4	1 % w/v PEG 3350	Bis Tris pH 5.5	$CaCl_2$
H5	25 % w/v PEG 3350	Bis Tris pH 5.5	Ammonium Acetate
H6	45 % v/v MPD	Bis Tris pH 5.5	0.1 M Ammonium Acetate
H7	45 % v/v MPD	Bis Tris pH 5.5	$(NH_4)_2SO_4$
H8	17 % w/v PEG 10K	Bis Tris pH 5.5	NaCl
H9	25 % w/v PEG 3350	Bis Tris pH 5.5	Li_2SO_4
H10	25 % w/v PEG 3350	Bis Tris pH 5.5	Ammonium Acetate
H11	25 % w/v PEG 3350	Bis Tris pH 5.5	$MgCl_2$
H12	25 % w/v PEG 3350	HEPES pH 7.5	Ammonium Acetate

APPENDIX VI

SUPPLEMENTARY INFORMATION

A6.1 Redox Potentiometry

The reduction potential of the Fe^{3+}/Fe^{2+} couple for wild type TDO and the TDO variants were analysed using two dyes, nile blue chloride, E^{Φ} = -116 mV (Figure A6.1A) and methylene blue, E^{Φ} = -11 mV (Figure A6.1B) as they both fall within the range of the reduction potentials for these enzymes (Chapter 7, section 7.5.9).

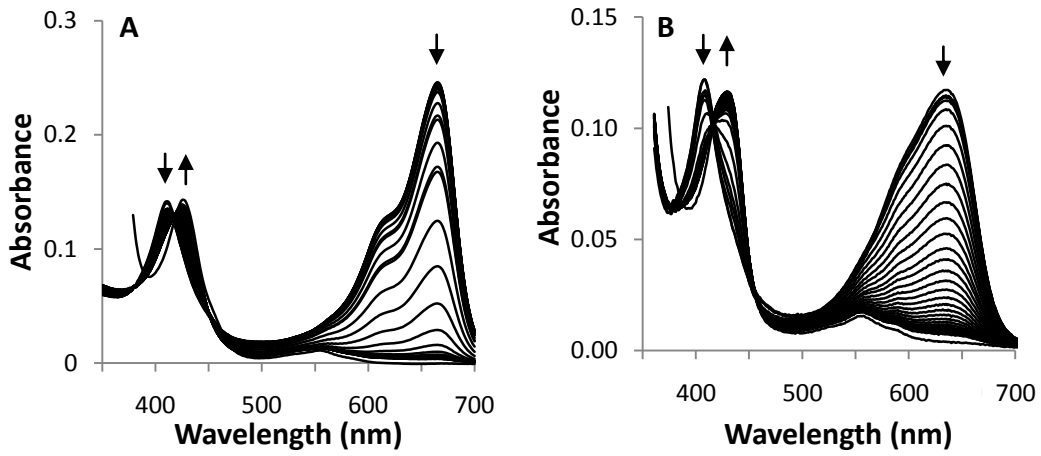

Figure A6.1. Spectral changes observed during determination of $Fe^{3+/}Fe^{2+}$ reduction potential for F140Y and H76S variants of TDO with the dyes (A) Nile Blue Chloride (B) Methylene blue respectively. For clarity, only certain spectra are shown; arrows indicate the direction of absorption change during the reductive titration.

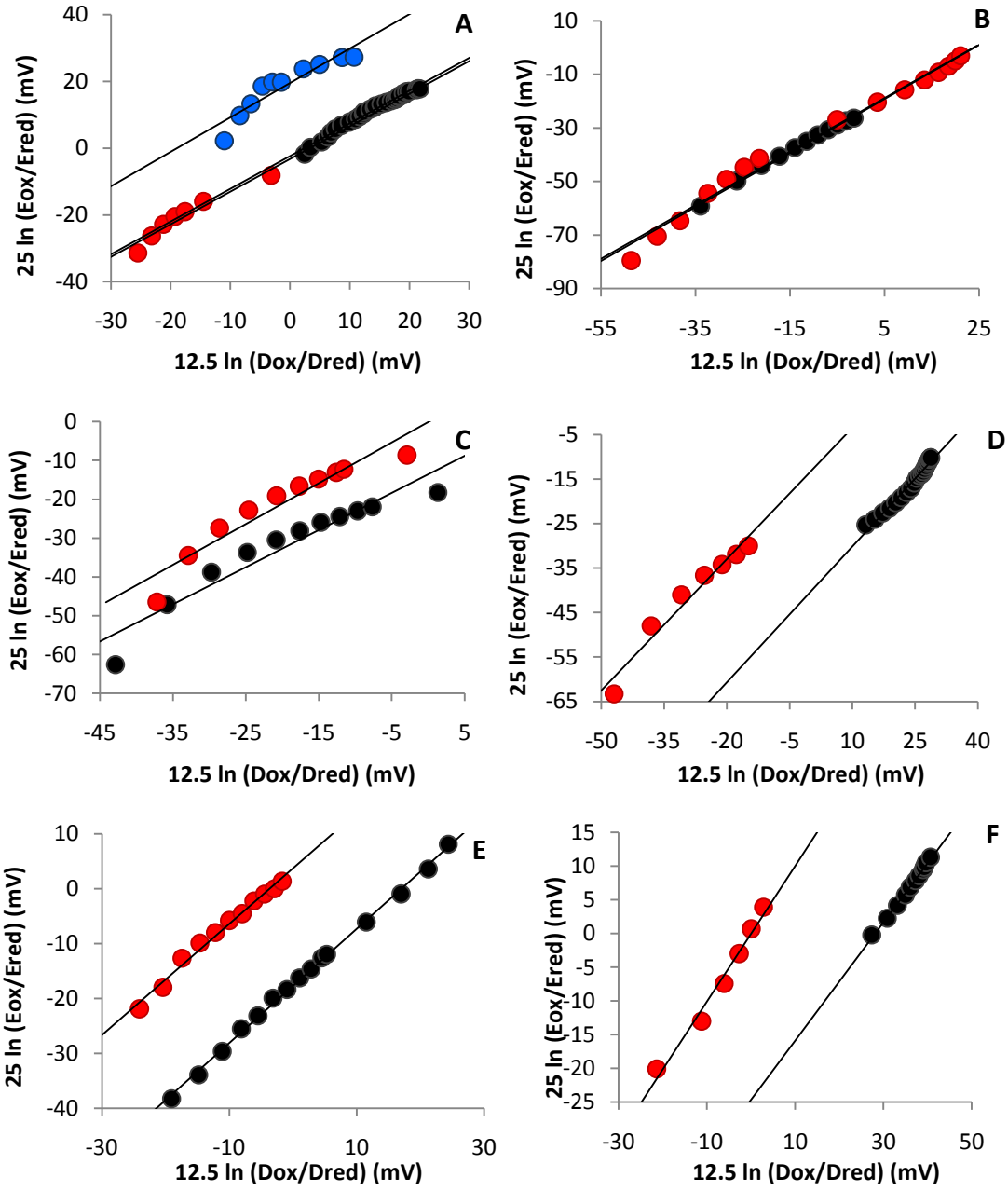

Figure A6.2 Redox Potentiometry for H76S, F72A, F140A, F140Y, R144A ad R144K variants of TDO in the absence of substrate (●), in the presence of 3 mM L-tryptophan (●) or 1 methyl- L-tryptophan (●). (A) Nernst plots for H76S ● -119 mV ● -113 mV ● -100 mV. (B) Nernst plot of F72A ● -140 mV ● -139 mV. (C) Nernst plots for F140A ● -129 mV ● -116 mV. (D) Nernst plots for F140Y ● -156 mV ● -129 mV. (E) Nernst plots for R144A ● -133 mV ● -112 mV. (F) Nernst plots for R144K ● -143 mV ● -116 mV. Reaction conditions: 100 mM potassium phosphate, pH 7.0, 25.0 ^{o}C.

A 6.2 L-Tryptophan Binding

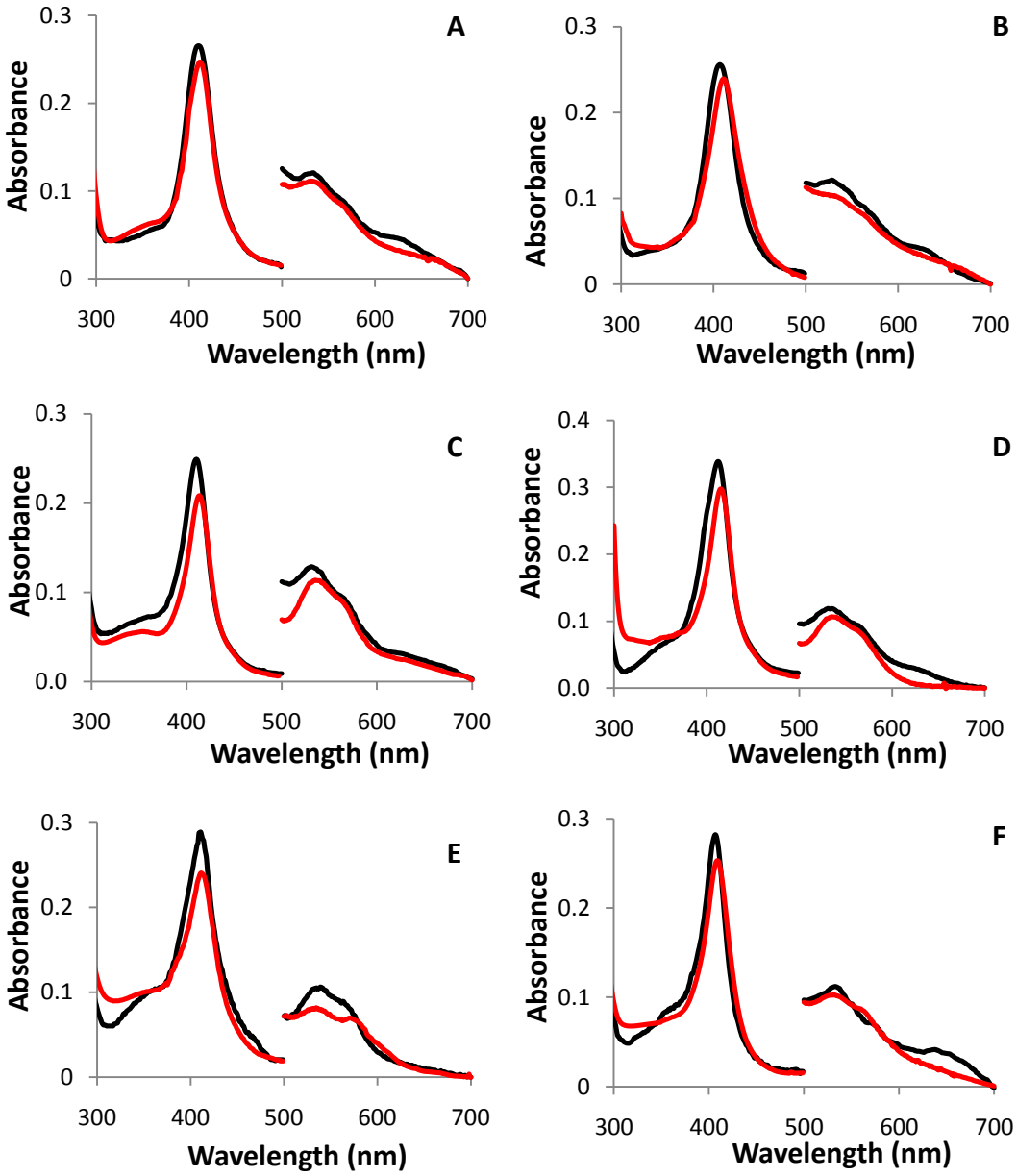

Figure A6.3 UV-visible spectra of ferric TDO variant enzyme (black) and in the presence of tryptophan (red) (**A**) H76A, (**B**) H76S, (**C**) F140A, (**D**) F72A, (**E**) R144A, (**F**) R144K. Absorbance values in the visible region have been multiplied by a factor of 5. Conditions: 50 mM Tris, pH 8.0.

A6.3 EPR

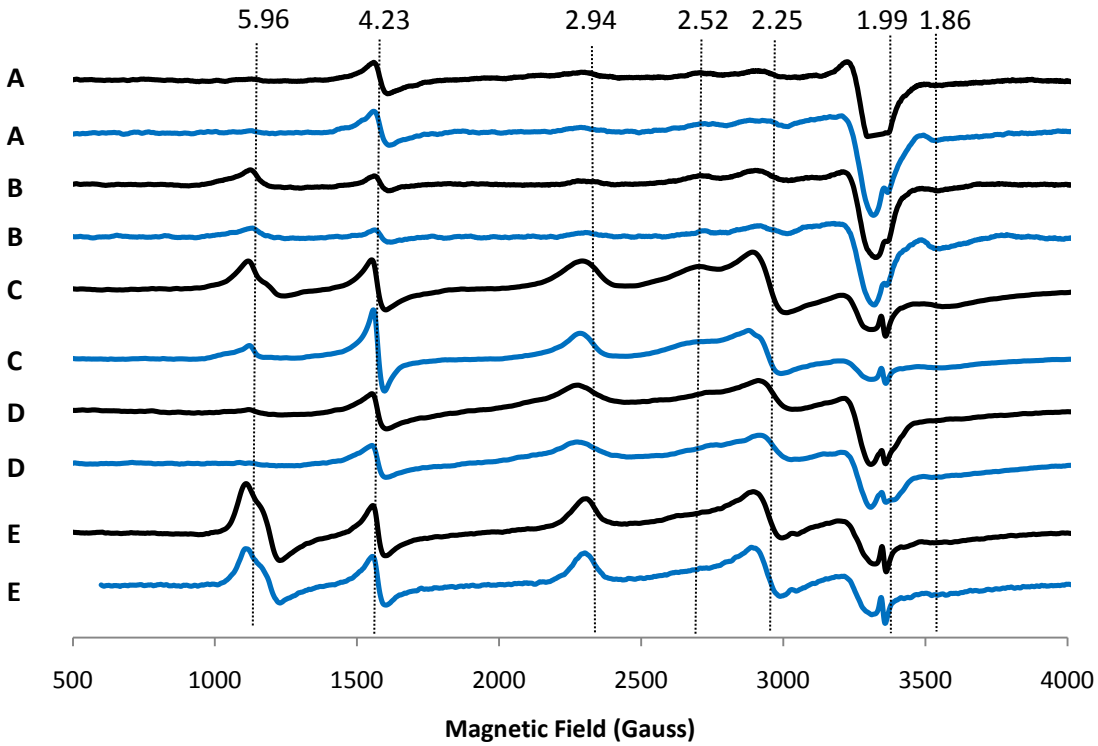

Figure A6.4 X-band EPR spectra of five rhTDO variants, (**A**) H76S, (**B**) F72A, (**C**) F140A, (**D**) F140Y and (**E**) R144K in the absence (Black) and presence (Blue) of 3 mM L-Tryptophan, which are similar to H76A spectra in Chapter 3. Spectra are adjusted to account for differences in receiver gain. Conditions: 11 K, 2.0 mW microwave power, frequency 9.51 GHz, modulation amplitude 1 mT.